ABSTRACT

Title of Document: STRUCTURE, LOCALIZATION AND FUNCTION OF MOUSE MYOSIN XVA IN THE INNER EAR

Erich T.A. Boger, Doctor of Philosophy, 2006

Directed By: Dr. Thomas B. Friedman, Laboratory of Molecular Genetics, National Institute on Deafness and Other Communication Disorders, National Institutes of Health, and Professor Arthur N. Popper, Department of Biology

Recessive mutations of *MYO15A* encoding unconventional myosin XVA are associated with sensorineural deafness in both humans (*DFNB3*) and the shaker 2 phenotype in mice, which are deaf and exhibit circling behavior due to a vestibular abnormality. Myosin XVa is extensively alternatively spliced and encodes approximately thirty protein isoforms. In mouse hair cells that are homozygous for the shaker 2 (*Myo15a*^{sh2}) missense mutation, stereocilia are abnormally short due to a failure of their actin filamentous core to elongate. The stereocilia bundle of homozygous *Myo15a*^{sh2} hair cells lack the characteristic staircase architecture found in wild type hair cell stereocilia bundles. I show that the inability of mutant myosin XVa to deliver whirlin, a scaffold protein, to stereocilia tips underlies the stereocilia dysmorphology in hair cells from homozygous *Myo15a*^{sh2} mice. The introduction of exogenous myosin XVa homozygous *Myo15a*^{sh2} hair cells results in restoration of

stereocilia elongation and staircase bundle formation. These results imply that the delivery of whirlin by myosin XVa is essential for stereocilia elongation and staircase formation. Using a series of GFP tagged myosin XVa expression constructs containing deletions of one or more domains, the regions necessary for localization to filopodia tips in COS-7 cells, as a model system, and to stereocilia tips of inner ear hair cells was determined. In COS-7 cells, the myosin XVa motor plus several combinations of domains of the myosin XVa tail are sufficient for filopodia tip targeting. The myosin XVa motor plus either the $MyTh4_1/FERM_1$ or $MyTh4_2/FERM_2$ domains are sufficient for stereocilia tip localization in inner ear hair cells. A preliminary assessment of the regions of myosin XVa necessary for the re-initiation of stereocilia elongation and staircase formation in homozygous *Myo15a*^{sh2} mutant inner ear hair cells is provided. These results provide a better understanding of the molecular mechanisms underpinning normal stereocilia morphogenesis.

STRUCTURE, LOCALIZATION AND FUNCTION OF MOUSE MYOSIN XVA IN THE INNER EAR

By

Erich Theodore August Boger

Dissertation submitted to the Faculty of the Graduate School of the
University of Maryland, College Park, in partial fulfillment
of the requirements for the degree of
Doctor of Philosophy
2006

Advisory Committee:
Dr. Arthur N. Popper, Chair
Dr. Thomas B. Friedman, Co-chair
Dr. Marco Colombini
Dr. Stephen M. Mount
Dr. Sergei Sukharev
Dr. Robert J. Wenthold

Dedication

Research science exists in a continuum, so I am indebted to the seminal observations of the generation of scientists who preceded me.

Acknowledgements

I wish to thank my mother and father for educating me, instilling a strong work ethic and imparting in me a passion for knowledge. To my wife Jennifer, your patience, encouragement and love made this accomplishment possible.

I am grateful to Dr. Arthur Popper, for serving as my University of Maryland advisor and encouraging me to matriculate into the Biology Doctoral Program at the University of Maryland. My deepest thanks to Lois Reid for answering my endless questions and guiding me through the academic maze at the University of Maryland. I wish to thank my dissertation committee members, Dr. Thomas B. Friedman, Dr. Arthur N. Popper, Dr. Marco Colombini, Dr. Sergei Sukharev, Dr. Stephen M. Mount and Robert J. Wenthold, for their time and guiding me through my doctoral research.

I wish to thank Dr. Ronald Schnaar (Johns Hopkins University) for opening my mind to the endless possibilities of research science and serving as my first scientific mentor. Dr. Robert Fridell, for instilling confidence in my abilities and introducing me to one of my great interests, myosin XVa. I am grateful to Dr. James Sellers, for his passion and knowledge of myosins, Dr. Zubair Ahmed, for friendship and intriguing scientific discussions, and to Dr. Inna Belyantseva, a remarkable friend, research scientist and mentor. I am indebted to Dr. Thomas Friedman, a scholar and gentleman, for giving me all measure of successes in my scientific career. His

passionate pursuit of knowledge, rigorous experimental method and tireless encouragement of my curiosity have inspired me.

Table of Contents

List of Tables

List of Figures

Chapter 1: Introduction

Overview

In vertebrates, inner ear cochlear and vestibular hair cells are the mechanosensory cells that underlie the processes of hearing and balance. Inner ear cochlear and vestibular hair cells convert mechanical stimuli of sound and head movement into electrical signals that are processed by the brain (Tilney et al. 1992 Gillespie et al. 2001; Frolenkov et al. 2004). Deflection of stereocilia, a specialized actin cytoskeletal structure projecting from the apical surface of inner ear hair cells, opens mechanically gated ion channels causing depolarization of hair cells (Pickles et al. 1984; Tilney et al. 1992; Denk et al. 1995; Holt et al. 2000; Kachar et al. 2000; Gillespie et al. 2001). To function as a mechanical transducer, stereocilia are organized into rows of increasing height forming a staircase pattern (Tilney et al. 1992; Frolenkov et al. 2004). The lengths of the stereocilia in the staircase are precisely determined as is the stereocilia number and width (Tilney et al. 1992). Underscoring its essential role in mechanotransduction, all vertebrate hair cell stereocilia are organized in a staircase pattern (Fay and Popper 2000; Manley 2000). In humans and mice, the normal process of stereocilia elongation and staircase formation is abolished by mutations in the unconventional myosin XVa and the scaffold protein whirlin (Probst et al. 1998; Wang et al. 1998; Liang et al. 1999; Anderson et al. 2000; Belyantseva et al. 2003a; Mburu et al. 2003; Belyantseva et al. 2005). The purpose of the research described in this dissertation is to examine the function of unconventional myosin XVa in stereocilia elongation and staircase formation.

In chapter 1 of this dissertation, I review the mammalian inner ear structure, discuss the structure and function of hair cell stereocilia, present a brief overview of the myosin superfamily and finally present an introduction to myosin XVa. In chapter 2, I describe mouse inner ear myosin XVa cDNA isoforms and speculate on possible function of the various myosin XVa protein isoforms. As a comparison to myosin XVa, I describe the structure of mouse inner ear myosins VIIa, VIIb and X. In chapter 3, I describe the interaction of myosin XVa with whirlin, its first reported protein partner. I demonstrate that the delivery of whirlin to stereocilia tips by myosin XVa is essential for the normal process of stereocilia elongation and staircase formation. In chapter 4, I experimentally determined the regions of myosin XVa protein that are necessary for accumulation at filopodia tips of COS-7 cells, a simple model system to evaluate the targeting of myosin XVa. In chapter 5, I describe the regions of myosin XVa protein that are necessary for localization at stereocilia tips of inner ear hair cells.

Structure of the mammalian inner ear

Within the mammalian inner ear there are two sensory organs, the vestibule and the cochlea. The vestibule is the organ of balance and equilibrium while the cochlea is the organ of hearing. The vestibular system is comprised of three canals oriented at perpendicular angles relative to each other and the fluid filled membranous labyrinth. Each of the three circular canals contain patches of sensory hair cells responsible for detection of various aspects of head movement. Linear acceleration is detected by

sensory hair cells located in the saccule and utricle while rotational movement is detected by hair cells in the ampulla.

The cochlea is a bone encapsulated spiral structure where the separation of sound into frequencies arises from the mechanical properties of the basilar membrane, a collagenous membrane that bisects the cochlear duct (Ashmore et al. 2001). The basilar membrane exhibits a stiffness gradient along its length that insures that different sound frequencies map to different positions along this membrane. The organ of Corti, which is located above the basilar membrane, contains the sensory epithelium and is composed of two types of mechanosensory hair cells, inner and outer hair cells.

Hair cell stereocilia

Inner ear cochlear and vestibular hair cells utilize a common mechanism to accomplish mechanosensory transduction. Stereocilia, which are rod-like, actin protrusions on the apical surface of cochlear and vestibular hair cells (figure 5-1C), enable the conversion of sound waves and movement into sensory information (Tilney et al. 1992; Gillespie et al. 2001; Frolenkov et al. 2004). Displacement of the stereocilia bundle opens mechanosensitive ion channels located either at the distal tips of stereocilia or at the attachment site of the obliquely oriented tip link to the next taller adjacent stereocilium (Pickles et al. 1984; Tilney et al. 1992; Denk et al. 1995; Holt et al. 2000 Kachar et al. 2000; Gillespie et al. 2001) resulting in a change in the

membrane voltages of cochlear and vestibular hair cells. These electrical changes are transmitted synaptically to afferent neurons of the eighth cranial nerve.

Stereocilia are organized into rows of increasing height forming a staircase pattern (Figure 5-1C; Tilney et al. 1992; Garcia-Anoveros et al. 1997; Frolenkov et al. 2004). Morphologically, the cell shape, the number, length and width of the stereocilia in the staircase differ among the four types of mechanosensory hair cells present in the inner ear, inner and outer hair cells of the organ of Corti and type I and II hair cells of the vestibular organs (Tilney et al. 1992). Each hair cell staircase is comprised of 30 to 300 stereocilium. The cytoskeletal core of each stereocilium is comprised of a rigid paracrystalline array of several hundred parallel, uniformly polarized cross-linked actin filaments (Tilney et al. 1983). The barbed ends of the actin filaments are located at the stereocilia tips while the pointed ends are located at the tapered base of the stereocilia (Tilney et al. 1983; Tilney et al. 1992). The actin cytoskeleton of stereocilia undergoes continuous renewal by the addition of actin monomers at the stereocilia tips, retrograde flow, and disassembly of actin monomers at the base (Schneider et al. 2002; Radzinska et al. 2004).

Three sets of extracellular links extending laterally in a symmetrical manner hold the stereocilia together (Garcia-Anoveros et al. 1997; Holt et al. 2000). A fourth set of links, known as tip links, extend upwards from the tip of the shorter stereocilium to the side of the next taller stereocilium (Pickles et al. 1984; Garcia-Anoveros et al. 1997; Holt et al. 2000; Kachar et al. 2000). The tip link is a stiff, inextensible right-

handed, coiled double extracellular filament that runs parallel to the bundle axis (Pickles et al. 1984; Garcia-Anoveros et al. 1997; Kachar et al. 2000). Recently, protocadherin 15 was shown to be a component of the tip link (Ahmed et al. 2006).

In the cochlea, the overlaying tectorial membrane contacts the tallest row of stereocilia of inner and outer hair cells. Vibrations of the basiliar membrane in response to auditory stimuli vertically displace auditory hair cells, resulting in the bending of the mechanosensitive stereocilia bundle against the tectorial membrane. Sensory hair cells of the vestibular organs share mechanistic features with cochlear hair cells. Horizontal or vertical head tilt movement displaces the otilithic membrane overlying the saccule and utricle hair cell stereocilia resulting in the opening of gated ion channels. Rotational head movement displaces the cupule causing bending of stereocilia bundles of ampulla hair cells, opening mechanically gated ion channels.

Gating-spring hypothesis

Deflection of the hair bundle towards the tallest stereocilia gates cation-selective transduction channels located either at the distal tips of stereocilia and/or at the attachment site of the tip link to the next taller adjacent stereocilium (Pickles et al. 1984; Denk et al. 1995). The mechanical force caused by the deflection of the stereocilia is transmitted to the transduction channel (Markin et al. 1995; Martin et al. 2000). Increased tension in a gating spring promotes the channel's transition from a closed to an open state, generating an electrical current of hundreds of picoamperes carried primarily by K^+ and Ca^{2+} ions (Holt et al. 2000). Positive deflection defined as

deflection of the bundle towards the tallest stereocilia, opens ion channels thereby increasing inward current and depolarizing the hair cell (Hudspeth et al. 1977).

A negative deflection closes all mechanically gated channels and hyperpolarizes the cell while a perpendicular deflection of the hair bundle has no effect (Shotwell et al. 1981). Within 10 microseconds of positive deflection of hair bundle deflection, ion channels open suggesting that the mechanical stimulus is directly coupled to the transduction channel. Electrophysiological and micromechanical data from *in vivo* and *in vitro* cultured hair cells confirmed the stimulus dependence of channel open probability and bundle stiffness (Howard et al. 1988; Markin et al. 1995).

The Ca^{2+} concentration near the transduction channels has a direct effect upon the gating of the transduction channel (Holt et al. 2000). The Ca^{2+} buffers within the stereocilia are unknown but Ca^{2+} binding proteins calmodulin, calbindin and calretinin appear to be strong candidates. Ca^{2+} extrusion from the stereocilia appears to be mediated by Ca^{2+} ATPases. Exposure to the calcium chelator BAPTA abolishes tip links and mechanotransduction (Assad et al. 1991) however tip links and mechanotransduction returned within 12 to 24 hours following BAPTA removal (Zhao et al. 1996; Ahmed et al. 2006).

Tip links were hypothesized to be the gating springs and are presumed to be connected directly to the transduction channel (Pickles et al. 1984; Kachar et al. 2000). The tension in the tip links between adjacent stereocilia connects the

mechanosensitive channels of the stereocilia to the energy stored in the tip links, thereby allowing fast channel gating without the involvement of second messenger cascades that are found in photoreceptors and olfactory cells (Ashmore et al. 2000; Gillespie et al. 2001). The exquisite sensitivity of the human cochlea is underscored by the observation that there are approximately 3,500 inner ear hair cells and 12,000 outer hair cells. By comparison, there are millions of photoreceptors in the retina and chemoreceptors in the olfactory center (Gillespie et al. 2001).

Hair Cell Adaptation

In response to sustained positive hair bundle deflection, the inward current in hair cells declines through the closure of transduction channels by a process known as adaptation (Eatock et al. 1987). Channel closure caused by maintained negative hair bundle deflection is followed by channel reopening (Eatock et al. 1987). These observations suggest an adaptation mechanism that moves the attachment point of the tip link without changing its stiffness (Howard et al. 1987). Hair cell adaptation continuously adjusts the tension in the tip links thereby influencing the open and closed states of the transduction cation channel (Eatock 2000; Holt et al. 2000). It was found that hair cells adapt to sustained deflections of the hair bundle through Ca^{2+}-dependent negative feedback on the probability of the mechanosensitive transduction channels (Assad et al. 1992; Garcia-Anoveros et al. 1997). Two distinct non-mutually exclusive models were proposed to explain the phenomena of hair cell adaptation. One model proposes mechanical adjustment by a molecular motor on the resting tension of the tip link (Howard et al. 1987) while the other model proposes that Ca^{2+}

binding directly or near the transduction channel alters the relationship between tip link tension and the open state of the channel (Crawford et al. 1989; Crawford et al. 1991).

The first model, the motor model of adaptation, postulates that in response to a maintained hair bundle deflection, the hair cell relieves the tension in the tip links between the stereocilia by repositioning the upper tip link insertion point along the side of the stereocilium (Holt et al. 2000). Maintaining the tension between the tip links probably requires a molecular motor, which is presumed to be a myosin due to the actin rich structure of the stereocilia. A complex of myosins, located adjacent to the upper tip link insertion point, hydrolyzes ATP in order to climb towards the barbed ends of stereocilia actin filaments (the actin filaments in the stereocilia are polarized in a single plane). The continuous climbing of the myosin motor complex is counterbalanced by the opposing force of the tautness in the tip link. Once the correct tautness is achieved in the tip link, the tension causes the motor to slip down the stereocilium. When the hair bundle is at rest, climbing rate equals the slipping rate, thereby keeping the tip links under a certain resting tension. During adaptation to continuous hair bundle deflection, influx of Ca^{2+} through the transduction channel is proposed to increase the slipping rate of the motor complex, thereby reducing the tension tip link and allowing the closure of the transduction channel (Holt et al. 2000).

During negative hair bundle deflections (deflections away from the tallest stereocilia), which decrease the tension in the tip links, the myosin complex climbs towards the tip of the stereocilia and restores the resting tension of the tip links. In this manner sensitivity or tension is restored to the tip link. Positive deflection (deflections towards the tallest stereocilia) of the hair bundle transmits a mechanical force greater than the opposing force generated by the myosin complex resulting in the myosin complex slipping and pulled down the actin filaments. Myosins contain a variable number of IQ domains that bind regulatory myosin light chains as well as calmodulin and therefore confer a Ca^{2+} dependence to myosin activity (Cheney et al. 1992). Calmodulin is found at high concentration [100 μM] near the tips of the stereocilia (Shepherd et al. 1989; Walker et al. 1993) and calmodulin inhibitors block adaptation (Walker et al. 1996). It seems plausible that the calmodulin mediates the Ca^{2+} regulation of the myosin adaptation motor (Garcia-Anoveros et al. 1997; Holt et al. 2000).

The second model, the Ca^{2+}-dependent closure model, suggests the rate of adaptation depends upon the Ca^{2+} concentration inside the tips of the stereocilia (Crawford et al. 1989; Crawford et al. 1991). Adaptation occurs when Ca^{2+} enters through the open transduction channel and binds directly or near the channel protein thereby stabilizing a closed state of the channel (Holt et al. 2000). High intracellular Ca^{2+} concentrations within the stereocilia show adaptation time constants of 0.3 msec, which is too fast to be mediated by a myosin ATPase cycle time estimated to be 4 to 8 msec (Holt et al.

2000). Elevated Ca^{2+} could cause a reduction in the stiffness of myosin's force generating lever arm.

Myosin Superfamily

Myosins comprise a superfamily of molecular motor proteins in which ATP hydrolysis causes a small conformational change in the globular motor domain that is amplified and translated into movement along actin filaments (Mooseker et al. 1995; Mermall et al. 1998; Sellers 2000; Schliwa et al. 2003; Vale 2003). The well-conserved 600 amino acid motor domain arose very early in eukaryotic development and its catalytic structure has been maintained (Schliwa et al. 2003; Vale 2003). All myosin molecules hydrolyze ATP by essentially the same mechanism (Mooseker et al. 1995; Mermall et al. 1998; Sellers 2000; Schliwa et al. 2003; Vale 2003). Based upon phylogenetic analyses of the motor domains, eighteen classes of heavy chain myosins can be distinguished in fungi, amoebas, plants, invertebrates, and vertebrates. (Hodge et al. 2000; Sellers 2000; Berg et al. 2001; Kendrick-Jones et al. 2001; Reilein et al. 2001). Each myosin class may contain multiple genes. Within the human genome, there are 39 myosin genes from twelve classes plus a single myosin gene that fails to group into any of the other classes (Berg et al. 2001). Conventional or class II myosins are found in muscle and other cell types. The seventeen other classes of myosins are known as unconventional myosins and are present in a variety of cell types.

Cell movement, muscular contraction, cytokinesis, membrane and vesicle trafficking, anchoring hair cell stereocilia, organelle localization, and signal transduction are driven by myosins (Baker et al. 1998; Hodge et al. 2000; Sellers 2000; Berg et al. 2001; Kendrick-Jones et al. 2001; Reilein et al. 2001). Despite their diverse cellular functions, all myosins have a motor, neck and tail domain (Sellers 2000; Kendrick-Jones et al. 2001). The conserved motor domain contains an open ATP binding pocket, an actin binding site, and a 'converter' region which links the motor domain to the neck (Sellers 2000; Kendrick-Jones et al. 2001). The neck region, which binds calmodulin and myosin light chains, is composed of a variable number of IQ motifs containing the consensus sequence (IQXXXRGXXXR; Mooseker et al. 1995). Among the unconventional myosins the tail domain is highly divergent and may contain multiple protein or lipid binding motifs (Mermall et al. 1998; Oliver et al. 1999). The characteristics of the tail domain are assumed to direct the interaction of a myosin with its protein partners, and direct the subcellular localization of the myosin (Mermall et al. 1998; Oliver et al. 1999). Interestingly, an identical phylogenetic pattern is observed if the tail domain is used for analysis suggesting that motor and tail domains did not evolve independently of each other but rather the motor and cargo binding tail has been optimized for their respective cellular function (Baker et al. 1998).

From my analysis of cDNA expression within mouse cochlear and vestibular tissue, mRNA transcripts of myosins 1a, 1b, 1c, 1d, 1e, 1f, 1h, 1h, IIIa, IIIb, Va, VI, VIIa, VIIb, X, XVa, XVI and XVIIIa are detected (Hasson et al. 1997; Liang et al. 1999;

Dumont et al. 2002; Walsh et al. 2002; Peters et al. 2006; unpublished data). Of these, at least six myosins are essential for auditory and vestibular as mutations of myosins IA, IIA, IIIA, VI, VIIA and XVA cause deafness in mice and humans (Avraham et al. 1995; Gibson et al. 1995; Wang et al. 1998; Lalwani et al. 2000; Seri et al. 2000; Walsh et al. 2002; Donaudy et al. 2003). Despite this wealth of expression and genetic data, the localization of only seven myosins was reported. Endogenous rat myosin Ib was present in support cells while myosin 1e was localized in the cuticular plate of hair cells (Dumont et al. 2002). Endogenous myosin Va was demonstrated to be present in afferent neurons of guinea pig utricle (Hasson et al. 1997). Myosin VI is not present in the stereocilia however it is localized within the cell body of the hair cell (Hasson et al. 1997). Subcellular localization of myosins 1c, VIIa and XVa were reported within the stereocilia bundle of sensory hair cells (Hasson et al. 1997; Anderson et al. 2000; Belyantseva et al. 2003a; Rzadzinska et al. 2004).

Myosin XVa background

Mutations in myosin XVA are associated with sensorineural deafness in both humans (*DFNB3*) and shaker 2 (*Myo15a*^{sh2}) mice (Friedman et al., 1995; Liang et al. 1998; Probst et al. 1998; Wang et al. 1998). The nonsyndromic congenital recessive deafness gene, *DFNB3* was mapped to human chromosome 17p11.2 using a large kindred from the village of Bengkala, Bali (Friedman et al. 1995). Based upon conserved synteny between mouse and human genomes, the shaker 2 mouse was proposed as a model of DFNB3 (Liang et al. 1998).

The shaker 2 phenotype is caused by an autosomal recessive mutation located on mouse chromosome 11 that arose in the progeny of an x-ray irradiated mouse (Dobrovolskaia-Zavasdkaia 1928; Snell et al. 1939). Affected mice lack the normal startle response to sound and demonstrate no auditory brainstem responses to high sound pressure levels, indicating profound deafness (Liang et al. 1998). Additionally, homozygous shaker 2 mice exhibit circling behavior and balance defects that are characteristically associated with vestibular dysfunction (Probst et al. 1998). The introduction of a **B**acterial **A**rtificial **C**hromosome containing the genomic sequence of mouse myosin XVa into homozygous shaker 2 embryonic stem cells resulted in the phenotypic rescue of the deafness and vestibular defects (Probst et al. 1998).

In homozygous shaker 2 mice, organ of Corti and vestibular hair cells have abnormally short stereocilia (Probst et al. 1998; Liang et al. 1999; Anderson et al. 2000). In wild type mouse hair cells, myosin XVa immunoreactivity is present in stereocilia, while myosin XVa immunoreactivity is absent from hair cell stereocilia of homozygous shaker 2 mice (Anderson et al. 2000).

Myosin XVa has a restricted tissue expression pattern in mice and humans. It is found exclusively in the cochlear and vestibular sensory hair cells of the inner ear and associated with secretory granules in cells of the anterior pituitary (Liang et al. 1999; Anderson et al. 2000 Lloyd et al. 2001; Belyantseva et al. 2003a).

Domain structure of myosin XVa protein

Based upon overlapping cDNA fragments from mouse inner ear, Liang (1999) predicted that two alternatively spliced *Myo15a* mRNA transcripts (figure 2-1A) encoded myosin XVa proteins of 2,324 and 3,511 amino acids (figure 2-1B). Alignment of the two myosin XVa protein sequences revealed that the two proteins shared identical motor, IQ motifs and domains in the tail region but differed by the inclusion or exclusion of exon 2, which encodes a 1,187 amino acid N-terminal extension preceding the motor domain. The tail of myosin XVa has two pairs of tandemly arrayed myosin tail homology 4 (MyTh4) and band 4.1/ezrin/radixin/moesin (FERM) domains, a Src homology 3 domain (SH3) and a predicted class I PDZ peptide ligand (I-T-L-L) at the carboxy terminus (Liang et al. 1999; Harris et al. 2001; Hung et al. 2002; Belyantseva et al., 2003a; Belyantseva et al. 2003b).

The **S**rc **H**omology **3** (SH3) domain is a small protein domain of about approximately 60 amino acids. SH3 domains are found in a variety of intracellular or membrane-associated proteins. SH3 domains mediate assembly of specific protein complexes by binding to specific proline-rich sequences in a diverse array of protein binding partners including cytoplasmic domains of transmembrane proteins as well as peripheral membrane proteins (Kay et al. 2000).

The **My**osin **T**ail **h**omology **4** (MyTh4) domain is an approximately 150 amino acid module which has been identified in eight proteins in the mouse genome including myosins VIIa, VIIb, X, XVa, XVBP, pleckstrin homology domain containing,

family H members 1, 2 and 3 (Plekhh1, Plekhh2 and Plekhh3). A MyTh4 domain is associated with a FERM domain (**F** for 4.1 protein, **E**zrin, **R**adixin and **M**oesin) in all eight proteins while it is associated with Pleckstrin Homology domains in five out of eight proteins. MyTh4 domains are predicted to be largely α-helical, interrupted by three or four turns. MyTh4 domains contain four highly conserved regions designated MGD (consensus sequence: L(K/R)(F/Y)MGDhP), LRDE (consensus sequence: LRDEhYCQhhKQHxxxN), RGW (consensus sequence: RGWxLh) and ELEA ((consensus sequence: RxxPPSxhELEA), where h is a hydrophobic residue and x is any residue.

The exact function of the MyTh4 domain is presently unknown, although several reports implicate roles in microtubule binding and dorsal filopodia formation. Weber and colleagues reported that disruption of microtubule binding by the MyTh4 domain of myosin X impaired meiotic spindle assembly and nuclear anchoring (Weber et al. 2004). In myosin X null cells unable to form dorsal filopodia, introduction of myosin X lacking the FERM domain resulted in dorsal filopodia formation while myosin X lacking the MyTh4 and FERM domains failed to promote filopodia formation (Bohil et al. 2006). These result suggest that either the MyTh4 domain or the combination of MyTh4 and FERM domains likely interact with an unidentified protein component essential for formation of filopodia (Bohil et al. 2006).

FERM domains (**F** for 4.1 protein, **E**zrin, **R**adixin and **M**oesin) are protein modules of approximately 300 amino acids that are involved in localizing proteins to the plasma membrane (Oliver et al. 1999). They are found in a large number of cytoskeletal-associated proteins that associate with various proteins at the interface between the plasma membrane and the cytoskeleton. In the majority of FERM-containing proteins, the FERM domain located at the N-terminus. The highly conserved three-dimensional structure of FERM domains is comprised of three subdomains (F1, F2, and F3) that together form a compact clover-shaped structure (Hamada et al. 2000; Pearson et al. 2000). One FERM subdomain interacts with cytoplasmic tails of adhesion proteins such as integrins while another subdomain electrostatically interacts with inositides (Pearson et al. 2000 Niggli 2001; Balla 2005).

The last four amino acids at the C-terminus sequence of myosin XVa (I-T-L-L) match the consensus class 1 PDZ-binding (ligand) motif (X-S/T-X-V/L). PDZ domains are protein-protein binding domains that commonly interact with transmembrane proteins allowing the assembly of supra-molecular signaling complexes (Sheng et al. 2001; Hung et al. 2002). A well-characterized example in sensory transduction is Drosophila INAD, containing five PDZ domains, that assembles the TRP ion channel complex at the rhabdomere of photoreceptors (Sheng et al. 2001; Harteneck et al. 2002).

In this dissertation, I examined the contributions of the various domains of myosin XVa to the subcellular localization in COS-7 filopodia and inner ear hair cell stereocilia. I show that 1) myosin XVa mRNA is alternatively spliced within the inner ear and encodes approximately thirty myosin XVa protein isoforms, 2) the delivery of whirlin to stereocilia tips by myosin XVa is essential for the elongation of stereocilia, 3) multiple redundant domains of myosin XVa can mediate filopodia tip targeting in COS-7 cells, and 4) the myosin XVa motor plus MyTh4 or MyTh4/FERM domains is sufficient for localization at hair cell stereocilia tips. The new questions raised by the data and conclusions from this work will be investigated by me for many years to come.

Chapter 2: Comparative Study of Alternatively Spliced cDNA transcripts of *Myo15a, Myo7a*, *Myo7b* and *Myo10*

Abstract

The cloning and sequencing analysis of 122 full-length *Myo15a* cDNA transcripts from mouse vestibular cDNA revealed that the mRNA transcripts from this gene are extensively alternatively spliced. Two major subclasses of *Myo15a* cDNA transcripts, termed class 1 and 2, were identified as having different transcription start sites. Class 1 *Myo15a* cDNA transcripts were comprised of exons 2 through 66 with an average transcript size of 10.6 kilobases (kb). Class 2 *Myo15a* cDNA transcripts were comprised of exon 1 and exons 3 through 66 and had an average transcript size of 7.3 kb. While alternate splicing of exons 8 and 26 were previously reported, the majority of *Myo15a* cDNA isoform diversity was accomplished by the retention of an entire intron or partial intronic sequence that resulted in novel translated sequence. On the basis of predicted protein products from the cloned full-length *Myo15a* cDNA transcripts, thirty different protein isoforms are possible. The majority of the predicted protein isoforms differ by the composition of domains of the tails, implying that the functional diversity of various myosin XVa protein isoforms is achieved by differences in the tail. In contrast to *Myo15a* cDNA, full-length mouse vestibular *Myo7a*, *Myo7b* and *Myo10* cDNA transcripts encode fewer protein isoforms.

Introduction

The mouse myosin XVa gene is comprised of 66 exons spanning 59.1 kilobases (kb) of genomic DNA of mouse chromosome 11. Initially it was reported that both mouse and human myosin XVa genes produced two alternatively spliced mRNA transcripts encoding two distinct myosin XVa proteins (figure 2-1A and 2-1B, Liang et al. 1999). One mouse *Myo15a* cDNA transcript was 11,769 base pairs in length and was comprised of exons 1 through 66. It was predicted to encode a 3,511 amino acid protein with a molecular mass of 395 kilodaltons (figure 2-1B). A second *Myo15a* cDNA transcript was 8,007 base pairs and comprised of exon 1 and exons 3 through 66. This cDNA transcript was predicted to encode a 2,324 amino acid protein with a molecular mass of 262 kilodaltons (figure 2-1B). A key difference between the two *Myo15a* cDNA transcripts was the inclusion or exclusion of exon 2. Exon 2 (3,762 base pairs) encodes a 1,187 amino acid domain termed the N-terminal extension that precedes the motor. In addition to exon 2, alternative splicing of exons 8 and 26 were observed in a few cDNA clones. No attempt to quantitate the occurrence of these transcripts in mouse inner ear mRNA transcripts was undertaken.

The presence of two alternatively spliced *Myo15a* cDNA transcripts reported by Liang and colleagues in 1999 were based upon the assembly of short, overlapping cDNA fragments cloned from mouse inner ear (Liang et al. 1999). By multiple tissue dot blot hybridization and RT-PCR analysis, human MYO15A cDNA expression was detected only within inner ear and pituitary tissue and was absent from many other tissue types (Liang et al. 1999; Lloyd et al. 2001). Thus, myosin XVA has an extremely limited tissue distribution. Due to the difficulty of obtaining several

micrograms of poly A+ RNA from inner ear tissue, pituitary poly A+ RNA was used for Northern blot analysis (Liang et al. 1999). A Northern blot using a cDNA probe common to both predicted *Myo15a* cDNA transcripts (exons 31-41) revealed a diffuse smear ranging in size from 6.0 kb to 12.0 kb. The same Northern blot was reprobed using a DNA probe specific to the first *Myo15a* cDNA transcript (exon 2) revealed a band of approximately 12.0 kb.

In situ hybridization of mouse inner ear tissue revealed the expression of *Myo15a* exclusively in sensory hair cells but absent from all other cell types within the cochlea and vestibular organs (Liang et al. 1999; Anderson et al. 2000). Immunolocalization of myosin XVa protein within the stereocilia of hair cells was observed using mouse whole-mount cochlear tissue (Liang et al. 1999).

Several unsuccessful attempts to Western Blot mouse inner ear protein extract using antiserum against a region of myosin XVa located between the first MyTh4 and FERM domains were performed. There were a few reasons for the failure to visualize myosin XVa protein on a Western blot. First, the large molecular weight of the two protein isoforms (262 and 395 kilodaltons) makes the transfer to nitrocellulose membranes technically demanding. Second, the presumed low copy number of myosin XVa protein complicates the task. At the cDNA transcript level, Massively Parallel Signature Sequencing (Brenner 2000) revealed that myosin XVa was present in the organ of Corti at three transcripts per million while in the vestibular organs it is present at approximately 400 transcripts per million (Peters et al. 2006). By

comparison, a ubiquitously expressed house keeping gene such as β-actin is present at 4,464 and 4,951 transcripts per million in the organ of Corti and vestibule, respectively. While no direct correlation exists between the amount of cDNA transcript and the level of steady state protein in mammals, the low amount of *Myo15a* cDNA transcript suggests a low myosin XVa protein level.

Methods

Cloning of Mouse Inner Ear Myo15a cDNA Transcripts.

To confirm the exon composition of *Myo15a* mRNA transcripts in the inner ear, full-length *Myo15a* cDNAs were cloned from mouse postnatal day 5 (P5) vestibular mRNA by RT-PCR. Approximately 2.7 μg of mouse P5 vestibular poly(A)$^+$ RNA was reverse transcribed using Powerscript Reverse Transcriptase (BD Biosciences) and an oligo dT primer [GAGGCCCTCGAGGACATG$(T)_{27}$VNNN where N is A, C or G]. Full-length *Myo15a* cDNA was generated by using LA Taq DNA polymerase (Takara Mirus Bio) using forward and reverse PCR primers located in the 5'-UTR and 3'-UTR regions. A single 10.5-kb PCR product for class 1 *Myo15a* cDNA transcripts was amplified with primers in exons 2 and 66 (Figure 2-1D). For class 2 *Myo15a* cDNA transcripts, PCR using primers located in exons 1 and 66 amplified three products of 6.9, 7.5, and 8.5 kb (Figure 2-1D).

PCR products were electrophoresed on a 0.7% agarose gel, gel slices containing the product bands were excised and the DNA was purified by electro-elution. The purified PCR products were cloned into pCR-XL-TOPO vector (Invitrogen) and transformed into DH5α Cells (Invitrogen). Bacterial clones were grown in CircleGrow media (MP Biomedical) for 18 hours at 37^{o}C and plasmid DNA was purified using QIAspin Miniprep Kit (Qiagen). EcoR I digest followed by electrophoresis of digest products on a 0.7% agarose gel determined the approximate cDNA insert size of *Myo15a* clones. Both strands of the cloned *Myo15a* cDNA inserts were sequenced by using Big Dye Terminator Version 3.0 and an ABI3730xl DNA Analyzer (Applied Biosystems). The sequence data was assembled and

analyzed using Seqman (DNAStar) and MacVector programs (Accelyrs). For each clone, the exon/intron composition and the longest open reading frame was determined. The primer sequences used for PCR amplification and sequencing of *Myo15a* cDNA clones is located in Table 1.

Cloning of Mouse Inner Ear Myo7a, Myo7b and Myo10 cDNA Transcripts. Full-length *Myo7a* cDNA (PCR product: 6.7 kb), full-length *Myo7b* cDNA (PCR product: 6.4 kb) and full-length *Myo10* cDNA (PCR product: 6.9 kb) were PCR amplified from mouse postnatal P5 vestibular cDNA using forward and reverse PCR primers located in the 5'-UTR and 3'-UTR regions. The PCR products were gel purified, cloned into pCR-XL-TOPO vector (Invitrogen) and transformed into DH5α Cells (Invitrogen). Both strands of thirty cloned *Myo7a* cDNA clones, of thirty-one cloned *Myo7b* cDNA clones and thirty-seven cloned *Myo10* cDNA clones were sequenced and analyzed. The primer sequences used for PCR amplification and sequencing of *Myo7a*, *Myo7b* and *Myo10* cDNA clones are located in Tables 2, 3 and 4.

Table 2-1. Primers used for the PCR amplification and sequencing of full-length mouse *Myo15a* cDNA

Primer	Sequence	Comment
Myo15a-F1 Myo15a-R1	ATGGCGGATGAGGAGAAGAAAGCGAAG CTGGCGGGAAGCAGTGAAAAGGTAGG	PCR amplification of full-length Class 1 *Myo15a* cDNA transcripts
Myo15a-F2 Myo15a-R1	GCAGACATAGGACCCCCAACAAACAGC CTGGCGGGAAGCAGTGAAAAGGTAGG	PCR amplification of full-length Class 2 *Myo15a* cDNA transcripts
Myo15a-1	TGTGGAGGCAGACATAGG	Sequencing of *Myo15a* cDNA
Myo15a-2	ACCTGCCTTCTATGCGGTC	"
Myo15a-3	CAAGCATTTTGGCGAAGG	"
Myo15a-4	TGGAAAGACTGAGGCTACG	"
Myo15a-5	CACAAACTTCCCAAAGCG	"
Myo15a-6	GCTGAGACCTACTACTACCTGAAC	"
Myo15a-7	GACATTGCCCAGGTGTAAG	"

Myo15a-8	CGGCACTCTCCACTGTTAG	“
Myo15a-9	ATCACCAGGGTCAACGCTC	“
Myo15a-10	CATCTCCCTGAAGCCCTAC	“
Myo15a-11	TGGCATCTTAGGCTTAGAGTAG	“
Myo15a-12	TCCTTCTTATGGTTGGGC	“
Myo15a-13	AAGATGGAGAGGTGTAACCC	“
Myo15a-14	CCCTTCCAGGTGTTTATCG	“
Myo15a-15	CGTTGGATGAAAAAACCTCG	“
Myo15a-16	GTCTGCTGAAGTTCCGTTC	“
Myo15a-17	CACGCAGAAGCCATAAGTG	“
Myo15a-18	GTAGGCATTGGGATTGCG	“
Myo15a-19	TGTCTCAGTGGCTTTGCG	“
Myo15a-20	CCAGGTCCAGCACATAGTC	“
Myo15a-21	TGCTGGACCTGGTATCAG	“
Myo15a-22	AGAAGCCGACAGCCATCGCCTACCG	“
Myo15a-23	GAGTTGAGTGTGGAATACCG	“
Myo15a-24	GCTCCAGAATCCATTTCG	“
Myo15a-25	ACCTTTCCACCATCCGTC	“
Myo15a-26	TTCTATGGCTACCAGGACATCCC	“
Myo15a-27	CCGCTTCACACTTTCTGTTAC	“
Myo15a-28	ATCTACTTCTCTCGCCTCTTCCCG	“
Myo15a-29	GTTCCAGAATGAAGGTGTCTAC	“
Myo15a-30	CACCAGTTTCTTGCGGACTACAC	“
Myo15a-31	TGACTTTGGCTGGAGGTTCG	“
Myo15a-32	GGTCTCGGAAATACTTCTGGGC	“
Myo15a-33	GCTTTGCTTCACTAAGGTCCCG	“
Myo15a-34	ACAATCTGGCAGTAGCATTC	“
Myo15a-35	GAAGCGAATGAGGTATGGATAG	“
Myo15a-36	AGGCTGGAGGCTGCTTTAC	“
Myo15a-37	AAAGGCTTCAGGGCGTGTC	“
Myo15a-38	CACCTGCTGTAGTTGTTGC	“
Myo15a-39	GAGCCAAGGACCACTTCTAC	“
Myo15a-40	TGACAGCGAGGATACAGG	“
Myo15a-41	TCGCTGTCAACCATAACG	“
Myo15a-42	CGGATGAGGAGAAGAAAGC	“
Myo15a-43	TAAGTGACTGGGCACGAG	“
Myo15a-44	TCGTGCCCAGTCACTTAGC	“
Myo15a-45	AGCCCATACAATGACTTGC	“
Myo15a-46	TACGACTACCATCGGGAAGGCGACG	“
Myo15a-47	GCTGTAAGGCGATGAATACC	“
Myo15a-48	CCTATCCACCCTATGACTTTC	“
Myo15a-49	TGGACCTGGCTGGTTTGTC	“
Myo15a-50	CAACAAGGTATGGACAAACCAG	“
Myo15a-51	GCACGGTTCCTCAAAAAAAC	“
Myo15a-52	TGTGGCTGACTTCGTCTC	“
Myo15a-53	ACCCCACCCTTCTCTCCAAC	“
Myo15a-54	AACCTCTGGGCTTGTTCC	“
Myo15a-55	AAGGGTGGCTGGAAAGGAC	“
Myo15a-56	ACTCACCACTGGGACCGTTG	“
Myo15a-57	CGTTGGTTCTCTTGCTGC	“
Myo15a-58	TGGACAGTTCCCCCATTGGC	“
Myo15a-59	CCAACACCTCCCAACAAAAATG	“
Myo15a-60	TGCTCTGGGTCTTGGTCTGG	“

Myo15a-61	TGGGGGCGAGTCTTTTTC	“

Table 2-2. Primers used for the PCR amplification and sequencing of full-length mouse *Myo7a* cDNA

Primer	Sequence	Comment
Myo7a-F Myo7a-R	CAGCAGAGGACTCCGTTACCC AGCAAACCCAGATGCCATAGG	PCR amplification of full-length 6.7 kb *Myo7a* cDNA
7A-1	CAGCAGAGGACTCCGTTAC	Sequencing of *Myo7a* cDNA
7A-2	GCTGCTCTCCATCTACTCG	“
7A-3	CGCCAAAATAGAGCAATACC	“
7A-4	CTTTGTCAAGGGCATCTATG	“
7A-5	TACGACCTGGAGAGCATCG	“
7A-6	TCCTGGAGAAGAACCGAG	“
7A-7	CGATGACTGGCAGATTGG	“
7A-8	GCCACCACTGTAGGAAAAAC	“
7A-9	ACTGAAGGAGAAGGAGGAGGCTCGG	“
7A-10	CAAACTCACAGAAGAGGTAACC	“
7A-11	CTTTGTCAACGGAACTCG	“
7A-12	CCTCTACATCGCTCTGTTCG	“
7A-13	CTTGCTCTTCTCCAGGTTTTAC	“
7A-14	ACCTTTCTGGAGGGGCTACG	“
7A-15	AGACCAGAGGCAGGATGTCG	“
7A-16	CAGAAAGCCCTGAGAAATG	“
7A-17	GACTGGATAAAGAAAGCACG	“
7A-18	TGACTGGAAACGGTCTATTG	“
7A-19	TGGAGTAGTGGCAACACC	“
7A-20	CATTGGGAACTTGGTCCG	“
7A-21	CGACTCCCCGCTGATAATAC	“
7A-22	CGTGATAGTTCCTCTCGTCAG	“
7A-23	CGCATCCAAGTTCTCAAATGTC	“
7A-24	GGTTGTCAGTGAACTCAATGTG	“
7A-25	AACTGGCTGCTGAGTGTAGGCGAGC	“
7A-26	ATCTGCCAGTCATCGTGCGTGC	“
7A-27	GCCTGGAACTCTATTATGCG	“
7A-28	TTCCTTCTTCCTCCGAGC	“
7A-29	TGGTCACCCTCATCGTCGTG	“
7A-30	GTGGATTCCCCATCGTTC	“
7A-31	GCTGTAGTTGCTGAATCTGTTAGC	“
7A-32	ACGGTCAGGGATGTAAGTG	“
7A-33	CATACTTAGACCTCTTCCGTAGC	“
7A-34	ATGACCTGCTCACCAGTATC	“
7A-35	TGTCATCGGGGAAGTAGAC	“
7A-36	TCCAGTCTGTCAGGTGTCGG	“
7A-37	GACCCTGTAGATGAGTGCG	“

Table 2-3. Primers used for the PCR amplification and sequencing of full-length mouse *Myo7b* cDNA

Primer	Sequence	Comment
Myo7b-F Myo7b-R	TTGACAAGGCTGAAGGAACTGC AGATGGGACCTGTTAGGGGTTG	PCR amplification of full-length 6.4 kb *Myo7b* cDNA
7B-1	GGATGGAGCCTGTGTAGG	Sequencing of *Myo7b* cDNA

7B-2	TGGGAAAGACCTTGATTGAG	“
7B-3	TGTATCATCAGTGGCGAGTC	“
7B-4	GATGTGGTAGTTGCGTTCC	“
7B-5	CGGAAGAGAAGCAAATGC	“
7B-6	TCCATCACATCAGACGAATC	“
7B-7	CACAATCCCTGTCCTTGGAGAG	“
7B-8	AGGTGCTCGTTGGCAAAG	“
7B-9	GGAACTACATCCACTACACCG	“
7B-10	TCAGGAAGGACTTGTTGTTGGC	“
7B-11	CGTGGACTCATCACAGACTAAG	“
7B-12	CTCATCAAATGTGTAGCGG	“
7B-13	GGTTTTCCCATCCGCTAC	“
7B-14	TGCTGTCGCACCAGGTAGC	“
7B-15	AGCCACCTGCTGATGAGACAGTTC	“
7B-16	TCACAGCAAACTTGGGGAAGG	“
7B-17	GAAGCGTAAGTCCATCTATGAC	“
7B-18	CACTGGCTCTGGAAGGTCACC	“
7B-19	ATGACACTGACCACTCGG	“
7B-20	ATTGGCGAAGGTGCGTTG	“
7B-21	CCCTTCTGTGCTGAACGG	“
7B-22	TCTCAGGGACAATCTGGGCTTC	“
7B-23	GGAGGACTTGGTGGTAAATG	“
7B-24	AAGGCGGGGACCAGAGAGTG	“
7B-25	CCACGGTGAAGAGTAACG	“
7B-26	TGCTGGGGGAGACGAACTCG	“
7B-27	CAGCAGCGTGGCTATTGC	“
7B-28	CAGGGTGTATGGCGACTC	“
7B-29	TCACAGAGTCGCCATACAC	“
7B-30	GAGGTCCCACCCTTAGAAC	“
7B-31	AGACCAGATGTTCTCGTTAGC	“
7B-32	TCCACAGGGTTCTAAGGG	“
7B-33	TTGAGCCACAGTTTCCGC	“
7B-34	GGAAACTGTGGCTCAACG	“
7B-35	GGAAGGCTCAGAGGTTTG	“
7B-36	CCAGACATTCTCCTCATCG	“
7B-37	CCGCTGTTTGTTCACTGTATTC	“

Table 2-4. Primers used for the PCR amplification and sequencing of full-length mouse *Myo10* cDNA

Primer	Sequence	Comment
Myo10-F Myo10-R	TCGGGAAGAATGTGCCACC AATCAGGCTGGGGAGGTTAGTG	PCR amplification of full-length 6.9 kb *Myo10* cDNA
10A-1	AGCACGGGTCTGGCTAAGAG	Sequencing of Myo10 cDNA
10A-2	GTCAGTGAACCCCTACCAG	“
10A-3	AAGCAGCGATAGCATTCG	“
10A-4	TCCCTCCCTGAATGTTTC	“
10A-5	AACAACAACTCCAGTCGCTTCG	“
10A-6	ACACCCAGACTGATTCAAGTAGTGG	“
10A-7	CCTTCAGACAAGTTATCACGG	“
10A-8	TGAGTCTCTGCTATCTACGGC	“
10A-9	TGCTCGCTGCTTTGAGTG	“
10A-10	ATCTTCCCACACCAATCC	“

10A-11	GCACCTCTCCAGCATAATG	“
10A-12	GGACACCTTGAAATGCGG	“
10A-13	GGTCTGGCATCTTCTGTGTG	“
10A-14	GATTCGGAAAGCAGGGTATGC	“
10A-15	TCGTGCCAAGTAGCCTAAG	“
10A-16	AGGCGGGAAGAGGAGATTG	“
10A-17	GATTTCCTTCTCCAGGCG	“
10A-18	CTGGAAAAGCAAAGGGAGAACAAG	“
10A-19	TTGAAGGCGTCGTCATCCG	“
10A-20	TTCAAGGACTCGCCCAACCC	“
10A-21	GGAGTTGGAGAAAGTCACG	“
10A-22	TATGGAAGCCAGTGGTCCC	“
10A-23	GGAACCACAGGAAGGTCTC	“
10A-24	GCAGGAAGCCCTCAAGCAAG	“
10A-25	ACAGAATCAATCAGCCCG	“
10A-26	GCTGATTGATTCTGTATGCG	“
10A-27	CCCAGTTTCAGAGCGTTC	“
10A-28	AAGAGACAGGCTACTGGAATG	“
10A-29	TCCTTCGCTACACGCATC	“
10A-30	GATGCCCTGGATGATAGG	“
10A-31	TCCACCTGAAAAGGATACG	“
10A-32	TTCATCTCGGGAAGGCAC	“
10A-33	CAACGGACAGGTGGACAAGG	“
10A-34	CATAAACGCAAACTCCACGCTG	“
10A-35	ATACCCCGCACACCTCCATC	“
10A-36	CACTTGTCAATGATGCTGGTGC	“
10A-37	GGCTCGCACCAGCATCATTG	“
10A-38	CACATCCACCACCTCACTC	“

Results

Cloning and Characterization of inner ear Myo15a cDNA transcripts

Based upon the known occurrence of alternative splicing in other myosin transcripts, I characterized the alternatively spliced mRNA transcripts of *Myo15a* in the inner ear. Using mouse postnatal day 5 (P5) vestibular mRNA as template, 122 *Myo15a* cDNA transcripts containing the 5'untranslated region (5' UTR), translational open reading frame and 3' UTR were PCR amplified, cloned and the entire cDNA insert was sequenced. The exon and intron composition and the longest translational open reading frame were determined for each cloned *Myo15a* transcript. These 122 *Myo15a* transcripts are predicted to encode 30 protein isoforms ranging in size from 92 kD to 395 kD. Two major subclasses of *Myo15a* cDNA transcripts, termed class 1 and 2, were identified and appear to utilize different transcription start sites (figure 2-1C).

Liang and colleagues (1999) reported that two *Myo15a* cDNA transcripts (8.0 kb and 11.8 kb) were transcribed from a single promoter and merely differed by the inclusion or exclusion of exon 2 (figure 2-1A). Therefore it was expected that PCR amplification of full-length *Myo15a* cDNA products using a forward and reverse PCR primers located in exons 1 and 66 respectively would yield both *Myo15a* cDNA transcripts. Predicted PCR products of 7.0 kb and 10.8 kb were expected, however only three bands at 6.9 kb, 7.5 kb and 8.5 kb were observed (figure 2-1D). Subsequent cloning and sequence analysis confirmed that the 6.9 kb, 7.5 kb and 8.5 kb PCR products correspond only to class 2 *Myo15a* cDNA transcripts that lack exon 2. No PCR product of 10.8 kb corresponding to a *Myo15a* transcript

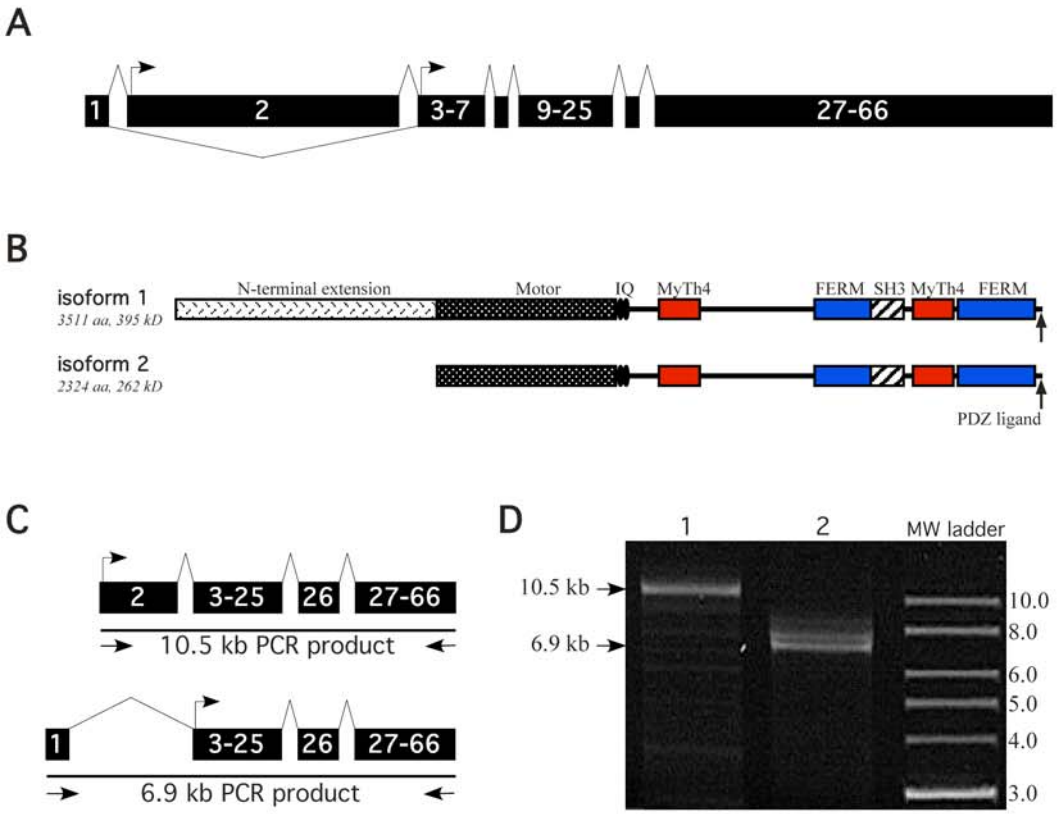

Figure 2-1. Mouse inner ear *Myo15a* mRNA isoforms. **(A)** Schematic representation of the exon composition of two predicted alternatively spliced *Myo15a* mRNA transcripts described in Liang et al. 1999 paper. *Myo15a* isoform 1 mRNA is comprised of exons 1 through 66 with a predicted translation start codon in exon 2 (right-pointing arrow). *Myo15a* isoform 2 mRNA, comprised of exon 1 and exons 3 through 66, has a predicted translation start codon in exon 3 (right-pointing arrow). **(B)** Representation of the two predicted myosin XVa protein isoforms encoded by *Myo15a* mRNA transcripts described in Liang et al. 1999 paper. The two myosin XVa protein isoforms were identical in sequence except isoform 2 lacks the 1,187 amino acid N-terminal extension preceding the motor. **(C)** Schematic representation of the exon composition of class 1 and 2 *Myo15a* cDNA transcripts, which are transcribed from different promoters. The predicted translation start codon in the two *Myo15a* cDNA transcripts is indicated (right-pointing arrow). **(D)** PCR amplification of full-length *Myo15a* cDNAs from mouse P5 vestibular cDNA. Class 1 *Myo15a* cDNA transcripts were PCR amplified with PCR primers located in exon 2 and 66 and yielded a single 10.5 kilobase (kb) cDNA product (lane 1). Class 2 *Myo15a* cDNA transcripts were PCR amplified with PCR primers located in exon 1 and 66 and yielded three cDNA products of 7.0 kb, 7.5 kb and 8.5 kb (lane 2).

containing exon 2 was observed, despite four PCR amplification experiments using different and sufficiently long PCR thermocycling extension times.

The failure to PCR amplify a *Myo15a* cDNA transcript containing exon 2 using PCR primers located in exons 1 and 66, suggested that perhaps a different first exon was utilized for class 1 *Myo15a* cDNA transcripts. Using forward and reverse PCR primers located in exons 2 and 66, respectively, PCR amplification yielded a single band of 10.5 kb. The predicted PCR product size was 10.5 kb (figure 2-1D). The complete mRNA transcript structure of class 1 *Myo15a* cDNA transcripts is unknown since the sequence of the 5' end of class 1 *Myo15a* cDNA transcripts is unknown. The translation start codon encoding class 1 myosin XVa protein isoforms is located 202 nucleotides down stream of the beginning of exon 2 suggesting that the 5' untranslated region is minimally 201 nucleotides in length. It is unclear whether any additional exons are located upstream of exon 2 in class 1 *Myo15a* cDNA transcripts. At the present time, no full-length cDNA or 5'-expressed sequence tag corresponding to the 5' end of exon 2 are available in a public database. The Cap-Analysis Gene Expression (CAGE) database (http://fantom.gsc.riken.go.jp/), which is a systematic attempt to profile the transcription start points using 21 nucleotide sequences derived from 5' ends of cDNA transcripts (Shiraki et al. 2003; Gustincich et al. 2006), has a single 5' CAGE tag located in intron 1, approximately 4,900 base pairs upstream of exon 2. I will attempt to PCR amplify a myosin XVa cDNA product from mouse vestibular cDNA using the 5' CAGE tag as a forward PCR primer and a reverse PCR primer located in exon 2. If I successfully PCR amplify a product, I will clone and

sequence the insert to determine the composition of exons within the product. Additionally, I will perform 5'-rapid amplification of cDNA ends (5'-RACE) to obtain the sequence of the 5' untranslated region upstream of the start codon. At this time, I speculate that class 1 *Myo15a* cDNA transcripts containing exon 2 are transcribed from an alternate promoter. Thus, *Myo15a* cDNA transcripts transcribed from exon 2 were designated as class 1 *Myo15a* cDNA transcripts, while *Myo15a* cDNA transcripts transcribed from exon 1 were designated as class 2 *Myo15a* cDNA transcripts.

Class 1 Myo15a transcripts encode thirteen predicted protein isoforms

Twenty-eight full-length class 1 *Myo15a* transcripts were cloned from mouse P5 vestibular cDNA that ranged in size from 9.1 kb to 12.2 kb with a mean insert size of 10.6 kb. For each *Myo15a* cDNA clone, the exon/intron composition and the longest open reading frame was determined. Twenty-five out of twenty-eight analyzed transcripts were predicted to translate a protein product, which clustered into thirteen protein isoforms ranging in deduced molecular weight from 203 kD to 395 kD (figure 2-2).

The most abundant class 1 *Myo15a* transcript encoded protein isoform 1a, which occurred in nine out of twenty-eight analyzed clones. The remaining predicted protein isoforms were ranked in descending order of molecular weight and were named isoforms 1b through isoform 1m (figure 2-2). Three out of twenty-eight cloned class 1 *Myo15a* cDNA transcripts were not predicted to encode a functional myosin motor

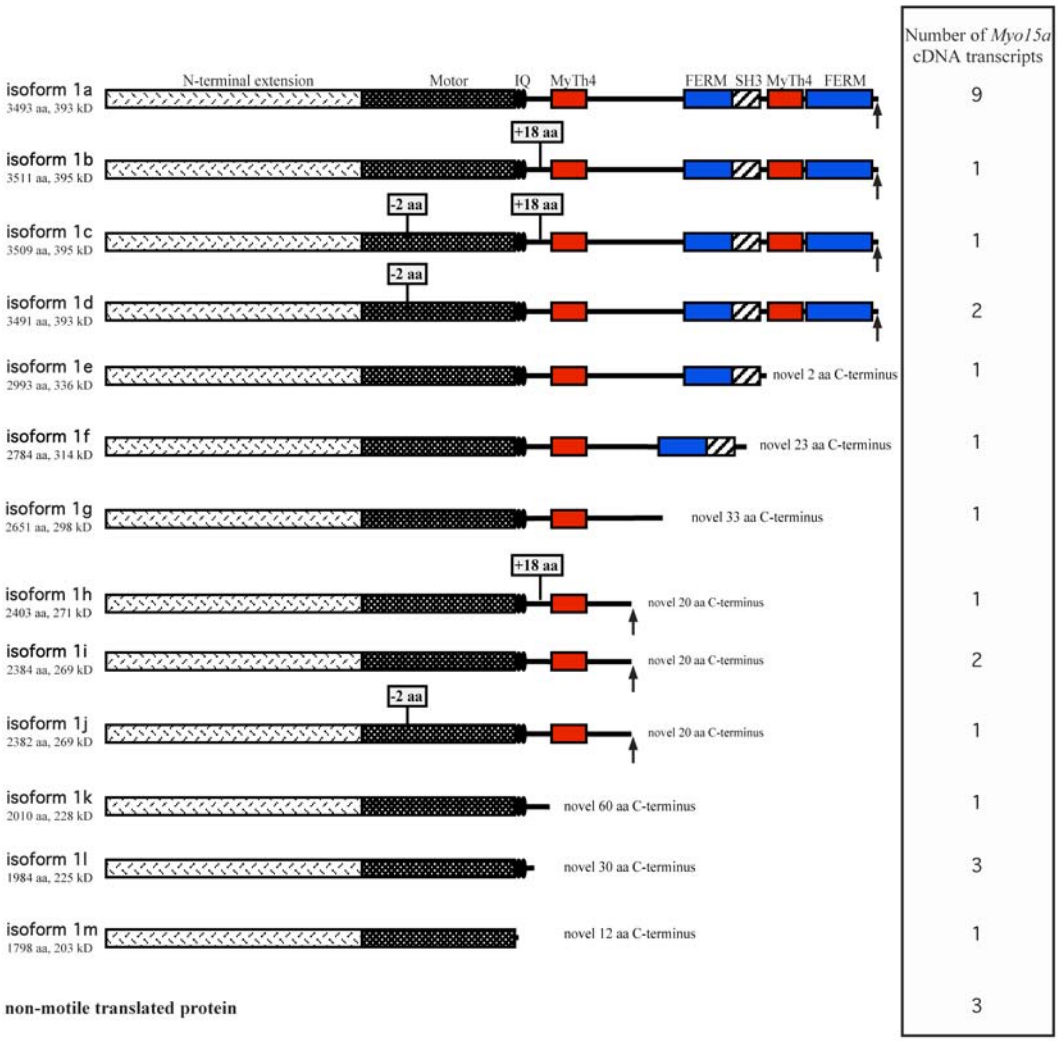

Figure 2-2. Myosin XVa protein isoforms predicted from 28 full-length class 1 *Myo15a* cDNA transcripts cloned from mouse P5 vestibular cDNA. Twenty-five out of twenty-eight *Myo15a* cDNA transcripts were predicted to encode a protein, which clustered into thirteen isoforms. Isoform 1a was the most abundant predicted protein product that occurred in nine out of twenty-eight *Myo15a* cDNA transcripts. Exclusion of exon 8 (denoted in grey box with "-2 aa") and inclusion of exon 26 (denoted in grey box with "+18 aa") in cDNA transcripts generated further proteomic diversity in predicted myosin XVa protein isoforms. The inclusion of intronic sequences in *Myo15a* cDNA transcripts altered the translational reading frame causing the premature truncation and generation of novel sequence at the C-terminus (isoforms 1e to 1m). Three class 1 *Myo15a* cDNA transcripts (denoted by "non-motile translated protein") were predicted to encode a non-functional myosin motor due to either the loss of multiple exons encoding the motor or retention of intronic sequence that disrupted the translational reading frame.

due either to the absence of multiple exons encoding the motor or the retention of intronic sequence that disrupted the translational reading frame within the motor. The pattern of disablements that disrupted the translational reading frame was different in each of the three clones.

Several of the *Myo15a* cDNA transcripts had identical exon/intron composition except for the inclusion or exclusion of alternatively spliced exons 8 and 26. Inclusion or exclusion in *Myo15a* cDNA transcripts of exon 8 (six base pairs) and exon 26 (fifty-four base pairs), which encode two and eighteen amino acids respectively, does not alter the translational open reading frame. Exon 8 encodes a two amino acid insert in the motor corresponding to surface loop 1. Inserts in surface loop 1 of other myosins are variable in sequence and length (Spudich 1994; Murphy 2000). Alternative splicing of Myosin IIb (Myh10), Myosin IIc (Myh14) and smooth muscle myosin heavy chain 11 (Myh11) mRNA yields transcripts in which an alternate exon that encodes either ten, eight or seven amino acids, respectively, are inserted into the surface loop 1 near the ATP-binding region. Baculovirus-expressed heavy meromyosins (HMM) of Myh10, Myh14 and Myh11 containing the larger surface loop 1 showed increased actin-activated MgATPase activity and *in vitro* motility in translocating actin filaments, compared to HMMs lacking the shorter surface loop 1 (Babu 2001; Clark 2005; Kim 2005; Ma 2006). In mice, the targeted knockout of the alternate exon encoding the insert in surface loop 1 in Myh10 and Myh11 resulted in a pathophysiological condition. The loss of an alternative exon encoding a seven amino acid insert in loop 1 of Myh11 resulted in decreased smooth muscle

contractility (Babu 2001) while the corresponding loss in Myh10 resulted in abnormal neuronal migration associated with hydrocephalus (Ma 2006).

At this time, I have no experimental data comparing the properties of myosin XVa motors containing and lacking the two amino acid insert in surface loop 1 encoded by exon 8. To address this question, I generated two baculovirus expression vectors encoding a myosin XVa HMM with the two amino acid loop 1 insert (encoded by exon 8) and without the two amino acid loop 1 insert (exon 8 spliced out of the cDNA transcript). In collaboration with Dr. James Sellers (Laboratory of Molecular Physiology, NHLBI/NIH), we will compare the kinetics of myosin XVa motors containing and lacking the two amino acid insert in surface loop 1. Overall, exon 8 is contained within 20 out of 25 class 1 *Myo15a* cDNA transcripts (80%) predicted to encode a protein.

Exon 26 encodes an eighteen amino acid insert of unknown function located between the IQ motifs and the first MyTh4 domain. No additional predicted protein motifs are apparent from its insertion. In *Myo15a* cDNA transcripts lacking exon 26, the exclusion of the eighteen amino acids does not result in a predicted protein motif within the region. The inclusion or exclusion of these eighteen amino acids might serve a structural role by increasing the distance between the motor and the tail.

Thirteen *Myo15a* cDNA transcripts were predicted to encode protein isoforms 1a, 1b, 1c and 1d, making this the most abundant isoform cluster. The exon composition of

Myo15a cDNA transcripts encoding protein isoforms 1a, 1b, 1c and 1d were identical except for the inclusion or exclusion of alternatively spliced exons 8 and 26 (figure 2-3). Ten out of thirteen *Myo15a* cDNA transcripts encoding protein isoforms 1a, 1b, 1c and 1d included the two amino acid surface loop in the motor (encoded by exon 8). It would be useful to know whether the presence or absence of the two amino acids affects the function of the myosin XVa motor. The eighteen amino acid insert (encoded by exon 26) located between the IQ motifs and the first MyTh4 domain occurred in two out of thirteen *Myo15a* cDNA transcripts encoding protein isoforms 1a, 1b, 1c and 1d.

Four *Myo15a* transcripts were predicted to encode protein isoforms 1h, 1i and 1j which differ by the inclusion or exclusion of a two amino acid insert in the motor encoded by exon 8 and an eighteen amino acid insert encoded by exon 26 (figure 2-4). Within these *Myo15a* cDNA transcripts, the retention of the entire intron 35 (429 base pairs) encodes twenty amino acids of novel sequence followed by an in-frame stop codon. The retention of intron 35 in these *Myo15a* cDNA transcripts encoding the novel twenty amino acid C-terminus is identical to the *Myo15a* cDNA transcripts encoding isoforms 2i and 2j. The last four amino acids of the C-terminus of myosin XVa isoforms 11h, 1i and 1j form a class II consensus PDZ binding ligand which is different from the class I consensus PDZ ligand found at the C-termini of isoforms 1a through 1d. None of the other predicted myosin XVa protein isoforms contains a predicted consensus PDZ ligand at their C-termini. The class II PDZ ligand in myosin XVa protein isoforms 1h, 1i and 1j would facilitate binding to a different PDZ

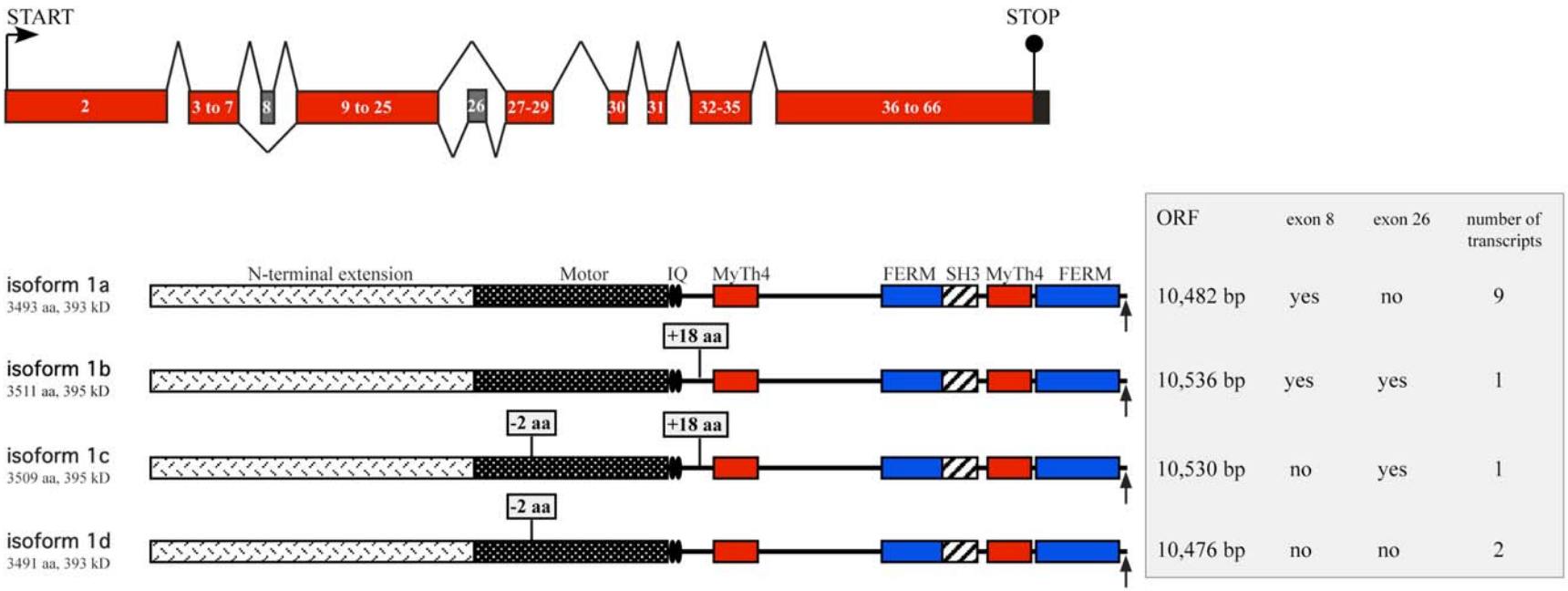

Figure 2-3. The exon structure of *Myo15a* cDNA transcripts encoding protein isoforms 1a, 1b, 1c and 1d.
Exclusion of exon 8 (denoted in grey box with "-2 aa") and inclusion of exon 26 (denoted in grey box with "+18 aa") in cDNA transcripts generated further proteomic diversity in predicted myosin XVa protein isoforms. The last four amino acids of the C-terminus form a class I PDZ ligand (denoted by upward facing arrow). The predicted translation start codon in the *Myo15a* cDNA transcripts is indicated (right-pointing arrow). Red colored rectangles represent exons encoding the open reading frame, grey colored rectangles represent alternatively spliced exons and black rectanges represent the untranslated region.
Abbreviation ORF = translational open reading frame.

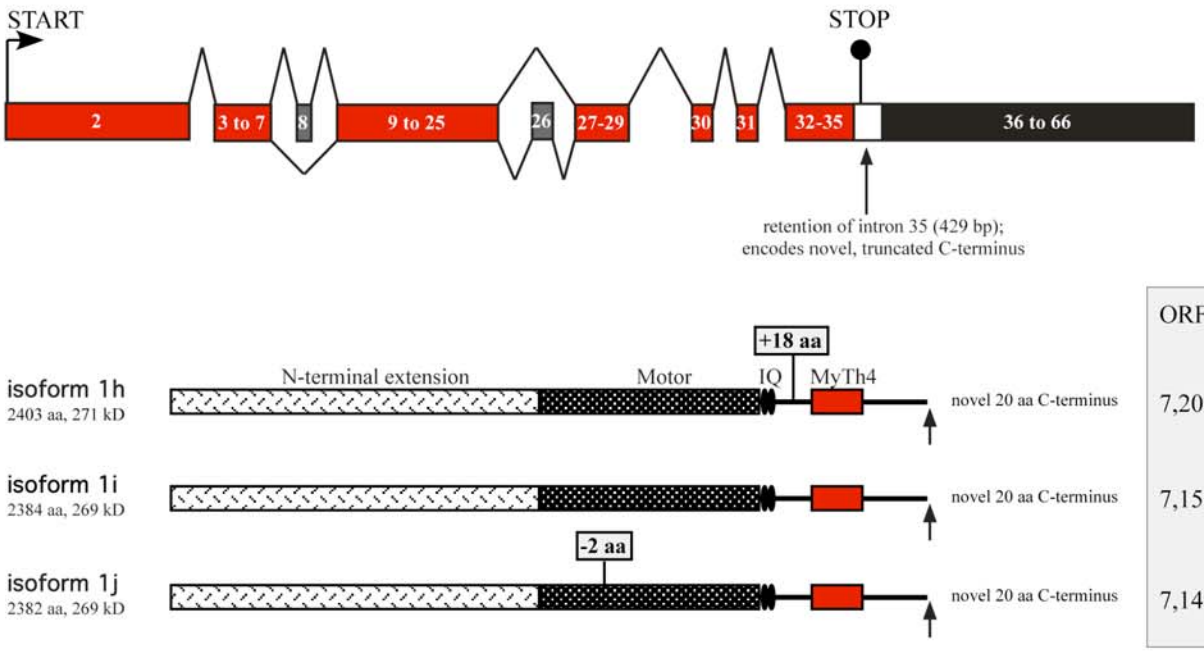

ORF	exon 8	exon 26	number of transcripts
7,209 bp	yes	yes	1
7,155 bp	yes	no	2
7,149 bp	no	no	1

Figure 2-4. The exon structure of *Myo15a* cDNA transcripts encoding protein isoforms 1h, 1i and 1j.
The retention of intron 35 in the cDNA transcript permits the translation of twenty amino acids of novel sequence at the C-terminus before encountering an in-frame stop codon. The last four amino acids of the C-terminus form a class II PDZ ligand (denoted by upward facing arrow). Exclusion of exon 8 (denoted in grey box with "-2 aa") and inclusion of exon 26 (denoted in grey box with "+18 aa") in cDNA transcripts generated further proteomic diversity in predicted myosin XVa protein isoforms. The predicted translation start codon in the two *Myo15a* cDNA transcripts is indicated (right-pointing arrow). Red colored rectangles represent exons encoding the open reading frame, grey colored rectangles represent alternatively spliced exons, white rectangles represent intronic sequence and black rectanges represent the untranslated region. Abbreviation ORF = translational open reading frame.

containing protein partner than bound by the class I PDZ ligand of isoforms 1a through 1d.

Three *Myo15a* cDNA transcripts were predicted to encode 1,984 amino acid protein isoform 1l (figure 2-5). Within these *Myo15a* cDNA transcripts, the retention of partial intron 25 (the last 89 base pairs preceding exon 26) causes a translational frame shift that encodes 30 amino acids of novel C-terminus sequence before encountering an in-frame stop codon. Since all of intron 25 (520 base pairs) was not retained in these transcripts, it is not clear whether a cryptic splice site accounts for the retention of partial intron 25 or whether it is a physiologically relevant mRNA isoform. Isoform 1l contains a truncated tail missing the $MyTh4_1$, $FERM_1$, SH3, $MyTh4_2$, $FERM_2$ domains and C-terminal PDZ ligand. Isoform 1l is likely to demonstrate a different hair cell localization pattern as compared to isoforms 1a, 1b, 1c and 1d.

Myo15a cDNA transcripts predicted to encode protein isoforms 1e, 1f, 1g, 1k and 1m (figure 2-2) occurred once each out of 28 analyzed cDNA transcripts. It is difficult to determine if they represent fully spliced *Myo15a* cDNA transcripts or mRNA splicing

intermediates. A Northern blot of inner ear poly A+ RNA would not resolve the matter since it would not distinguish between mature and immature mRNA splicing intermediates. Given the large size of the class 1 *Myo15a* mRNA messages (approximately 12 kb), it would be difficult to visualize differences of several

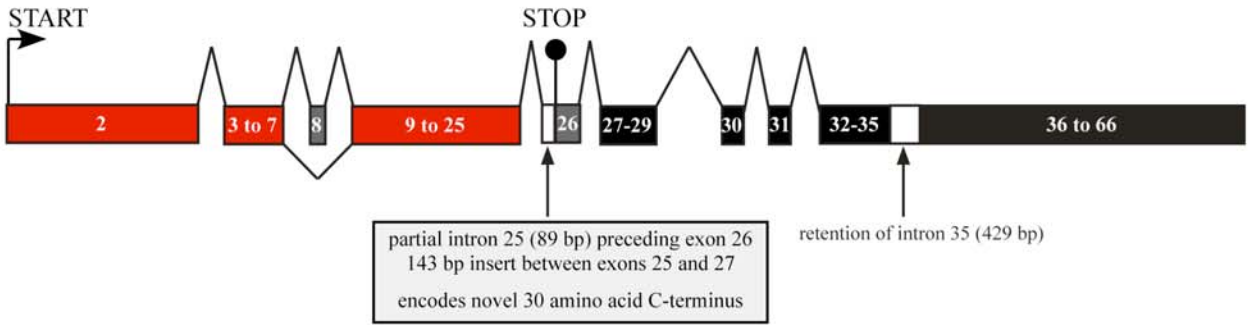

ORF	exon 8	exon 26	number of transcripts
5,955 bp	yes	yes	3

Figure 2-5. The exon structure of *Myo15a* cDNA transcripts encoding protein isoform 1l.
The retention of partial intron 25 (the last 89 base pairs preceding exon 26) in the cDNA transcript causes a translational frame shift that encodes thirty amino acids of novel C-terminus sequence before encountering an in-frame stop codon. The retention of intron 35 in the cDNA transcript increases the length of the 3' untranslated region. The predicted translation start codon in the *Myo15a* cDNA transcript is indicated (right-pointing arrow). Red colored rectangles represent exons encoding the open reading frame, grey colored rectangles represent alternatively spliced exons, white rectangles represent intronic sequence and black rectanges represent the untranslated region. Abbreviation ORF = translational open reading frame.

hundred base pairs on a denaturing gel. Visualizing protein product bands on a Western blot of inner ear protein extract using a monoclonal antibody raised against the myosin XVa motor would unequivocally resolve whether the various *Myo15a* mRNA transcripts encode myosin XVa protein isoforms.

N-terminal extension of Myosin XVa

The 1,187 amino acid N-terminal extension found in myosin XVa protein isoforms 1a through 1m has several unusual features. The function of the N-terminal extension is unknown and presently it bears no obvious similarity to any other protein in the mouse proteome. A comparison of the amino acid sequences of the N-terminal extension from several species reveals significant sequence conservation between the various myosin XVa homologs (table 2-5). While the function of the N-terminal extension of myosin XVa remains unknown, the sequence conservation among the various species suggests a conserved cellular function. A large number of proline-tyrosine repeats are arranged in a regular periodicity in the distal two thirds of the N-terminal extension suggesting an alpha helical structural conformation similar to collagen. Curiously, the number and locations of proline-tyrosine repeats are conserved between human and mouse orthologs.

Table 2-5. Percentage amino acid identity and similarity of several myosin XVa orthologs to the N-terminal extension of mouse myosin XVa.

Species	% amino acid identity	% amino acid similarity
Rat	90	92
Cow	65	72
Rheus monkey	73	79
Human	71	78

A predicted partial formin homology 2 (FH2) domain was found although it only contained approximately 111 amino acids of the consensus 450 amino acid FH2 domain. Formin proteins, which contain tandemly arrayed FH1 and FH2 domains, control actin assembly and are involved in a wide variety of actin based processes in eukaryotes including cell polarization, cytokinesis, hair cell stereocilia formation, sperm cell acrosome formation and embryonic developmental (Evangelista et al. 2003). Results suggest that a FH1 domain facilitates membrane localization by binding to a SH3 domain of a protein partner while FH2 domain appears to mediate actin nucleation and assembly by binding effector proteins (Alberts 2001). Conflicting data makes it unclear whether subdomains within the FH2 domain are responsible for distinct actin functions (Evangelista et al. 2003). It is presently not known if the 110 amino acid partial FH2 motif found in the N-terminal extension of myosin XVa has any actin nucleation function.

The presence of a protein region greater than 100 amino acids preceding a myosin motor is unusual, as N-terminal extensions are found only in eight out of the forty mouse myosin genes, namely *Myo3a*, *Myo3b*, *Myo9a*, *Myo9b*, *Myo15a*, *Myo16*, *Myo18a* and *Myo18b* (NCBI Unigene database). Myosins IIIa and IIIB proteins have a 300 amino acid Serine/Threonine kinase domain preceding the motor. Myosins IXa and IXb proteins contain a 110 amino acid Ras-GTP binding domain preceding the motor. Myosin XVIIIa protein contains a PDZ domain within the 300 amino acid domain preceding the motor. Myosin XVIIIb protein also has a 300 amino acid N-terminal extension, which does not contain a predicted protein domain. Thus, the presence of an N-terminal extension that does not contain a predicted protein motif is rare as it is found only in 2 out of 40 myosins found in the mouse or human proteome, namely myosins XVa and XVIIIb.

It appears that the N-terminal extension of myosin XVa is not necessary for trafficking to stereocilia tips as evidenced by the demonstration that GFP-myosin XVa isoform 2a, which is identical to isoform 1a except that it lacks the 1,187 amino acid N-terminal extension, localizes to stereocilia tips of transfected inner ear hair cells (Figure 3-7A; Belyantseva et al. 2003a; Belyantseva et al. 2005). The majority of attempts to transfect inner ear hair cells with a GFP-myosin XVa expression construct encoding isoform 1a were unsuccessful, although in a single transfected hair cell GFP-myosin XVa isoform 1a was observed at tips of stereocilia (Belyantseva, personal communication). The lack of more transfected hair cells makes interpretation of these result problematic.

Class 2 Myo15a transcripts encode seventeen predicted protein isoforms

Ninety-four full-length class 2 *Myo15a* transcripts were cloned from mouse P5 vestibular cDNA in two experiments. The ninety-four *Myo15a* cDNA clones ranged in size from 6.0 kb to 8.6 kb with a mean insert size of 7.3 kb. For each *Myo15a* cDNA clone, the exon/intron composition and the longest open reading frame was determined. Eighty-five out of ninety-four analyzed transcripts were predicted to translate a protein product, which clustered into seventeen putative protein isoforms ranging in predicted molecular weight from 92 kD to 262 kD (figure 2-6).

The most abundant class 2 *Myo15a* transcript encoded protein isoform 2a, which occurred in 22 out of 94 analyzed clones. The remaining predicted protein isoforms were ranked in descending order of molecular weight and were named isoforms 2b through isoform 2q (figure 2-6). Some of the *Myo15a* cDNA transcripts occurred only once out of 94 analyzed cDNA transcripts. Seven out of ninety-four cloned *Myo15a* cDNA transcripts were not predicted to encode a protein due either to the inclusion of intronic sequences or exclusion of multiple exons predicted to encode the motor. The failure to remove the intronic sequence resulted in a disruption of the translational open reading frame and the presence of multiple in-frame stop codons. None of the seven clones would encode a functional myosin XVa motor due to the disablements described.

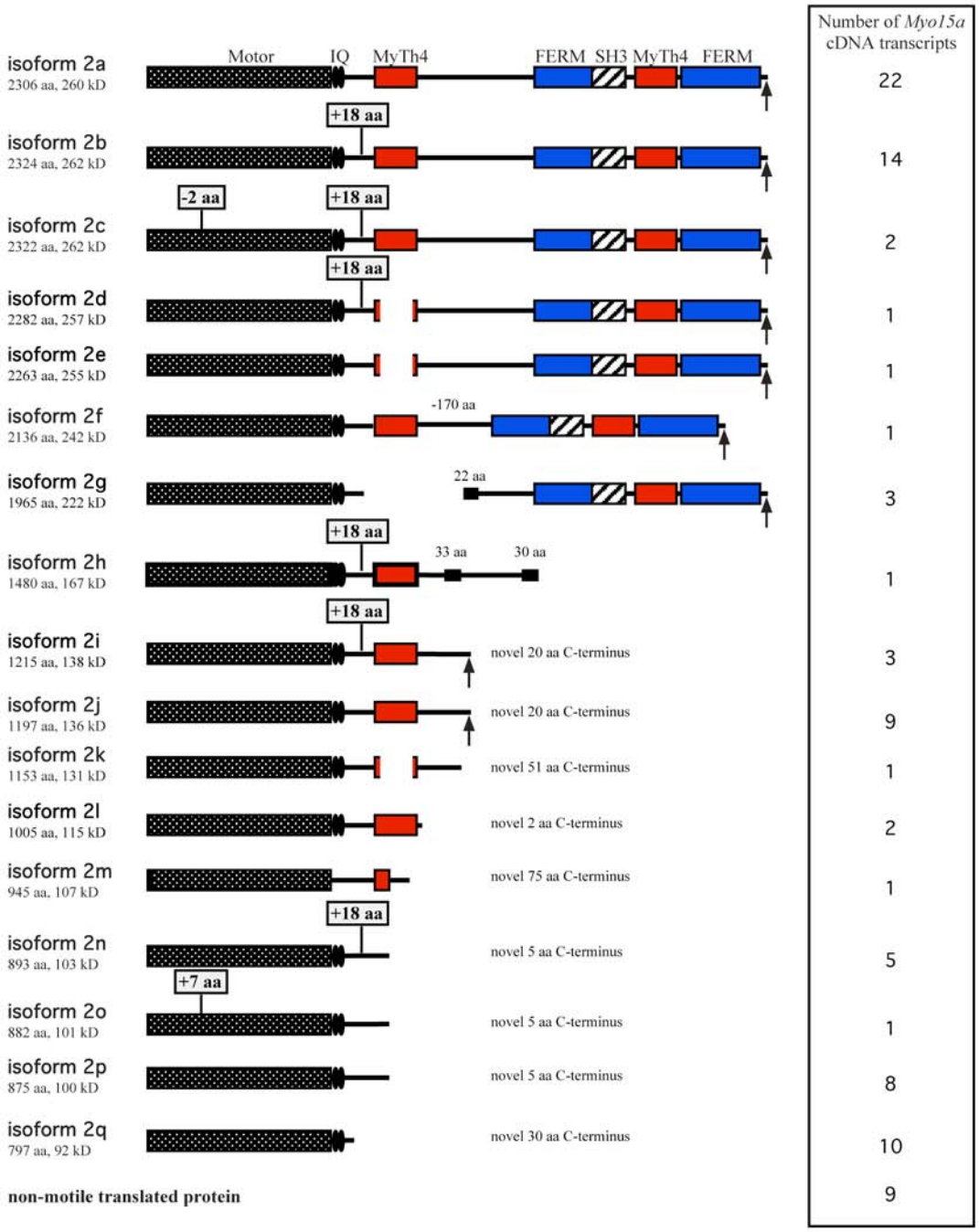

Figure 2-6. Myosin XVa protein isoforms predicted from ninety-four full-length class 2 *Myo15a* cDNA transcripts cloned from mouse P5 vestibular cDNA. Eighty-five out of ninety-four *Myo15a* cDNA transcripts were predicted to encode a protein, which clustered into seventeen isoforms.

Several of the *Myo15a* cDNA transcripts had identical exon/intron composition except for the inclusion or exclusion of alternatively spliced exons 8 and 26. The implications of the inclusion or exclusion of exons 8 and 26 were previously discussed in the section entitled “Class 1 *Myo15a* transcripts encode thirteen predicted protein isoforms”. Overall, exon 8 is contained within eighty-three out of eighty-five class 2 *Myo15a* cDNA transcripts (98%) predicted to encode a protein. This suggests that *Myo15a* cDNA transcripts lacking exon 8 are exceedingly rare. Exon 26 is contained within thirty-five out of eighty-five class 2 *Myo15a* cDNA transcripts (41%) predicted to encode a protein. The occurrence of exon 26 within *Myo15a* cDNA transcripts suggests that alternative splicing of this exon is common.

Thirty-eight *Myo15a* cDNA transcripts were predicted to encode protein isoforms 2a, 2b and 2c, making it the most abundant isoform cluster. The exon composition of *Myo15a* cDNA transcripts encoding protein isoforms 2a, 2b and 2c were identical except for the inclusion or exclusion of alternatively spliced exons 8 and 26 (figure 2-7). Thirty-six out of thirty-eight *Myo15a* cDNA transcripts encoding protein isoforms 2a, 2b and 2c included the two amino acid surface loop in the motor (encoded by exon 8). Previously we demonstrated that in transfected inner ear hair cells, GFP-myosin XVa isoform 2a localizes to stereocilia tips (Belyantseva et al. 2003a; Belyantseva et al. 2005). It is unclear whether myosin XVa isoform 2c that lacks two amino acids (encoded by exon 8) in loop 1 of the motor will demonstrate a different localization pattern within inner ear hair cells.

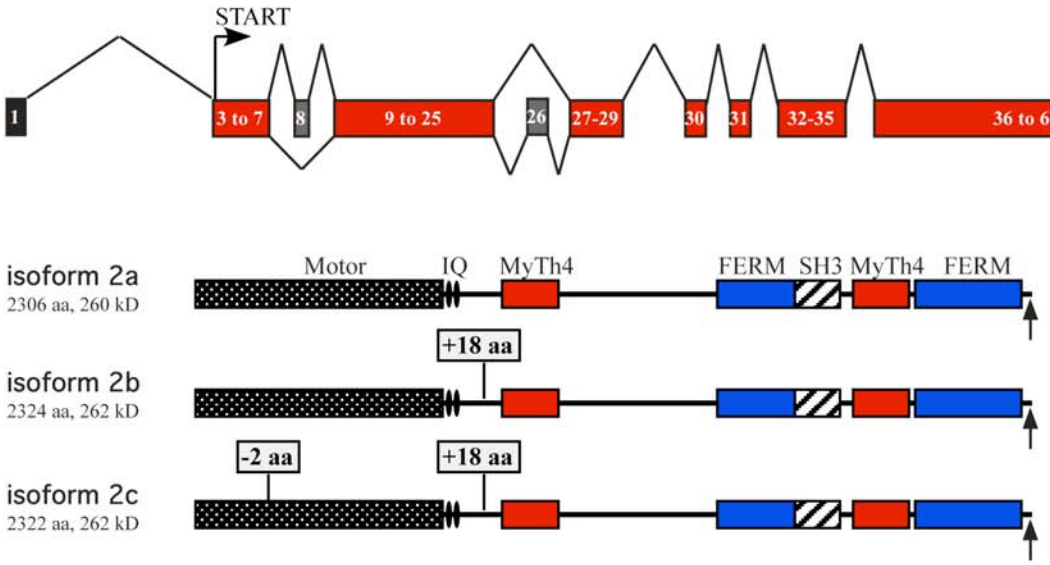

ORF	exon 8	exon 26	number of transcripts
6,921 bp	yes	no	22
6,975 bp	yes	yes	14
6,969 bp	no	yes	2

Figure 2-7. The exon structure of *Myo15a* cDNA transcripts encoding protein isoforms 2a, 2b and 2c.
Exclusion of exon 8 (denoted in grey box with "-2 aa") and inclusion of exon 26 (denoted in grey box with "+18 aa") in cDNA transcripts generated further proteomic diversity in predicted myosin XVa protein isoforms. The last four amino acids of the C-terminus form a class I PDZ ligand (denoted by upward facing arrow). The predicted translation start codon in the *Myo15a* cDNA transcripts is indicated (right-pointing arrow). Red colored rectangles represent exons encoding the open reading frame, grey colored rectangles represent alternatively spliced exons and black rectanges represent the untranslated region.
Abbreviation ORF = translational open reading frame.

To investigate this question, I have generated a GFP-myosin XVa isoform 2c expression vector and plan to transfect it into inner ear hair cells and COS7 cells to determine whether its localization is different than GFP-myosin XVa isoform 2a. If no discernable difference is observed, then I will conclude that any effect on stereocilia localization is subtle or negligible.

The eighteen amino acid insert (encoded by exon 26) located between the IQ motifs and the first MyTh4 domain occurred in sixteen out of thirty-eight *Myo15a* cDNA transcripts encoding protein isoforms 2a, 2b and 2c. Since the domain composition of the tail, $MyTh4_1$, $FERM_1$, SH3, $MyTh4_2$, $FERM_2$ domains and C-terminal PDZ ligand, is identical between myosin XVa protein isoforms 2a, 2b and 2c, the eighteen amino acid insert is unlikely to affect stereocilia tip localization. This conjecture is based upon the experimental observation that myosin XVa protein comprised of the motor plus either the $MyTh4_1$, $FERM_1$ or $MyTh4_2$, $FERM_2$ domains is sufficient for stereocilia tip localization (see Chapter 5). I speculate that the eighteen amino acid insert will affect binding of a protein partner at either the IQ motif or at the first MyTh4 domain. Protein partners binding IQ motifs of myosins are known to influence the enzymatic properties of myosin motors (Sellers 2000).

Two *Myo15a* cDNA transcripts are predicted to encode protein isoforms 2d and 2e which differ by the inclusion or exclusion of an eighteen amino acid insert encoded by exon 26 (figure 2-8). Within these two *Myo15a* cDNA transcripts, the splicing of partial exon 30 (missing 108 out of 236 base pairs) to partial exon 31 (missing 21 out

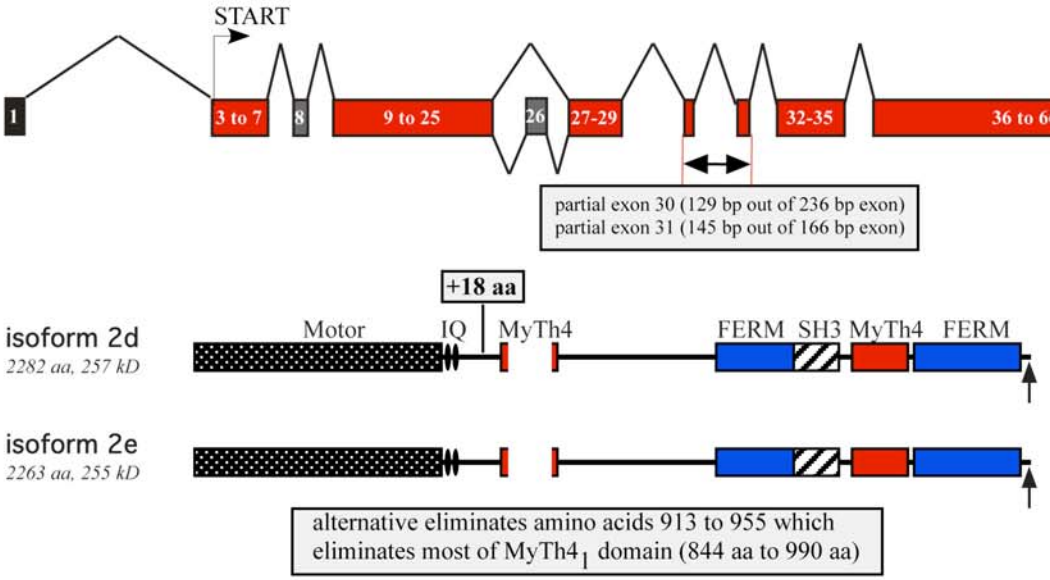

ORF	exon 8	exon 26	number of transcripts
6,849 bp	yes	yes	1
6,742 bp	yes	no	1

Figure 2-8. The exon structure of *Myo15a* cDNA transcripts encoding protein isoforms 2d and 2e.
The splicing of partial exon 30 to partial exon 31 eliminates cDNA sequence encoding 43 amino acids but does not alter the translational open reading frame. At the protein level, isoforms 2d and 2e would likely lack the structural fold of the first MyTh4 domain due to the loss of 43 amino acids located in the middle of this 147 amino acid domain. The inclusion of exon 26 (denoted in grey box with "+18 aa") in cDNA transcripts generated further proteomic diversity in predicted myosin XVa protein isoforms. The last four amino acids of the C-terminus form a class I PDZ ligand (denoted by upward facing arrow). The predicted translation start codon in the *Myo15a* cDNA transcripts is indicated (right-pointing arrow). Red colored rectangles represent exons encoding the open reading frame, grey colored rectangles represent alternatively spliced exons and black rectanges represent the untranslated region. Abbreviation ORF = translational open reading frame.

of 166 base pairs) eliminates cDNA sequence encoding forty-three amino acids but does not alter the translational open reading frame. At the protein level, isoforms 2d and 2e would likely lack the structural fold of the first MyTh4 domain due to the loss of forty-three amino acids located in the middle of this one hundred and forty-seven amino acid domain.

Three *Myo15a* cDNA transcripts were predicted to encode a 1,965 amino acid protein isoform 2g (figure 2-9). The splicing of a partial exon 28 (missing 71 out of 131 base pairs) to partial intron 35 (the last 65 base pairs preceding exon 36) eliminates cDNA sequence encoding 363 amino acids, introduces coding sequence in partial intron 35 that encodes twenty-two amino acids of novel sequence but does not alter the translational open reading frame. Isoform 2g protein would lack the first MyTh4 domain and approximately 40% of the spacer region between the first MyTh4 and first FERM domains.

Twelve *Myo15a* transcripts were predicted to encode protein isoforms 2i and 2j which differ by the inclusion or exclusion of an eighteen amino acid insert encoded by exon 26 (figure 2-10). Within these *Myo15a* cDNA transcripts, the retention of entire intron 35 (429 base pairs) encodes twenty amino acids of novel sequence before encountering the first of several in-frame stop codons. The retention of intron 35 in these *Myo15a* cDNA transcripts encoding the novel twenty amino acid C-terminus is identical to the Myo15a *cDNA* transcripts encoding isoforms 1h, 1i and 1j. The last four amino acids of the C-terminus of myosin XVa isoforms 2i and 2j form a

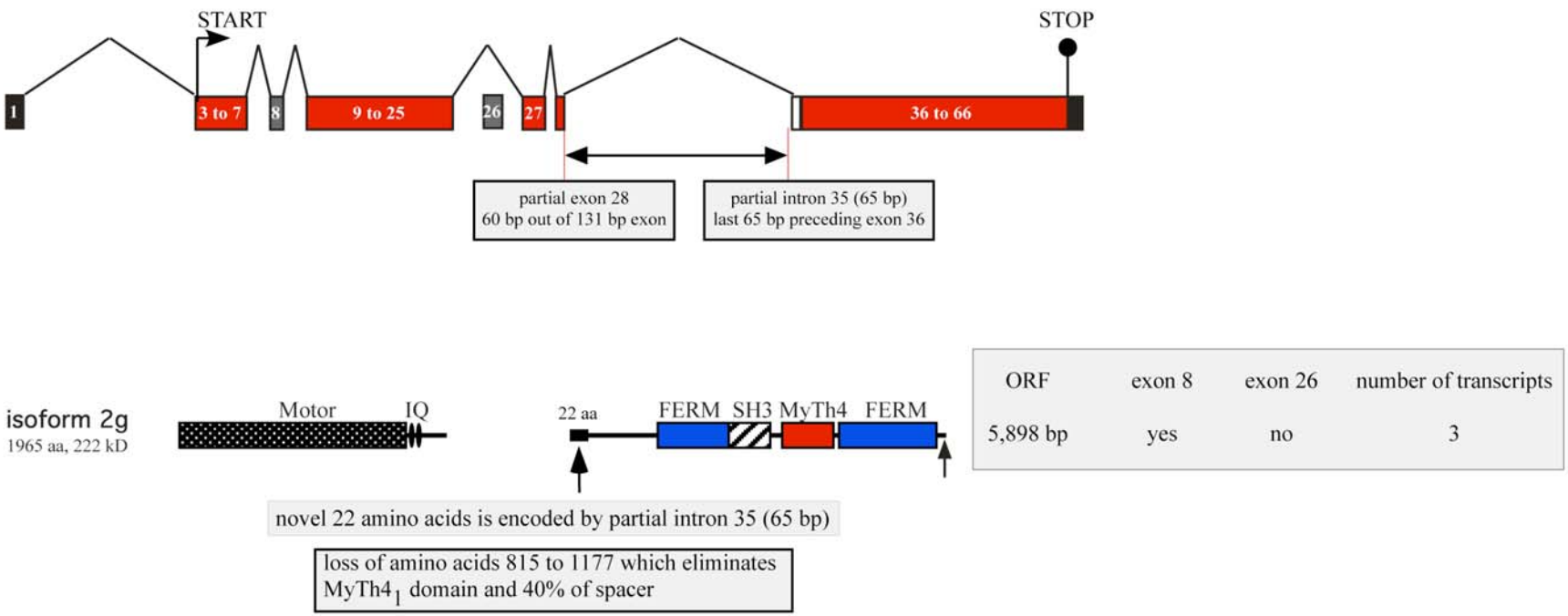

Figure 2-9. The exon structure of *Myo15a* cDNA transcripts encoding protein isoform 2g.
The splicing of a partial exon 28 to partial intron 35 eliminates cDNA sequence encoding 363 amino acids, introduces coding sequence in partial intron 35 that encodes 22 amino acids of novel sequence but does not alter the translational open reading frame. Isoform 2g protein would lack the first MyTh4 domain and approximately 40% of the spacer region between the first MyTh4 and first FERM domains. The predicted translation start codon in the *Myo15a* cDNA transcript is indicated (right-pointing arrow). Red colored rectangles represent exons encoding the open reading frame, grey colored rectangles represent alternatively spliced exons, white rectangles represent intronic sequence and black rectanges represent the untranslated region. Abbreviation ORF = translational open reading frame.

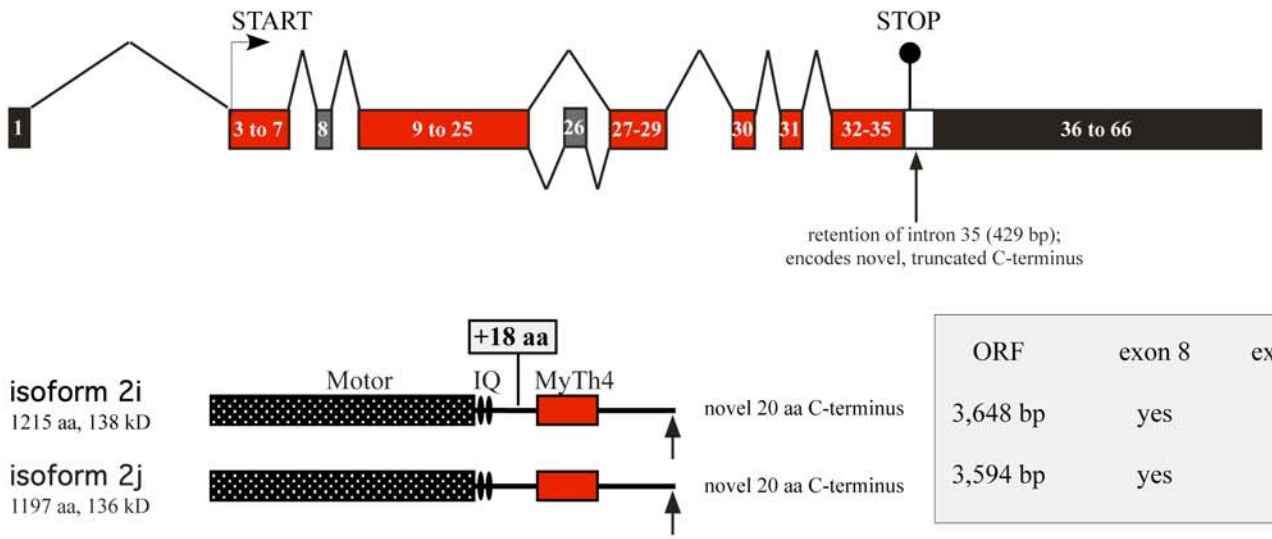

ORF	exon 8	exon 26	number of transcripts
3,648 bp	yes	yes	3
3,594 bp	yes	no	9

Figure 2-10. The exon structure of *Myo15a* cDNA transcripts encoding protein isoforms 2i and 2j.
The retention of intron 35 in the cDNA transcript permits the translation of 20 amino acids of novel sequence at the C-terminus before encountering an in-frame stop codon. The last four amino acids of the C-terminus form a class II PDZ ligand (denoted by upward facing arrow). The inclusion of exon 26 (denoted in grey box with "+18 aa") generated further proteomic diversity. The predicted translation start codon in the *Myo15a* cDNA transcripts is indicated (right-pointing arrow). Red colored rectangles represent exons encoding the open reading frame, grey colored rectangles represent alternatively spliced exons, white rectangles represent intronic sequence and black rectanges represent the untranslated region. Abbreviation ORF = translational open reading frame.

predicted class II consensus PDZ binding ligand. On the basis of binding specificity to PDZ ligands, PDZ domains can be classified into at least four groups (Harris et al. 2001; Sheng et al. 2001; Jelen et al. 2003; Kim et al. 2004). The interaction of a PDZ ligand with a PDZ domain is restricted to its sub-group, such that class II PDZ domains appear only interact with class II PDZ ligands.

Myosin XVa isoforms 2a, 2b, 2c, 2d, 2e, 2f and 2g have a C-terminal class I consensus PDZ ligand. In the case of myosin XVa isoform 2a, this class I PDZ ligand was demonstrated to bind the third PDZ domain of whirlin (Belyantseva et al. 2005). None of the other myosin XVa protein isoforms contains a consensus PDZ ligand at their C-termini. The class II PDZ ligand in myosin XVa protein isoforms 2i and 2j would facilitate binding to a different group of PDZ containing proteins. The identity of these PDZ domain containing proteins capable of binding to the class II PDZ ligand of myosin XVa as well as the functional relevance of the putative interaction remain to be investigated.

In addition to the class II PDZ ligand, the truncated tail of protein isoforms 2i and 2j lack the first FERM, SH3, second MyTh4 and second FERM domains. The loss of these domains may alter the localization in hair cells. Our localization experiments in hair cells as well as in a green monkey kidney COS7 cell line revealed that a functional myosin XVa motor is not sufficient for correct localization implying that domains within the tail contribute to the localization specificity (see Chapters 4 and 5). In transfected COS7 cells, GFP-myosin XVa isoform 2j localized in the cell body

and along the length of filopodia but did not accumulate at the filopodia tips like GFP-myosin XVa isoform 2a (figure 4-9B). Collectively taken, the truncated tail of protein isoforms 2i and 2j is likely to affect the cellular localization, promote binding of different protein partners and allow participation in a macromolecular complex distinct from protein isoforms 2a, 2b and 2c.

Two *Myo15a* cDNA transcripts were predicted to encode 1,005 amino acid protein isoform 2l (figure 2-11). Within these *Myo15a* cDNA transcripts, the retention of entire intron 31 (217 base pairs) encodes two amino acids of novel sequence before encountering an in-frame stop codon. Isoform 2l protein contains a shortened tail that truncates after the first MyTh4 domain.

Fourteen *Myo15a* cDNA transcripts are predicted to encode protein isoforms 2n, 2o and 2p which primarily differ by the inclusion or exclusion of an eighteen amino acid insert encoded by exon 26 (figure 2-12). The retention of entire intron 29 (875 base pairs) encodes five amino acids of novel sequence before encountering an in-frame stop codon. Protein isoforms 2n, 2o and 2p contain a truncated tail missing the $MyTh4_1$, $FERM_1$, SH3, $MyTh4_2$, $FERM_2$ domains and C-terminal PDZ ligand. The *Myo15a* cDNA transcript encoding isoform 2n, retained 21 base pairs of intronic sequence preceding exon 8. The 21 base pair intronic sequence would encode seven novel amino acids in loop 1 of the motor. This splice variant was observed once out of ninety-four *Myo15a* cDNA transcripts and may be a splicing intermediate.

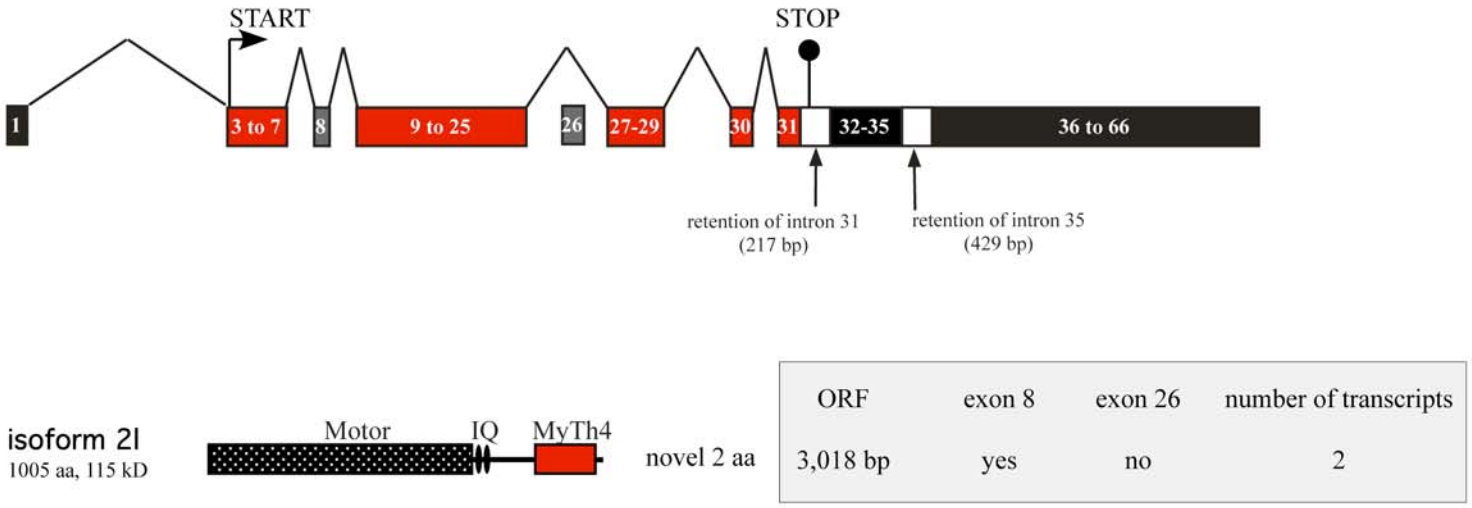

Figure 2-11. The exon structure of *Myo15a* cDNA transcripts encoding protein isoform 2l.
The retention of entire intron 31 (217 bp) encodes two amino acids of novel sequence before encountering an in-frame stop codon. The retention of intron 35 in the cDNA transcript increases the length of the 3' untranslated region. The predicted translation start codon in the *Myo15a* cDNA transcript is indicated (right-pointing arrow). Red colored rectangles represent exons encoding the open reading frame, grey colored rectangles represent alternatively spliced exons, white rectangles represent intronic sequence and black rectanges represent the untranslated region. Abbreviation ORF = translational open reading frame.

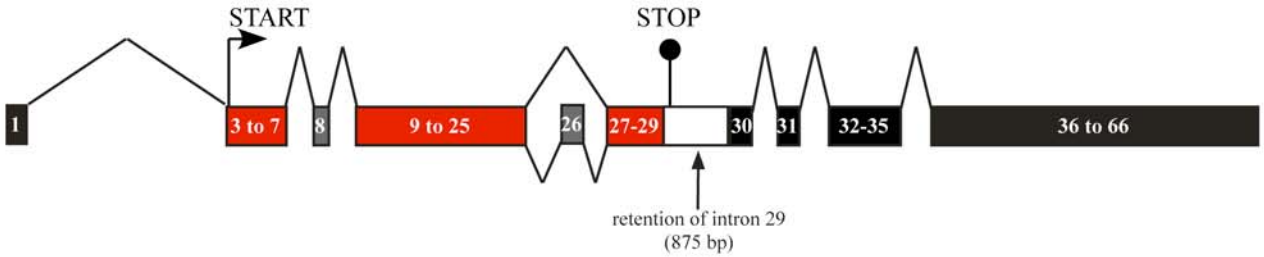

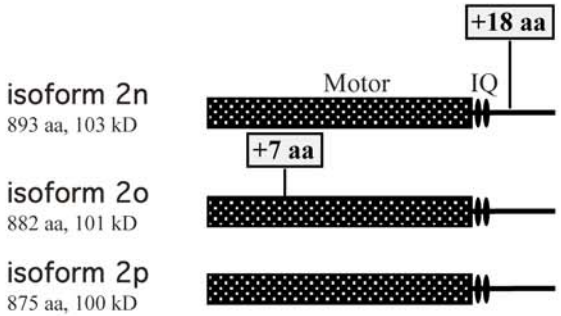

	ORF	exon 8	exon 26	number of transcripts
novel 5 aa C-terminus	2,682 bp	yes	yes	5
novel 5 aa C-terminus	2,649 bp	yes	no	1
novel 5 aa C-terminus	2,649 bp	yes	no	8

Figure 2-12. The exon structure of *Myo15a* cDNA transcripts encoding protein isoforms 2n, 2o and 2p.
The retention of entire intron 29 (875 base pairs) in these cDNA transcripts encodes five amino acids of novel sequence before encountering an in-frame stop codon. The inclusion of exon 26 (denoted in grey box with "+18 aa") generated further proteomic diversity. The predicted translation start codon in the *Myo15a* cDNA transcripts is indicated (right-pointing arrow). Red colored rectangles represent exons encoding the open reading frame, grey colored rectangles represent alternatively spliced exons, white rectangles represent intronic sequence and black rectanges represent the untranslated region. Abbreviation ORF = translational open reading frame.

Ten *Myo15a* cDNA transcripts were predicted to encode a 797 amino acid protein isoform 2q (figure 2-13). Within these *Myo15a* cDNA transcripts, the retention of partial intron 25 (the last 89 base pairs preceding exon 26) causes a translational frame shift that encodes thirty amino acids of novel C-terminus sequence before encountering an in-frame stop codon. Similar to protein isoforms 2n, 2o and 2p, isoform 2q contains a truncated tail missing the $MyTh4_1$, $FERM_1$, SH3, $MyTh4_2$, $FERM_2$ domains and C-terminal PDZ ligand. GFP myosin XVa isoform 2q accumulated in the cell body of transfected COS7 cells and did not accumulate at filopodia tips.

Characterization of inner ear Myo7a, Myo7b and Myo10 cDNA transcripts

I wanted to determine if the retention of partial and full intronic sequences in *Myo15a* cDNA transcripts was typical of other myosins. If partial and full intronic sequences were commonly found in other cloned myosin cDNA transcripts, one explanation is that immature mRNA splice intermediates were present in my mouse vestibular cDNA sample used to PCR amplify my full-length *Myo15a* cDNA transcripts. On the other hand, if we failed to observe retention of partial and full intronic sequences in other cloned myosin cDNA transcripts, this would suggest one or two possibilities. The first possibility is that the kinetics of exon/intron splicing in *Myo15a* transcripts is slow and less efficient as compared to other myosins. The second possibility is that the retention of partial and full intronic sequences in *Myo15a* cDNA transcripts may be physiologically relevant.

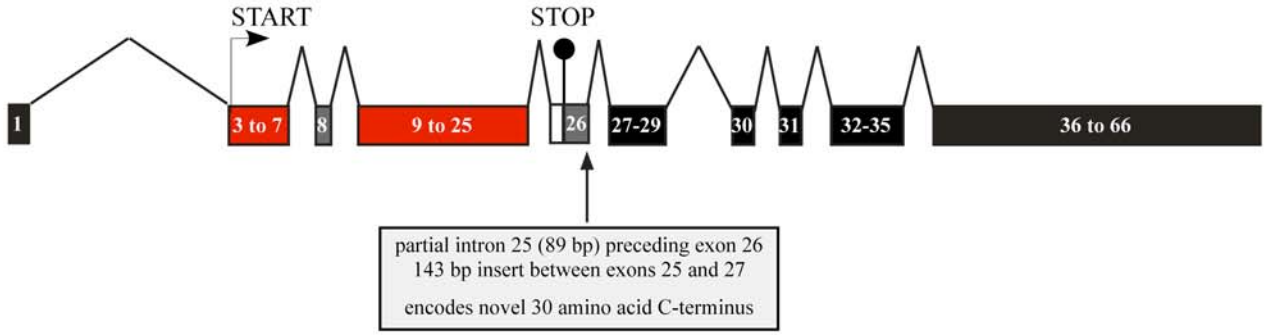

ORF	exon 8	exon 26	number of transcripts
2,394 bp	yes	yes	10

Figure 2-13. The exon structure of *Myo15a* cDNA transcripts encoding protein isoform 2q.
The retention of partial intron 25 (the last 89 base pairs preceding exon 26) in the cDNA transcript causes a translational frame shift that encodes thirty amino acids of novel C-terminus sequence before encountering an in-frame stop codon. The predicted translation start codon in the *Myo15a* cDNA transcript is indicated (right-pointing arrow). Red colored rectangles represent exons encoding the open reading frame, grey colored rectangles represent alternatively spliced exons, white rectangles represent intronic sequence and black rectanges represent the untranslated region. Abbreviation ORF = translational open reading frame.

In order to address these questions, I analyzed the alternative splicing of full-length *Myo7a*, *Myo7b* and *Myo10* cDNA transcripts in the inner ear using the same cDNA source previously used for the cloning of *Myo15a* transcripts. Myosin VIIa, myosin VIIb and myosin X were chosen for analysis because they are the closest relatives of myosin XVa (Hodge et al. 2000; Sellers 2000; Berg et al. 2001; Chen et al. 2001). At the protein level, myosins VIIa, VIIb, X and XVa are characterized as containing one or more MyTh4/FERM domains. Phylogenetic analysis of the protein sequences of all myosin motors clusters myosins VIIa, VIIb, X and XVa together (Hodge et al. 2000; Sellers 2000; Berg et al. 2001). Similar analysis using the protein sequences of tails yields a similar clustering of myosins VIIa, VIIb, X and XVa together (Korn 2000; Chen et al. 2001).

Myo7a encodes two protein isoforms

Thirty full-length *Myo7a* cDNA transcripts were cloned from mouse P5 vestibular cDNA. The sequence of my thirty *Myo7a* cDNA transcripts (Accession Numbers AY821853 and AY821854) differed in four different aspects from the reported mouse *Myo7a* cDNA sequence found in the NCBI database (Accession Number U81453). First, the NCBI record for mouse *Myo7a* cDNA contained a truncated 5' UTR sequence and an incorrectly predicted ATG start codon. All attempts to PCR amplify *Myo7a* PCR products using forward PCR primers based upon the erroneous 5' UTR sequence found in the NCBI database were unsuccessful. In contrast, I determined that transcription of *Myo7a* transcripts initiated from a 111 base pair exon upstream (termed exon 0) of the previously identified exon 1 found in the NCBI

database. PCR amplification of full-length mouse *Myo7a* cDNA transcripts using a forward PCR primer in exon 0 was successful and generated a robust product. The identification of the transcription start site in exon 0 instead of exon 1 correctly identified the 129 base pairs comprising the 5' UTR sequence.

Second, I determined that the sequence of exon 1 is twenty-six base pairs shorter at the 5' end of the exon than predicted in the NCBI database. These twenty-six base pairs do not exist within the mouse genome so their inclusion in the NCBI mouse *Myo7a* cDNA transcript is an error (NCBI Accession Number: NM_008663). The previously predicted ATG start codon resided within these nonexistent twenty-six base pairs. Instead, an alternate ATG start codon in exon 1 was identified. Translation from this newly identified ATG start codon results in a predicted myosin VIIa protein product that is eleven amino acids shorter at the N-terminus than predicted by the NCBI record for mouse myosin VIIa protein.

Third, a novel alternatively spliced coding exon (exon 2a) was identified and present in nine out of thirty *Myo7a* cDNA transcripts. Exon 2a (18 base pairs) encodes a six amino acid insert within the motor. The implications of the six amino acid insert within the motor will be discussed later when describing the protein structure.

Fourth, exon 33 was found to be shorter than predicted by the NCBI database, as it contained 170 base pairs instead of the 284 base pairs predicted. Twenty-nine out of thirty cloned *Myo7a* cDNA transcripts contained the shortened exon 33. The loss of

the 114 base pairs in exon 33 did not affect the translational open reading frame but rather caused the loss of thirty-eight amino acids.

The exon and intron composition of each cloned *Myo7a* transcript was determined and the longest translational open reading frame was ascertained. Twenty-six out of thirty analyzed clones were predicted to translate a protein product. The predicted protein products clustered into four putative protein isoforms.

The most abundant *Myo7a* cDNA transcript (19 out of 30 clones) was predicted to encode 2,166 amino acid protein termed isoform 1 (figure 2-14A). This predicted protein product differs from the mouse myosin VIIa protein sequence found in the NCBI database in two regions. It is eleven amino acids shorter at the N-terminus and it lacks thirty-eight amino acids in the spacer region located between the first FERM domain and the SH3 domain. The translational open reading frame of Myo7a isoform 1 was cloned into N-terminally GFP tagged expression vector. In transfected inner ear hair cells, GFP-myosin VIIa localized along the length of the stereocilia in a pattern identical to endogenous myosin VIIa (figure 3-7E; Hasson et al. 1997; Rzadzinska et al. 2004; Belyantseva et al. 2005). Localization of myosin VIIa along the length of stereocilia contrasts with the stereocilia tip localization of myosin XVa in hair cells (Belyantseva et al. 2003; Belyantseva et al. 2005) implying distinct trafficking mechanisms for these two proteins in hair cells.

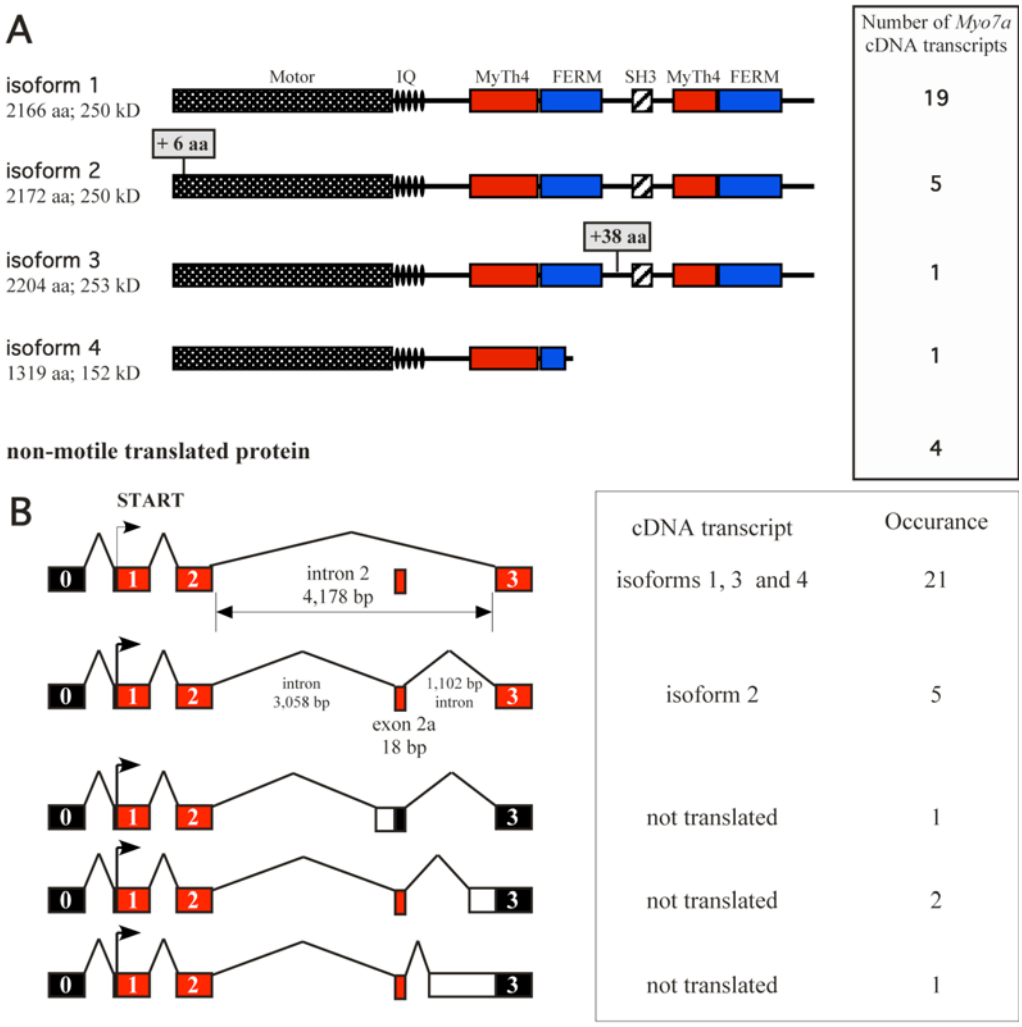

Figure 2-14. (A) Myosin VIIa protein isoforms predicted from 30 full-length *Myo7a* cDNA transcripts cloned from mouse P5 vestibular cDNA.Twenty-six out of thirty *Myo7a* cDNA transcripts were predicted to encode a protein, which clustered into four isoform classes. Isoform 1 was the most abundant predicted protein product that occurred in 19 out of 30 *Myo7a* cDNA transcripts. Isoform 2 contained a six amino acid insert adjacent to the Sh1-SH2 helix in the motor due to inclusion of alternatively spliced exon 2a within these *Myo7a* cDNA transcripts. Isoform 3 contains an additional 38 amino acids in the spacer region between the first FERM domain and the SH3 domain due to the retention of a longer exon 33 (284 bp instead of 170 bp) in the *Myo7a* cDNA transcript. Isoform 4 contains a truncated tail that terminates 56 amino acids into the first FERM domain. The *Myo7a* cDNA transcript encoding isoform 4 retains full intron 28 (703 base pairs) causing translation of 21 amino acids of novel sequence before encountering an in-frame stop codon. The last four amino acids of the C-terminus (F-A-C-M) does not conform to a consensus PDZ ligand. **(B)** Incomplete processing of intronic sequence surrounding exon 2a causes disruption of the translational reading frame in four *Myo7a* cDNA transcripts . The predicted translation start codon in the *Myo7a* cDNA transcripts is indicated (right-pointing arrow). Red colored rectangles represent exons encoding the open reading frame, black rectanges represent untranslated region and white rectangles represent intronic sequence.

The second most abundant *Myo7a* cDNA transcript (5 out of 30 clones) was predicted to encode 2,172 amino acid protein termed isoform 2 (figure 2-14A). Inclusion of alternative spliced exon 2a (18 base pairs) in *Myo7a* transcripts encodes a six amino acid insert within the motor. Other than the six amino acid insert within the motor, isoform 2 is identical in protein sequence to isoform 1. Based upon the crystal structure of chicken smooth muscle myosin II, the six amino acid insert is adjacent to the Sh1-SH2 helix. The impact of this six amino acid insert on the functional properties of the motor remains unclear, although no precedent suggests that a hydrophobic loop adjacent to the Sh1-SH2 helix will enhance the properties of the motor. A GFP-Myo7a expression vector encoding isoform 2 was generated. However we have not transfected it into inner ear hair cells to determine its cellular localization. It is tempting to speculate that GFP-myosin VIIa isoform 2 will demonstrate a different localization pattern in transfected hair cells than GFP-myosin VIIa isoform 1, although this awaits experimental validation.

Myosin VIIa isoform 3 is identical in protein sequence to isoform 1 except that it contains an additional thirty-eight amino acids in the spacer region between the first FERM domain and the SH3 domain due to a larger exon 33 (284 base pairs instead of 170 base pairs found in other *Myo7a* cDNA transcripts). Because this cDNA transcript occurred once out of thirty *Myo7a* cDNA transcripts, it appears to be an aberrant splicing intermediate.

Myosin VIIa isoform 4 contains a truncated tail which includes a novel twenty-one amino acid C-terminus. The retention of full intron 28 (703 base pairs) in this *Myo7a* cDNA transcript alters the translational reading frame resulting in the truncation fifty-six amino acids into the first FERM domain. The last four amino acids at the carboxyl terminus of myosin VIIa isoform 4 do not form a consensus PDZ binding ligand. Since this cDNA transcript occurred once out of thirty *Myo7a* cDNA transcripts, it may be an aberrant splicing intermediate similar to cDNA clone encoding myosin VIIa isoform 3.

Four out of thirty *Myo7a* cDNA transcripts were not predicted to encode a protein (figure 2-14B). All four clones contained exon 2a but were unable to splice out partial intronic sequence preceding exon 2a or preceding exon 3. The failure to remove the intronic sequence resulted in a disruption of the translational open reading frame and the presence of multiple in-frame stop codons.

Myo7b encodes two protein isoforms

Thirty-one full-length *Myo7b* cDNA transcripts were cloned from mouse P5 vestibular cDNA. For each clone, the exon/intron composition and the longest open reading frame was determined. Twenty-eight out of thirty-one clones were predicted to encode a protein. The protein products clustered into two isoform classes. The most abundant *Myo7b* transcript, which occurred in twenty-four out of thirty-one transcripts, was predicted to encode a 2,113 amino acid protein (figure 2-15). The protein sequence of myosin VIIb isoform 1 was identical to the sequence reported in

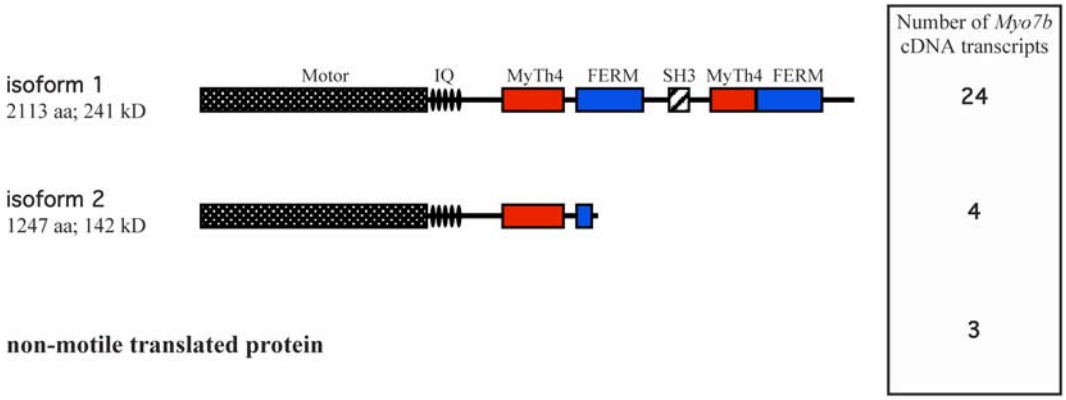

Figure 2-15. Myosin VIIb protein isoforms predicted from 31 full-length *Myo7b* cDNA transcripts cloned from mouse P5 vestibular cDNA. Twenty-eight out of thirty-one *Myo7b* cDNA transcripts were predicted to encode a protein, which clustered into two isoform classes. Isoform 1 was the most abundant predicted protein product that occurred in 24 out of 31 *Myo7b* cDNA transcripts. The protein sequence of isoform 1 is identical to the sequence listed in the NCBI database (NP_115770), while the protein sequence of isoform 2 is novel. Isoform 2 contains a truncated tail that terminates fifty amino acids into the first FERM domain. The *Myo7b* cDNA transcript encoding isoform 2 retains partial intron 28 (66 base pairs) causing translation of three amino acids of novel sequence before encountering an in-frame stop codon. The last four amino acids of the C-terminus (K-E-A-F) does not conform to any consensus PDZ ligand. The three *Myo7b* cDNA transcripts not predicted to encode a protein contained two disruptions in the translational open reading frame due to the retention of full intron 3 (1,075 base pairs) and partial intron 14 (73 base pairs). These retained intronic sequences would prevent these *Myo7b* cDNA transcripts from encoding a motor domain in two different regions.

the NCBI database. A GFP tagged Myo7b expression construct was generated and the subcellular localization was examined in transfected inner ear hair cells and COS-7 cells. In wild type hair cells, GFP-myosin VIIb accumulated in the cell body but was absent from stereocilia (figure 5-14B). In transfected COS7 cells, GFP-myosin VIIb was uniformly distributed throughout the cytoplasm and along the length of filopodia (figure 3-10). In proximal tubule cells of kidney and enterocytes of the intestine,

endogenous myosin VIIb was immunolocalized at distal tips of apical microvilli (Chen et al. 2001). No information on the cell type nor the cellular localization of endogenous myosin VIIb protein within the inner ear is published.

A second group of *Myo7b* transcripts is predicted to encode 1,247 amino acid myosin VIIb isoform 2 (figure 2-15). This *Myo7b* cDNA transcript contains 66 base pairs of partial intronic sequence between exons 28 and 29 that causes the inclusion of an in-frame stop codon. This novel isoform contains a shortened tail that truncates fifty amino acids into the first FERM domain. The truncated tail of myosin VIIb isoform 2 structurally resembles myosin XVa isoforms 1h and 2f. However the last four amino acids at the carboxyl terminus of myosin VIIb isoform 2 do not form a consensus PDZ binding ligand.

Three out of thirty-one cloned *Myo7b* cDNA transcripts were not predicted to encode a protein due to the inclusion of two intronic sequences. The retention of full intron 3 (875 base pairs) leads to multiple in-frame stop codons as well as a translational frameshift. The retention of 73 base pairs of partial intronic sequence between exons 14 and 15 causes a second translational frameshift in these *Myo7b* transcripts.

Myo10 encodes two motile protein isoforms and five non-motile isoforms

Thirty-seven full-length *Myo10* cDNA transcripts were cloned from mouse P5 vestibular cDNA. For each clone, the exon/intron composition and the longest open reading frame was determined. All thirty-seven *Myo10* cDNA transcripts were

predicted to encode a protein, which cluster into seven isoform classes. Five of the seven myosin X isoform classes appear to be non-motile proteins.

The most abundant *Myo10* transcript, which occurred in twenty-eight out of thirty-seven analyzed clones, is predicted to encode a 2,062 amino acid protein (figure 2-16A). The protein sequence of myosin X isoform 1 is identical to the sequence reported in the NCBI database. In transfected inner ear hair cells, GFP-myosin X remained in the cell body, which contrasted with the stereocilia localization of GFP-myosin VIIa and GFP-myosin XVa proteins. The cell type distribution and cellular localization of endogenous myosin X within the inner ear is unknown, so it is difficult to interpret the significance of cell body localization of GFP-myosin X.

The second most abundant *Myo10* cDNA transcript (2 out of 37 clones) was predicted to encode a 1,192 amino acid protein termed isoform 2, which truncates prior to the first pleckstrin homology domain (figure 2-16A). The exclusion of exon 28 (244 base pairs) in these *Myo10* cDNA transcripts causes a translational frameshift that encodes two amino acids of novel sequence before encountering an in-frame stop codon. Berg and colleagues reported that the myosin X motor by itself was the primary determinant of filopodia tip localization in epithelial cells (Berg et al. 2002). It appears unlikely that the exclusion of the three pleckstrin homology, MyTh4 and FERM domains in isoform 2 will affect cellular localization. However, the loss of these domains in the tail will produce binding to a set of protein partners distinct from

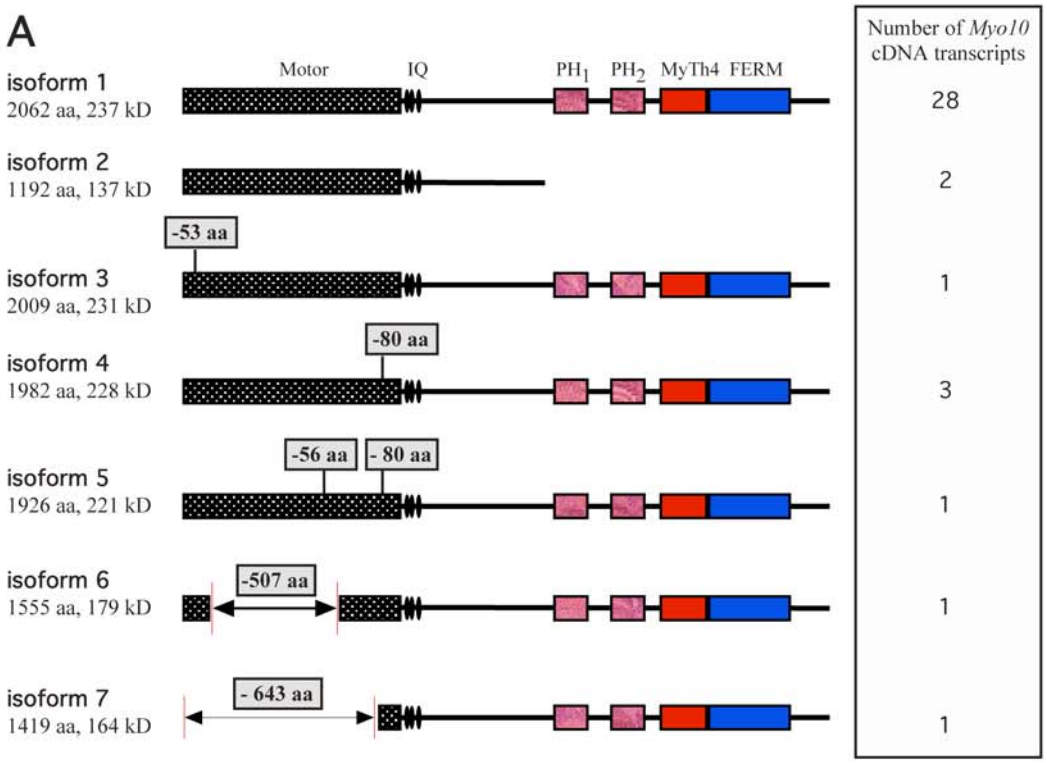

B

isoform class	missing amino acids within protein	cDNA transcript comments	translational frameshift
3	41 to 93	Splices out exon 3	no
4	643 to 722	Splices out exons 20 to 22	no
5	444 to 499	Splices out exons 13 to 15	no
	643 to 722	Splices out exons 20 to 22	no
6	112 to 618	Splices out exon 4 to 19	no
7	1 to 643	Retained partial intron 19 (28 base pairs)	yes

Figure 2-16. (A) Myosin X protein isoforms predicted from 37 full-length *Myo10* cDNA transcripts cloned from mouse P5 vestibular cDNA. All 37 full-length *Myo10* cDNA transcripts were predicted to encode a protein, which clustered into seven isoforms.Isoform 1 was the most abundant predicted myosin X protein product that occurred in 28 out of 37 *Myo10* cDNA transcripts. The protein sequence of isoform 1 is identical to the sequence listed in the NCBI database (NP_062345) while protein sequences of isoforms 2 to 7 are novel. Isoform 2 truncates prior to the first pleckstrin homology (PH) domain. This *Myo10* cDNA transcript splices out exon 28 (244 base pairs), causing a translational frameshift that encodes two amino acids of novel sequence before encountering an in-frame stop codon. The last four amino acids (K-G-R-S) at the C-terminus do not conform to any consensus PDZ ligands. **(B)** Myosin X protein isoforms 3 to 7 are likely to be non-motile due to the loss of amino acids in the motor. The *Myo10* cDNA transcripts encoding these protein isoforms lack exons encoding the motor (isoforms 3-6) or retention of an intron that disrupted the translational reading frame (isoform 7).

those bound by isoform 1 (Zhang et al. 2004). Whether any protein partners are bound as cargo by the truncated tail of myosin X will be worth investigating.

Myo10 cDNA transcripts encoding protein isoforms 3, 4, 5 and 6, splice out one or more exons encoding the motor yet the translational reading frame is unaffected (Figure 2-16B). The loss of these amino acids would likely disrupt the globular folding of subdomains within the motor leading to a diminished ability to transmit mechanical force. Curiously, the exclusion of exons in other regions of *Myo10* transcripts was not observed.

In the *Myo10* cDNA transcript encoding isoform 7, the retention of partial intron 19 (twenty-eight base pairs) disrupts the translational reading frame. The longest translational reading frame would initiate from a methionine residue located at amino acid 644. The predicted protein sequence of isoform 7 is identical to the human "headless" myosin X protein reported by Sousa and colleagues (Sousa et al. 2006) that lacked the first 643 amino acids of the full-length myosin X protein. Although the translational reading frames were identical, the human *MYO10* cDNA transcript predicted to encode a headless myosin X contained a novel 5'-UTR region and lacked the first 19 exons. In contrast, my mouse *Myo10* cDNA transcript, encoding isoform 7, was comprised of all 48 exons plus partial intron 19. Perhaps it is coincidental but it seems unlikely that two distinctly different cDNA transcripts from two different species would encode the same myosin X motor-less protein product.

Discussion

The diversity of mammalian protein coding mRNA transcripts is generated through four mechanisms. First, the usage of alternate promoters may allow alternative exons to encode different N-terminus domains of proteins. Second, the inclusion or exclusion of exons within the translational reading frame can alter the amino acid sequence of the protein. Third, the retention of an intron or part of an intron in the mature mRNA transcript can encode novel amino acid sequence or prematurely truncate the protein due to the inclusion of a stop codon, allowing for the translation of novel C-terminus domains. Finally, the usage of alternate polyadenylation sites can produce an alternative C-terminus domain in proteins or alternative 3' untranslated regions. My analysis of *Myo15a* cDNA transcripts suggests that the first three aforementioned mechanisms are utilized to generate alternatively spliced myosin XVa mRNA transcripts.

The cloning and sequencing analysis of 122 mouse vestibular full-length *Myo15a* cDNA transcripts, which contained the 5' untranslated region, translational open reading frame and the 3' untranslated region, revealed that mRNA transcripts from this gene are extensively alternatively spliced. Thirty myosin XVa protein isoforms ranging in molecular weight from 92 to 395 kilodaltons were predicted to be encoded. *Myo15a* cDNA transcripts generated multiple translational reading frames through three distinct mechanisms. First, *Myo15a* cDNA transcripts are transcribed from two different promoters. This allows them to be characterized into two major subclasses, class 1 and 2 *Myo15a* cDNA transcripts. Class 1 transcripts, which are transcribed from an unidentified promoter, are readily distinguished by the inclusion of exon 2

(3,762 base pairs). This unusually large exon encodes a 1,187 amino acid N-terminal extension that precedes the motor. Class 2 *Myo15a* cDNA transcripts, which are transcribed from a promoter adjacent to exon 1, splice from exon 1 to exon 3 thereby excluding exon 2. Thus the inclusion or exclusion of exon 2 in *Myo15a* cDNA transcripts allows them to be categorized into one or two subclasses.

Second, alternative splicing of exons 8 and 26 generates further diversity within the translational reading frames of *Myo15a* cDNA transcripts. The inclusion of exon 8 was found in 94% of *Myo15a* cDNA transcripts (103 out of 110 clones) encoding a protein, suggesting that the alternative splicing of exon 8 rarely occurred. On the other hand, alternative splicing of exon 26 was commonly found as 39% of *Myo15a* cDNA transcripts (43 out of 110 clones) encoding a protein contained exon 26. With the exception of exon 26, it appears that alternative splicing of exons within *Myo15a* cDNA transcripts is not a commonly used mechanism to generate diverse translational reading frames.

Third, the retention of intronic sequence from partial and entire introns within *Myo15a* cDNA transcripts generated multiple translational reading frames that encoded a diverse array of tail domains containing novel sequence at their C-termini. Initially, the discovery of retained intronic sequence in a large number of class 1 and 2 *Myo15a* cDNA transcripts suggested that I had cloned immature mRNA splice intermediates. If we discounted any *Myo15a* cDNA transcript containing retained intronic sequence, this meant that only 43% of *Myo15a* cDNA transcripts (53 out of

122 clones) encoded a protein product, suggesting that the mRNA processing of *Myo15a* is inefficient. Retained intronic sequences were found in *Myo7a*, *Myo7b* and *Myo10* cDNA transcripts at frequencies of 17%, 23% and 3%, respectively. Given the observation that the *Myo7a* (55.7 kb genomic DNA containing 50 exons), *Myo7b* (77.7 kb genomic DNA containing 48 exons), *Myo10* (147 kb genomic DNA containing 42 exons) and *Myo15a* (59.1 kb genomic DNA containing 66 exons) genes contain approximately an equal number of exons spread over a similar sized region of genomic DNA, it seems unusual that only *Myo15a* cDNA transcripts retain intronic sequences with a high frequency. It is worth noting that the cloning and sequence analysis of full-length whirlin and α-actinin 2 cDNA transcripts from the same mouse vestibular cDNA used to clone *Myo7a*, *Myo7b*, *Myo10* and *Myo15a* cDNA transcripts revealed no retained intronic sequences.

Ultimately determining whether or not *Myo15a* cDNA transcripts containing partial and full intronic sequences encode proteins will be answered by visualizing protein product bands on a Western blot using monoclonal antiserum raised against the motor, the only region common to all myosin XVa protein isoforms. If the corresponding protein products are observed on a Western blot, it will suggest that the retention of partial and full intronic sequences in *Myo15a* cDNA transcripts is a mechanism of generating proteomic diversity for myosin XVa.

At this time, it is difficult to determine if alternatively spliced myosin XVa mRNA isoform homologs are present in human, rat, and other species. Two factors appear to

confound this analysis. First, only a small number of myosin XVa expressed sequence tags (ESTs) are present in public databases examined (NCBI, UCSC Genome Browser, TIGR, Ensembl and FANTOM3). For myosin XVa, there are 6 mouse ESTs, 4 rat ESTs, 4 dog ESTs, 36 human ESTs and 2 monkey ESTs. Second, the majority of the myosin XVa ESTs are located in the distal 3' end of the myosin XVa cDNA transcript. My results indicated that the majority of mouse myosin XVa cDNA isoform diversity was generated by retention of partial or entire intronic sequence located between exons 24 and 36. As of the present time, there are no mouse, rat, dog, human or monkey myosin XVa ESTs containing exons 24 to 36. It appears the only way to determine if myosin XVa cDNA isoforms exist in other species will be to clone and sequence analyze full-length myosin XVa cDNA transcripts from these species.

The cloning and sequence analysis of full-length *Myo7a*, *Myo7b*, *Myo10* and *Myo15a* cDNA transcripts predicted the presence of numerous novel protein isoforms. Many of these predicted protein isoforms differ in molecular weight by less than 10 kilodaltons, making the electrophoretic separation and visualization of these 200 to 300 kilodalton proteins difficult on a Western blot. Based upon a biochemical purification approach, it is likely that many of these protein isoforms would be missed, thereby underestimating the proteomic diversity of myosins VIIa, VIIb, X and XVa.

Each of the genes encoding *Myo7b*, *Myo10* and *Myo15a* transcripts appears to utilize a distinct set of mechanisms for producing alternative spliced mRNA transcripts. Alternative splicing of exon 2a in *Myo7a* cDNA transcripts accounts for the protein sequence difference between myosin VIIa isoforms 1 and 2. Inclusion of the six amino acid insert within the motor encoded by exon 2a, may profoundly influence the enzymatic properties of myosin VIIa isoform 2. Whether this six amino acid insert affects localization within inner ear hair cells remains to be investigated.

In contrast, the inclusion or exclusion of partial intron 28 sequence in *Myo7b* cDNA transcripts accounts for the difference in the two encoded myosin VIIb protein isoforms. The retention of partial intron 28 causes the truncation of the encoded protein within the first FERM domain. Isoform 2, which lacks most of the first FERM domain, the SH3 and second MyTh4 and FERM domains, may bind a distinct set of protein partners relative to isoform 1. In the case of myosin VIIb protein, it is unknown whether the motor, the tail or a combination of both regions directs the correct cellular localization. A comparison of the cellular localization of myosin VIIb isoforms 1 and 2 will provide insight towards resolving this matter.

Alternative splicing of exon 28 in *Myo10* cDNA transcripts accounts for the protein sequence difference between myosin X isoforms 1 and 2, which differ in protein sequence at the C-terminus. The exclusion of exon 28 in *Myo10* cDNA transcripts causes truncation of the encoded protein prior to the first pleckstrin homology domain in isoform 2. The exclusion of the three pleckstrin homology, MyTh4 and FERM

domains in isoform 2 may not affect localization but may bind different protein partners than isoform 1. The inefficient splicing of exons encoding the motor in *Myo10* transcripts encoding protein isoforms 3, 4, 5 and 6 appears energetically wasteful unless there is a biological advantage to producing a non-motile myosin X protein.

Future Plans

Generation and validation of monoclonal antiserum against myosin XVa motor

A key remaining question is whether or not *Myo15a* cDNA transcripts containing intronic sequence encode a protein. Retained introns in functional, mature transcripts have been reported for several mammalian genes (Chang et al. 1999; Graveley 2001; Lo et al. 2004). The most definitive approach to validate the existence of the various predicted myosin XVa isoforms will be to visualize the protein products of the predicted molecular weights on a Western blot of mouse inner ear tissue. Although the thirty predicted myosin XVa protein isoforms vary in their composition at the amino and carboxyl terminus, the 697 amino acids comprising the motor is nearly invariant for all of the isoforms (figure 2-2 and 2-6). To verify the presence of the various predicted myosin XVa isoforms, we will develop monoclonal antiserum against purified, recombinant mouse myosin XVa motor.

To determine the specificity of our monoclonal antiserum, I will determine if it immunoreacts with mouse myosins VIIa, VIIb and X in two different assays. Myosins VIIa, VIIb and X are the closest protein relatives of myosin XVa (Hodge et al. 2000; Korn 2000; Sellers 2000; Berg et al. 2001; Chen et al. 2001). First, I will determine if

our monoclonal antiserum cross-reacts with purified protein products of mouse myosins VIIa, VIIb and X heavy meromyosins in a protein slot blot. Next I will determine the utility of the antiserum for recognizing denatured proteins by immunoblotting mouse myosins VIIa, VIIb, X and XVa motor heavy meromyosins electrophoresed on a SDS acylamide gel. If there is no cross-reactivity with myosins VIIa, VIIb and X, then it suggests the antiserum will work well for Western blots.

Second, I will determine if the monoclonal antiserum non-specifically recognizes GFP-mouse myosins VIIa, VIIb or X in transfected COS7 cells. Following fixation, the cells with be stained with our monoclonal antiserum and the immunolocalization pattern will be determined by confocal microscopy. Previously it was demonstrated that GFP-tagged myosin XVa isoform 2a distinctly localized to filopodia tips in transfected COS7 cells (Belyantseva et al. 2003a; Belyantseva et al. 2005), so I optimistically expect co-localization of our monoclonal antiserum with GFP-myosin XVa at filopodia tips. Since myosin XVa is not expressed endogenously in COS7 cells (Belyantseva et al. 2003a), staining of mock-transfected COS7 cells will determine if our antiserum recognizes endogenous myosins. If co-localization of our antiserum with GFP-myosins VIIa, VIIb and X in transfected COS7 cells is observed, then I will conclude that our antiserum is not specific for myosin XVa.

Confirmation of inner ear myosin XVa protein isoforms

To confirm the existence of myosin XVa protein isoforms predicted by my cloned *Myo15a* cDNA transcripts, I will perform a western blot on whole mouse inner ear

tissue. Although a wide size range of protein products is predicted from my cloned full-length *Myo15a* cDNA transcripts, I predict that eight distinct bands of 92, 100, 115, 136, 225, 260, 270 and 393 kilodaltons will be observed. These eight bands correspond to the most abundant predicted protein isoforms from my 122 full-length *Myo15a* cDNA transcripts (isoforms 1a, 1b, 1c, 1d, 1h, 1i, 1j and 1l and isoforms 2a, 2b, 2c, 2d, 2e, 2g, 2i, 2j, 2l, 2n, 2o, 2p and 2q). If the molecular weights corresponding to predicted protein products from myosin XVa isoforms are observed on a Western blot, this suggests that the *Myo15a* cDNA transcripts encode proteins. In particular, protein products of 92, 100, 115, 136, 225 and 270 kilodaltons represent the predicted proteins encoded by *Myo15a* cDNA transcripts containing partial and full intronic sequences.

Immunolocalization of myosin XVa isoforms within the inner ear.

To address the possibility of myosin XVa protein isoforms have different subcellular localizations within hair cells, I will stain mouse and rat inner ear sensory epithelia explants using our monoclonal antiserum directed against an epitope of the myosin XVa motor. From analyses, we know that myosin XVa isoform 2a (discussed in Chapter 3) localizes to stereocilia tips. I anticipate that myosin XVa isoforms containing truncated C-termini will localize to the cell body and basolateral surface of hair cells. All of the truncated C-termini contain unique amino acid sequences, which will be used to design isoform specific antiserum. For instance, antiserum specific for isoforms 1h, 1i, 1j, 2i and 2j, containing a unique 20 amino acid C-terminus, was generated but has not been experimentally evaluated. In addition, the hair cell

localization of GFP-myosin XVa isoforms 2j, 2p and 2q transfected into inner ear sensory epithelia explants will corroborate the localization of endogenous myosin XVa protein.

Chapter 3: Whirlin and Myosin XVa are Protein Partners

Abstract

In humans and mice, mutations of myosin XVa and whirlin are associated with deafness and vestibular dysfunction. The *in vivo* interaction of myosin XVa's carboxy-terminal PDZ ligand with the third PDZ domain of whirlin is demonstrated in transfected COS-7 and mouse inner ear hair cells. Myosin XVa, which is not endogenously present in COS-7 cells, binds whirlin as cargo and delivers whirlin to the tips of filopodia in COS-7 cells. Disruption of the interaction, either by deleting the carboxy-terminal PDZ ligand of myosin XVa or the third PDZ domain of whirlin, eliminates delivery of whirlin to filopodia tips. The addition of the four amino acid PDZ ligand to the carboxy-terminus of myosin X resulted in the transport and delivery of whirlin to filopodia tips of COS-7 cells. In mice, the failure of myosin XVa to deliver whirlin to inner ear hair cell stereocilia results in deafness in the mouse mutants shaker 2 and whirler, which harbor mutations in myosin XVa and whirlin, respectively. The stereocilia of shaker 2 and whirler inner ear hair cells are abnormally short due to a failure of the actin cytoskeleton to elongate and the stereocilia bundle lacks the characteristic staircase structure found in normal hair cells. The introduction of exogenous myosin XVa into shaker 2 and whirlin into whirler inner ear hair cells results in restoration of stereocilia elongation and staircase bundle formation. These results imply that the delivery of whirlin by myosin XVa is essential for stereocilia elongation and staircase formation.

Introduction

PDZ domains are 90 amino acid modular protein-interaction domains that are specialized for binding to short peptide motifs that are usually located at the carboxy termini of proteins, although interaction can occur with internal peptide sequences that adopt a β-hairpin structure (Harris et al. 2001; Sheng et al. 2001; Jelen et al. 2003; Kim et al. 2004). PDZ domains are named after the proteins (**P**SD-95, **D**iscs Large and **Z**ona Occludins 1) in which these motifs were originally described. Although degenerate PDZ homologs are present in bacteria and yeast, the presence of more than 400 PDZ domain containing proteins in the mouse proteome, suggests that they co-evolved with multicellularity (Harris et al. 2001; Jelen et al. 2003). PDZ domains are often arranged in tandem arrays and/or associated with other protein interaction domains to form multidomain scaffold proteins. The binding of specific C-terminal peptides to PDZ domains, allows PDZ domain containing proteins to assemble large molecular complexes. Typically, the PDZ scaffold protein and its associated multiprotein complex are targeted to a specific subcellular site to perform a specialized local function (Harris et al. 2001; Sheng et al. 2001; Jelen et al. 2003; Kim et al. 2004).

PDZ domains are classified on the basis of the sequence of their preferred carboxy-terminal peptide ligands. The carboxy-terminal-terminal amino acid is termed the P_0 residue, while subsequent amino acids towards the amino-terminus are termed P_{-1}, P_{-2} and P_{-3} (Harris et al. 2001; Sheng et al. 2001). Crystal structures, site directed

mutagenesis and peptide library screening revealed that P_0, P_{-2} and P_{-3} residues are critical for recognition (Harris et al. 2001; Sheng et al. 2001; Jelen et al. 2003). On the basis of their preferences at the P_0 and P_{-2} positions, PDZ domains can be divided into at least three classes. Class I PDZ domains bind ligands with the consensus sequence X-S/T-X-V/L, class II PDZ domains bind the motif X-ϕ-X-ϕ and class III PDZ domains bind X-D-X-V where X is any amino acid and ϕ is a hydrophobic amino acid (Harris et al. 2001; Sheng et al. 2001; Jelen et al. 2003).

PDZ domains are comprised of six β strands that form a partially open barrel and two α helices that flank each side of the open barrel. Carboxy-terminal peptide ligands bind to an extended groove formed by the βB strand and the αB helix of the PDZ domain. Binding of a carboxy-terminal peptide ligand imparts little conformational change to a PDZ domain. The side chains of the P_0 and P_{-2} amino acids point directly at the βB/ αB groove while the side chains of the P_{-1} and P_{-3} amino acids face the surface of the protein and are solvent accessible (figure 3-1). The hydrophobic side chain of the amino acid at the P_0 position points into a hydrophobic pocket of the PDZ domain, where it makes several hydrogen bonds. The differential preference of PDZ domains for glycine, valine, alanine, leucine, isoleucine or phenylalanine at the P_0 position of the carboxyl ligand is explainable by the variations in the size and geometry of the hydrophobic pocket (Harris et al. 2001; Sheng et al. 2001; Jelen et al. 2003). The side chain of the P_{-2} amino acid points into a separate pocket, which in class I PDZ domains contains a histidine residue that makes a hydrogen bond with a serine or threonine P_{-2} residue of the PDZ ligand (figure 3-1A). In class II PDZ

domains, histidine is replaced by leucine or methionine that recognizes a hydrophobic residue at the P_{-2} position (figure 3-1B). Variations in the P_{-2} binding pocket can

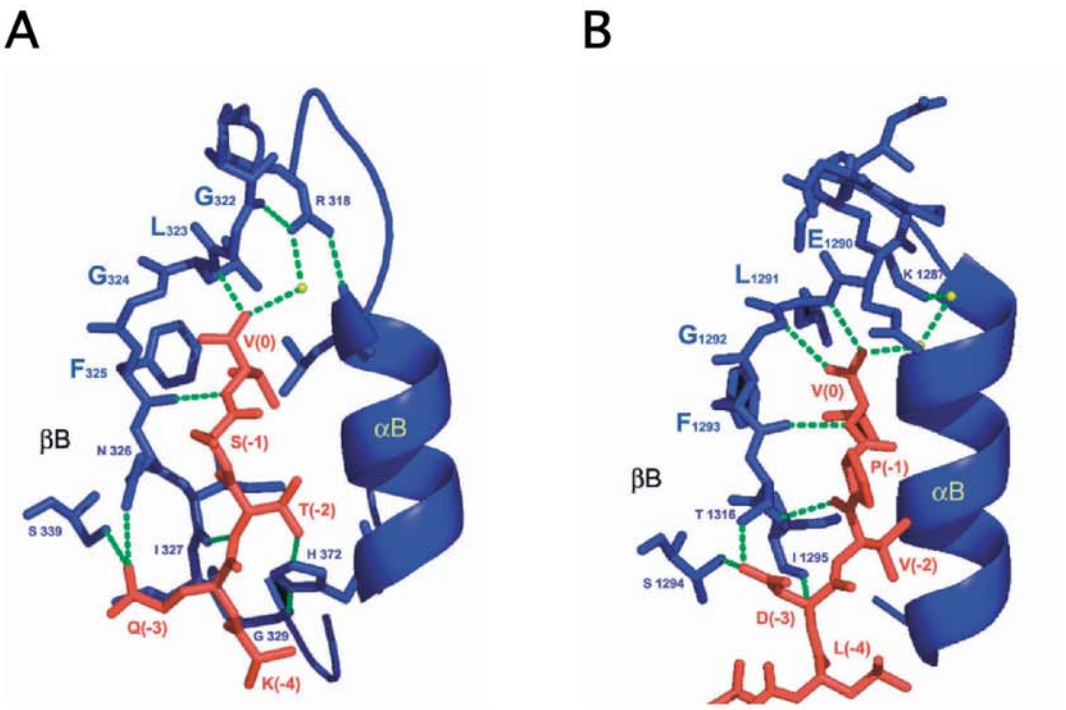

Figure 3-1. Classification of PDZ domains according to specificity for carboxy terminal ligand peptides. **(A)** The ligand binding pocket of a class I PDZ domain. The class I PDZ ligand of CRIPT (colored in red) makes several hydrogen bonds (green dashed lines) with βB strand and αB helix of PDZ3 domain of PSD-95 (colored blue). The P_0, P_{-2} and P_{-3} residues of the PDZ ligand are most critical for the interaction. Valine, the P_0 residue of the PDZ ligand, makes several hydrogen bonds with the amino acids in the βB strand. The side chain of threonine, the P_{-2} residue of the PDZ ligand, points into a pocket and makes a hydrogen bond with a histidine residue of the PDZ domain. Glutamine, the P_{-3} residue, contacts the binding groove, contributing further binding specificity. **(B)** The ligand binding pocket of a class II PDZ domain. The class II PDZ ligand of ErbB2 receptor (colored in red) makes several hydrogen bonds (green dashed lines) with PDZ domain of Erbin (colored blue). Valine, the P_0 residue of the PDZ ligand, makes several hydrogen bonds within a hydrophobic pocket of the PDZ domain. No hydrogen bonds are formed between the αB helix of the PDZ domain and valine, the P_{-2} residue of the PDZ ligand. Aspartic acid, the P_{-3} residue, contacts the binding groove, contributing further binding specificity. This figure was taken from from Jelen (2003) with permisssion of the author.

generate distinct preferences for hydroxylated, charged or hydrophobic amino acids in the ligand (Harris et al. 2001; Sheng et al. 2001). The side chain of P_{-3} amino acid contacts the binding groove, contributing further binding specificity (Doyle et al. 1996; Karthikeyan et al. 2001; Jelen et al. 2003). The amino acid at the P_{-1} position plays a supplementary role in fine-tuning the binding specificity and affinity to PDZ domains (Harris et al. 2001; Sheng et al. 2001; Zhang et al. 2003).

PDZ-based protein complexes can be moved around the cell as pre-assembled packages by one of three mechanisms. In some instances, PDZ domains directly interact with the molecular motor such as the direct interaction of PDZ domains of PSD-95 (**p**ost-**s**ynaptic **d**ensity protein **95**), SAP97 (**s**ynapse-**a**ssociated **p**rotein **97**) and S-SCAM (**s**ynaptic **sca**ffolding **m**olecule) with the C-terminal ligand of kinesin 1Bα (Mok et al. 2002). The PDZ1 domain of Drosophila INAD interacts with C-terminal ligand of myosin IIIa while the interaction of GRIP (**g**lutamate-**r**eceptor-**i**nteracting-**p**rotein) with conventional kinesin KIF5 was demonstrated (Chevesich et al. 1997; Setou et al. 2002). A second method of transporting PDZ-based protein complexes involves an interaction between the motor protein and other protein domain within the PDZ domain containing protein. SAP97 protein is comprised of a L27, three PDZ, a SH3 and guanylate kinase-like domains. The guanylate kinase-like domain of SAP97 directly binds kinesin family member 13B while L27 domain of SAP97 interacts with myosin VI (Asaba et al. 2003; Wu et al. 2002).

Finally, PDZ-based protein complexes can associate with molecular motors indirectly through adaptor proteins. PSD-95 protein is comprised of L27, three PDZ, a SH3 and guanylate kinase-like domains. The guanylate kinase-like domain of PSD-95 binds GKAP (**g**uanylate **k**inase-**a**ssociated **p**rotein), which in turn binds dynein light chain (DLC). DLC is a light chain that is bound by myosin Va and cytoplasmic dynein (Naisbitt et al. 2000), allowing trafficking of the PSD-95 complex to postsynaptic site.

Whirlin

Whirlin is a PDZ domain containing protein comprised of three PDZ domains each predicted to bind class I PDZ ligands, a proline-rich region and carboxy-terminal class II PDZ ligand (Belyantseva et al. 2003b; Mburu et al. 2003; Yap et al. 2003). Orthologs of whirlin are present in the genomes of humans, monkey, mice, rats, dogs, chicken, cow, frog, zebrafish and puffer fish (Ensembl Genome Browser). RT-PCR of human and rat multiple tissue cDNA panels revealed strong expression of whirlin in brain, heart, pancreas, spleen, lung, liver and kidney while lower expression levels were observed in skeletal muscle, ovary and testis (Nagase et al. 2000; Yap et al. 2003). The distribution of whirlin expressed sequence tags from mouse and human tissue indicate expression in bone, brain, cervix, colon, ear, eye, kidney, liver, lung, mammary gland, muscle, ovary, pancreas, placenta, prostate, spleen, skin, stomach, testis, thymus, uterus and embryonic tissue (NCBI Unigene). Although not ubiquitous, whirlin is widely expressed in many tissues in human, rat and mice.

Yap and co-authors identified whirlin, which they named CIP98 (**C**ASK **I**nteracting **P**rotein-**98** kilodaltons), as a protein partner of CASK (**Ca**lmodulin-dependent **S**erine **K**inase) in a yeast two-hybrid screen of a rat brain library (Yap et al. 2003). Using a series of deletion constructs in the yeast two-hybrid system, Yap and colleagues showed that the guanylate kinase-like (GK) domain interacted with a minimal region of whirlin that included the third PDZ domain and the 76 amino acids that preceded it. Loss of the 76 amino acids preceding the third PDZ domain abolished the interaction, since the third PDZ domain alone could not bind it. The interaction between the two proteins was demonstrated by co-immunoprecipitation of a brain protein extract. Whirlin and CASK colocalized in the dendritic processes of neurons in the cerebral cortex, the thalamus and the molecular layer of the cerebellum (Yap et al. 2003). Yap and colleagues speculated that whirlin-CASK interaction formed a complex necessary for the trafficking of synaptic vesicles for neurotransmission.

Positional Cloning Identifies Whirlin

The whirler mouse (*whirler*^{wi}) phenotype, which is deaf and exhibits circling behavior consistent with vestibular dysfunction, was first reported by Fleming and colleagues (Fleming et al. 1994). The whirler phenotype is caused by an autosomal recessive mutation located on mouse chromosome 4. Eight years later, Mustapha and colleagues identified a consanguineous Palestinian family segregating recessive, non-syndromic sensorineural deafness (DFNB31) that mapped to human chromosome 9q32-34, a region syntenic to the *whirler*^{wi} locus (Mustapha et al. 2002).

In 2003, Mburu and colleagues identified mutations in a novel gene encoding whirlin. Mutations in whirlin are associated with deafness and vestibular dysfunction phenotype in *whirler*^{wi} mice and affected members of Palestinian family previously ascertained by Mustapha and colleagues (Mburu et al. 2003). The mouse and human whirlin genes are comprised of 12 exons spanning approximately 100 kilobases of genomic DNA. Based upon the predicted exon structure of the gene, the expressed sequence tag database and PCR amplification of small cDNA fragments from mouse inner ear, Mburu and colleagues (2003) predicted that two cDNA transcripts, termed long and short whirlin, were transcribed (figure 3-2A; Mburu et al. 2003). Mouse long whirlin cDNA transcript was comprised of exons 1 through 12 while the short whirlin cDNA transcript contained a novel 5' UTR sequence in intron 4 followed by exons 5 through 12. The long whirlin cDNA transcript encodes a 907 amino acid protein containing three PDZ domains, a proline-rich domain and C-terminal class II PDZ ligand while the short whirlin cDNA transcript encodes a 465 amino acid protein that lacks the first and second PDZ domains (figure 3-3A). The causative mutation in the *whirler*^{wi} mouse was a 14,351 base pair deletion of the genomic DNA that eliminated 592 base pairs of coding sequence in the whirlin cDNA transcript (figure 3-2C; Mburu et al. 2003). The 592 base pair deletion in exons 6 through 9 of *whirler*^{wi} cDNA transcripts is predicted to shift the translational reading frame in long and short cDNA transcripts (figure 3-2A and 3-2C).

Scanning electron microscopy examination of the inner ear tissue from *whirler*^{wi} mice revealed that stereocilia bundles of auditory and vestibular hair cells were properly positioned but abnormally short (figure 3-4). The stereocilia bundle did not show the

characteristic staircase structure found in wild type hair cells (Holme et al. 2002; Mburu et al. 2003; Frolenkov et al. 2004). A nearly complete restoration of the hearing defect and the stereocilia architecture of *whirler*^{wi} hair cells was observed after a Bacterial Artificial Chromosome predicted to encode a short whirlin protein containing the proline-rich, third PDZ domain and carboxy-terminal PDZ ligand was introduced (figure 3-3A; Mburu et al. 2003). Since the Bacterial Artificial Chromosome lacked the genomic DNA containing the first three exons of the gene, the authors speculated that the short whirlin cDNA transcript was transcribed (figure 3-2A). The apparent restoration of the stereocilia bundle by short whirlin protein containing the proline-rich domain, third PDZ domain and carboxy-terminal PDZ ligand, suggested that the first and second PDZ domains were not critical for the elongation and maintenance of stereocilia in sensory hair cells in the inner ear (Mburu et al. 2003). Kikkawa and colleagues reported two whirlin protein bands (33 and 49 kilodaltons) on a Western blot of protein extract from *whirler*^{wi} inner ear, which had been phenotypically rescued by the introduction of Bacterial Artificial Chromosome containing the partial genomic sequence of the whirlin gene (Kikkawa et al. 2005).

Methods

For this Ph.D. dissertation, I initiated and completed all of the molecular biology, performed the COS-7 cell transfections and captured the images of co-transfected COS-7 cells. Inna Belyantseva M.D., Ph.D. performed all of the immunohistochemistry of hair cells and used my expression constructs to capture the high-resolution confocal images of gene-gun transfected hair cells (Belyantseva et al., 2005). Dr. Sadaf Naz, a postdoctoral fellow in the Friedman laboratory, expressed and purified two recombinant whirlin proteins, which were used as antigens for the generation of rabbit anti-whirlin antisera.

Genotyping.

Tail snip samples were taken from mouse pups and genomic DNA was purified using the DNeasy Tissue Kit (Qiagen) and eluted in 200 microliters. For the genotyping of shaker 2 mice, a 1,158 base pair PCR product was amplified. Five microliters of PCR product was digested with Tse I for 1.5 hours at 65^{o}C. The Tse I restriction digest products were electrophoresed on a 2.0% agarose gel. The shaker 2 mutation eliminates a Tse I recognition site. A Tse I restriction enzyme digest of 1,158 base pair PCR product results in different sized Tse I restriction enzyme digest products for wild type (**416**, 224, 223, 140, 121 and 34 base pairs), heterozygous shaker 2 (**639**, **416**, 224, 223, 140, 121 and 34 base pairs) and homozygous shaker 2 animals (**639**, 224, 223, 140, 121 and 34 base pairs).

In order to genotype whirler mice, we took advantage of the 14, 351 base pair *whirler* deletion in genomic DNA of the whirlin gene (Mburu et al. 2003). PCR reactions

were performed with primers annealing to nucleotides in exon 6 and exon 9 of whirlin, which amplified a 171 base pair product from genomic DNA of homozygous or heterozygous *whirler*^{wi} mice but not from wild type animals. The PCR product (14,523bp) from the wild type allele is too long for conventional PCR conditions. In the same PCR reaction we detected the wild type allele (544 base pairs) using primers annealing to sequence in intron 6 and intron 7 of whirlin, which is absent in homozygous *whirler*^{wi} mice. The PCR primers used for shaker 2 and whirler genotyping are listed in Table 3-1.

Antibodies.

Rabbit polyclonal TF1 antiserum was raised against a fusion protein of GST with a proximal segment of the myosin XVa tail region between the first MyTH4 and FERM domains (Fig. 2A and ref. 41) corresponding to amino acid residues number 2139 to 2354 (NCBI accession AY331132), and affinity purified on a Pierce AminoLink column. The anti-myosin XVa antibody (TF1) was characterized previously (Anderson et al., 2000; Belyantseva et al., 2003a). In order to raise antibodies to whirlin, cDNA constructs encoding amino acid residues 362 to 509 and 711 to 815 of mouse whirlin (Accession # AY739114) were introduced individually into pGEX5.1 (Amersham Biosciences) and expressed in E. coli (BL21 Gold DE3 pLysS, Stratagene). Fusion proteins were isolated by incubating with glutathione sepharose 4B (Amersham Biosciences), and the purity confirmed by denaturing PAGE. Each fusion protein was used to immunize three rabbits (Covance). cDNAs encoding amino acids 362 to 509 or 711 to 815 of mouse whirlin were also introduced into

pMAL-c2x (New England Biolabs), transformed into E. coli Rosetta (DE3, Novagen), and induced to express the corresponding maltose binding (MBP) fusion protein. The expressed fusion proteins were isolated using amylose resin and bound to a column of 4% beaded agarose support (AminoLink plus coupling gel, Pierce). Antisera from the immunized rabbits were affinity purified using chromatography columns containing the corresponding MBP whirlin fusion protein.

Immunocytochemistry.

Whole mount samples from the organs of Corti (OC) and vestibular tissues as well as inner ear sensory epithelia explants were fixed in 4% paraformaldehyde and immunostained as described (ref). The cochleae of adult and postnatal, C57BL/6 (Charles River Labs), shaker 2 (Jax Labs), and whirler (Jax Labs) mice, ranging from P0 to P30 as well as adult (120-150 g) and postnatal P0-P10 Sprague-Dawley rats (Taconic), were dissected and fixed with 4% paraformaldehyde in PBS for 2 hrs. Cultured inner ear sensory epithelia explants were fixed overnight with 4% paraformaldehyde at 4°C. Immunostaining using TF1 and HL5136, HL5137, HL5140, HL5141 antibodies was performed as described (Belyantseva et al., 2003a). F-actin was visualized by rhodamine-phalloidin or Alexa Fluor 633 phalloidin staining.

Myosin XVa expression constructs.

GFP-myosin XVa expression construct, whose sequence corresponded to mouse myosin XVa isoform 2a (Accession # AY331133), was described previously as [-

N]Myo15a-GFP (Belyantseva et al., 2003a). To generate the GFP-myosin XVa expression construct lacking the PDZ ligand (deletion of the sequence encoding amino acids 2303-2306, Accession # AY331133), the open reading frame was PCR amplified using Pfu Ultra DNA polymerase (Stratagene, La Jolla, CA) from the aforementioned cloned GFP-myosin XVa cDNA, inserted into the EcoR I and Sal I sites of EGFP-C2 plasmid (Clontech, Palo Alto, CA) and sequence verified. The sequence of PCR primers is given in Table 3-2 while the sequencing primers are listed in Table 2-1 of Chapter 2.

Myosins Ic, VI, VIIa, VIIb and X expression vectors

The open reading frame of mouse myosin Ic was PCR amplified from IMAGE clone 5344331 using Pfu Ultra DNA polymerase (Stratagene, La Jolla, CA). The PCR product was cloned into the Hind III and Sac II sites of EGFP-C3 plasmid (Clontech, Palo Alto, CA) and sequence verified. The open reading frame of human myosin VI was PCR amplified from human kidney cDNA and cloned into the EcoR I and Sal I sites of EGFP-C2 plasmid (Clontech, Palo Alto, CA) and sequence-verified. The open reading frames of myosin VIIa isoform 1, myosin VIIb isoform 1 and myosin X isoform 1 were PCR amplified from mouse P5 vestibular cDNA and cloned into the EcoR I and Sal I sites of EGFP-C2, Xho I and Sal I sites of EGFP-C3 and Bgl II and Kpn I sites of EGFP-C3 plasmid, respectively. All inserts were sequence verified. To generate the mouse GFP-myosin X[+PDZ_L] expression vector, the fifteen base pair myosin XVa cDNA sequence encoding the class I PDZ ligand (I-T-L-L-stop codon) was added to a reverse PCR primer. The myosin X open reading frame was PCR

amplified and cloned into the Bgl II and Kpn I sites of GFP-C3 plasmid (Clontech). The sequence of PCR primers is listed in Table 3-2.

Whirlin expression constructs.

Using mouse P5 vestibular cDNA as template, full-length whirlin cDNA containing the entire open reading frame including the 5'untranslated region (UTR) and 3' UTR was PCR amplified with LA Taq DNA Polymerase (Takara Mirus, Madison, WI), cloned into PCR-XL-TOPO (Invitrogen, Carlsbad, CA), transformed into XL10 Gold cells (Stratagene, La Jolla, CA) and the entire insert was sequence verified. The predominant vestibular whirlin cDNA isoform encoded the expected 907 amino acid protein (Accession # AY739114; Mburu et al. 2003). Additionally, eight novel whirlin isoforms encoding predicted protein products of 366, 403, 465, 476, 550, 906, 911 and 918 amino acid residues were found (Accession # AY739115- AY739122, figure 3-2B).

To construct a wild type cDNA encoding the 907 amino acid isoform of whirlin, the entire open reading frame was PCR amplified from cloned whirlin cDNA using LA Taq DNA Polymerase (Takara Mirus, Madison, WI) and inserted into the EcoR I and Sal I sites of EGFP-C2 plasmid (Clontech, Palo Alto, CA). We also constructed a mutant cDNA encoding the whirlin protein that lacks the third PDZ domain (-PDZ_3) equivalent to the R778X mutant allele reported by Mburu (2003). The wild type dsRed-whirlin and dsRed-whirlin (-PDZ_3) expression constructs were generated using an identical procedure as described above and inserted into the EcoR I and Sal I sites

of dsRed2-C1 (Clontech, Palo Alto, CA). PCR primer sequences are given in Table 2 while the sequencing primers are listed in Table 3.

Culture and transfection of inner ear sensory epithelium.

Inner ear sensory epithelium cultures were prepared from OC, saccule, utricle and ampulae of P1 toP4 C57Bl/6, shaker 2, and whirler mice and from OC of P2-P3 rats as described (Belyantseva et al., 2003a). Cultures were then transfected using a Helios gene gun (Bio-Rad Labs). Gold particles (1.0 μm, Bio-Rad) were coated with plasmid DNA at a ratio of 2 μg plasmid DNA to 1 μg of gold particles and precipitated onto the inner wall of Tefzel tubing, which was cut into individual cartridges containing ~1 μg of plasmid DNA. For some experiments cartridges were prepared using a mix of GFP-Myo15a and DsRed-Whrn precipitated on the same gold particles. Samples were bombarded with the gold particles from one cartridge per culture using 120 psi of helium. After an additional 8 hrs to 4 days in culture, samples were fixed in 4% paraformaldehyde, stained with rhodamine-phalloidin or Alexa Fluor 633 phalloidin and observed using a Zeiss LSM510 confocal microscope equipped with a 100x, N.A.=1.45 objective.

COS-7 cell culture and time-lapse imaging.

African green monkey kidney cells (COS-7) were cultured at 37ºC and 5% CO_2 in DMEM supplemented by 10% Fetal Bovine Serum and 10 mM HEPES. Using Lipofectamine 2000 (Life Technologies) cells were transfected with wild type and mutant GFP-Myo15a expression constructs and wild type and mutant GFP- and

DsRed-Whrn expression constructs. In fixed tissue samples, co-localization of myosin XVa and whirlin were analyzed with Zeiss software for the LSM510 confocal microscope.

For time-lapse imaging, COS-7 cells were grown and transfected in the glass-bottom Petri dishes. Cells were observed with a Nikon TE300 inverted microscope equipped with a 100x, 1.3 NA objective. Temperature was maintained at 37±2ºC using an objective heater and a heating stage. Epifluorescent and bright field images were acquired every 10 or 20 s with a ORCA-II-ER cooled CCD camera (Hamamatsu Co.) controlled with MetaMorph software (Universal Imaging Co.). The same software controlled fast exchange of the fluorescent filters, acquiring GFP and DsRed images sequentially within 1-1.5 s, which covered no more than 15% of the shortest time-lapse interval.

Table 3-1. PCR primers for genotyping shaker 2 and whirler mice

PCR product	Primer Sequence
Shaker 2	forward primer 5'-CAGCCCTATCACCTGCTCATCAG-3' reverse primer 5'-GCCACCACCCAGTAAGAGAAGAC-3'
544 bp whirler PCR product	forward primer 5'-TGGATGCTTCCTCAAGGACACCAGA-3' reverse primer 5'-TATCCCCAGACTGAGAGCCCCAGAA-3'
171 bp whirler PCR product	forward primer 5'-GGGGAATCAGACTCGTGCACTGCT-3' reverse primer 5'-GGTGCACCTCCACCAGAACAAAGTG-3'

Table 3-2. PCR primers for synthesizing myosin and whirlin expression constructs

PCR product	Primer Sequence
Myo15a isoform 2a	Forward primer, 5'- cgattc**gaattc**ATGCACTCCATACGCAACCTGCCTTC-3' Reverse primer, 5'- cgattc**gtcgac**TCACAAGAGGGTGATCTCGCTGGGAGG-3'
Myo15a isoform 2a (-PDZ ligand)	Forward primer, 5'- cgattc**gaattc**ATGCACTCCATACGCAACCTGCCTTC-3' Reverse primer, 5'- cgattc**gtcgac**TCACTCGCTGGGAGGCAGTGTGAGCC-3'
Myosin Ic	Forward primer, 5'- cgattc**aagctt**ATGGAGAGCGCCTTGACTGCCCG-3' Reverse primer, 5'- cgattc**ccgcgg**TCACCGAGAATTCAGCCGTGGGGC-3'
Myosin VI	Forward primer, 5'- cgattc**gaattc**ATGGAGGATGGAAAGCCCGTTTGG-3' Reverse primer, 5'-cgattc**gtcgac**CTACTACTTTAACAGACTCTGCAGCATGGCTG-3'
Myosin VIIa isoform 1	Forward primer, 5'- cgattc**gaattc**ATGGACCTGAAGTCAGGCCAGGAG-3' Reverse primer, 5'- cgattc**gtcgac**TCACCTCCCGCTCCTGGAGTTC-3'
Myosin VIIb isoform 1	Forward primer, 5'-cgattc**ctcgag**ATGTCCGTGTTCCGGCTGGGTG-3' Reverse primer, 5'-cgattg**gtcgac**TTAGGGGTTGGCCGGGGCG-3'
Myosin X isoform 1	Forward primer, 5'-cgattc**agatct**cATGGACAGCTTCTTTCCCGAGGGAGCAC-3' Reverse primer, 5'-cgattc**ggtacc**TCACCTGGAGCTGCCCTGGCTGCTC-3'
Myosin X[+PDZ$_L$]	Forward primer, 5'-cgattc**agatct**cATGGACAGCTTCTTTCCCGAGGGAGCAC-3' Reverse primer, 5'-cgattc**ggtacc**TCACAAGAGGGTGATCCTGGAGCTGCCCTGGCTGCTC-3'
whirlin cDNA isoforms 1 to 7	Forward primer, 5'- CCAGTTTCACCTGCCTTCGC-3' Reverse primer, 5'- TGCCTTCCTTCCCTTCACCTAAC-3'
whirlin cDNA isoforms 8 & 9	Forward primer, 5'- GTAGGAGATGCGAGCACTTTGTACGC-3' Reverse primer, 5'- TGCCTTCCTTCCCTTCACCTAAC-3'
whirlin	Forward primer, 5'- cgattc**gaattc**ATGAACGCACAGCTGGACGGC-3'

isoform 1	Reverse primer, 5'- cgattg**gtcgac**CTAGAGCATCACGTTGAACTCAGTGACC-3'
whirlin [–PDZ_3]	Forward primer, 5'- cgattc**gaattc**ATGAACGCACAGCTGGACGGC-3' Reverse primer, 5'- cgattg**gtcgac**CTCAGCCTGAGGTGCTGGCCTC-3'

Uppercase letters denote cDNA sequence, lowercase bold letters are restriction enzyme recognition sites and lowercase letters denote extra primer sequence

Table 3-3. Primers for sequencing whirlin cDNA

Primer	Primer Sequence
Whirl-5	AGTGAACTGCTCCCGCTCG
Whirl-6	AGCGGGAGCAGTTCACTCAC
Whirl-7	TGAAGCCCAAGCCCTCGTGG
Whirl-8	CTGTCAAGGCTCTCAAAGG
Whirl-9	CCCAGGTGTAGATGTGGTTG
Whirl-10	GCAGAGTGGAGATGAGAAAAAG
Whirl-11	CCACACCAGTGATGTAAATGC
Whirl-12	AATCCTGGCTTGCTTGTCC
Whirl-13	CACAGAAGAAGGGACAAGC
Whirl-14	ACACACACGCCAAGTTCTC
Whirl-15	GGTTCCTTCCAGGTCTAATG
Whirl-16	TGGTTTCCTACAGCGACAC
Whirl-17	GATGTGTCTGTGGATGATGTC
Whirl-18	TGGTGCTGAGAAGACAATG
Whirl-19	CCCATTTATGCCTCCATC
Whirl-20	TTCACATCAGGCTCACTGTCCG
Whirl-21	CCTTGCCATTCTTGTTCTTAGC
Whirl-22	ACAGACAGCATCCGCTAAG
Whirl-23	TGTCTGCCCATTCACTTCC

Results

Whirlin encodes nine protein isoforms

A more detailed analysis of whirlin cDNA transcripts in mouse inner ear in this dissertation revealed a more complex distribution of alternatively spliced cDNA transcripts (figure 3-2B). Nine whirlin cDNA transcripts including eight novel cDNA transcripts were identified from the cloning and sequence analysis of full-length whirlin cDNA transcripts. Using PCR primers located in exons 1 and 12, whirlin cDNA isoforms 1 to 7 were identified. The whirlin cDNA isoforms 1 to 4 differed by alternative splicing of novel exon 7a (isoform 2), extra coding sequence at the end of exon 4 (isoform 3) or loss of the first codon in exon 9 (isoform 4). Whirlin cDNA isoforms 5 and 6 lacked exons 2 through 5 and differed by the alternative splicing of exon 7a while whirlin cDNA isoform 7 lacked exons 2 through 6.

Despite numerous attempts using PCR primers located in the distal sequence of intron 4 and exon 12, I was unsuccessful in PCR amplifying the short whirlin transcript as described by Mburu and colleagues (figure 3-2A). The mouse short whirlin cDNA transcript reported by Mburu (2003) was assumed to be a homolog of human teratocarcinoma expressed sequence tag (NCBI Accession Number: AK022854). Despite the wide tissue expression pattern of whirlin, a mouse short whirlin expressed sequence tag was not detected (NCBI Unigene database). However, I did identify two whirlin cDNA transcripts (isoforms 8 and 9) that were structurally similar to short whirlin cDNA transcript using PCR primers located in intron 5 and exon 12. Whirlin cDNA isoforms 8 and 9 were comprised of novel 5'UTR sequence from intron 5 followed by exons 6 through 12 and differed by alternative splicing of exon 7a.

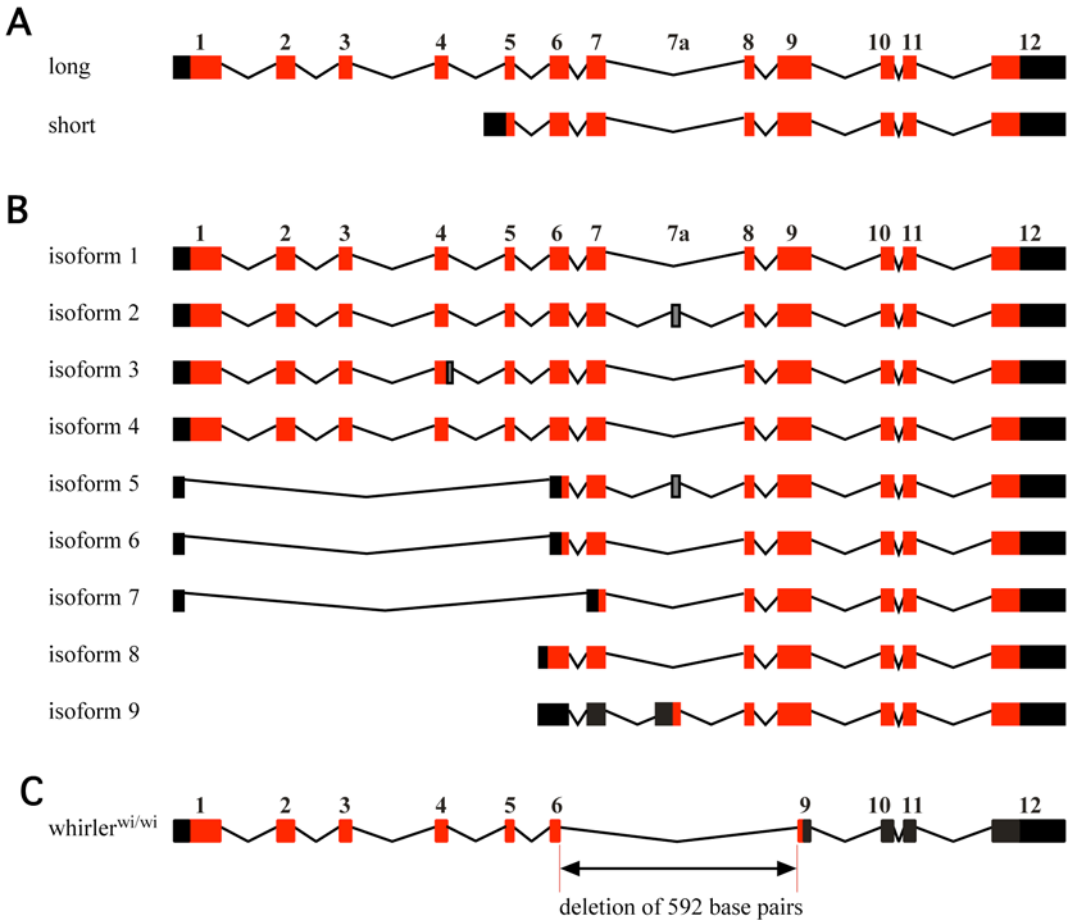

Figure 3-2. The exon composition of alternatively spliced mouse vestibular whirlin mRNA transcripts. **(A)** Structure of mouse wild-type whirlin cDNA transcripts reported by Mburu (2003). The long whirlin cDNA transcript was comprised of exons 1 to 12 while the short transcript contained a novel 5' untranslated region sequence located in intron 4 followed by exons 5 to 12. Exons encoding the translational open reading frame are represented by red rectangles and black rectanges represent 5‘ and 3’ untranslated regions. **(B)** Structure of mouse wild-type whirlin cDNA transcripts reported by Belyantseva (2005). Seven splice variants of cloned mouse whirlin cDNAs (NCBI Accession # AY739114 - AY739120) were cloned using PCR primers located in exon 1 and exon 12. Exons encoding the translational open reading frame are represented by red rectangles, alternatively spliced coding exons are grey rectangles and black rectanges represent 5‘ and 3’ untranslated regions. Two splice variants of cloned mouse whirlin cDNAs (NCBI Accession # AY739121 - AY739122) were cloned using PCR primers located in intron 5 and exon 12. The short whirlin cDNA transcript in panel A was not identified. **(C)** Structure of mutant mouse whirler (whirler$^{wi/wi}$) cDNA transcript that has a 592 base pair deletion of coding sequence that includes part of exon 6, all of exons 7 and 8 and part of exon 9 resulting in a translational frameshift at the codon encoding amino acid 433. The 592 base pair deletion in exons 6 through 9 of whirler mutant mouse is predicted to shift the translational reading frame of all nine whirlin cDNA isoforms depicted in panel B.

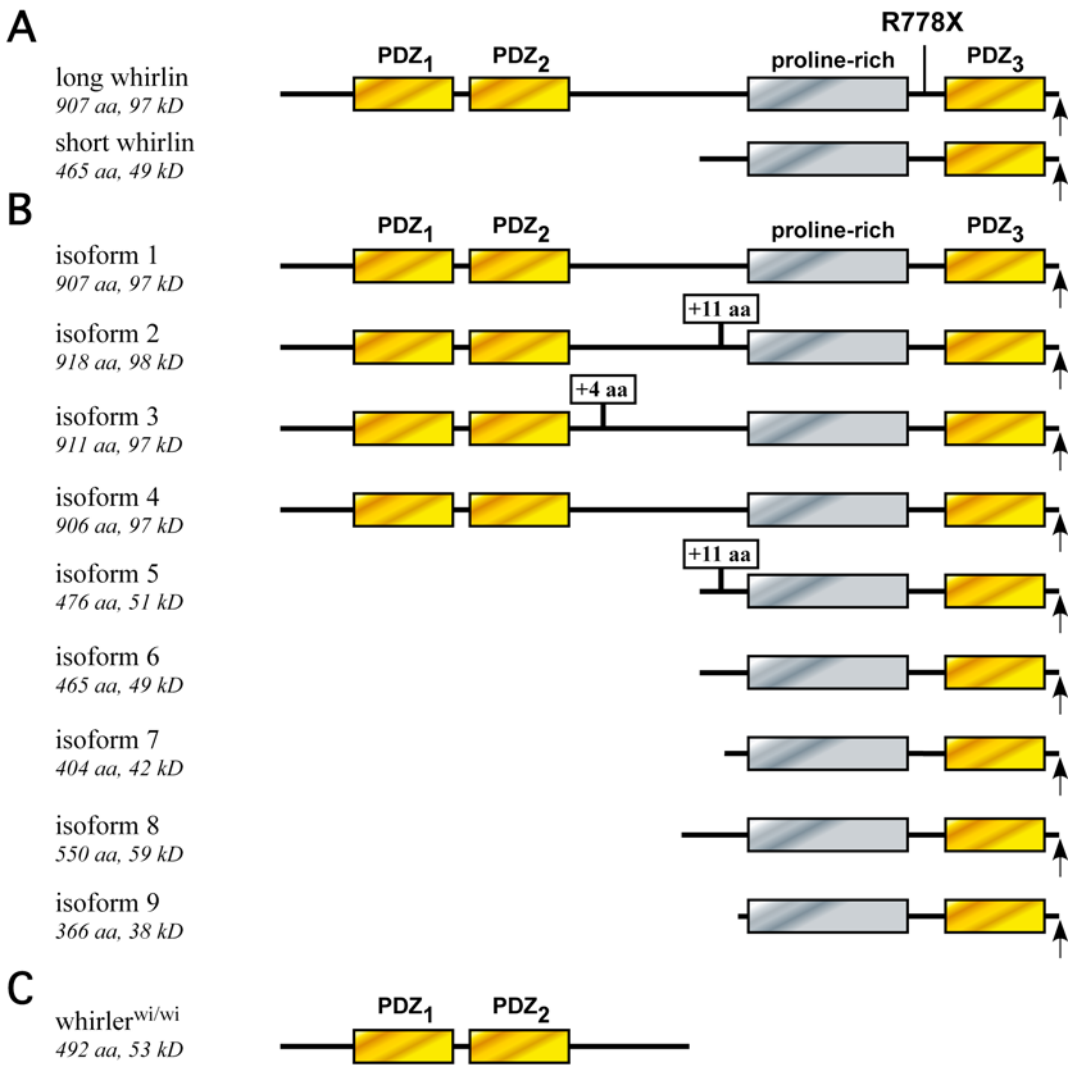

Figure 3-3. Structure of mouse vestibular whirlin protein isoforms. **(A)** Structure of mouse whirlin proteins reported by Mburu (2003). Long whirlin protein was comprised of three class I PDZ domains (yellow rectangles), a proline-rich region (grey rectangle) and a carboxy terminal class II PDZ ligand (denoted by upward facing arrow). The location of the R778X nonsense mutation reported by Mburu (2003) that prematurely truncates human whirlin is depicted. Short whirlin protein contained the proline-rich, PDZ3 domains and carboxy terminal class II PDZ ligand. **(B)** Structure of mouse whirlin proteins reported by Belyantseva (2005). In addition to the 907 amino acid protein isoform reported by Mburu, eight novel whirlin protein isoforms encoding polypeptides of 366, 403, 465, 476, 550, 906, 911 and 918 amino acid residues. Alternative splicing of exon 4 (denoted in grey box with "+4 aa") and exon 7a (denoted in grey box with "+11 aa") encoded inserts of 4 and 11 amino acids respectively. **(C)** Structure of mutant mouse whirler (whirler$^{wi/wi}$) protein that truncates prior to the proline-rich region (Mburu 2003). A translational frameshift at the codon encoding amino acid 433 results in translation of an additional fifty-eight amino acids before encountering an in-frame stop codon.

The deduced protein products from the nine whirlin cDNA transcripts clustered into two subgroups (figure 3-3B). The first group of whirlin proteins (isoforms 1 through 4) contained three PDZ domains, a proline-rich domain and carboxy-terminal PDZ ligand. The second group of whirlin proteins lacked the first two PDZ domains but contained the proline-rich domain, third PDZ domain and carboxy-terminal PDZ ligand (isoforms 5 through 9). The 592 base pair deletion in exons 6 through 9 of *whirler*^{wi} cDNA transcripts is predicted to shift the translational reading frame in all nine whirlin cDNA transcripts (figure 3-2B and 3-2C). The deletion causes a translational frameshift at amino acid 433 in whirlin isoforms 1 through 4, causing the translation of fifty-eight novel amino acids before encountering a stop codon. The resulting truncated protein lacks the proline-rich domain, third PDZ domain and carboxy-terminal PDZ ligand (figure 3-3C). For whirlin cDNA isoforms 5 through 9, the longest in-frame predicted protein product is approximately 50 amino acids. Western blot analysis of bovine protein extracts from retina, brain, testis, small intestine, stomach, kidney and lung revealed protein bands corresponding to the molecular weights of my predicted inner ear whirlin protein isoforms (van Wijk et al. 2006), indirectly suggesting that my cloned mouse whirlin cDNA transcripts encoded proteins *in vivo*.

Endogenous myosin XVa and whirlin protein co-localize at stereocilia tips

In homozygous whirler^{wi} mice, the abnormally short stereocilia, which fail to normally elongate and achieve a staircase-like architecture, were similar to the stereocilia dysmorphology of homozygous *Myo15a*^{sh2} mice (figure 3-4; Probst et al. 1998; Wang et al. 1998). Based upon these defects, it was proposed that myosin XVa and whirlin were protein partners in a macromolecular complex that mediated

stereocilia elongation and staircase formation (Holme et al. 2002; Belyantseva et al. 2003a; Belyantseva et al. 2003b; Frolenkov et al. 2004).

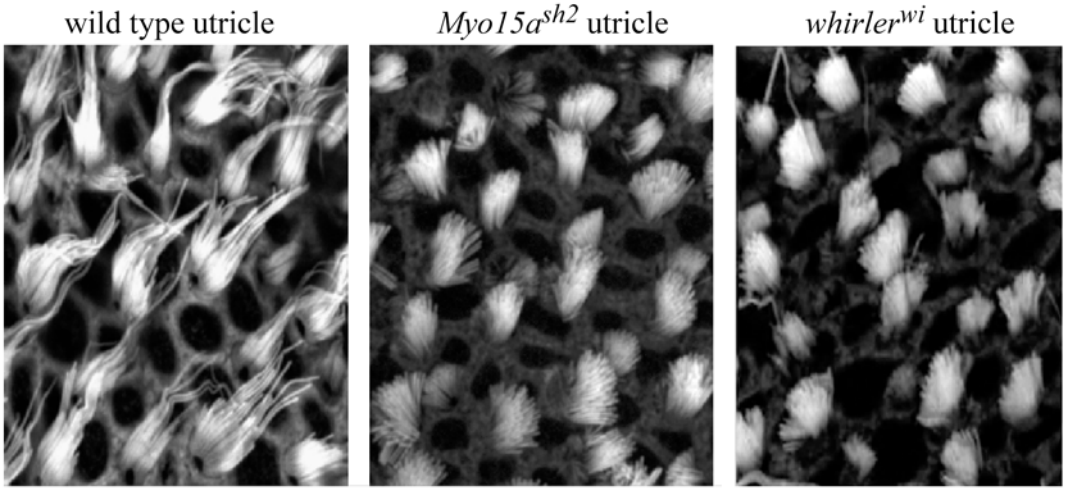

Figure 3-4. Homozygous whirler (*whirler*^{wi}) and shaker 2 (*Myo15a*^{sh2}) mice show similar defects of elongation and staircase formation of hair cell stereocilia bundles.Scanning electron micrographs revealed the stereocilia bundles of homozygous *Myo15a*^{sh2} and *whirler*^{wi} mice are short and fail to elongate and achieve a staircase architecture characteristic of wild type mouse utricle hair cell.

To determine whether myosin XVa could bind to whirlin and transport it to the tips of stereocilia, we raised antisera against myosin XVa and whirlin (figure 3-5A) and determined the localization of endogenous protein. We found myosin XVa and whirlin were concentrated at the stereocilia tips of auditory and vestibular hair cells in newborn and adult mice (figure 3-5B; Belyantseva et al. 2003a; Belyantseva et al. 2005). The distal tip localization of these two proteins at the barbed ends of the actin filaments of the stereocilia coincided with the site of growth and remodeling of the

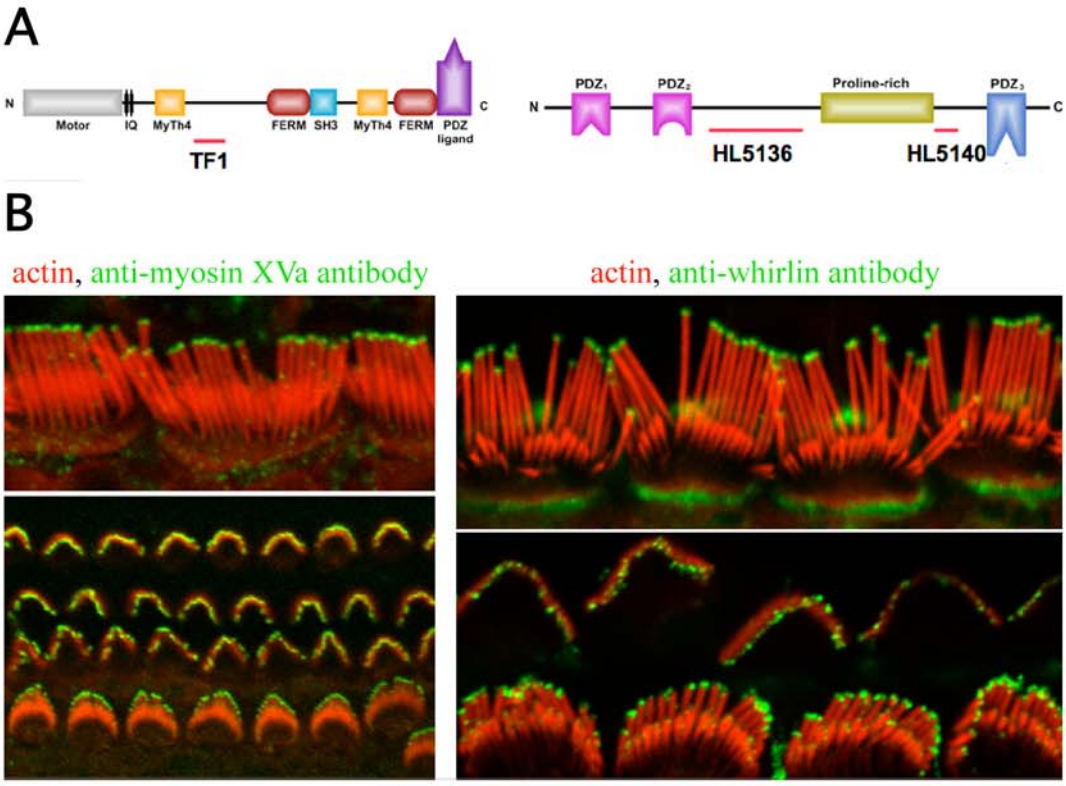

Figure 3-5. Endogenous myosin XVa and whirlin are localized to the tips of wild type hair cell stereocilia. **(A)** Stick figures illustrating the domain composition of myosin XVa and whirlin. The red lines underneath myosin XVa and whirlin stick figures represent the regions of recombinant purified protein used as antigen to raise polyclonal antisera. For whirlin, two different polyclonal antisera were raised while single polyclonal antiserum was generated for myosin XVa. **(B)** Myosin XVa immunoreactivity (green) was observed at every stereocilia tip in mouse wild type inner and outer hair cells using TF1 antisera (left panel). Whirlin immunoreactivity (green) was detected at stereocilia tips of wild type inner and outer hair cells using HL5136 and HL5140 antisera (right panel). The actin cytoskeleton is visualized by rhodamine-phalloidin (red) in all panels.

actin core (Tilney et al. 1981; Schneider et al. 2002; Belyantseva et al. 2003a; Rzadzinska et al. 2004; Belyantseva et al. 2005). Other researchers independently and contemporaneously confirmed that myosin XVa and whirlin are localized at tips of stereocilia (Rzadzinska et al. 2004; Delprat et al. 2005; Kikkawa et al. 2005).

Whirlin is mislocalized in hair cells of shaker 2 mice

We reasoned that if myosin XVa bound and transported whirlin to stereocilia tips of wild type hair cells, then the *Myo15a*^{sh2} mutation causing a disablement of motor function should result in mislocalization of whirlin in homozygous *Myo15a*^{sh2} hair cells. Consistent with our hypothesis, Inna Belyantseva observed no myosin XVa or whirlin immunoreactivity at stereocilia tips of homozygous *Myo15a*^{sh2} auditory and vestibular hair cells (figures 3-6A and 3-6B; Belyantseva et al. 2003a; Belyantseva et al. 2005). Next, we sought to ascertain whether whirlin was required for stereocilia tip localization of myosin XVa by examining the localization of both proteins in homozygous *whirler*^{wi} hair cells. Myosin XVa was present at stereocilia tips of *whirler*^{wi} hair cells while whirlin was absent (figures 3-6C and 3-6D). Collectively, this suggested that whirlin was not required for the targeting or tethering of myosin XVa at the tips of stereocilia, however myosin XVa was necessary for the whirlin localization at stereocilia apices.

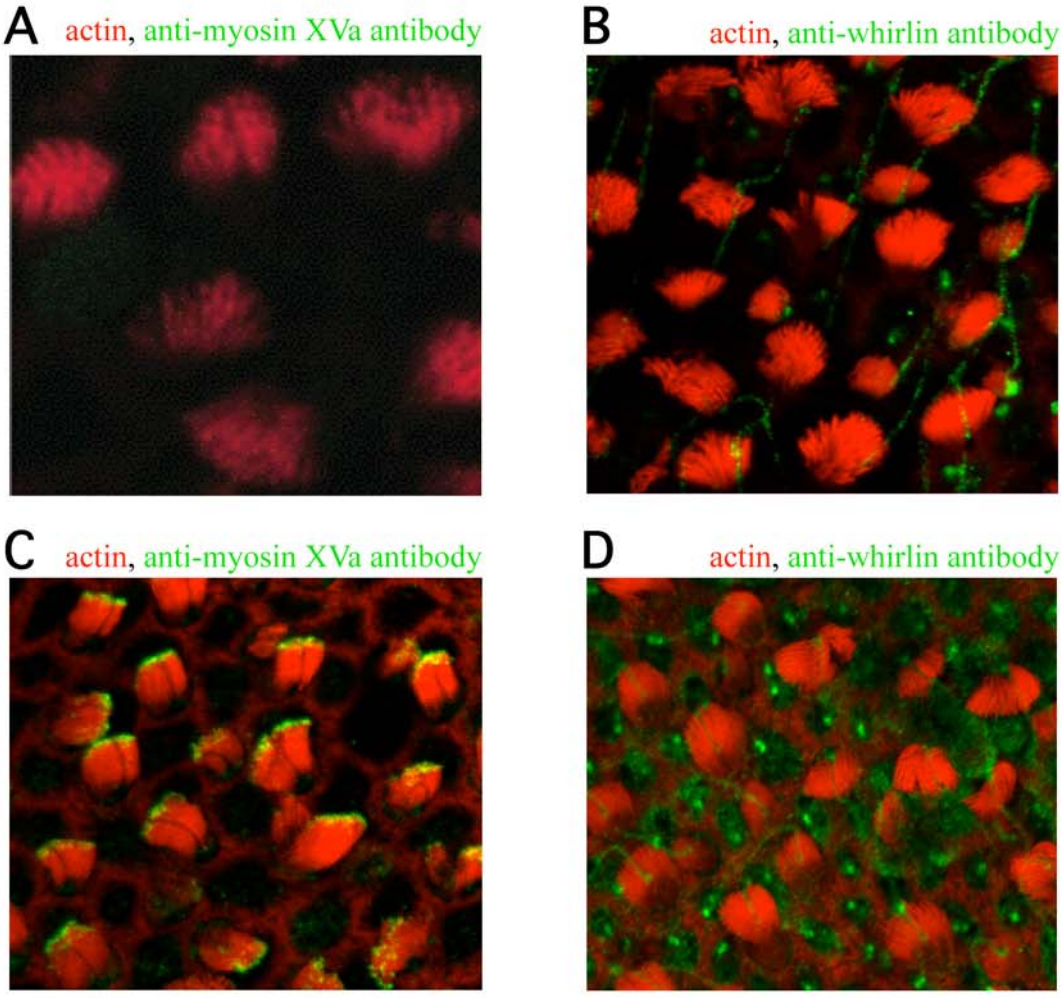

Figure 3-6. Myosin XVa is required for whirlin localization at the tips of stereocilia; however whirlin is not necessary for myosin XVa localization at the stereocilia tips. **(A)** No myosin XVa immunoreactivity was observed in utricle hair cell stereocilia of homozygous *Myo15a*^{sh2} mice. **(B)** Whirlin is absent from utricle hair cell stereocilia of homozygous *Myo15a*^{sh2} mice. **(C)** Myosin XVa immunoreactivity (green) was observed at stereocilia tips of homozygous *whirler*^{wi} utricle hair cells. **(D)** Whirlin is absent from hair cell stereocilia of homozygous *whirler*^{wi} mice. The actin cytoskeleton is visualized by rhodamine-phalloidin (red) in all panels.

Exogenous myosin XVa and whirlin co-localize at stereocilia tips

The targeting of whirlin and myosin XVa to stereocilia tips of wild type hair cells was demonstrated by Inna Belyantseva M.D., Ph.D. using gene gun transfection of mouse and rat sensory epithelial explants. Gold particles, coated with plasmid DNA of either green fluorescent protein (GFP) tagged-myosin XVa or GFP-whirlin expression construct, were ballistically fired into dissected living inner ear tissue that is adhered to a coverslip (figures 3-7A and 3-7B). After 24 to 48 hours of transfection, the tissue was fixed and the actin cytoskeleton was counterstained. The localization of the GFP signal within transfected hair cells was examined by confocal microscopy (figure 3-7C). As one experimental control, we determined that transfection of GFP expression vector without a cDNA insert resulted in the uniform distribution of GFP signal throughout the cell body and stereocilia (Belyantseva et al. 2003a). This demonstrated that the GFP protein alone was incapable of specifically localizing to tips of stereocilia. Next, full-length GFP-myosin XVa and GFP-whirlin cDNA expression constructs were individually transfected into wild type rat and mouse vestibular and auditory hair cells. Accumulation of GFP-myosin XVa and GFP-whirlin were observed at the distal tip of every stereocilium of transfected hair cells (figures 3-8A and 3-8B; Belyantseva et al. 2003a; Belyantseva et al. 2005). The localization of GFP-myosin XVa and GFP-whirlin in transfected hair cells was consistent with the observed endogenous location of these two proteins. The over-expression of GFP-myosin XVa and GFP-whirlin in transfected wild type hair cells did not result in over-elongation of stereocilia length as compared to neighboring non-transfected hair cells (Belyantseva et al. 2003a; Belyantseva et al. 2005).

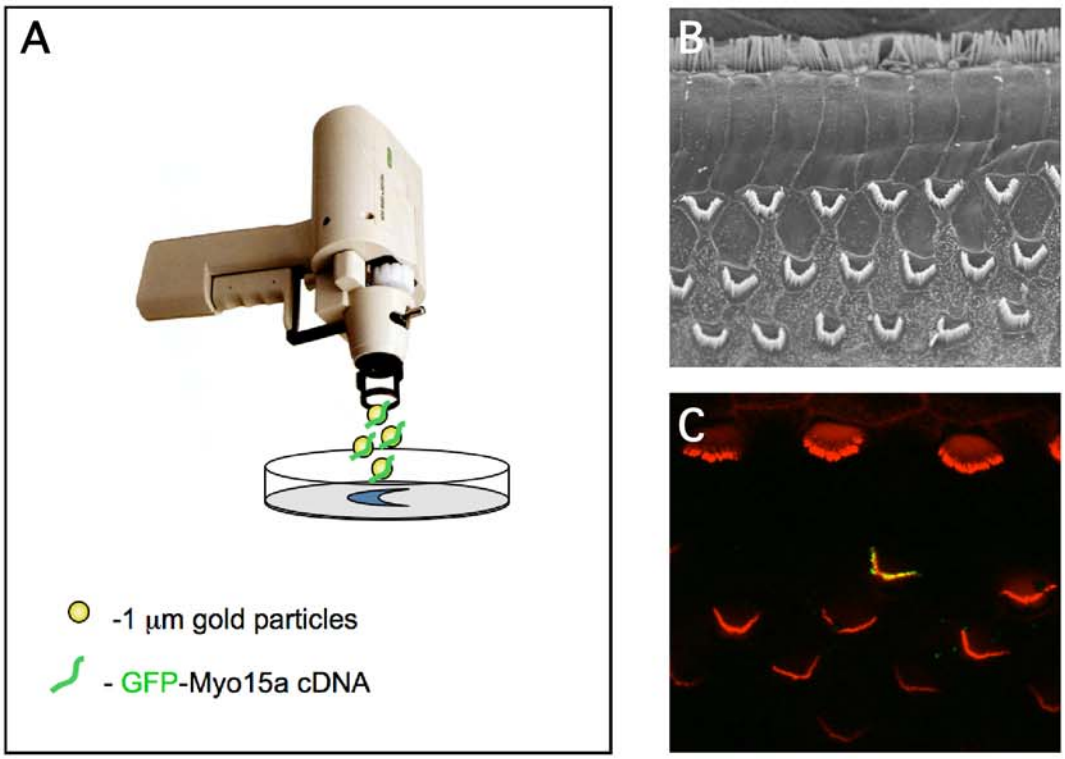

Figure 3-7. Helios gene gun transfection of a mouse inner ear sensory epithelium *in vitro*. **(A)** Small gold particles coated with plasmid DNA are ballistically fired into the apical surface of dissected sensory epithelium tissue. **(B)** Image of the apical surface of organ of Corti illustrating the one row of inner hair cells and three rows of outer hair cells. **(C)** After 24 to 48 hours of transfection, sensory epithelium tissue is fixed; the actin cytoskeleton counterstained with rhodamine-phalloidin (red) and the slide is examined by confocal microscopy. The co-localization of GFP-myosin XVa (green) and actin cytoskeleton (red) at stereocilia tips (yellow) is observed in a single transfected hair cell.

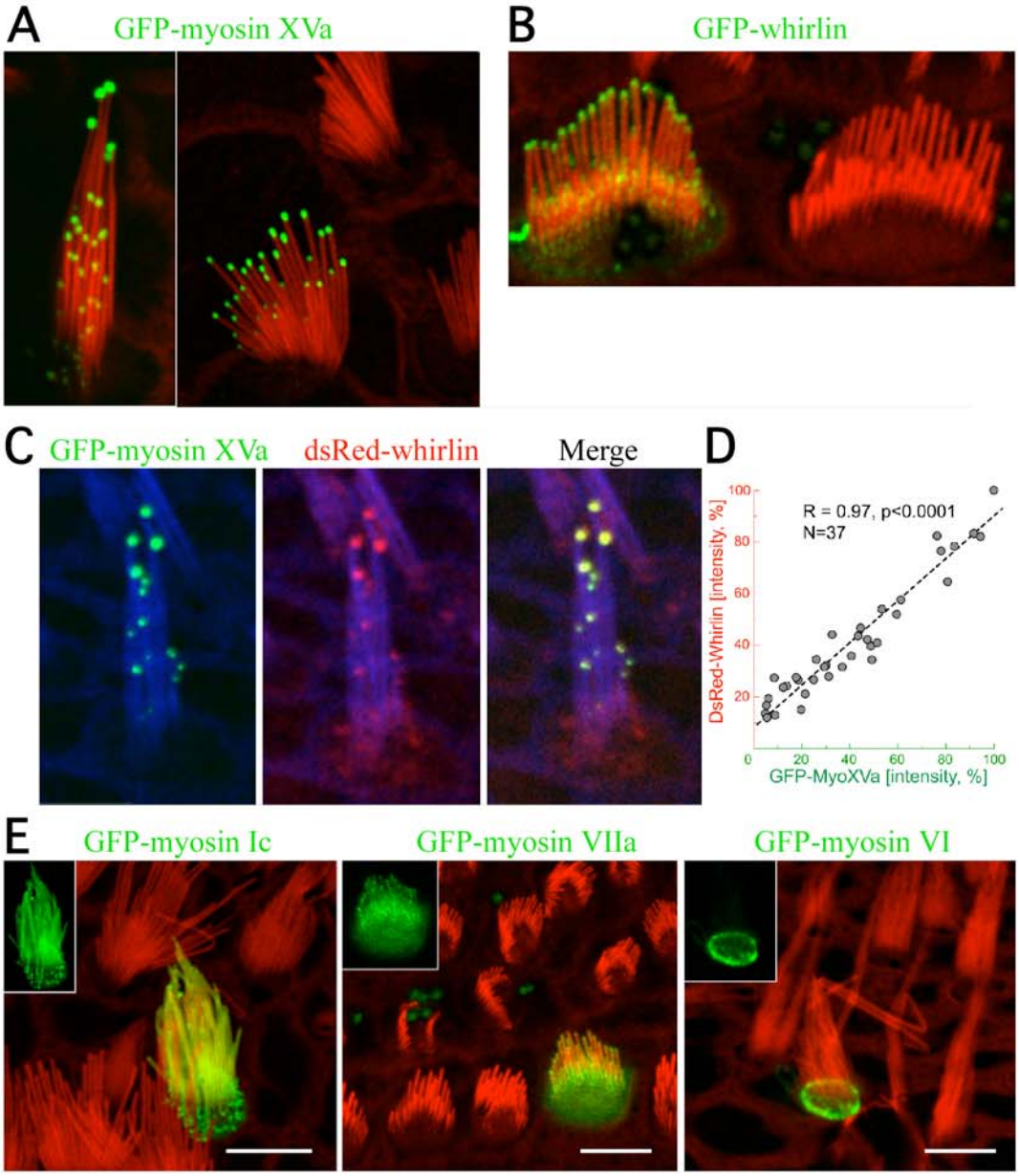

Figure 3-8. Targeting of fluorescently epitope-tagged myosin XVa and whirlin to stereocilia tips of wild type hair cells following Helios gene gun transfection. **(A)** GFP-myosin XVa accumulates at stereocilia tips of mouse wild-type vestibular hair cells after 48 hours of transfection. **(B)** GFP-whirlin at stereocilia tips of rat inner hair cell after 21 hours transfection. Overexpression of GFP-whirlin does not perturb the length of stereocilia bundle relative to a untransfected neighbor hair cell. **(C)** Co-transfection of GFP-myosin XVa and dsRed-whirlin into mouse wild-type vestibular hair cell results in accumulation of both fluorescently epitopes at stereocilia tips. **(D)** Direct proportionality of GFP-myosin XVa and dsRed-whirlin fluorescence in hair cell stereocilia after co-transfection. **(E)** Other transfected myosins fail to only target to stereocilia tips. The actin cytoskeleton is visualized by rhodamine-phalloidin (red) in all panels except panel C, in which it was stained with Alexa Fluor 633 (blue). Scale bars, 5 μm.

When gold bullets, prepared with equal amounts of GFP-myosin XVa and red fluorescent protein tagged (dsRed) whirlin plasmid DNA, were transfected into wild type hair cells, both fluorescently epitope tagged proteins were observed at stereocilia tips (figure 3-8C; Belyantseva et al. 2005). Quantitative analysis of the fluorescence at the tips of stereocilia of different lengths revealed that the amount of dsRed-whirlin was directly proportional to GFP-myosin XVa (figure 3-8D). Intriguingly, the concentration of GFP-myosin XVa and dsRed-whirlin was greater at tips of longer stereocilia than shorter stereocilia within the same cell. Neither the functional significance nor the molecular mechanism that establishes this length dependent gradient of myosin XVa is known. In summary, the co-localization of GFP-myosin XVa and dsRed-whirlin in transfected hair cells was similar to the stereocilia tip localization of endogenous myosin XVa and whirlin.

Other myosins do not localize to stereocilia tips

Because the majority of myosins are plus-end directed motors, it would seem that upon encountering the base of stereocilium, a myosin would translocate along the unidirectional actin filament until it reached the stereocilia tip. Rather than being a general property of all myosins, so far, only myosin XVa specifically localizes to tips of stereocilia. The transfection of mouse GFP-myosin Ic, human GFP-myosin VI, mouse GFP-myosin VIIa and mouse GFP-myosin X into mouse hair cells revealed that none of the myosins specifically localized to stereocilia tips (figure 3-8E and figure 5-14C). GFP-myosin Ic and GFP-myosin VIIa localized along the length of the stereocilia with a slight concentration towards the tips (Belyantseva et al. 2005).

These results were consistent with previously reported localization of endogenous myosin Ic and myosin VIIa in hair cells (Hasson et al. 1997; Rzadzinska et al. 2004).

GFP-myosin VI localized in the pericuticular necklace and was absent from the stereocilia (figure 3-8E; Belyantseva et al. 2005). Our results for myosin VI were similar to localization of endogenous myosin VI in hair cells (Hasson et al. 1997). In transfected hair cells, GFP-myosin X accumulated in the cell body of hair cells and was absent from the stereocilia (figure 5-14C). It is not known whether myosin X is endogenously present within hair cells. The absence of GFP-myosin X from stereocilia was surprising for two reasons. First, myosin X is a plus-end directed motor that accumulates at filopodia tips of transfected epithelial cells similar to myosin XVa. Second, since the myosin X tail, like myosins VIIa and XVa, contains a MyTh4 and FERM domain, it was expected that it would accumulate in stereocilia like myosins VIIa and XVa. Collectively taken, these results suggest that myosin XVa may be the only molecular motor in hair cells that selectively delivers cargo to the tips of stereocilia.

Myosin XVa binds whirlin and transports it to filopodia tips in COS-7 cells

Since filopodia and stereocilia of inner ear hair cells are comprised of parallel, bundled actin filaments that elongate by actin polymerization at their tips, we used COS-7 cells as a cell culture model to demonstrate the interaction of myosin XVa and whirlin. In transfected COS-7 cells, GFP-myosin XVa localized to the tips of filopodia in the absence of whirlin (data not shown; Belyantseva et al. 2003a). To

evaluate whether GFP-myosin XVa could bind dsRed-whirlin and transport it to tips of filopodia, full-length GFP-myosin XVa and dsRed-whirlin cDNA expression constructs were co-transfected into COS-7 cells. Both GFP-myosin XVa and dsRed-whirlin accumulated at filopodia tips of transfected COS-7 cells (figure 3-9B; Belyantseva et al. 2005). Next, dsRed-whirlin was co-transfected with one of two myosin XVa expression constructs containing mutations in the motor (GFP-myosin XVa(C592Y) or GFP-myosinXVa(R167A/G388A). Neither GFP-myosin XVa(C592Y), GFP-myosin XVa(R167A/G388A) nor whirlin was observed at the tips of filopodia (figure 3-9C and data not shown; Belyantseva et al. 2005). The transfection of dsRed-whirlin or GFP-whirlin expression constructs without myosin XVa resulted in no whirlin accumulation at filopodia tips (data not shown). This indicated that whirlin was not transported to filopodia tips by an endogenous myosin present in COS-7 cells. These results indicated that GFP-myosin XVa could interact with dsRed-whirlin, and a functional myosin XVa motor was necessary to transport whirlin to the tips of filopodia.

The presence of a PDZ binding ligand on the carboxy terminus of myosin XVa suggested that it might bind one of whirlin's three PDZ domains. Based upon a classification of PDZ domains (Bezprozvanny et al. 2001), all three PDZ domains of whirlin are class I PDZ domains predicted to specifically bind a class I PDZ ligand such as myosin XVa's class I PDZ binding ligand. In the mouse myosin XVa mutant, *Myo15a*^{sh2J}, the encoded myosin XVa protein has a deletion of the C-terminal 268 amino acids that includes the last four amino acids (I-T-L-L), which encode a class I

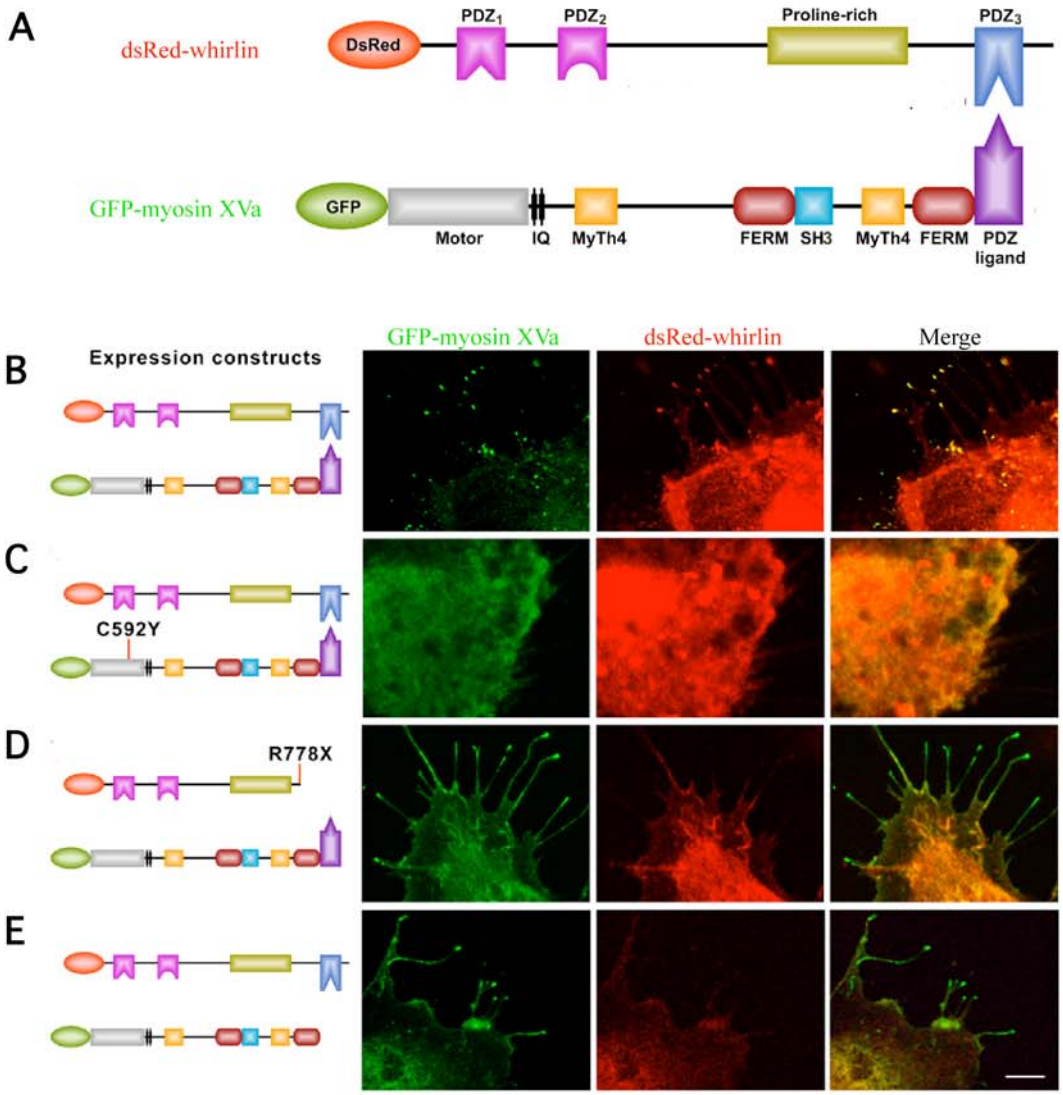

Figure 3-9. Myosin XVa carboxy PDZ ligand interaction with whirlin's PDZ3 domain is required for colocalization in transfected COS-7 cells.
(A) Representation of the wild type dsRed tagged whirlin and GFP tagged myosin XVa and their domains. The carboxy PDZ ligand of myosin XVa binds the third PDZ domain of whirlin. **(B)** Co-transfection of GFP-Myosin XVa (green, left panel) and dsRed-whirlin (red, middle panel) results in the accumulation of both fluorescent signals at filopodia tips of COS-7 cells (merge, right panel).
(C) Co-transfection of GFP-Myosin XVa(C592Y), which contains a mutation in the motor, and dsRed-whirlin results in accumulation in the cell body (right panel). **(D)** GFP-Myosin XVa accumulates at filopodia tips but is unaccompanied by dsRed-whirlin[-PDZ_3], which lacks the third PDZ domain necessary for interaction (right panel). **(E)** GFP-Myosin XVa[-PDZ_L], which lacks the carboxy PDZ ligand, accumulates at filopodia tips but is unaccompanied by dsRed-whirlin (right panel). Scale bar, 10 μm.

PDZ binding ligand. The stereocilia of *Myo15a*^{sh2J} auditory and vestibular hair cells are short and fail to form a staircase structure, similar to *Myo15a*^{sh2} and *whirler*^{wi} short stereocilia phenotypes (Anderson et al. 2000; Holme et al. 2002; Belyantseva et al. 2003a; Belyantseva et al. 2005). In humans, a nonsense mutation, Q3492X that eliminates the carboxy 36 amino acids, is associated with deafness (Nevra Nal, unpublished data). Underscoring its importance, the C-terminal PDZ ligand of myosin XVa is conserved in human, mouse, rat, dog, frog, pufferfish and zebrafish. In deaf individuals of the Israeli family segregating the R778X allele and homozygous whirler mice, the loss of the third PDZ domain of whirlin is the common molecular denominator, which suggested that the third PDZ domain of whirlin might interact with carboxy-terminal PDZ binding ligand of myosin XVa.

To test this hypothesis, the interaction of myosin XVa lacking the PDZ ligand and whirlin missing its third PDZ domain were evaluated in COS-7 cells. A whirlin cDNA expression construct lacking the third PDZ domain (dsRed-whirlin[-PDZ_3]), equivalent to the previously reported human whirlin R778X mutant allele was generated (Mburu et al. 2003). DsRed-whirlin[-PDZ_3] remained in the cell body and failed to co-localize with GFP-myosin XVa at filopodia tips in co-transfected COS-7 cells (figure 3-9D). This result suggested that the third PDZ domain of whirlin was necessary for the interaction with myosin XVa. In the reciprocal experiment, GFP-myosin XVa[-PDZ_L] expression construct, which encodes 2302 amino acids out of 2306 amino acids except for the last four amino acids encoding a class I PDZ ligand, was co-transfected with dsRed-whirlin into COS-7 cells. Accumulation of GFP-

myosin XVa[-PDZ_L] at filopodia tips was observed, however it was not accompanied by dsRed-whirlin, which remained in the cell body (figure 3-8E). These results indicated that the PDZ binding ligand of myosin XVa and the third PDZ domain of whirlin were necessary for localization of whirlin at filopodia tips.

Myosin XVa and whirlin move concurrently in COS-7 cells

Live cell imaging was used to demonstrate that whirlin was cargo of myosin XVa in COS-7 cells. When GFP-myosin XVa and dsRed-whirlin were co-transfected into COS-7 cells, simultaneous accumulation of green and red fluorescence at filopodia tips was observed (Belyantseva et al. 2005). We were unable to detect individual molecules or small patches of green and red fluorescence moving together towards filopodia tips. GFP-myosin XVa may move as a single molecule or in small numbers that are below the threshold detection limit of our instruments. In contrast, patches of GFP-myosin X are observed in live cell imaging moving along the filopodia towards tips (Berg et al. 2002).

Retrograde movement of GFP-myosin XVa and dsRed-whirlin moving synchronously together towards the cell body was observed (Belyantseva et al. 2005). In cells co-transfected with GFP-myosin XVa and dsRed-whirlin[-PDZ_3], GFP-myosin XVa accumulated alone at the tips of filopodia and relocated in patches towards the cell body unaccompanied by dsRed-whirlin[-PDZ_3], which remained in the cell body. Identical results were obtained by the co-transfection of GFP-myosin XVa[-PDZ_L] and dsRed-whirlin, further confirming the necessity of the PDZ ligand

of myosin XVa and the third PDZ domain for localization of whirlin at filopodia tips. However, we can not exclude the possibility that an intermediate adaptor protein simultaneously binds the third PDZ domain of whirlin and PDZ ligand of myosin XVa. Such a hypothetical intermediate adaptor protein would need to be present in both inner ear hair cells and COS-7 cells, which do not endogenously express myosin XVa (Belyantseva et al. 2003a). To distinguish between these two possibilities, the interaction between myosin XVa and whirlin could be studied in the following manner. First, whirlin protein would be purified to homogeneity. Biotinylated whirlin would be immobilized on streptavidin-biosensor chips, and binding rates with purified myosin XVa would be measured by surface plasmon resonance (Han et al. 2006, Klaavuniemi et al. 2004 and Marfatia et al. 1997). The binding of myosin XVa to whirlin would indicate a direct interaction between the two proteins.

Other myosins do not transport whirlin to filopodia tips in COS-7 cells

To determine if whirlin could be a cargo of other unconventional myosins, dsRed-whirlin was co-transfected into COS-7 cells with either mouse GFP-myosin Ic, human GFP-myosin VI, mouse GFP-myosin VIIa, mouse GFP- myosin VIIb or mouse GFP-myosin X. In co-transfected COS-7 cells, GFP-myosin Ic was distributed along the length of the filopodia and concentrated at the filopodia tips, but it was not accompanied by dsRed-whirlin (figure 3-10A; Belyantseva et al. 2005). GFP-myosin VI was not targeted to tips of filopodia and no co-localization with dsRed-whirlin was observed (figure 3-10A; Belyantseva et al. 2005). GFP-myosin VIIa was distributed along the length of filopodia but was not concentrated nor colocalized with whirlin at

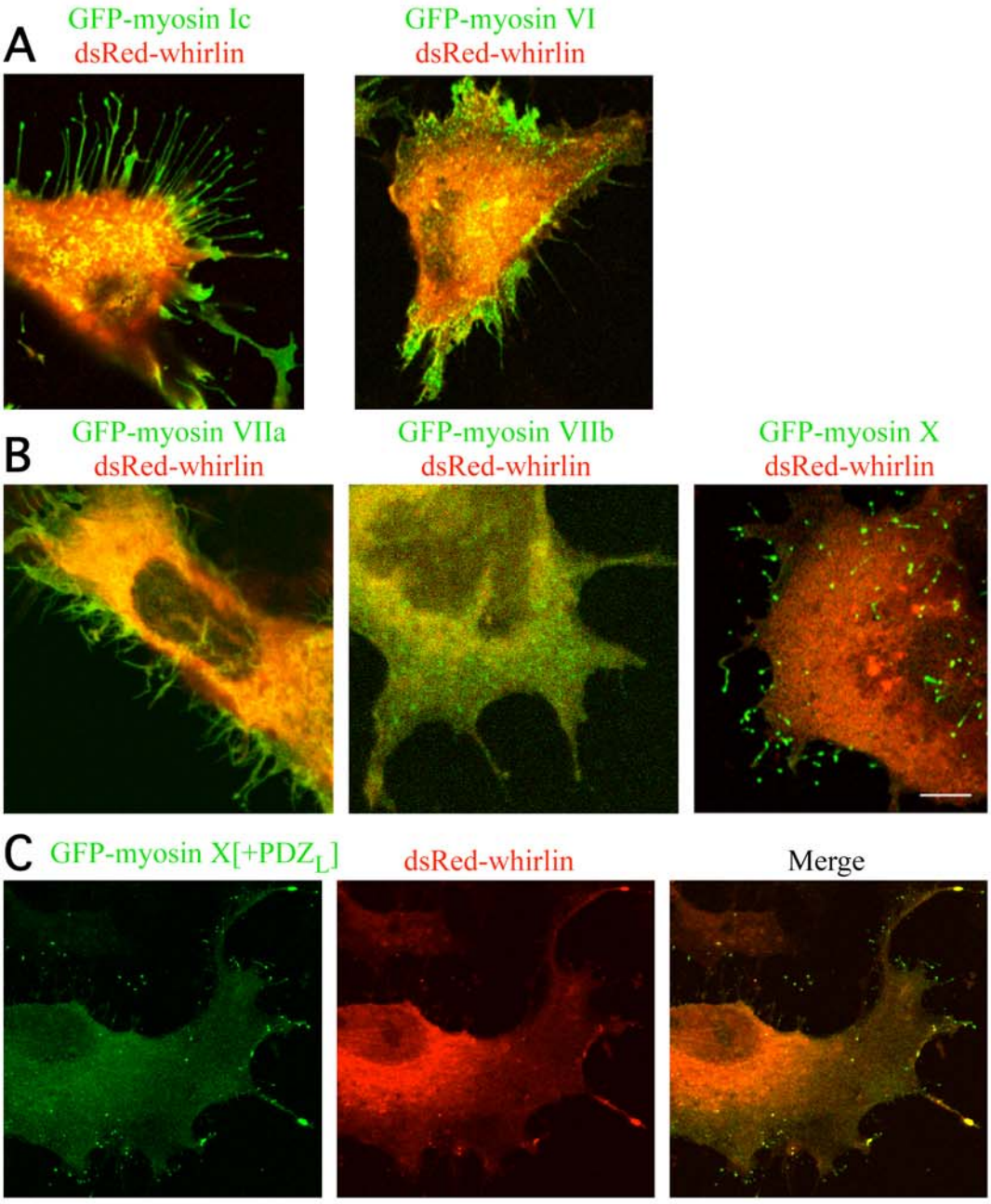

Figure 3-10. Other unconventional myosins do not transport whirlin to filopodia tips of transfected COS-7 cells. **(A)** Co-transfection of COS-7 cells with either GFP-myosin Ic (left panel) or GFP-myosin VI (right panel) revealed no co-localization of these myosins with dsRed-whirlin in filopodia.
(B) Co-transfection of COS-7 cells with either GFP-myosin VIIa (left panel), GFP-myosin VIIb (middle panel) or GFP-myosin X (right panel) revealed no co-localization of these myosins with dsRed-whirlin in filopodia.
(C) Co-transfection of GFP-myosin X[+PDZ_L], containing the myosin XVa PDZ ligand inserted at the carboxy terminus (green, left panel), and dsRed-whirlin (red, middle panel) resulted in the accumulation of both fluorescent signals at filopodia tips of COS-7 cells (merge, right panel). Scale bar, 10 μm.

filopodia tips (figure 3-10B; Belyantseva et al. 2005). GFP-myosin VIIb was uniformly distributed throughout the cytoplasm and filopodia and did not specifically co-localize with dsRed-whirlin (figure 3-10B). In co-transfected COS-7 cells, GFP-myosin X was concentrated at filopodia tips but was not accompanied by dsRed-whirlin (figure 3-10B; Belyantseva et al. 2005). Our GFP-myosin X results were consistent with previous reports that demonstrated that endogenous and GFP tagged bovine myosin X target to filopodia tips of CPAE, HeLa and COS-7 cells (Berg et al. 2002; Belyantseva et al. 2005). These data indicate that whirlin is not a promiscuous cargo of unconventional myosins, but binds selectively to the PDZ ligand of myosin XVa for transport to the tips of filopodia.

Myosin X with added PDZ ligand delivers whirlin to filopodia tips

If the C-terminal four amino acids (I-T-L-L) that form the PDZ ligand of myosin XVa were the sole determinant of binding to the third PDZ domain of whirlin, then a GFP-myosin X construct with the myosin XVa PDZ binding ligand added at the C-terminus should deliver whirlin to filopodia tips. The last twelve base pairs of cDNA encoding the four amino acid PDZ binding ligand of myosin XVa was added to a mouse full-length myosin X expression construct (GFP-myosin X [+PDZ_L]). In COS-7 cells co-transfected with GFP-myosin X [+PDZ_L] and dsRed-whirlin, both GFP-myosin X [+PDZ_L] and whirlin protein accumulated at tips of some filopodia within a cell (figure 3-10C). It should be noted that the delivery of whirlin to filopodia tips by GFP-myosin X [+PDZ_L]) was less efficient than the delivery by GFP-myosin XVa. Nonetheless, this experiment indicated that the myosin XVa PDZ binding ligand is

both sufficient and necessary for the interaction with whirlin and delivery of it to tips of filopodia.

Re-initiation of stereocilia elongation and staircase formation in transfected hair cells

The stereocilia bundles of homozygous *Myo15a*^{sh2} and *whirler*^{wi} auditory and vestibular hair cells are properly positioned but are abnormally short and fail to form the characteristic staircase structure found in wild type hair cells. This indicated that myosin XVa and whirlin are not required for the emergence, initial elongation or increase in thickness of stereocilia within the hair bundle. To determine if myosin XVa contributed to elongation and staircase formation of stereocilia by delivering whirlin, homozygous *Myo15a*^{sh2} auditory and vestibular hair cells were transfected with GFP-myosin XVa. We observed re-initiation of elongation and staircase formation of stereocilia in transfected *Myo15a*^{sh2} hair cells. After 48 hours, the stereocilia of inner hair cells within the organ of Corti were approximately two-fold longer than neighboring non-transfected hair cells, and developed staircase architecture similar to wild type inner hair cells (figure 3-11A; Belyantseva et al. 2005). Elongation and partial restoration of the stereocilia bundle was observed in mouse *Myo15a*^{sh2} vestibular hair cells after 43 hours of transfection (figure 3-11B). An apparent restoration of stereocilia staircase architecture was observed in transfected *Myo15a*^{sh2} vestibular hair cells after 67 hours of transfection (figure 3-11C). Over-elongation of the stereocilia bundle was not observed, suggesting that an excessive amount of myosin XVa did not perturb the regulated process of stereocilia elongation and staircase formation. In addition to the restoration of stereocilia

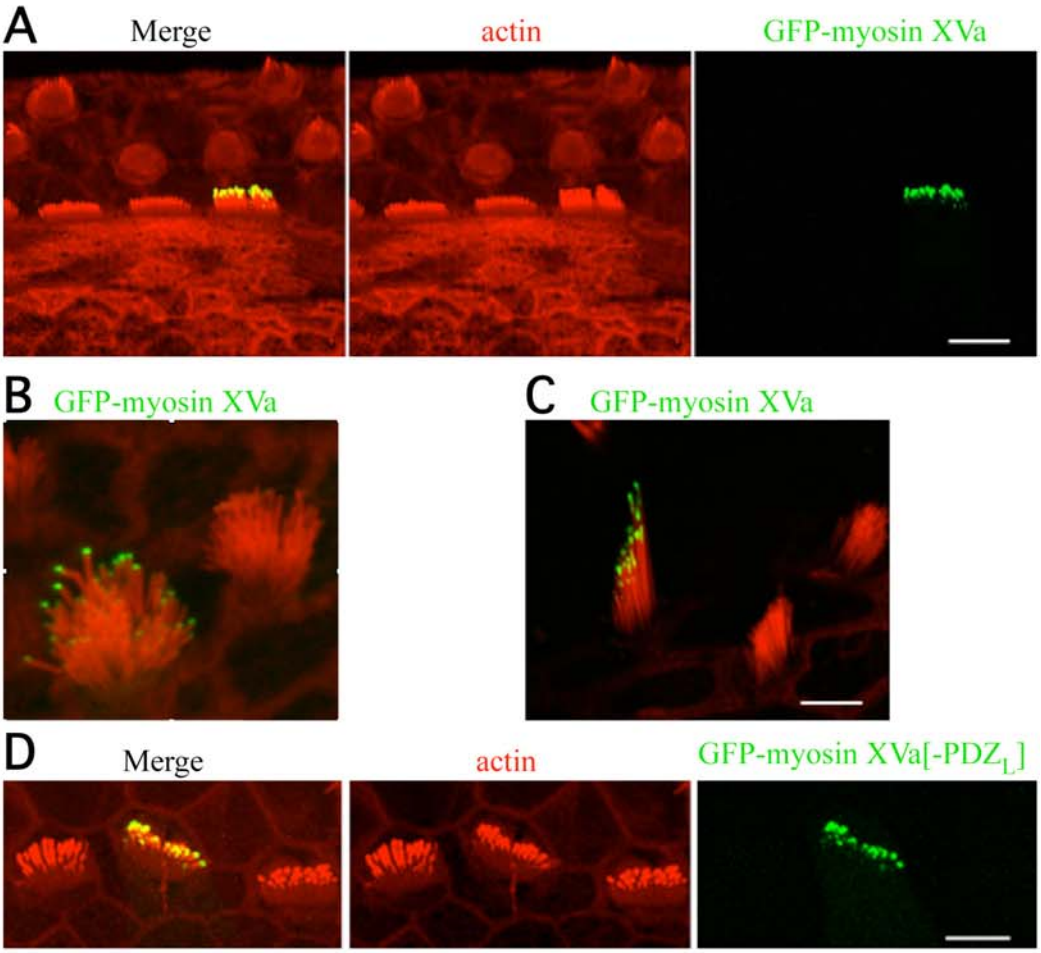

Figure 3-11. GFP-myosin XVa causes elongation and staircase formation of stereocilia bundles in transfected *Myo15a*^{sh2} hair cells. **(A)** The stereocilia of a transfected *Myo15a*^{sh2} organ of Corti inner hair cell is approximately two-fold longer than neighboring non-transfected hair cells after 48 hours of transfection. The stereocilia bundle of the transfected hair cell has developed staircase architecture similar to wild type inner hair cells. **(B)** Re-initiation of stereocilia elongation and staircase bundle formation in mouse *Myo15a*^{sh2} utricle hair cell after 43 hours of transfection. **(C)** Restoration of the staircase shape of a stereocilia bundle of a transfected mouse *Myo15a*^{sh2} utricle hair cell after 67 hours of transfection. The average height of stereocila bundles: control homozygous *Myo15a*^{sh2} cells, 2.9 ± 0.6 µm , n = 24; transfected cells: 7.3 ± 2.2 µm , n = 12; normal stereocilia bundles of heterozygous *Myo15a*^{sh2} cells: 9.6 ± 1.5 µm , n = 22; student *t*-test $p<0.00001$. **(D)** GFP-myosin XVa[-PDZ$_L$], which lacks the carboxy PDZ ligand, fails to re-initiate elongation or develop a staircase architecture in transfected *Myo15a*^{sh2} organ of Corti inner hair cells although it accumulated at apices of stereocilia. The average height of stereocila bundles: control homozygous *Myo15a*^{sh2} cells, 2.9 ± 0.6 µm , n =24; transfected cells: 2.8 ± 0.7 µm , n =6; student *t*-test $p>0.5$. The actin cytoskeleton is visualized by rhodamine-phalloidin (red) in all panels. Scale bars, 5 µm.

staircase architecture, supernumerary rows of stereocilia were reabsorbed on the apical cell surface, consistent with the normal process of stereocilia bundle maturation. The transfection of GFP- myosin XVa[-PDZ_L], which lacked the C-terminal PDZ ligand, into *Myo15a*^{sh2} hair cells did not promote stereocilia elongation and staircase formation, however it concentrated at the tips of all short stereocilium (figure 3-11D).

Next we wished to determine whether stereocilia architecture restoration was due to exogenous myosin XVa transporting endogenous whirlin to stereocilia tips. *Myo15a*^{sh2} hair cells transfected with GFP-myosin XVa and stained with anti-whirlin antibody showed that GFP-myosin XVa bound and transported endogenous whirlin to the stereocilia tips, thereby enabling stereocilia elongation and staircase formation (figure 3-12A). In *Myo15a*^{sh2} hair cells transfected with GFP-myosin XVa[-PDZ_L] and stained with anti-whirlin antibody, endogenous whirlin remained in the cell body and did not colocalize with GFP-myosin XVa[-PDZ_L] at stereocilia tips (figure 3-12B). While the deletion of the PDZ ligand of myosin XVa abolished the interaction with whirlin, the presence GFP-myosin XVa[-PDZ_L] at stereocilia tips implies its localization was not influenced by its interaction with whirlin. In control experiments, full-length mouse GFP-myosin Ic and GFP-myosin VIIa were transfected into *Myo15a*^{sh2} hair cells. While GFP-myosin Ic and GFP-myosin VIIa were distributed along the length of abnormally short stereocilia of *Myo15a*^{sh2} hair cells, neither myosin stimulated restoration of stereocilia elongation and staircase formation (data not shown). When GFP-whirlin was transfected into *Myo15a*^{sh2} hair cells, whirlin

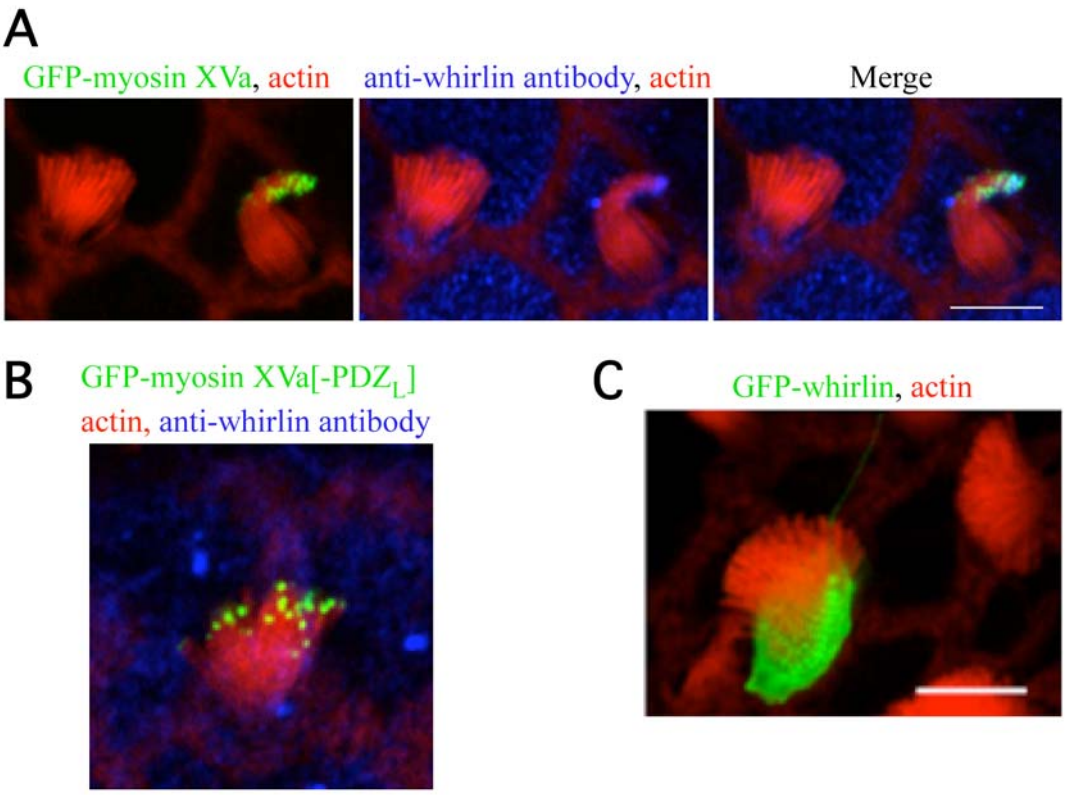

Figure 3-12. Delivery of endogenous whirlin to stereocilia tips by GFP-myosin XVa is essential to re-initiation of elongation and staircase formation in transfected *Myo15a^{sh2}* hair cells. **(A)** GFP-Myosin XVa (green, left panel) binds and transports endogenous whirlin (blue, middle panel) to stereocilia tips of transfected *Myo15a^{sh2}* vestibular hair cell (merged image, right panel). There is no anti-whirlin immunoreactivity in the stereocilia of a neighboring non-transfected hair cell. **(B)** GFP-myosin XVa lacking the PDZ ligand accumulates at apices of stereocilia but does not tranport endogenous whirlin to the tips. No stereocilia elongation or staircase formation is observed in the transfected *Myo15a^{sh2}* vestibular hair cell. **(C)** Over-expression of GFP-whirlin in a transfected *Myo15a^{sh2}* vestibular hair cell does not result in transport of whirlin to tips nor restoration of stereocilia bundle defects. The actin cytoskeleton is visualized by rhodamine-phalloidin (red) in all panels. Scale bars, 5 µm.

remained in the cell body and no restoration of stereocilia architecture was observed (figure 3-12C). This result suggests that regardless of the steady state levels of whirlin within a hair cell, functional myosin XVa is required for delivery of whirlin to

stereocilia tips. Our results demonstrate that stereocilia elongation and staircase formation occurs only when myosin XVa delivers whirlin to stereocilia tips.

The transfection of GFP-whirlin into *whirler*^{wi} hair cells restored the stereocilia bundle length and staircase architecture similar to wild type inner hair cells (figures 3-13A). The over-expression of GFP-whirlin in *whirler*^{wi} hair cells did not cause stereocilia over-elongation, suggesting that whirlin is a component of a regulated process of stereocilia elongation and staircase formation. Co-localization of GFP-whirlin and whirlin antisera at stereocilia tips of transfected *whirler*^{wi} hair cells was observed (figure 3-13B). No anti-whirlin immunoreactivity was observed in the stereocilia tips of neighboring non-transfected cells.

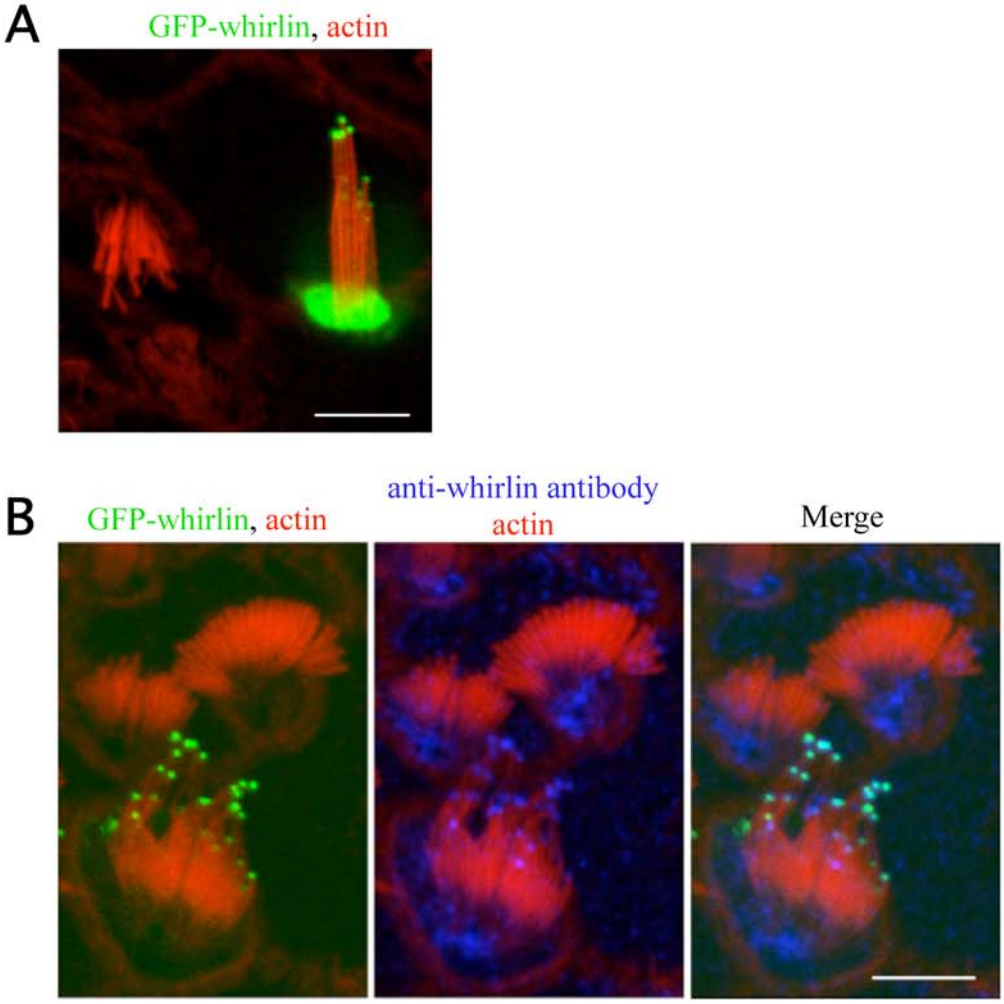

Figure 3-13. GFP-whirlin causes elongation and staircase formation of stereocilia bundles in transfected *whirler*^{wi} hair cells. **(A)** Restoration of the staircase shape of a stereocilia bundle of a transfected mouse *whirler*^{wi} saccule hair cell after 48 hours of transfection. The average height of stereocila bundles: control homozygous *whirler*^{wi} cells, 3.1 ± 0.5 µm , n = 37; transfected cells: 7.0 ± 1.9 µm , n =18; normal stereocilia bundles of heterozygous *whirler*^{wi} cells: 9.5 ± 1.4 µm , n =21; student *t*-test $p<0.00001$. **(B)** Co-localization of GFP-whirlin (green, left panel) and anti-whirlin antibody staining (blue, middle panel) in a at the stereocilia tips of a transfected *whirler*^{wi} vestibular hair cell (merge, right panel). No anti-whirlin immunoreactivity is observed at stereocilia tips of neighboring non-transfected hair cells. The actin cytoskeleton is visualized by rhodamine-phalloidin (red) in all panels. Scale bars, 5 µm.

Discussion

Other interpretations of the myosin XVa and whirlin interaction

In this chapter, I demonstrated the *in vivo* interaction of the myosin XVa carboxy-terminal PDZ ligand with the third PDZ domain of whirlin in transfected COS-7 and inner ear hair cells. We interpret our data to indicate that once whirlin is bound as cargo, myosin XVa transports and delivers whirlin to filopodia tips of COS-7 cells and to stereocilia tips of inner ear hair cells. Disruption of the interaction, either by deletion of carboxy-terminal PDZ ligand of myosin XVa or the third PDZ domain of whirlin, eliminated delivery of whirlin to filopodia and stereocilia tips.

Contemporaneously with the publication of our results (Belyantseva et al. 2005); the interaction of myosin XVa and whirlin was reported by two other groups (Delprat et al. 2005; Kikkawa et al. 2005). In contrast to our findings that myosin XVa's PDZ ligand interacted with the third PDZ domain of whirlin (figure 3-14A), Delprat and colleagues (2005) reported that other regions of the myosin XVa and whirlin proteins mediated this interaction (Delprat et al. 2005). Using *in vitro* binding assays, Delprat (2005) concluded that the $MyTh4_2/FERM_2$ region of myosin XVa bound the first and second PDZ domains of full-length whirlin (figure 3-14B). The PDZ ligand of myosin XVa was not necessary for the interaction between myosin XVa and whirlin. If true, then the interaction between myosin XVa and whirlin should not be affected by the whirler mutation in which a translational frameshift truncates whirlin prior to the proline-rich and third PDZ domains.

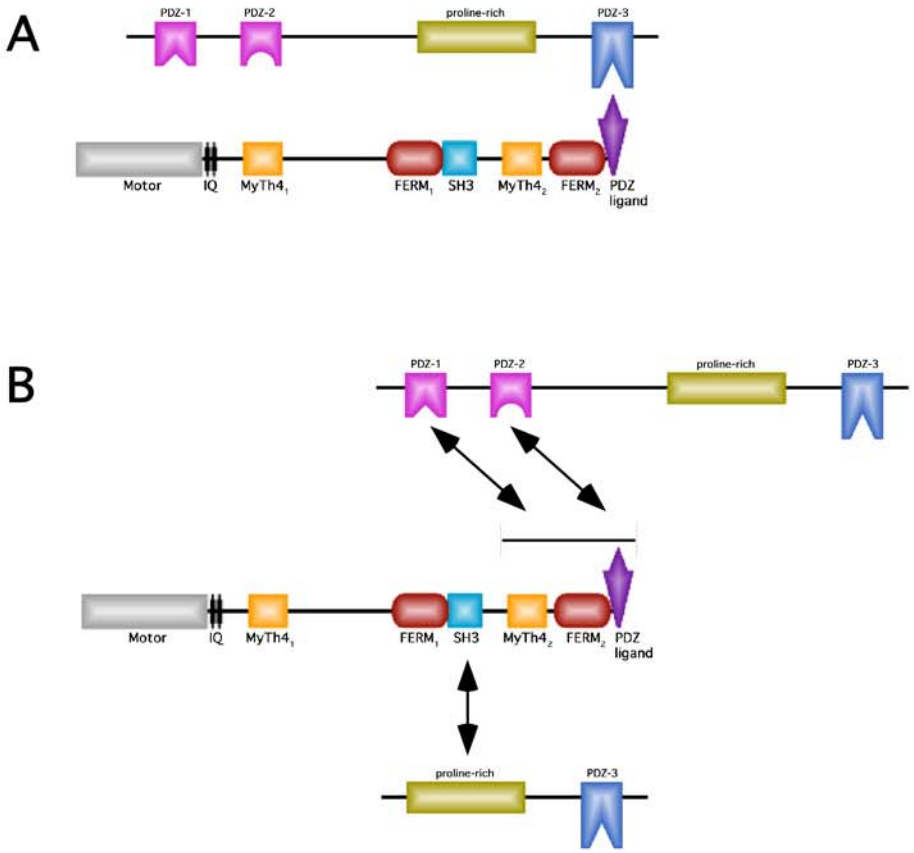

Figure 3-14. A comparison of the regions necessary for the interaction of myosin XVa and whirlin reported by Belyantseva et al. 2005 and Delprat et al. 2005. **(A)** The carboxyl terminal PDZ ligand of myosin XVa binds the third PDZ domain of whirlin (Belyantseva et al. 2005). Disruption of the interaction by the deletion of either the PDZ ligand in myosin XVa or the third PDZ domain in whirlin resulted in a failure of the two proteins to co-localize at filopodia tips of transfected COS-7 cells. Myosin XVa lacking the PDZ ligand was unable to transport whirlin to stereocilia tips in transfected *Myo15a*^{sh2} hair cells. **(B)** The MyTh4$_2$/FERM$_2$ region of myosin XVa presumably binds both the first and second PDZ domains of whirlin (Delprat et al. 2005). Evidence of the interaction was obtained using an *in vitro* GST binding assay. The authors reported that the myosin PDZ ligand was not necessary for the interaction. Using an *in vitro* GST binding assay, Delprat (2005) reported that the SH3 domain of myosin XVa binds the proline-rich region of whirlin of a whirlin isoform comprised of the proline-rich and third PDZ domain. The putative interacting regions of myosin XVa and whirlin were not assayed in an *in vivo* system such as co-localization at filopodia tips of transfected COS-7 cells.

However, in mouse *whirler*^{wi} hair cells, whirlin is absent from stereocilia tips while myosin XVa is present at apices of stereocilia. Thus, the subcellular localization of whirlin in mouse *whirler*^{wi} hair cells argues against a strong molecular interaction proposed by Delprat (2005) that is sufficient to allow myosin XVa to bind the truncated whirlin protein as cargo and deliver it to stereocilia tips.

Delprat (2005) also inferred by *in vitro* binding assays, that the SH3 domain of myosin XVa bound the proline-rich region of a whirlin isoform lacking the first and second PDZ domains (figure 3-14B). But the authors failed to experimental test their premise in either an *in vitro* or *in vivo* assay. In addition, their *in vitro* binding assay has technical problems. The authors concluded that a region of myosin XVa containing SH3 and MyTh4$_2$ domains bound an isoform of whirlin containing the proline-rich and third PDZ domains. However, the region of myosin XVa containing SH3 and MyTh4$_2$ domains also bound to GST resin alone. The intensity of the band observed for the putative myosin XVa SH3/MyTh4$_2$ region and whirlin interaction was approximately four fold stronger than the non-specific binding of myosin XVa SH3/MyTh4$_2$ region to GST resin alone. Delprat (2005) was unable to demonstrate an interaction between the tail of myosin XVa, which included the MyTh4$_1$, FERM$_1$, SH3, MyTh4$_2$, FERM$_2$ domains and PDZ ligand, and the full-length whirlin protein in either a GST pull-down assay or after immunoprecipitation of extracts from co-transfected cells. These results conflicted with filopodia tip co-localization of myosin XVa and full-length and partial whirlin in transfected COS-7 cells demonstrated by Delprat (2005) as well as by my work (Belyantseva et al. 2005; Delprat et al. 2005).

A primary drawback of using small partial fragments of proteins to resolve interacting regions is that the small protein fragments may fail to fold into their native conformation in the absence of their neighboring protein domains and/or may promiscuously bind to other protein domains. Thus, regions of myosin XVa and whirlin interaction predicted from *in vitro* binding assays need to be tested in an *in vivo* cellular environment using full-length proteins or nearly full-length proteins containing disablements or domain deletion that disrupt predicted interacting regions.

Our results of the filopodia tip co-localization assay in COS-7 cells disprove that the $MyTh4_2/FERM_2$ region of myosin XVa interacts with the first and second PDZ domains of full-length whirlin reported by Delprat (2005). In co-transfected COS-7 cells, both Delprat (2005) and I reported that full-length myosin XVa and whirlin accumulated at filopodia tips (figures 3-9B and 3-15A; Belyantseva et al. 2005; Delprat et al. 2005). When myosin XVa[$-PDZ_L$], which lacked the carboxy four amino acid PDZ ligand, was co-transfected into COS-7 cells with full-length whirlin, myosin XVa[$-PDZ_L$] accumulated at filopodia tips but was unaccompanied by whirlin (figures 3-9E and 3-15B; Belyantseva et al. 2005). In the reciprocal experiment, co-transfection of full-length myosin XVa with whirlin lacking the third PDZ domain resulted in accumulation of myosin XVa at filopodia tips but it was unaccompanied by whirlin (figures 3-9D and 3-15C; Belyantseva et al. 2005). Deletion of myosin XVa's PDZ ligand or whirlin's third PDZ domain was sufficient to prevent transport of whirlin to filopodia tips. The $MyTh4_2/FERM_2$ region of myosin XVa and whirlin's

	COS-7 filopodia tip localization	Reference
A 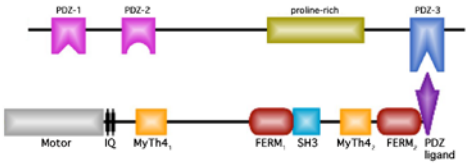	yes yes	Belyantseva et al. 2005 Delprat et al. 2005
B 	no yes	Belyantseva et al. 2005
C 	no yes	Belyantseva et al. 2005
D 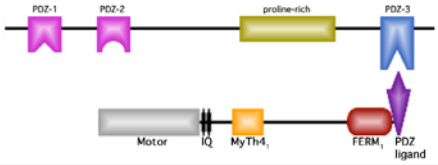	yes yes	Boger, unpublished
E 	yes yes	Delprat et al. 2005
F 	not tested yes	
G 	not tested yes	
H 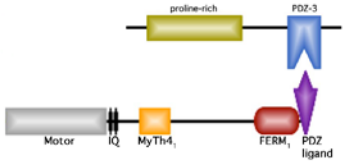	not tested yes	

Figure 3-15

Figure 3-15. A summary of the filopodia tip localization results of multiple pairs of myosin XVa and whirlin expression constructs in transfected COS-7 cells reported by Belyantseva et al. 2005 and Delprat et al. 2005. **(A)** Full-length myosin XVa and full-length whirlin co-localize at filopodia tips of transfected COS-7 cells. **(B)** Deletion of the carboxy four amino acid PDZ ligand of myosin XVa or **(C)** the third PDZ domain of whirlin results in a failure to accumulate at filopodia tips. **(D)** Myosin XVa lacking the SH3, $MyTh4_2$ and $FERM_2$ domains co-localized with whirlin at filopodia tips. **(E)** Co-localization at filopodia tips of myosin XVa and whirlin lacking the first and second PDZ domains was reported. **(F)** Proposed experiment to determine if myosin XVa lacking the SH3 domain can co-localize at filopodia tips with a whirlin isoform lacking first and second PDZ domains. **(G)** Proposed experiment to determine if full-length myosin XVa can co-localize at filopodia tips with a whirlin deletion construct comprised of only the third PDZ domain. **(H)** Proposed experiment to determine if myosin XVa lacking the SH3, $MyTh4_2$ and $FERM_2$ domains can co-localize at filopodia tips with a whirlin isoform lacking first and second PDZ domains.

first and second PDZ domains although present, were not able to interact sufficiently to allow the transport of whirlin to filopodia tips by myosin XVa. In another experiment, myosin XVa[-SH3,-$MyTh4_2$,-$FERM_2$] transported full-length whirlin to filopodia tips (figure 3-15D; Belyantseva et al. 2005). The ability of myosin XVa[-SH3,-$MyTh4_2$,-$FERM_2$,+PDZ_L], which contains the PDZ ligand at the carboxy terminus, to transport whirlin to filopodia tips despite lacking the SH3, $MyTh4_2$ and $FERM_2$ domains, appears to refute Delprat's (2005) conclusion that the $MyTh4_2$/$FERM_2$ region of myosin XVa bound the first and second PDZ domains of whirlin. Collectively, our results in COS-7 cells (figures 3-15A, B, C and D) demonstrate the myosin XVa's $MyTh4_2$ and $FERM_2$ domains are not sufficient to interact with whirlin's first and second PDZ domains to permit delivery of whirlin to filopodia tips by myosin XVa in an *in vivo* environment. However, we cannot rule out the possibility that the interaction between myosin XVa $MyTH4_2$/$FERM_2$ region

whirlin's first and second PDZ domains stabilizes the interaction between the two proteins at filopodia and stereocilia tips after the delivery of whirlin by myosin XVa.

Delprat (2005) reported that myosin XVa's SH3 domain interacted with the proline-rich region of an isoform of whirlin containing the proline-rich and third PDZ domains. In transfected COS-7 cells, full-length myosin XVa transported partial whirlin product comprised of the proline-rich and third PDZ domain to filopodia tips (figure 3-15E; Delprat et al. 2005). To evaluate this putative interaction, I propose the following three experiments in transfected COS-7 cells. First, I will co-transfect myosin XVa[-SH3], which lacks the SH3 domain, and partial whirlin product into COS-7 cells (figure 3-15F). If the SH3 domain is critical to the interaction, then myosin XVa[-SH3] should accumulate at filopodia tips unaccompanied by whirlin. Next, I will co-transfect full-length myosin XVa with a whirlin deletion protein comprised of only the third PDZ domain (figure 3-15G). If the proline-rich region is critical to the interaction, then myosin XVa[-SH3] should accumulate at filopodia tips unaccompanied by whirlin. Finally I will co-transfect myosin XVa[-SH3,-MyTh4$_2$,-FERM$_2$] and partial whirlin product into COS-7 cells (figure 3-15H). If accumulation of myosin XVa[-SH3,-MyTh4$_2$,-FERM$_2$] and partial whirlin is observed at filopodia tips, it will suggest that the SH3 domain and proline-rich regions does not mediate a strong interaction of myosin XVa and whirlin in an *in vivo* cellular environment. The proposed experiments in COS-7 cells will directly test whether myosin XVa's SH3 domain interacts with the proline-rich region of whirlin. Resolving the domains required for myosin XVa and whirlin interaction to permit delivery of whirlin to

filopodia tips would allow future investigations to focus on putative protein partners of the remaining domains of myosin XVa and whirlin.

Passive diffusion of whirlin to stereocilia tips

Rather than myosin XVa delivering whirlin to stereocilia and filopodia tips, an alternate explanation is that whirlin diffuses to stereocilia and filopodia tips where it interacts with myosin XVa. At this time, I have no evidence that directly refutes the possibility of whirlin diffusing to stereocilia and filopodia tips. In our live cell imaging of COS-7 cells co-transfected with GFP-myosin XVa and dsRed-whirlin, the simultaneous accumulation of green and red fluorescence at filopodia tips was observed, consistent with the delivery of whirlin by myosin XVa. We were unable to detect individual molecules or small patches of green and red fluorescence moving together towards filopodia tips, although synchronous retrograde flow of myosin XVa and whirlin was observed. GFP-myosin XVa may move as a single molecule or in small numbers that are below the threshold detection limit of our instruments suggesting that a more sensitive method of detection is needed.

To determine whether GFP-myosin XVa and dsRed-whirlin move together along actin filaments, I propose using total internal reflection fluorescence microscopy (TIRF). TIRF microscopy allows the visualization of single-fluorophores in living cells (Sako and Uyemura 2002; Schneckenburger 2005). First, I would attempt to visualize GFP-myosin XVa and dsRed-whirlin moving concurrently *in vitro* on actin filaments. Next, I would attempt to visualize GFP-myosin XVa and dsRed-whirlin

moving concurrently *in vivo* towards filopodia tips in transfected COS-7 cells. If we obtained evidence of GFP-myosin XVa and dsRed-whirlin moving together along actin filaments, this would provide strong evidence for delivery of whirlin by myosin XVa.

Several observations indirectly suggest that the passive diffusion of whirlin to stereocilia tips does not occur. Our anti-whirlin antiserum revealed that endogenous whirlin is present in two subcellular locations in wild type hair cells. Whirlin is present at stereocilia tips and at the base of the stereocilia where stereocilia emerge from the cuticular plate. At tips of stereocilia, co-localization of endogenous whirlin and myosin XVa is observed while no myosin XVa immunoreactivity is observed at the base of stereocilia. The function of whirlin at the base of stereocilia is unknown. Whirlin may assemble a macromolecular complex that performs an essential function at the stereocilia base or perhaps whirlin awaits the arrival of myosin XVa to be loaded as cargo for transport to the stereocilia tips much like a passenger at a train station awaiting their train's arrival.

In shaker 2 mice, endogenous myosin XVa and whirlin are absent from the tips of the abnormally short stereocilia of *Myo15a*^{sh2} hair cells however whirlin is present at the base of stereocilia. Transfection of GFP-whirlin into *Myo15a*^{sh2} hair cells does not result in accumulation of whirlin at stereocilia tips nor along the length of stereocilia despite the over-expression of whirlin (figure 3-12C; Belyantseva et al. 2005). High levels of GFP-whirlin are observed at the base of stereocilia of transfected *Myo15a*^{sh2}

hair cells relative to the endogenous whirlin in wild type hair cells. The height of inner and outer *Myo15a*^{sh2} inner and outer hair cell stereocilia are 21% and 14%, respectively, the height of wild type stereocilia (Mustapha et al. 2006, in press). However, I did not observe GFP-whirlin along the length of these short stereocilia in transfected *Myo15a*^{sh2} hair cells. In contrast, transfection of GFP alone, containing no cDNA insert, results in accumulation of GFP along the entire length of stereocilia in wild type and *Myo15a*^{sh2} hair cells. Given the observation that *Myo15a*^{sh2} hair cells are capable of mechanotransduction (Stepanyan et al. 2006), this suggests that protein components of the mechanotransduction complex and tip links are present at stereocilia tips; dispelling the notion that proteins are incapable of accumulating at stereocilia tips of *Myo15a*^{sh2} hair cells. Over-expressed GFP-whirlin was not observed along the length of abnormally short stereocilia of *Myo15a*^{sh2} hair cells (figure 3-12C; Belyantseva et al. 2005) which is inconsistent with a passive diffusion of whirlin to stereocilia tips.

***In vivo* assay system**

In mice, the failure to deliver whirlin to inner ear hair cell stereocilia results in deafness in the mouse mutants shaker 2 (*Myo15a*^{sh2}) and whirler (*whirler*^{wi}), which contain mutations in myosin XVa and whirlin, respectively. The stereocilia of *Myo15a*^{sh2} and *whirler*^{wi} inner ear hair cells are abnormally short due to a failure of the actin cytoskeleton to elongate and the stereocilia bundle lacks the characteristic staircase structure found in normal hair cells. The introduction of exogenous myosin

XVa into homozygous *Myo15a*^{sh2} and whirlin into *whirler*^{wi} inner ear hair cells resulted in restoration of stereocilia elongation and staircase bundle formation.

The restoration of the stereocilia bundle architecture in transfected *Myo15a*^{sh2} hair cells by GFP-myosin XVa offers an *in vivo* cellular assay to dissect the contributions of individual domains of myosin XVa in the process. We observed two events that are critical to re-initiation of stereocilia elongation and stair case formation in transfected *Myo15a*^{sh2} hair cells. The first event was that GFP-myosin XVa must localize at stereocilia tips. In our control experiments, we showed that GFP tagged myosins Ic, VIIa and X were incapable of specifically accumulating at stereocilia tips of transfected hair cells. The accumulation of myosin XVa at distal tips of stereocilia appeared to be an intrinsic property of the motor and/or tail domains of myosin XVa. The second event critical for restoration of the stereocilia bundle architecture in transfected *Myo15a*^{sh2} hair cells was the ability of GFP-myosin XVa to bind and deliver endogenous whirlin to stereocilia tips.

These data raises a central question of whether myosin XVa's sole function is to transport whirlin to stereocilia tips? If true, then re-initiation of stereocilia elongation and stair case formation in transfected *Myo15a*^{sh2} hair cells might be unaffected by GFP-myosin XVa protein lacking one or more domains within the tail. Would a minimal myosin XVa protein capable of trafficking to stereocilia tips and also delivering whirlin in transfected *Myo15a*^{sh2} hair cells promote stereocilia elongation? If GFP-myosin XVa, which lacks one or more domains, is capable of delivering

whirlin to stereocilia tips but fails to re-initiate stereocilia elongation and staircase formation, then it suggests that the deleted region either mediates either a critical protein-protein or protein-lipid interaction, or it destabilizes the normal folding conformation. The contributions of myosin XVa domains to the stereocilia elongation and staircase formation were investigated and these data are described in chapter 5.

What is myosin XVa's function at the tips of stereocilia?

The stereocilia of *Myo15a*^{sh2} hair cells are short and lack the stair case bundle characteristically found in wild type hair cells, however scanning electron microscopy images suggest that tip links are present in young mouse hair cell bundles (Frolenkov GI, personal communication). Recently, molecular identity of a component of tip link, protocadherin 15-CD3, was reported (Ahmed et al. 2006). Myosin XVa does not transport protocadherin 15-CD3 to stereocilia tips as evidenced by the correct localization of protocadherin 15-CD3 at stereocilia tips of *Myo15a*^{sh2} hair cells (Ahmed ZM and Belyantseva IA, personal communication). Moreover, in patch clamped *Myo15a*^{sh2} hair cells, mechanically induced positive deflection of the hair bundle resulted in a measurable depolarization (Frolenkov, submitted for publication). While *Myo15a*^{sh2} hair cells are capable of mechanotransduction, the depolarization peak is very shallow and not sustained. The mechanotransduction capacity of *Myo15a*^{sh2} hair cells is present; implying that myosin XVa neither transports components nor stabilizes the hair cell mechanotransduction channel complex (Frolenkov, personal communication).

The localization of myosin XVa and whirlin under the apical membrane and overlapping with the barbed ends of the actin filaments of the stereocilia core coincides with the location of growth and remodeling of the actin core (Tilney et al. 1981; Schneider et al. 2002; Belyantseva et al. 2003a; Rzadzinska et al. 2004; Belyantseva et al. 2005). The delivery of whirlin to stereocilia tips by myosin XVa appears to be a critical event in stereocilia elongation and staircase formation. After delivery, it is unclear whether myosin XVa and whirlin remain associated or whether another protein partner at the stereocilia tip binds to third PDZ domain of whirlin. The co-localization of endogenous as well as fluorescently tagged myosin XVa and whirlin proteins at stereocilia tips of wild type hair cells suggest that if the two proteins are dissociated, they remain in proximity to each other. It was speculated that myosin-generated forces enhance actin polymerization at the tip by pushing the plasma membrane away from the barbed end, thereby creating space for the addition of actin monomers (Lin et al. 2005; Sousa et al. 2005). If plasma membrane bound actin mediators were pulled away from the barbed ends of actin filaments by myosin generated mechanical force, the net effect could strongly stimulate actin polymerization (Kozlov et al. 2004).

The failure of *whirler*^{wi} stereocilia to elongate and form a staircase structure despite the localization of myosin XVa at tips of short stereocilia, suggests that protein partners of whirlin assemble a macromolecular complex involved in regulating actin polymerization. Members of the Rho-GTPase, formin and Rho-GEF families are attractive candidates of this putative complex. The Rho-GTPase family consists of

twenty-two members that each affect cytoskeletal organization in a characteristic manner and participate in processes important for the formation of lamellipodia, filopodia and stress fibers, focal adhesion assembly and membrane ruffling (Aspenstrom et al. 2004; Sorokina et al. 2005). While Cdc42 is frequently mentioned as a key mediator of filopodia formation, the projections induced by Cdc42 are generally short and arise from the cell periphery (Pellegrin et al. 2005). Rho-GTPase members Rhod, Rhof, Rhoq and Rhou induce the formation of filopodia in epithelial cells (Aspenstrom et al. 2004; Passey et al. 2004; Pellegrin et al. 2005; Sorokina et al. 2005). In particular, constitutively active forms of RhoD and RhoF cause the formation of numerous very long filopodia (Aspenstrom et al. 2004; Sorokina et al. 2005). The cell type distribution and subcellular localization of Rhod, Rhof, Rhoq and Rhou within the inner ear will provide a useful starting point for investigation their potential role in stereocilia elongation. In a general sense, the dearth of information regarding the function of Rho-GTPase members in the formation of microvilli derived structures such as filopodia and stereocilia, highlights the necessity of addressing this aspect of cell biology.

Rho-GTPase guanine nucleotide-exchange factors (Rho-GEFs) are responsible for activation of Rho-GTPases in response to a variety of cellular stimuli. Perturbations in Rho-GEF function result in a variety of cancers, developmental and neurological disorders in humans (Rossman et al. 2005). The specificity of the effectors of RhoA, Rac1 and Cdc42 has been reported, however analysis of the remaining nineteen Rho-GTPases is incomplete. While it remains to be delineated, it appears that each of the

sixty-nine members of the Rho-GEF family will modulate the activity of a specific member or subset of Rho-GTPases (Rossman et al. 2005). Determination of which Rho-GEFs are expressed in the mouse inner ear will narrow the possible candidates.

The ability of unbranched parallel actin filaments such as stereocilia to elongate by the addition of actin monomers at their barbed end is dependent upon the factors that antagonize the function of barbed end capping protein. Several molecules influence the actin-binding ability of capping protein, either by binding directly to capping protein or by binding to filament barbed ends and thereby preventing capping protein from binding. Phosphatidylinositol (4,5)-bisphosphate, myotrophin and CARMIL antagonize the function of capping protein by binding directly to it (Schafer et al. 1996; Taoka et al. 2003; Yang et al. 2005). Capping protein can be regulated indirectly by proteins that bind the barbed end of the actin filament such as members of the formin family.

Formins are a conserved superfamily present in all eukaryotes including fifteen formin proteins in the mammalian proteome (Wallar et al. 2003; Zigmond 2004; Higgs 2005a; Higgs et al. 2005b). They are multi-domain proteins comprised of two functional domains, formin homology 1 and 2. Formin homology 1 domain influences Formin homology 2 domain function through binding to the actin monomer-binding protein, profilin. Formin homology 2 domains alter actin polymerization dynamics by accelerating *de novo* filament nucleation, altering filament barbed end elongation/depolymerization rates and antagonize barbed-end

capping proteins (Evangelista et al. 2003; Wallar et al. 2003; Zigmond 2004; Higgs 2005a). Processive capping allows the addition of actin subunits despite the presence of formin bound at the barbed end of the actin filament (Zigmond et al. 2003; Harris et al. 2004). The formin Diap3, which localizes to filopodia tips (Schirenbeck et al. 2005), is necessary for stimulation of filopodia formation by Rho-GTPase Rif (Pellegrin et al. 2005). The role of formins in the formation of filopodia makes these proteins compelling molecular candidates in the regulation of the actin cytoskeleton during stereocilia morphogenesis. Characterization of the cell type expression pattern of the fifteen formin genes within the mouse inner ear will serve as a useful starting point.

Reported protein partners of whirlin

Recently it was reported that a region of whirlin comprised the third PDZ domain and the 58 amino acids preceding it was capable of binding the GK domain of **m**embrane **p**rotein, **p**almitoylated **1** (Mpp1, also known as p55) in an *in vitro* and *in vivo* pull-down assay (Mburu et al. 2006). Partial co-localization of whirlin and Mpp1 were observed at the stereocilia apices of mouse outer hair cells, however a significant fraction of Mpp1 was observed in other regions of stereocilia in the absence of whirlin. It is unclear whether the co-localization of whirlin and Mpp1 at stereocilia tips is co-incidental or reflects temporal *in vivo* interaction.

Usherin, a transmembrane protein containing a extracellular region comprised of numerous lamin-EGF-like modules, fibronectin and laminin repeats, is reported to be another protein partner of whirlin in mouse inner ear (Adato 2005). Using an *in vitro* binding assay, the first and second PDZ domains of whirlin bound the carboxy-terminal class I PDZ ligand of the usherin. Adato and colleagues provided no images of whirlin and usherin co-localization within inner ear hair cells, so it is difficult to evaluate whether the two proteins co-localize or interact *in vivo*.

In adult rat retina, the interaction of whirlin with usherin and G protein-coupled receptor 98 (Gpr98, also known as Vlgr1) was reported (van Wijk et al. 2006). Co-localization of whirlin and usherin was observed at the outer plexiform layer, outer limiting membrane and inner segments of the retina while G protein-coupled receptor 98 and whirlin co-localized at the outer limiting membrane and connecting cilium. The reported protein partners of whirlin in the inner ear and retina suggest that whirlin may be a cytoplasmic scaffold protein capable of interacting with many cell-type specific protein partners for the assembly of multi-protein signaling complexes near the plasma membrane.

Future Plans

Identification of myosin XVa and whirlin protein partners

Yeast two-hybrid screening of mouse inner ear and vestibular cDNA libraries identified multiple putative protein partners of myosin XVa and whirlin. As an initial screening step to determine if these putative partners interact *in vivo*, I will use the

myosin XVa protein-protein assay described in chapter 4 (figure 4-13). For putative protein partners of myosin XVa, the cDNA insert (referred to hereafter as protein A) from the two-hybrid prey plasmid will be cloned into a dsRed monomer plasmid. The dsRed-protein A plasmid will be co-transfected along with full-length GFP-myosin XVa plasmid into COS-7 cells. If myosin XVa interacts with protein A, then GFP-myosin XVa will transport protein A to filopodia tips of transfected COS-7 cells (figure 4-13). The co-localization of green and red fluorescent signals at filopodia tips, indicated by the yellow color in the merge panel, would indicate an interaction between myosin XVa and protein A. If only a green fluorescent signal was observed at filopodia tips while red fluorescent signal was distributed throughout the cytoplasm, then this would indicate that no protein interaction had occurred.

For putative protein partners of whirlin, the cDNA insert (referred to hereafter as protein B) from the two-hybrid prey plasmid will be inserted in-frame into a multiple cloning site located upstream of the minimal myosin XVa cDNA insert or into a different plasmid with the multiple cloning site located after the minimal myosin XVa cDNA insert (figure 4-13). The encoded protein would be comprised of GFP-myosin XVa fused to protein B. The dsRed-whirlin plasmid will be co-transfected along with GFP-myosin XVa-protein B plasmid into COS-7 cells. Co-localization of green and red fluorescent signals at filopodia tips will indicate an interaction between protein B and whirlin.

Next I will generate polyclonal antiserum against interacting protein partners identified from the myosin XVa protein-protein assay, and determine if myosin XVa, whirlin and the protein partner co-localize within inner ear hair cells. Additionally, I will determine if the protein partner is mislocalized in *Myo15a*^{sh2} and *whirler*^{wi} hair cells based upon the assumption that myosin XVa or whirlin is required for correct localization of the protein partner within hair cells. In summary, three different approaches will be used to evaluate putative protein partners of myosin XVa and whirlin identified from two-hybrid screening.

Chapter 4: The domains of myosin XVa necessary for filopodia tip targeting in COS-7 cells

Abstract

In wild type mouse inner ear hair cells, myosin XVa is localized at tips of each stereocilium. When GFP tagged myosin XVa expression construct was transfected into cultured COS-7 cells, GFP-myosin XVa accumulated at filopodia tips. Filopodia in COS-7 cells and stereocilia of inner ear hair cells are comprised of parallel bundled actin filaments with the barbed ends located at the tips. I tested the hypothesis that filopodia tip targeting in COS-7 cells is a good model to study myosin XVa trafficking to stereocilia tips. The ability of GFP-myosin XVa containing deletions of one or more regions of the tail to localize at filopodia tips in transfected COS-7 cells was examined. While a functional motor was necessary, the motor plus IQ motifs did not traffic to filopodia tips. Based upon results of many different GFP-myosin XVa deletion constructs, I observed that the motor, IQ motifs plus several combinations of domains of the myosin XVa tail are sufficient for targeting of this unconventional myosin to filopodia tips. The motor, IQ motifs plus $MyTh4_1/FERM_1$, the motor, IQ motifs plus $MyTh4_2/FERM_2$ domains and the motor, IQ motifs plus $FERM_2$ domain target filopodia tips but the motor, IQ motifs plus $FERM_1$ domain does not target filopodia tips. The motor, IQ motifs plus $FERM_1$/SH3 domains or motor, IQ motifs plus $FERM_1$/SH3/$FERM_2$ domains are sufficient for filopodia tip targeting. Finally, the combination of motor, IQ motifs plus $MyTh4_1$, SH3 and $MyTh4_2$ domains targeted the distal region of the filopodia but accumulation at tips of filopodia was altered. Therefore, there are multiple redundant domains of the myosin XVa tail for

filopodia tip targeting, while the majority of the domains in the tail are required for stereocilia tip localization in inner ear hair cells (see Chapter 5).

Introduction

To investigate the subcellular localization behavior of myosin XVa in epithelial cells, I used COS-7 cells as a model. COS-7 cells are an easily transfected monkey kidney epithelial cell line that form filopodia when the cells are not confluent. Filopodia are thin cellular extensions containing a core of bundled, non-branched actin filaments that participate in diverse biological processes such as growth cone guidance (O'Connor et al. 1990), wound-healing (Wood et al. 2002), angiogenesis (Gerhardt et al. 2003) and cell-cell signaling (Ramirez-Weber et al. 2000). Actin polymerization occurs at the barbed ends of the actin filaments, which are located at the tip of the filopodium (Edds 1977; Tilney et al. 1981). Since the majority of myosin motors are expected to have plus end directed motility, it would seem that upon encountering the actin cytoskeleton of a filopodium, a myosin would translocate along the unidirectional actin filament until it reached the filopodia tip. To date, only 6 out of 24 unconventional myosins in the mouse proteome localize at the tips of filopodia. Ten myosins, myosins Ia, Ib, Id, Vb, VI, VIIb, IXa, IXb, XVIIIa and XVIIIb do not accumulate in filopodia while the subcellular localization of the remaining eight myosins is unknown. Myosin IIIa (Les Erickson et al. 2003), myosin Va (Espreafico et al. 1992; Wang et al. 1996), myosin X (figure 3-10B; Berg et al. 2002) and myosin XVa (figure 3-9B; Belyantseva et al. 2003a; Belyantseva et al. 2005) target to filopodia tips. Two myosins, myosin Ic (figure 3-10A) and myosin VIIa (figure 3-10B), localize along the length of filopodia in transfected cells.

The molecular properties that allow some myosins to localize at filopodia tips are not known. For unconventional myosins, it is assumed that the tail domain is involved in

targeting and membrane binding (Mermall et al. 1998), suggesting that the differences in myosin tails account for targeting to filopodia. Another possibility is that myosin localization or exclusion at specific intracellular sites is due to differential myosin motor activity along tropomyosin-coated actin filaments (Tsakraklides et al. 1999). Several tropomyosins have been demonstrated to differentially regulate the functional properties of myosin I, II and V motor domains (Wolenski 1995). The targeting of myosin Va to sites of polarized growth in budding yeast was directed by tropomyosin-coated actin filaments (Pruyne et al. 1998). The selective impediment of the actin binding or motility of some myosin motors due to interactions with actin associated proteins coating the filament might lower the net rate of forward movement to below the opposing rate of retrograde actin flow, resulting in a failure to reach filopodia tips (Sousa et al. 2005). Another possibility is that all plus end directed myosins may traffic to filopodia tips, but only a small number accumulate at filopodia tips due to retention by protein-protein or protein-phosphoinositide interactions. To date, no reports support or refute the possibility of retention of myosins at filopodia tips by protein or phosphoinositide interaction.

Methods

Myosin XVa expression constructs containing cDNA deletions.

Full-length GFP-myosin XVa mouse cDNA and GFP-myosin XVa[-PDZ_l] expression constructs were previously described in the methods section of Chapter 3. Using full-length GFP-myosin XVa cDNA expression construct as template, PCR products encoding various regions of myosin XVa were amplified using Pfu Ultra DNA polymerase (Stratagene, figure 4-1). The PCR products, which contained Xho I or Cla I restriction enzyme recognition sites that were introduced into the PCR primer sequences, were digested with either Xho I or Cla I restriction enzyme (New England BioLabs) and ligated together using T4 DNA ligase (New England BioLabs). The ligated PCR products were used as template and the entire cDNA insert was PCR amplified using Pfu Ultra DNA polymerase (Stratagene). The cDNA insert was digested with EcoR I and Sal I restriction enzymes (New England BioLabs) and ligated into the EcoR I and Sal I sites of EGFP-C2 plasmid (Clontech). Both strands of the cloned myosin XVa cDNA inserts were sequenced by using Big Dye Terminator Version 3.0 and an ABI3730xl DNA Analyzer (Applied Biosystems). The sequence data was assembled and analyzed using Seqman (DNAStar) and MacVector programs (Accelyrs). A representation of the PCR products used to generate the various myosin XVa cDNA inserts is depicted in figure 4-1. The sequence of PCR primers used to generate the various myosin XVa cDNA fragments is listed in Table 4-1. The combinations of myosin XVa cDNA fragments ligated together to generate the open reading frames of the various myosin XVa deletion constructs is given in Table 4-2.

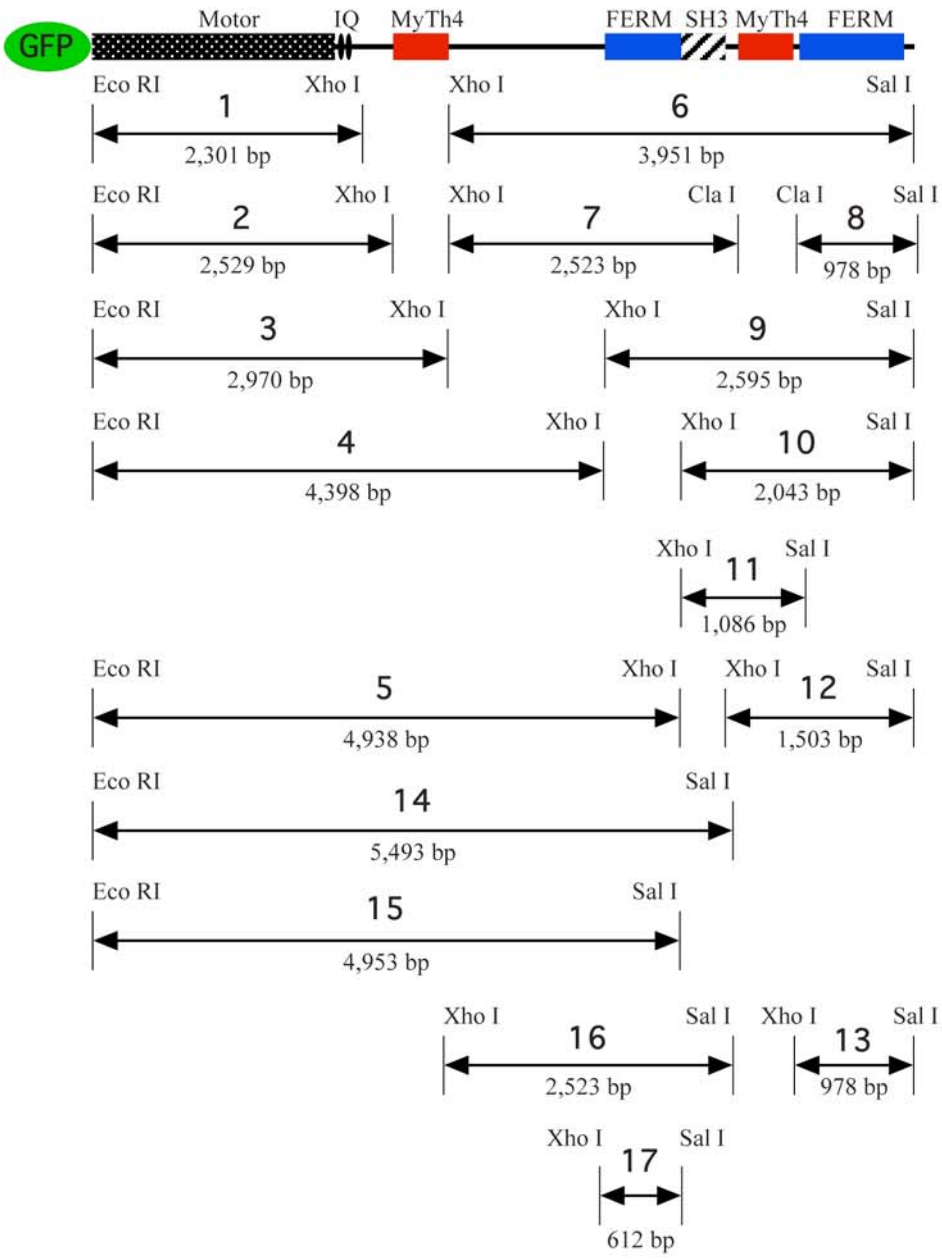

Figure 4-1. Myosin XVa cDNA fragments used to generate the translational open reading frames of myosin XVa deletion cDNA constructs. Seventeen different myosin XVa cDNA fragments were PCR amplified. Combinations of myosin XVa cDNA fragments were ligated together (Table 4-2) to generate the open reading frames of the various myosin XVa cDNA deletion constructs used in this study. Restriction enzyme recognition sites were incorporated into the forward and reverse PCR primers to facilitate the ligation of cDNA fragments. Ligation of two cDNA fragments using a Xho I recognition site sequence (CTC GAG) inserts two amino acids (L-E) into the translated protein product while the Cla I recognition site sequence (ATC GAT) inserts two amino acids (I-D) into the protein product.

Myosin XVa isoform 2j and 2q expression constructs.

The open reading frames myosin XVa cDNA isoforms 2j and 2q were PCR amplified using Pfu Ultra DNA polymerase (Stratagene). The PCR products, which contained EcoR I and Sal I restriction enzyme recognition sites in the forward and reverse PCR primers, were digested with EcoR I and Sal I restriction enzyme and ligated into the EcoR I and Sal I sites of GFP-C2 plasmid (Clontech). The sequence of the cDNA insert was verified by sequencing both DNA strands as described in the preceding paragraph. PCR primer sequences are listed in Table 4-1.

Myosins VIIa, VIIb and X expression constructs.

The methods used to construct mouse GFP-myosins VIIa, VIIb and X cDNA expression constructs were described in the Methods Section of Chapter 3.

Table 4-1. PCR primers for synthesizing myosin XVa expression constructs

PCR product	Primer Sequence
1	Forward primer, 5'-cgattc**gaattc**ATGCACTCCATACGCAACCTGCCTTC-3' Reverse primer, 5'- cgattc**ctcgag**CTTGAGGTAGCGGCGGCGGTTC-3'
2	Forward primer, 5'-cgattc**gaattc**ATGCACTCCATACGCAACCTGCCTTC-3' Reverse primer, 5'- cgattc**ctcgag**CCCAAAGGAGGGTTCCTTGAAGTGGC-3'
3	Forward primer, 5'-cgattc**gaattc**ATGCACTCCATACGCAACCTGCCTTC-3' Reverse primer, 5'-cgattc**ctcgag**CTGAATGGCAGTCCACTCCAGCTGAG-3'
4	Forward primer, 5'-cgattc**gaattc**ATGCACTCCATACGCAACCTGCCTTC-3' Reverse primer, 5'-cgattc**ctcgag**GTCCTGGTAGCCATAGAAGTTGGGGTTG-3'
5	Forward primer, 5'-cgattc**gaattc**ATGCACTCCATACGCAACCTGCCTTC-3' Reverse primer, 5'-cgattc**ctcgag**ATCAGAATCCTTCTTCAGTTCCAGAATGAAGG-3'
6	Forward primer, 5'-cgattc**ctcgag**GAGAAGGCCAGTATGGCTCTAGATGTGAGCTG-3' Reverse primer, 5'-cgattc**gtcgac**TCACAAGAGGGTGATCTCGCTGGGAGG-3'

7	Forward primer, 5'- cgattc**ctcgag**GAGAAGGCCAGTATGGCTCTAGATGTGAGCTGCTTCAATGG-3' Reverse primer, 5'- cgattc**atcgat**GAAGCAAAGCACGTCCTCCAGAGTTTTG-3'
8	Forward primer, 5'-cgattc**atcgat**GGCCGCAGTTCCAAGAGGCAGCTC-3' Reverse primer, 5'-cgattc**gtcgac**TCACAAGAGGGTGATCTCGCTGGGAGG-3'
9	Forward primer, 5'-cgattc**ctcgag**GATCCTGTGCAGACACAGCTGCACCG-3' Reverse primer, 5'-cgattc**gtcgac**TCACAAGAGGGTGATCTCGCTGGGAGG-3'
10	Forward primer, 5'-cgattc**ctcgag**GCGCAGCAGGTCAAGACCCTAGTAGACACC-3' Reverse primer, 5'-cgattc**gtcgac**TCACAAGAGGGTGATCTCGCTGGGAGG-3'
11	Forward primer, 5'- cgattc**ctcgag**GCGCAGCAGGTCAAGACCCTAGTAGACACC-3' Reverse primer, 5'-cgattc**gtcgac**TCACAAGAGGGTGATGCGGCCTGCCAACATAGCACG-3'
12	Forward primer, 5'-cgattc**ctcgag**CTCAAGCTGAAGTCTAAGGAGGATCGGGAGTCC-3' Reverse primer, 5'-cgattc**gtcgac**TCACAAGAGGGTGATCTCGCTGGGAGG-3'
13	Forward primer, 5'-cgattc**ctcgag**GCAGGCCGCAGTTCCAAGAGGCAG-3' Reverse primer, 5'-cgattc**gtcgac**TCACAAGAGGGTGATCTCGCTGGGAGG-3'
14	Forward primer, 5'- cgattc**gaattc**ATGCACTCCATACGCAACCTGCCTTC-3' Reverse primer, 5'- cgattc**gtcgac**TCACAAGAGGGTGATGAAGCAAAGCACGTCCTCCAGAGTTTTG-3'
15	Forward primer, 5'- cgattc**gaattc**ATGCACTCCATACGCAACCTGCCTTC-3' Reverse primer, 5'- cgattc**gtcgac**ATCAGAATCCTTCTTCAGTTCCAGAATGAAGG-3'
16	Forward primer, 5'- cgattc**ctcgag**GAGAAGGCCAGTATGGCTCTAGATGTGAGCTGCTTCAATGG-3' Reverse primer, 5'- cgattc**gtcgac**TCACAAGAGGGTGATGAAGCAAAGCACGTCCTCCAGAGTTTTG-3'
17	Forward primer, 5'- cgattc**ctcgag**GATCCTGTGCAGACACAGCTGCACCGCCTAGTCAACCC-3' Reverse primer, 5'- cgattc**gtcgac**ATCAGAATCCTTCTTCAGTTCCAGAATGAAGG-3'
Isoform 2j	Forward primer, 5'- cgattc**gaattc**ATGCACTCCATACGCAACCTGCCTTC-3' Reverse primer, 5'-cgattg**gtcgac**TTACCCTAAGAAATGGTACACACACTGAGCCTG-3'
Isoform 2q	Forward primer, 5'- cgattc**gaattc**ATGCACTCCATACGCAACCTGCCTTC-3' Reverse primer, 5'- cgattg**gtcgac**TCAGCTGCAGGAGAGCAAATGGTCAGAG-3'

Uppercase letters denote cDNA sequence, lowercase bold letters are restriction enzyme recognition sites and lowercase letters denote extra primer sequence

Table 4-2. PCR product combinations used to generate myosin XVa expression constructs

Expression construct	Ligated PCR products	Additional amino acids inserted as result of restriction site
[-SH3]	5 + 12	+L-E
[-MyTh4$_1$]	2 + 6	+L-E
[-FERM$_1$]	4 + 10	+L-E
[-linker]	3 + 9	+L-E
[-MyTh4$_1$,-MyTh4$_2$]	2 + 7 + 8	+L-E, +I-D
[-FERM$_1$,-FERM$_2$]	4 + 11	+L-E
[-MyTh4$_1$,-FERM$_1$]	1 + 10	+L-E
[-MyTh4$_1$,-FERM$_1$,-SH3]	1 + 12	+L-E
[-MyTh4$_1$,-FERM$_1$,-SH3,-MyTh4$_2$]	1 + 13	+L-E
[-MyTh4$_2$,-FERM$_2$]	14	None
[-SH3,-MyTh4$_2$,-FERM$_2$]	15	None
[-MyTh4$_1$,-SH3,-MyTh4$_2$,-FERM$_2$]	1 + 17	+L-E
[-MyTh4$_1$,-MyTh4$_2$,-FERM$_2$]	2 + 16	+L-E

COS-7 cell culture.

African green monkey kidney cells (COS-7) were cultured at 37ºC and 5% CO_2 in DMEM media (Invitrogen), containing 10% fetal bovine serum (Invitrogen) and 10 mM HEPES (Invitrogen). Using Lipofectamine 2000 (Invitrogen), cells were transfected with GFP-myosin XVa expression constructs. In fixed tissue samples, subcellular localization of myosin XVa was analyzed with Zeiss software for a LSM510 confocal microscope.

Results

In order to determine which region(s) of myosin XVa are sufficient for filopodia tip localization, a series of green fluorescent protein (GFP) tagged mouse myosin XVa expression constructs containing deletions of the cDNA encoding individual or multiple regions were transfected into COS-7 cells and the localization was determined by confocal microscopy. The domain(s) missing from GFP-myosin XVa deletion protein products were designated in brackets. For example, if the cDNA encoding the SH3, second MyTh4 and second FERM domains were deleted, the protein was designated GFP-myosin XVa[-SH3,-MyTh4$_2$,-FERM$_2$]. Two myosin XVa motor mutants containing engineered missense mutations in the motor domain predicted to abolish motility were used in this study. The missense mutation(s) in the myosin XVa motor domain are listed in parenthesis. For example, GFP-myosin XVa(R167A/G388A) contains two missense mutations in the motor domain. Two myosin XVa isoforms, cloned from mouse inner ear cDNA, were used in the study. The two isoforms were designated GFP-myosin XVa isoform 2p and GFP-myosin XVa isoform 2q.

Myosin XVa is not endogenously present in COS-7 cells

In COS-7 cells, our anti-mouse myosin XVa antiserum (TF1) failed to detect any endogenous myosin XVa epitope at filopodia tips in either non-transfected or mock-transfected cells (figure 4-2). In COS-7 cells transfected with GFP-myosin XVa cDNA expression construct, anti-myosin XVa antiserum staining co-localized with GFP-myosin XVa at filopodia tips (figure 4-2A, B and C; Belyantseva et al. 2003a).

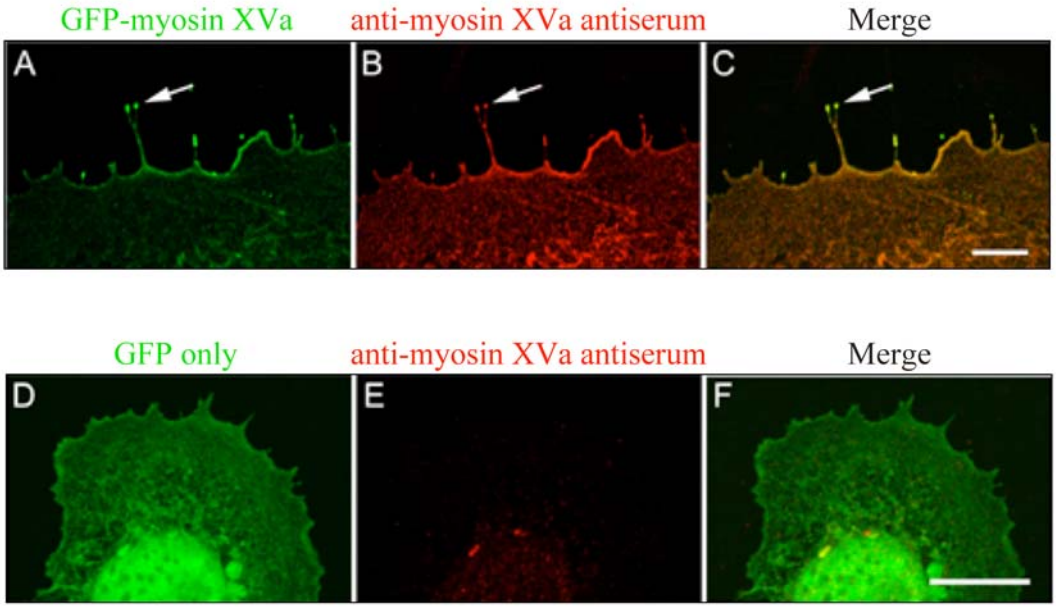

Figure 4-2. Myosin XVa is not endogenously present in COS-7 cells.**(Panels A through C)**. COS-7 cell tranfected with GFP-myosin XVa (green) and stained with anti-myosin XVa antibody (red). **(A)** GFP-myosin XVa is concentrated at filopodia tips (white arrow) and is present in the cell body. **(B)** Anti-myosin XVa antiserum (red) recognizes GFP-myosin XVa at filopodia tips (white arrow) and in the cell body. **(C)** Colocalization of GFP-myosin XVa and anti-myosin XVa antiserum staining. **(Panels D through F)**. COS-7 cell tranfected with GFP-C2 vector without myosin XVa cDNA insert (green) and stained with anti-myosin XVa antibody (red). **(D)** COS-7 cell transfected with GFP-C2 without myosin XVa cDNA insert (green) is distributed diffusely throughout the cytoplasm. **(E)** The same COS-7 cell stained with anti-myosin XVa antibody (red). **(F)** Merged image of GFP-C2 and anti-myosin XVa antibody staining. No detectable amounts of myosin XVa is observed at filopodia tips. (scale bars, 10 μm).

Conversely, COS-7 cells transfected with a EGFP-C2 plasmid without myosin XVa insert showed no anti-myosin XVa immunoreactivity at filopodia tips (figure 4-2D, E and F; Belyantseva et al. 2003a). The lack of anti-myosin XVa antiserum immunoreactivity suggests that either myosin XVa is not endogenously present or

that our anti-myosin XVa antiserum fails to recognize the green monkey myosin XVa homolog in COS-7 cells.

Alignment analysis of the region of the mouse myosin XVa protein recognized by the TF1 antiserum reveals that this "epitope region" is conserved among vertebrates (Table 4-3). Given the conservation of the TF1 epitope region and that our TF1 antiserum recognizes mouse, rat and guinea pig myosin XVa homologs at stereocilia tips of hair cells (Belyantseva et al. 2003a) and human myosin XVa protein in anterior pituitary cells (Lloyd et al. 2001), it seems likely that our TF1 antiserum would recognize green monkey myosin XVa homolog. In COS-7 cells transfected with GFP-whirlin, no accumulation of whirlin was observed at filopodia tips, suggesting that endogenous myosins present within COS-7 cells were incapable of transporting whirlin to filopodia tips.

Table 4-3. Percentage amino acid identity and similarity of several myosin XVa orthologs to the mouse myosin XVa TF1 epitope.

Species	% amino acid identity	% amino acid similarity
Rat	97	97
Dog	77	81
Cow	78	85
Rheus monkey	82	88
Human	81	86

In order to definitively determine if myosin XVa is expressed in COS-7 cells, I would reverse transcribe poly A+ RNA purified from COS-7 cells and use this cDNA template to PCR amplify regions of myosin XVa cDNA using PCR primers derived from Rheus monkey genomic sequence (Ensembl database). As positive PCR controls, I would amplify myosins VIIa and X cDNA, which are expressed in human and mouse kidney tissue. If I was able to PCR amplify short myosin XVa cDNA fragments from COS-7 cDNA, I would attempt to determine the sequence of the full-length myosin XVa cDNA transcript. If the predicted protein sequence of monkey myosin XVa was divergent within the TF1 epitope region, it might explain the failure of TF1 antiserum to recognize myosin XVa homologs in COS-7 cells.

The motor domain is necessary but not sufficient for filopodia tip localization

To determine whether a functional motor is required for filopodia tip trafficking, two myosin XVa motor mutants, GFP-myosin XVa proteins (GFP-myosin XVa(C592Y) and GFP-myosin XVa(R167A/G388A), were transfected into COS-7 cells. Both of the myosin XVa motor mutants remained in the cell body (figure 3-9C and data not shown; Belyantseva et al. 2005). To examine the possibility that these two myosin XVa motor mutants were strongly locked onto actin filaments and were unable to translocate to filopodia tips, co-sedimentation assays in transfected COS-7 cells were carried out by Drs. Belyantseva and Sellers, Both GFP-myosin XVa(C592Y) and GFP-myosin XVa(R167A/G388A) were found distributed equally between the supernatant and the insoluble actin pellet in the presence and absence of ATP (data not shown). Moreover, myosins locked onto actin filaments are expected to highlight

the actin cytoskeleton pattern of the cell, which is not observed with either GFP-myosin XVa(C592Y) or GFP-myosin XVa(R167A/G388A). These observations indicate that GFP-myosin XVa(C592Y) and GFP-myosin XVa(R167A/G388A) are not bound to actin in a rigor like manner.

In order to determine if the motor of myosin XVa was the sole determinant of filopodia tip localization in COS-7 cells, GFP-myosin XVa comprised of the motor and IQ motifs GFP-myosin XVa isoform 2q, a predicted endogenous inner ear myosin XVa isoform described in chapter 2 (figure 2-13), was transfected into COS-7 cells. GFP-myosin XVa isoform 2q accumulated in the cell body, along the length of filopodia but did not specifically accumulate at filopodia tips (figure 4-3A). The inability of the motor and IQ motifs to target filopodia tips suggested one or more domains of the tail are necessary for subcellular accumulation at the tips of filopodia.

PDZ ligand and SH3 domain are not necessary for filopodia tip localization

The transfection of GFP-myosin XVa[-PDZ_L], which lacked the carboxy terminal four amino acids comprising the class I PDZ ligand, resulted in the accumulation at filopodia tips (figure 3-9E; Belyantseva et al. 2005). This suggested that the protein interaction mediated by the PDZ ligand is not essential for filopodia tip localization. Next, I sought to determine whether the deletion only of the SH3 domain would affect localization. In transfected COS-7 cells, GFP-myosin XVa[-SH3] accumulated at filopodia tips (figure 4-3B). These results suggested that neither the deletion of the

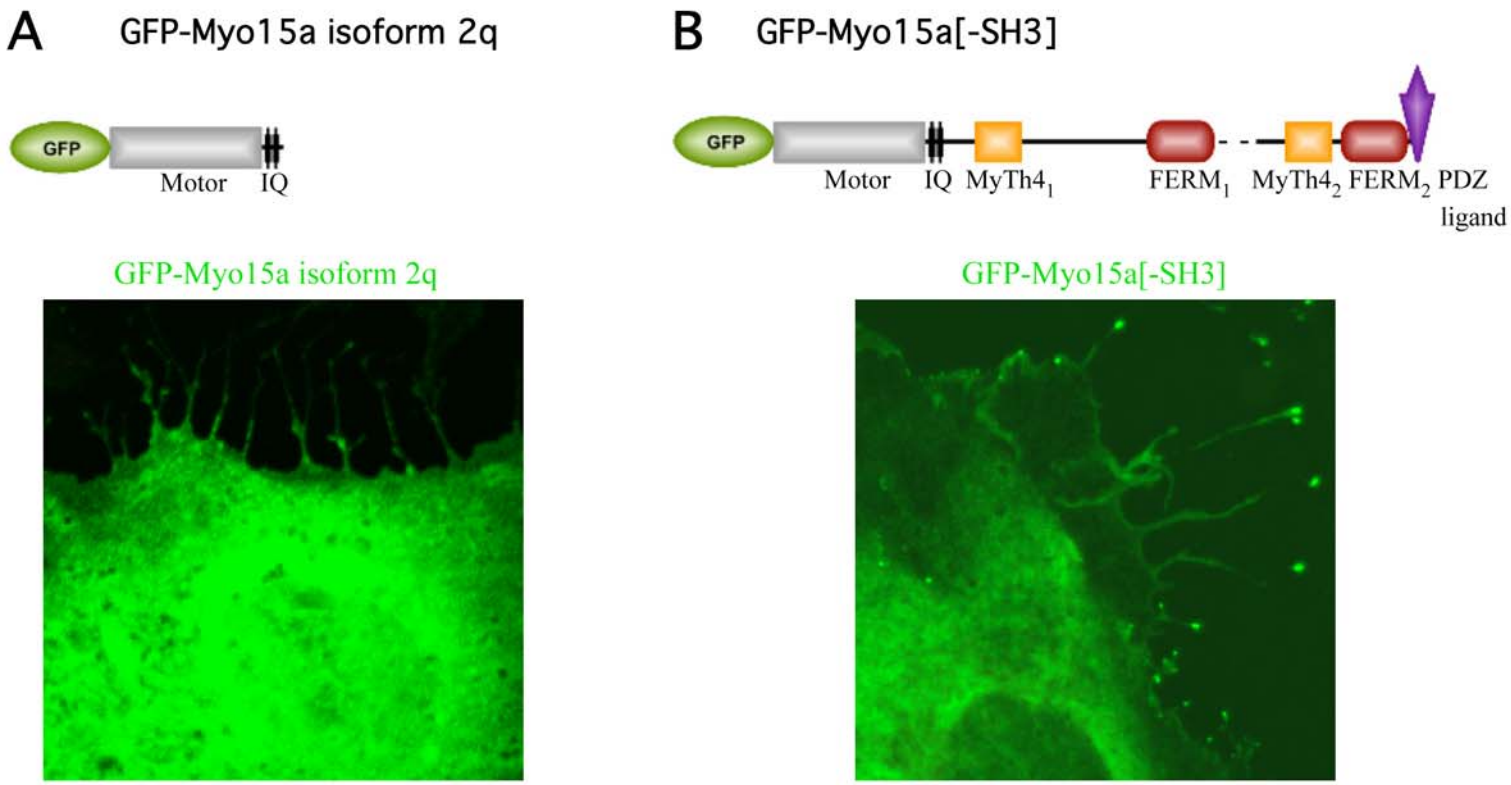

Figure 4-3. A myosin XVa motor and IQ motifs is insufficient for filopodia tip targeting while the deletion of the SH3 domain in GFP-myosin XVa protein does not affect targeting to filopodia tips. **(A)** GFP-myosin XVa isoform 2q, an endogenous inner ear myosin XVa isoform comprised of the motor and IQ motifs, is found distributed throughout cytoplasm, and along the length of the filopodia but does not specifically accumulate at filopodia tips. **(B)** GFP-myosin XVa[-SH3], which lacks the SH3 domain, accumulates at filopodia tips. Dotted lines represent deleted regions of myosin XVa.

SH3 domain nor the PDZ ligand affected the targeting of GFP-myosin XVa to filopodia tips.

Deletion of $MyTh4_1$ or $FERM_1$ domains does not affect filopodia tip targeting

The role of the first MyTh4 ($MyTh4_1$) and FERM ($FERM_1$) domains in filopodia targeting were evaluated. In each case, the deletion of either the $MyTh4_1$ and $FERM_1$ domains did not affect targeting to filopodia tips. Both GFP-myosin XVa[-$MyTh4_1$] and GFP-myosin XVa[-$FERM_1$] accumulated at filopodia tips in transfected COS-7 cells (figure 4-4). To determine if the region located between the $MyTh4_1$ and $FERM_1$ domains, which I termed the "linker", contributed to filopodia targeting, GFP-myosin XVa[-linker] lacking the 450 amino acids between the $MyTh4_1$ and $FERM_1$ domains was transfected into COS-7 cells (figure 4-5A). GFP-myosin XVa[-linker] targeted to filopodia tips suggesting that the loss of this "linker" region did not affect targeting. It also implied that the spacing between the $MyTh4_1$ and $FERM_1$ domains was not critical for filopodia tip targeting. Collectively taken, these results suggest that either the individual loss of the $MyTh4_1$ and $FERM_1$ domains and linker region were not critical for targeting to filopodia tips or that some other region of the protein was capable of targeting myosin XVa to filopodia tips in the absence of the $MyTh4_1$ and $FERM_1$ domains and linker region.

Deletion of both FERM domains affects filopodia tip localization

To address the possibility that functionally redundant regions of myosin XVa were capable of filopodia targeting in GFP-myosin XVa containing single deleted domain,

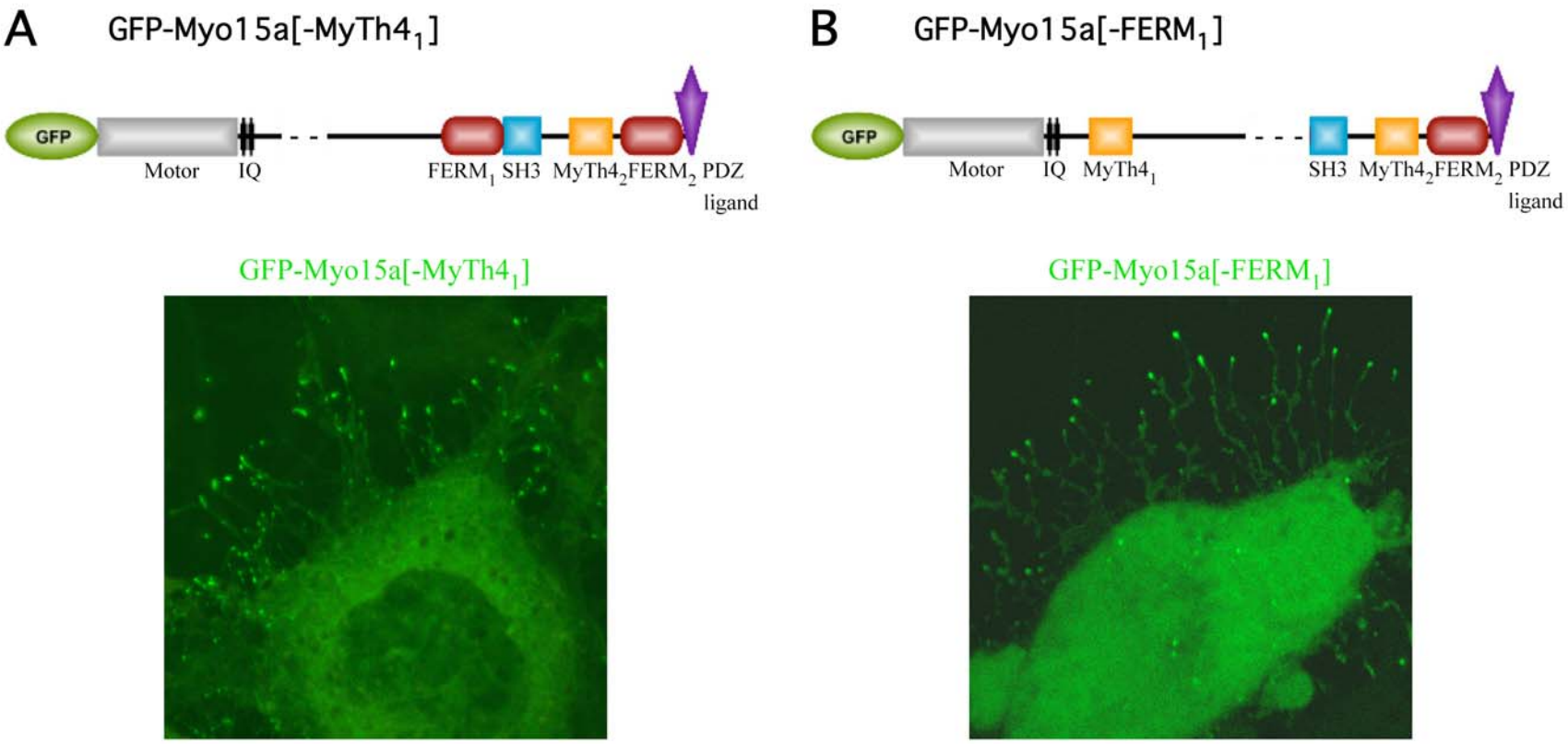

Figure 4-4. Deletion of either the MyTh4$_1$ or FERM$_1$ domain in GFP-myosin XVa protein does not affect targeting to filopodia tips. **(A)** GFP-myosin XVa[-MyTh4$_1$] accumulates at filopodia tips of transfected COS-7 cells. **(B)** GFP-myosin XVa[-FERM$_1$] accumulates at filopodia tips.Dotted lines represent deleted regions of myosin XVa.

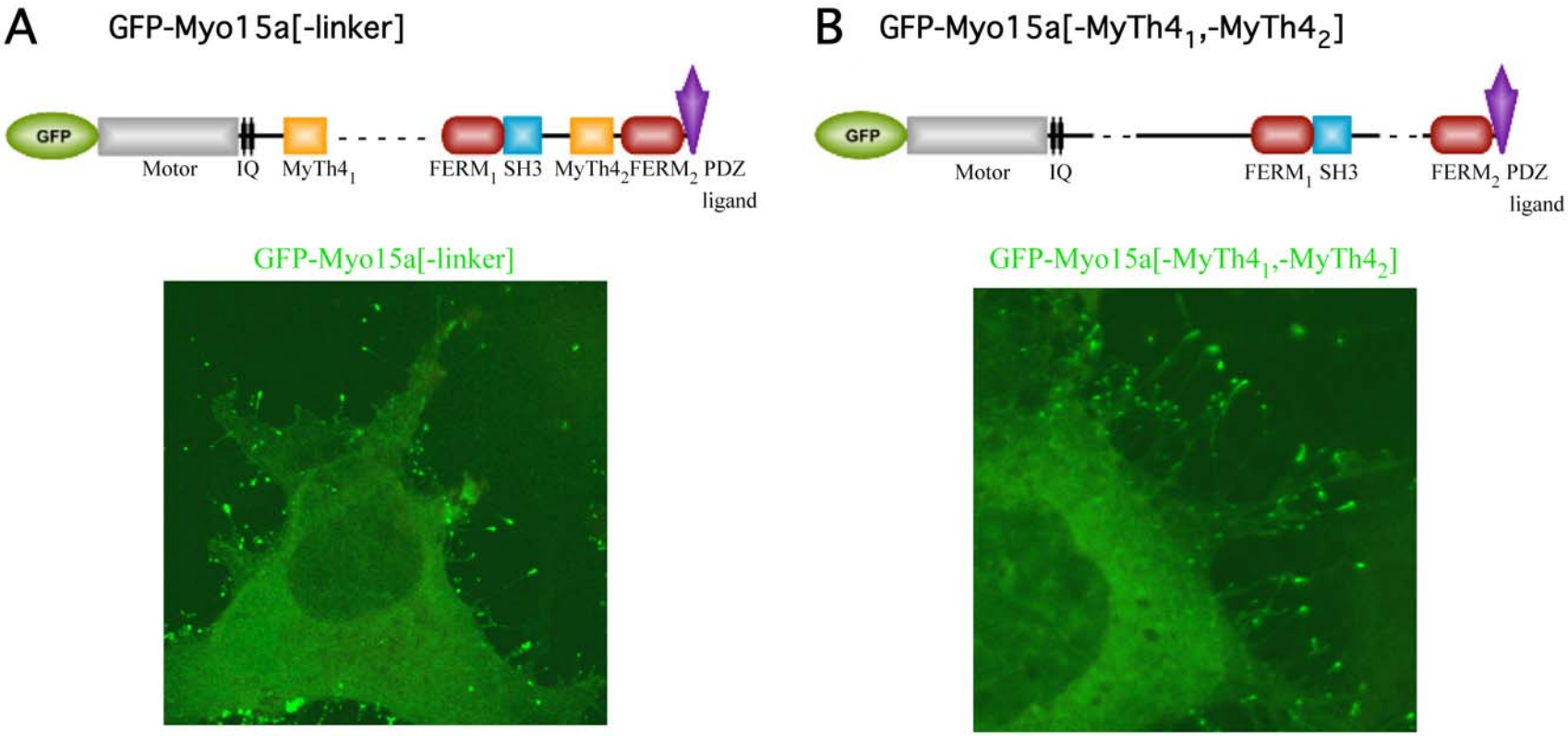

Figure 4-5. The deletion of 450 amino acids located between MyTh4$_1$ and FERM$_1$ domains nor the deletion of both MyTh4 domains of myosin XVa affects targeting to filopodia tips. **(A)** GFP-myosin XVa[-linker], which lacks the 450 amino acids between the MyTh4$_1$ and FERM$_1$ domains, accumulated at filopodia tips of transfected COS-7 cells. **(B)** GFP-myosin XVa[-MyTh4$_1$, -MyTh4$_2$], which lacks both MyTh4 domains, targets to filopodia tips. Dotted lines represent deleted regions of myosin XVa.

I generated GFP-myosin XVa expression constructs that either lacked both $MyTh_4$ domains or both FERM domains. The transfection of GFP-myosin XVa[-$MyTh4_1$,-$MyTh4_2$], lacking both MyTh4 domains, resulted in accumulation at filopodia tips (figure 4-5B). This result suggested at least two possibilities. One possibility was that neither of the MyTh4 domains contributed to filopodia targeting. A second possibility is that another region of myosin XVa such as the $FERM_1$, SH3 and $FERM_2$ domains are capable of targeting in the absence of both MyTh4 domains.

The deletion of both FERM domains (figure 4-6A) affected the dynamics of filopodia tip localization. In multiple experiments, the transfection of GFP-myosin XVa[-$FERM_1$,-$FERM_2$], lacking both FERM domains, resulted in an unusual localization pattern. In approximately half of the transfected COS-7 cells, GFP-myosin XVa[-$FERM_1$,-$FERM_2$] was distributed diffusely throughout the cytoplasm (figure 4-6B). The grainy appearance of the cytoplasm and the large number of vacuoles within the cell body suggest that these transfected cells are sick. While the process of transfection damages mammalian cells, the failure to observe similar cell transfection toxicity with other GFP-myosin XVa constructs transfected in parallel, suggests that GFP-myosin XVa[-$FERM_1$,-$FERM_2$] is responsible for the sickly appearance of the COS-7 cells. The other half of transfected cells show GFP-myosin XVa[-$FERM_1$,-$FERM_2$] accumulation at the distal region of filopodia rather than exclusively at the filopodia tips (figure 4-6C). The localization of GFP-myosin XVa[-$FERM_1$,-$FERM_2$] along the distal end of filopodia is an aberrant pattern of retention at filopodia tips.

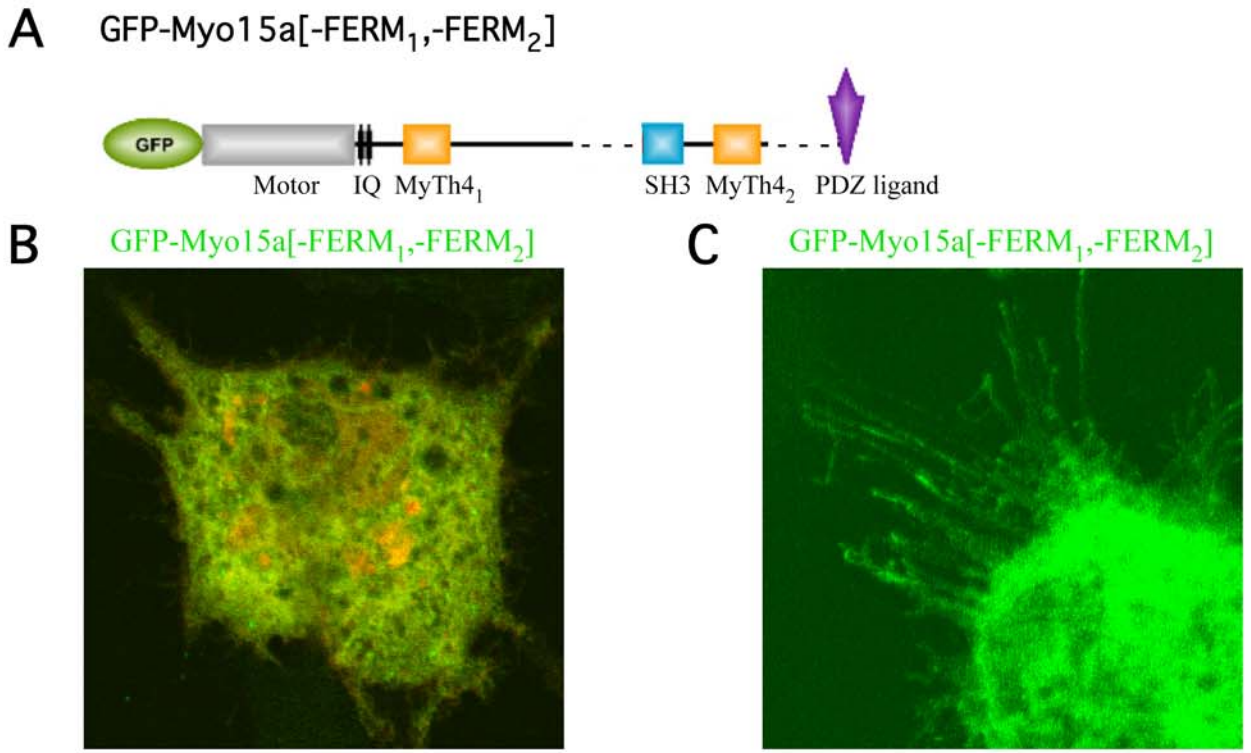

Figure 4-6. The deletion of both FERM domains of myosin XVa affects the dynamics of filopodia tip accumulation in transfected COS-7 cells. **(A)** Schematic representation of the GFP-myosin XVa[-$FERM_1$,-$FERM_2$] protein product which lacks both FERM domains. Dotted lines represent deleted regions of myosin XVa. **(B)** GFP-myosin XVa[-$FERM_1$,-$FERM_2$] is distributed diffusely throughout the cytoplasm of a transfected COS-7 cell. **(C)** Accumulation of GFP-myosin XVa[-$FERM_1$,-$FERM_2$] at the distal ends of filopodia is observed in transfected COS-7 cells. Approximately half of transfected COS-7 cells have diffuse cytoplasmic distribution of GFP-myosin XVa[-$FERM_1$,-$FERM_2$] while in the other half of transfected COS-7 cells, GFP-myosin XVa[-$FERM_1$,-$FERM_2$] accumulates along the distal ends of filopodia.

Motor plus $FERM_2$ domain is sufficient for filopodia tip localization

In the next group of experiments, I sought to determine if the second MyTh4 and FERM domains ($MyTh4_2$ and $FERM_2$ domains) were sufficient for filopodia tip targeting. First, I tested the ability of GFP-myosin XVa lacking the $MyTh4_1$ and $FERM_1$ domains to target filopodia tips. Transfection of GFP-myosin XVa[-$MyTh4_1$,$FERM_1$] resulted in robust accumulation at filopodia tips (figure 4-7A). Next, I transfected GFP-myosin XVa[-$MyTh4_1$,$FERM_1$,-SH3], comprised of the motor, IQ motifs, $MyTh4_2$ and $FERM_2$ domains, and observed accumulation at filopodia tips at levels indistinguishable from full-length GFP-myosin XVa (figure 4-7B). The equally robust filopodia tip accumulation of GFP-myosin XVa[-$MyTh4_1$,$FERM_1$] and GFP-myosin XVa[-$MyTh4_1$,$FERM_1$,-SH3] confirmed that the absence of the SH3 domain did not affect targeting. Transfection of GFP-myosin XVa[-$MyTh4_1$,$FERM_1$,-SH3,-$MyTh4_2$], comprised of the motor, IQ motifs and $FERM_2$ domain resulted in weaker accumulation at filopodia tips (figure 4-8A). Thus, the motor, IQ motifs and $FERM_2$ domain was sufficient for targeting filopodia tips. The accumulation of GFP-myosin XVa[-$MyTh4_1$,$FERM_1$,-SH3,-$MyTh4_2$] at filopodia tips was noticeably less than GFP-myosin XVa[-$MyTh4_1$,$FERM_1$,-SH3], although I did not attempt to quantitate the difference. These results suggest that the $MyTh4_2$ and $FERM_2$ domains function synergistically to promote robust targeting to filopodia tips.

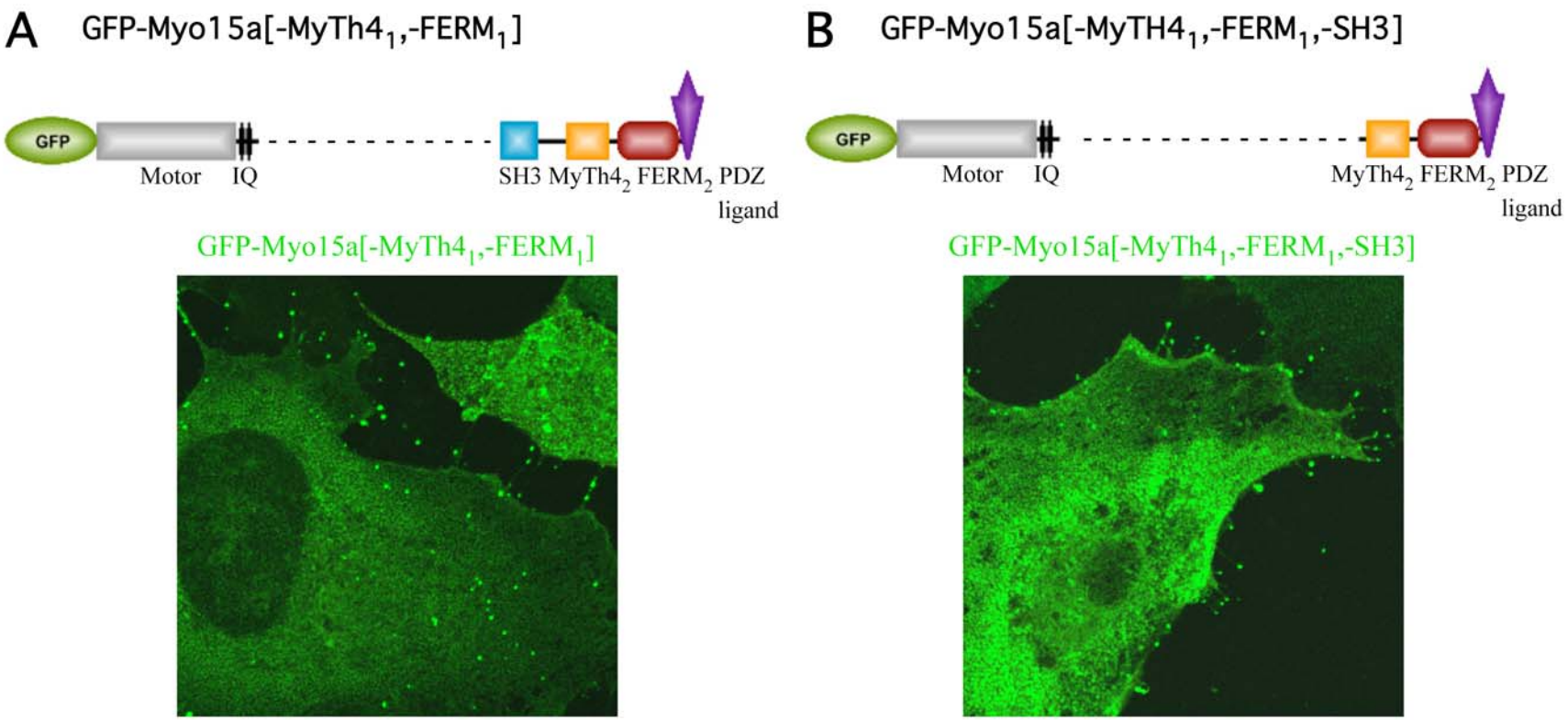

Figure 4-7. Subcellular localization of minimal myosin XVa comprised of the motor plus MyTh4$_1$ and FERM$_2$ domains. **(A)** Myosin XVa motor plus SH3, MyTh4$_1$ and FERM$_2$ domains is sufficient for targeting filopodia tips. **(B)** Myosin XVa motor plus MyTh4$_1$ and FERM$_2$ domains is sufficient for targeting filopodia tips. Dotted lines represent deleted regions of myosin XVa.

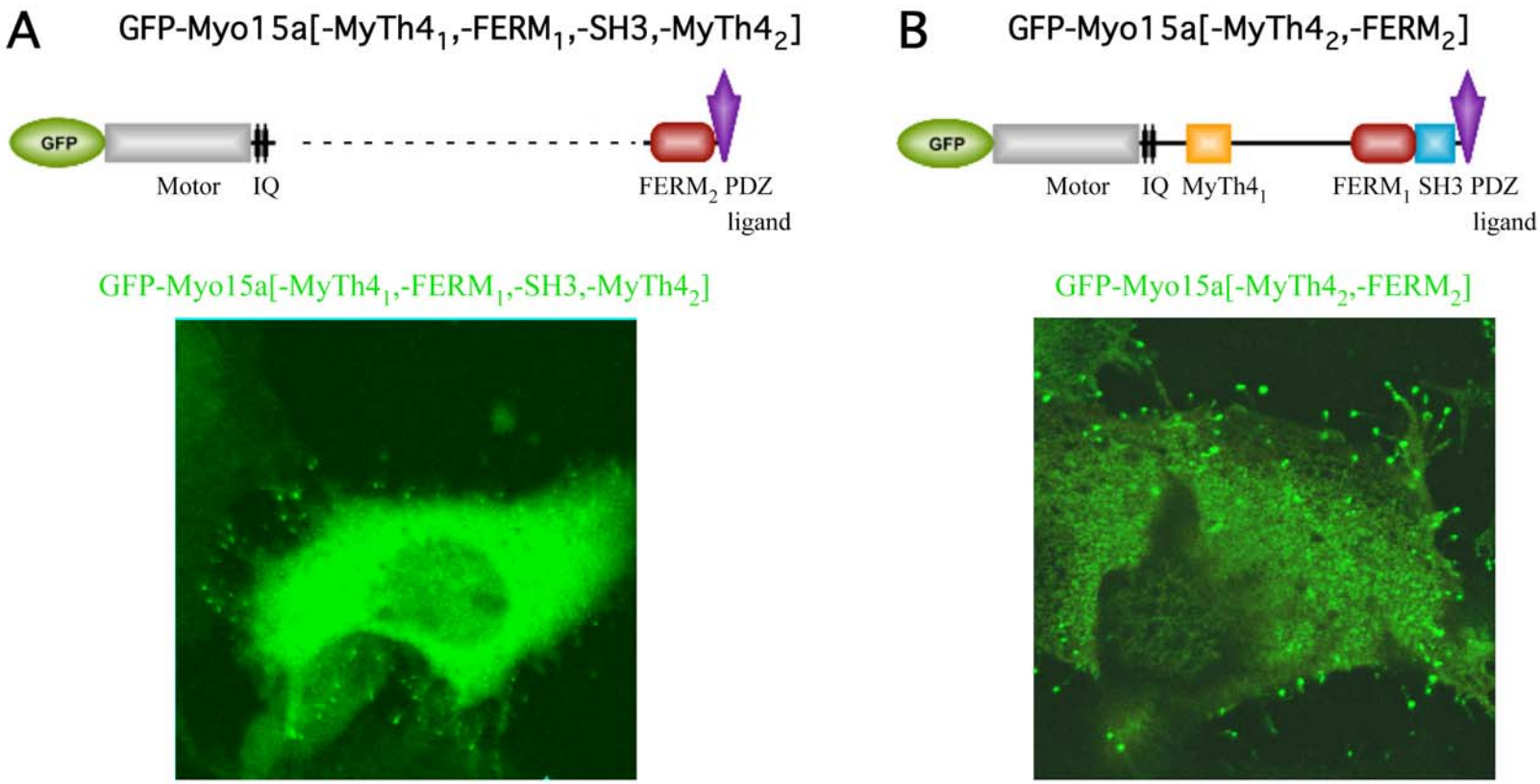

Figure 4-8. Myosin XVa comprised of the motor plus FERM$_2$ domain or motor plus MyTh4$_1$, FERM$_1$ and SH3 domains is sufficient for targeting to filopodia tips. **(A)** Myosin XVa motor plus FERM$_2$ domain accumulates at filopodia tips. **(B)** Myosin XVa motor plus MyTh4$_1$, FERM$_1$ and SH3 domains accumulates at filopodia tips of transfected COS-7 cells. Dotted lines represent deleted regions of myosin XVa.

Motor plus MyTh4$_1$ /FERM$_1$ or FERM$_1$/SH3 domains are sufficient for filopodia tip localization

In this set of experiments, I wish to determine if the myosin XVa motor plus the MyTh4$_1$ and FERM$_1$ domains were sufficient for filopodia tip localization. The transfection of GFP-myosin XVa[-MyTh4$_2$,-FERM$_2$], comprised of the motor, IQ motifs, MyTh4$_1$, FERM$_1$ and SH3 domains, resulted in the accumulation at filopodia tips (figure 4-8B). Next, I transfected GFP-myosin XVa[-SH3,-MyTh4$_2$,-FERM$_2$] into COS-7 cells and observed accumulation at filopodia tips (figure 4-9A). To determine if the motor, IQ motifs and MyTh4$_1$ domain are sufficient for filopodia tip localization, GFP-myosin XVa isoform 2j, a predicted inner ear myosin XVa isoform described in chapter 2 (figure 2-10), was transfected into COS-7 c ells. GFP-myosin XVa isoform 2j was diffusely distributed throughout the cytoplasm and along the length of filopodia (figure 4-9B), implying that the motor plus MyTh4$_1$ domain was not sufficient. Transfection of GFP-myosin XVa[-MyTh4$_1$,-SH3,-MyTh4$_2$,-FERM$_2$], comprised of the motor, IQ motifs and FERM$_1$ domain, resulted in diffuse cytoplasmic distribution (figure 4-10A) similar to motor, IQ motifs and MyTh4$_1$ domain. In contrast to the ability of the motor, IQ motifs and FERM$_2$ domain to target filopodia tips (figure 4-8A), the motor, IQ motifs and FERM$_1$ domain is not sufficient (figure 4-10A). Individually, motor, IQ motifs and MyTh4$_1$ domain nor the motor, IQ motifs and FERM$_1$ domain is capable of targeting to filopodia tips. However, the myosin XVa motor plus the MyTh4$_1$ and FERM$_1$ domains promoted robust targeting to filopodia tips (figure 4-9A), as did the myosin XVa motor plus the MyTh4$_2$/FERM$_2$ domains (figure 4-7B).

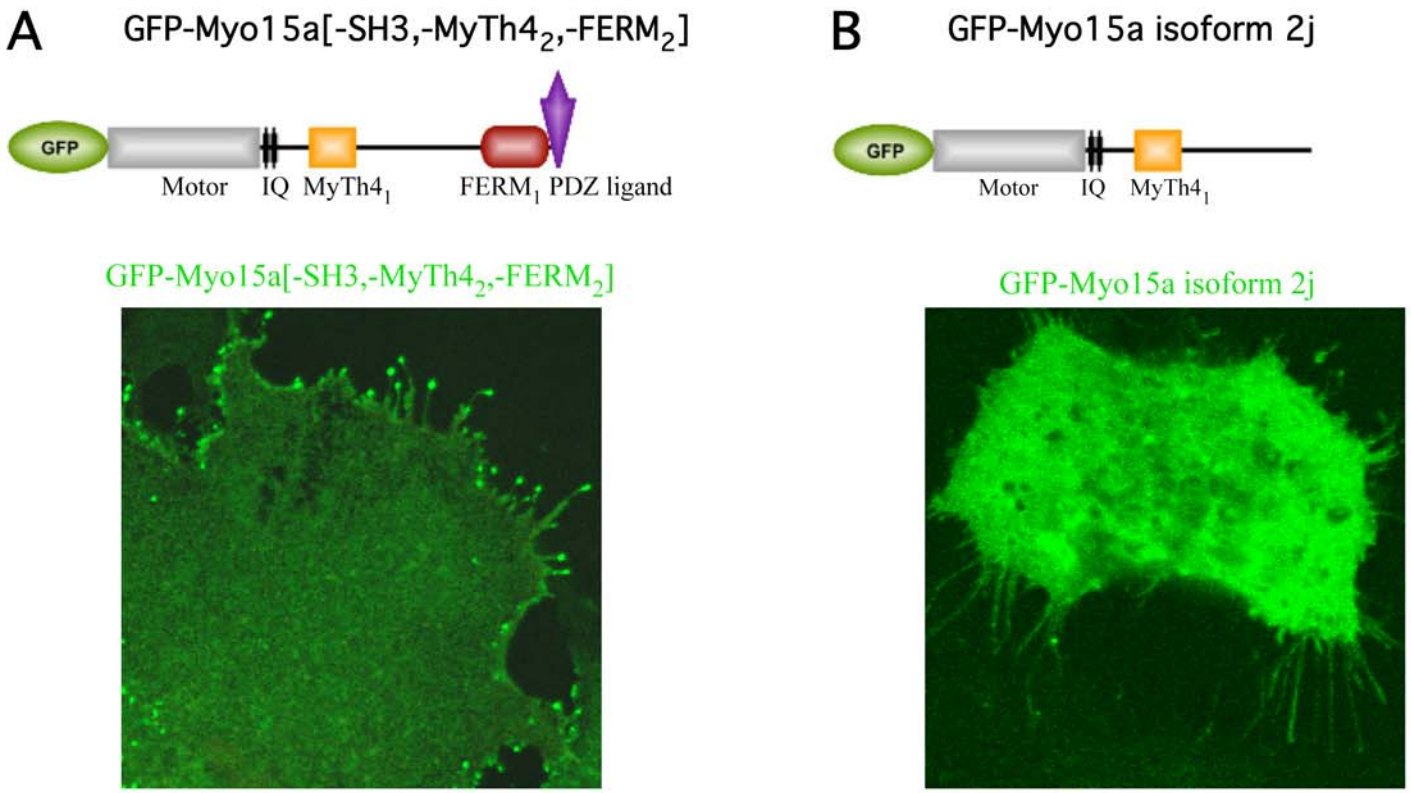

Figure 4-9. Myosin XVa comprised of the motor plus MyTh4$_1$ and FERM$_1$ domains is sufficient for targeting to filopodia tips. **(A)** Myosin XVa motor plus MyTh4$_1$/FERM$_1$ is sufficient for targeting filopodia tips. **(B)** Myosin XVa isoform 2j does not specifically accumulate at filopodia tips but instead is distributed alog the length of filopodia and within the cell body of a transfected COS-7 cell. Dotted lines represent deleted regions of myosin XVa.

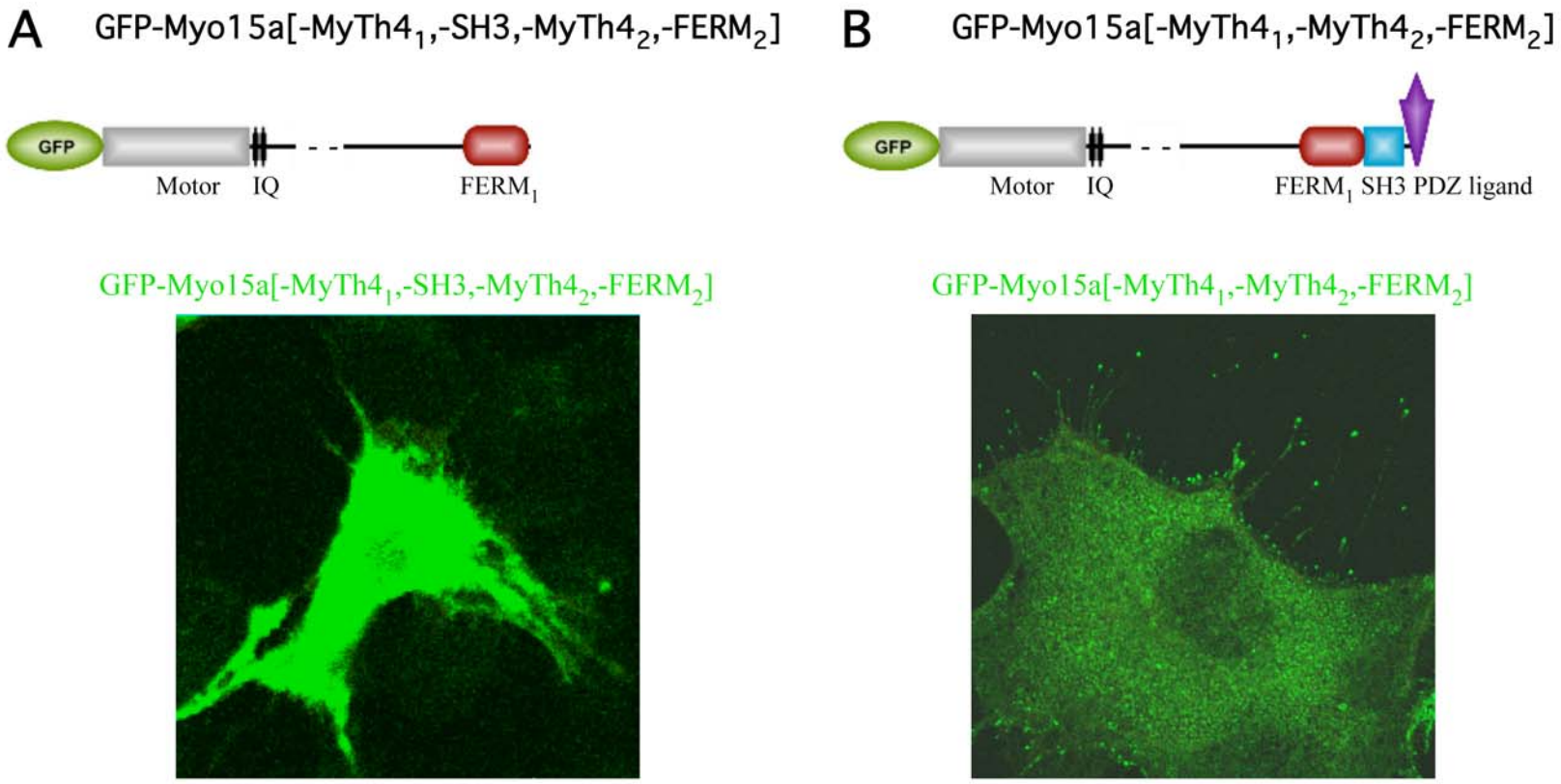

Figure 4-10. Myosin XVa comprised of the motor plus FERM$_1$ and SH3 domains is sufficient for targeting to filopodia tips. **(A)** Myosin XVa motor plus FERM$_1$ domain does not specifically accumulate at filopodia tips but instead is diffusely distributed throughout the cell body and along the length of filopodia. **(B)** Myosin XVa motor plus FERM$_1$ and SH3 domains accumulates at filopodia tips of transfected COS-7 cells. Dotted lines represent deleted regions of myosin XVa.

In my previous COS-7 cell transfection experiments, the absence of the SH3 domain did not result in a noticeable difference in filopodia tip accumulation (figures 4-3, 4-7, 4-8B and 4-9A). However, the addition of the SH3 domain to a myosin XVa deletion protein, incapable of targeting filopodia tips, enabled accumulation at filopodia tips. For example, although the motor, IQ motifs and $FERM_1$ domain was insufficient to target filopodia tips (figure 4-10A), a myosin XVa deletion protein comprised of the motor, IQ motifs and $FERM_1$ and SH3 domains (GFP-myosin XVa[-$MyTh4_1$,-$MyTh4_2$,-$FERM_2$]) was capable of targeting filopodia tips (figure 4-10B). This experiment suggested that the $FERM_1$ and SH3 domain could function as a filopodia tip targeting unit in addition to the $MyTh4_1/FERM_1$ and $MyTh4_2/FERM_2$ domains.

Discussion

Redundant domains for filopodia tip targeting

The limited tissue expression pattern of myosin XVa in anterior pituitary gland secretory cells and inner ear hair cells, suggests that it is a highly specialized motor protein adapted to trafficking within these cell types. In wild type mouse inner ear hair cells, myosin XVa is localized at tips of each stereocilium. Since filopodia in COS-7 cells and stereocilia of inner ear hair cells are comprised of parallel bundled actin filaments whose barbed ends are located at the respective tips, filopodia tip targeting in COS-7 cells was used as a first approximation to a model for myosin XVa trafficking to stereocilia tips.

The results of COS-7 subcellular localization experiments using various GFP-myosin XVa proteins containing deletions of various regions suggests that myosin XVa has multiple redundant domains that are sufficient for targeting to filopodia tips (figure 4-11). The motor plus MyTh4 and FERM domains functions as one possible basic unit for targeting. Both the $MyTh4_1/FERM_1$ and $MyTh4_2/FERM_2$ tandems function with the motor and IQ motifs to promote tip localization. The contributions of the MyTh4 and FERM domains appear to act synergistically, as individually the motor plus $FERM_1$ domain is incapable of filopodia targeting while the motor plus $FERM_2$ domain weakly targets filopodia tips. The motor plus $MyTh4_1$ or $MyTh4_2$ domains appear incapable of targeting filopodia tips.

A second combination of FERM and SH3 domains was sufficient for trafficking to filopodia tips. Motor plus $FERM_1$ and SH3 domains as well as motor plus $FERM_1$, SH3 and $FERM_2$ domains accumulated at filopodia tips. Finally, a third combination of the motor plus $MyTh4_1$, SH3 and $MyTh4_2$ domains targeted to the distal region of filopodia in approximately half of all transfected cells. Collectively taken, these data suggest that the SH3, MyTh4 and FERM domains work in combination with the myosin XVa motor and IQ motifs to promote robust filopodia tip targeting.

The necessity of the myosin XVa motor plus combinations of SH3, MyTh4 and FERM domains for filopodia tip targeting suggests at least two models for the specific accumulation at filopodia tips. The first model predicts that one or more of the of SH3, MyTh4 and FERM domains of myosin XVa interact with a protein

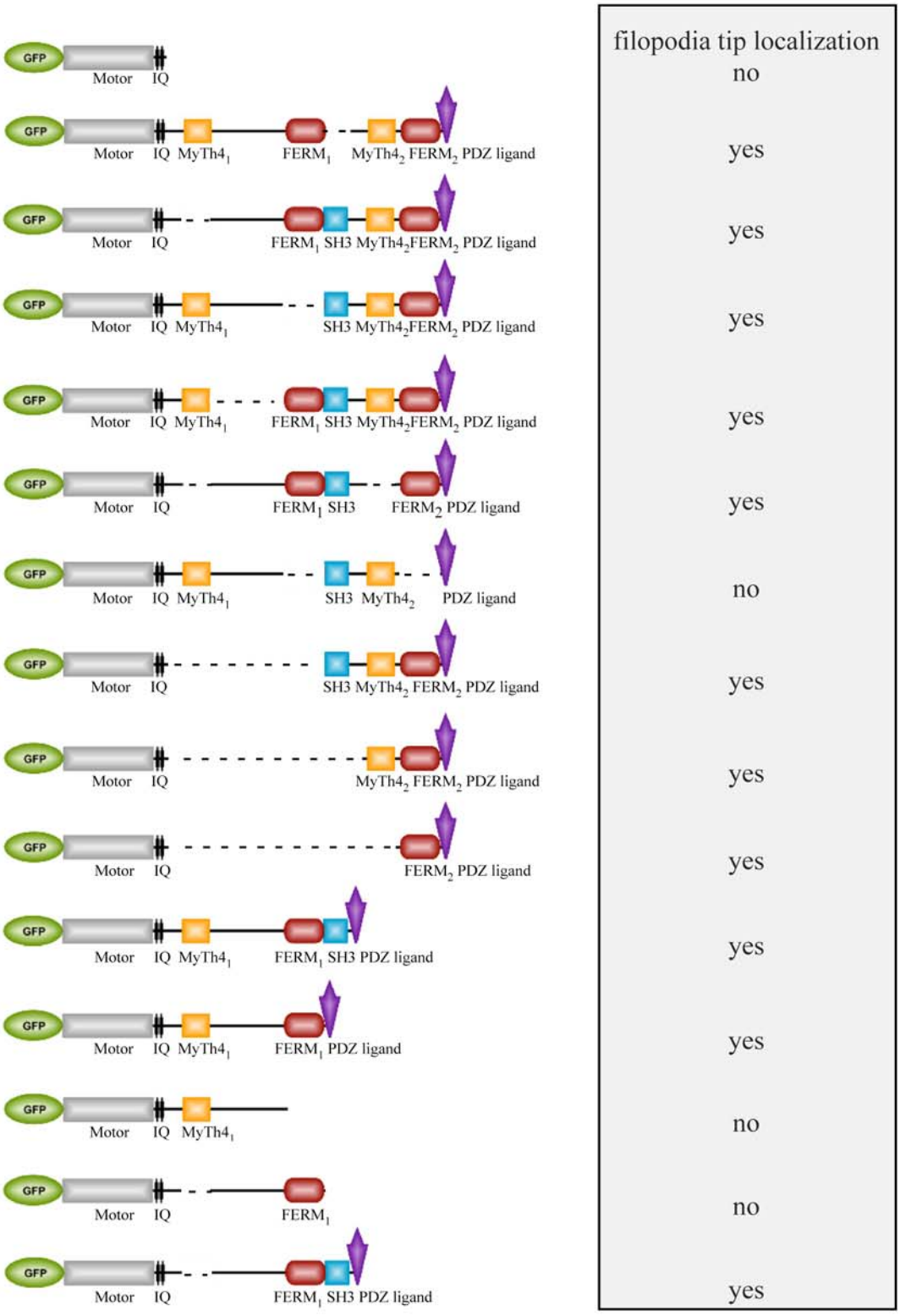

filopodia tip localization
no
yes
yes
yes
yes
yes
no
yes
yes
yes
yes
yes
no
no
yes

Figure 4-11. Summary of COS-7 subcellular localization of GFP-Myosin XVa deletion expression cDNA constructs used in chapter 4. Dotted lines represent deleted regions of myosin XVa.

component of the filopodia tip. Proteins containing SH3 domains interact with specific proline-rich sequences in a diverse array of protein binding partners including cytoplasmic domains of transmembrane proteins as well as peripheral membrane proteins (Kay et al. 2000). The MyTh4 domain of myosin X binds microtubules (Weber et al. 2004), also is essential to formation of dorsal filopodia and likely interacts with an unidentified protein component (Bohil et al. 2006). FERM domains are postulated to mediate protein-protein contacts with integral and peripheral membrane proteins (Oliver et al. 1999).

The second model predicts that one or both of the FERM domains of myosin XVa interact with phosphoinositide-enriched region at the filopodia tip. The highly conserved three-dimensional structure of FERM domains is comprised of three subdomains (Hamada et al. 2000; Pearson et al. 2000). One FERM subdomain interacts with cytoplasmic tails of adhesion proteins such as integrins while another subdomain electrostatically interacts with inositides (Pearson et al. 2000 Niggli 2001; Balla 2005). It remains to be determined if the FERM domains of myosin XVa demonstrate a binding specificity of inositides.

Over-expressed myosin XVa does not promote substrate attached filopodia formation in COS-7 cells

Myosin XVa does not appear to promote substrate-attached filopodia formation since over-expression of GFP-myosin XVa does not appear to result in an increase in the number or length of filopodia relative to non-transfected COS-7 cells. In contrast, over-expression of myosin X in COS-7 cells results in approximately a four fold

increase in the number of substrate-attached filopodia and approximately two and half fold increase in the length of substrate-attached filopodia (Berg et al. 2002). Additionally, over-expression of myosin X induced a five hundred fold increase in filopodia formation on dorsal surfaces of transfected COS-7 cells (Bohil et al. 2006). At this time, we have not determined if over-expression of myosin XVa in COS-7 cells induces increase in dorsal filopodia.

Not all MyTh4/FERM containing myosins target filopodia tips

The presence of a MyTh4/FERM group in a myosin does not assure filopodia tip targeting as demonstrated by the subcellular localizations of myosins VIIa, VIIb and X in transfected COS-7 cells (figure 3-10B). GFP-Myosins VIIa and VIIb, which each contain a SH3 domain and two MyTh4/FERM groups in their tails, accumulate along the length of filopodia and within the cell body of transfected COS-7 cells respectively (figure 3-10B). GFP-myosin X, which contains two pleckstrin homology domains and one MyTh4/FERM group in its tail, targets filopodia tips in COS-7 cells (figure 3-10B). Berg and colleagues reported that a GFP-myosin X heavy meromyosin (HMM) fragment, comprised of the motor, IQ motifs and coiled-coil motif, was the primary determinant of filopodia tip localization in epithelial cells (Berg et al. 2002). There is however, an alternate explanation. GFP-myosin X HMM may have dimerized with an endogenous full-length myosin X molecule, thereby permitting targeting of GFP-myosin X HMM to filopodia tips.

Future Plans

Chimeric Myosins

Based upon the differences in COS-7 localization of mouse myosins VIIa, VIIb, X and XVa, it remains to be investigated whether chimeric myosins containing mixed combinations of motors and tails of myosins VIIa, X and XVa will exhibit different subcellular localizations. For instance, would the myosin VIIa motor plus the myosin XVa tail localize to filopodia tips analogous to GFP-myosin XVa or would it distribute along the length of filopodia like GFP-myosin VIIa? Conversely, would the myosin XVa motor plus the myosin VIIa tail localize to filopodia tips or along the length of filopodia? It is my speculation that the chimeric myosins will acquire the localization property of the tail and behave accordingly. Clearly the tails of myosins VIIa, VIIb, X and XVa represent more than cargo loading sites for proteins to be delivered to their cellular destination and appear to play a role in the dynamic process of trafficking. Likewise, I believe that the motors of myosins VIIa, VIIb, X and XVa are not merely “mindless” plus end directed motors, but rather have evolved to work cooperatively with the tail to direct the myosin to its correct localization.

To address these questions, I will generate six chimeric myosin expression constructs that contain all possible combinations of the motor and tails of myosins VIIa, X and XVa (figure 4-12). To date, I have made four out of six chimeric myosin cDNA inserts, which await cloning into the EGFP-C2 plasmid. These GFP-chimeric myosins will be transfected into COS-7 cells and their subcellular localization will be assessed by confocal microscopy.

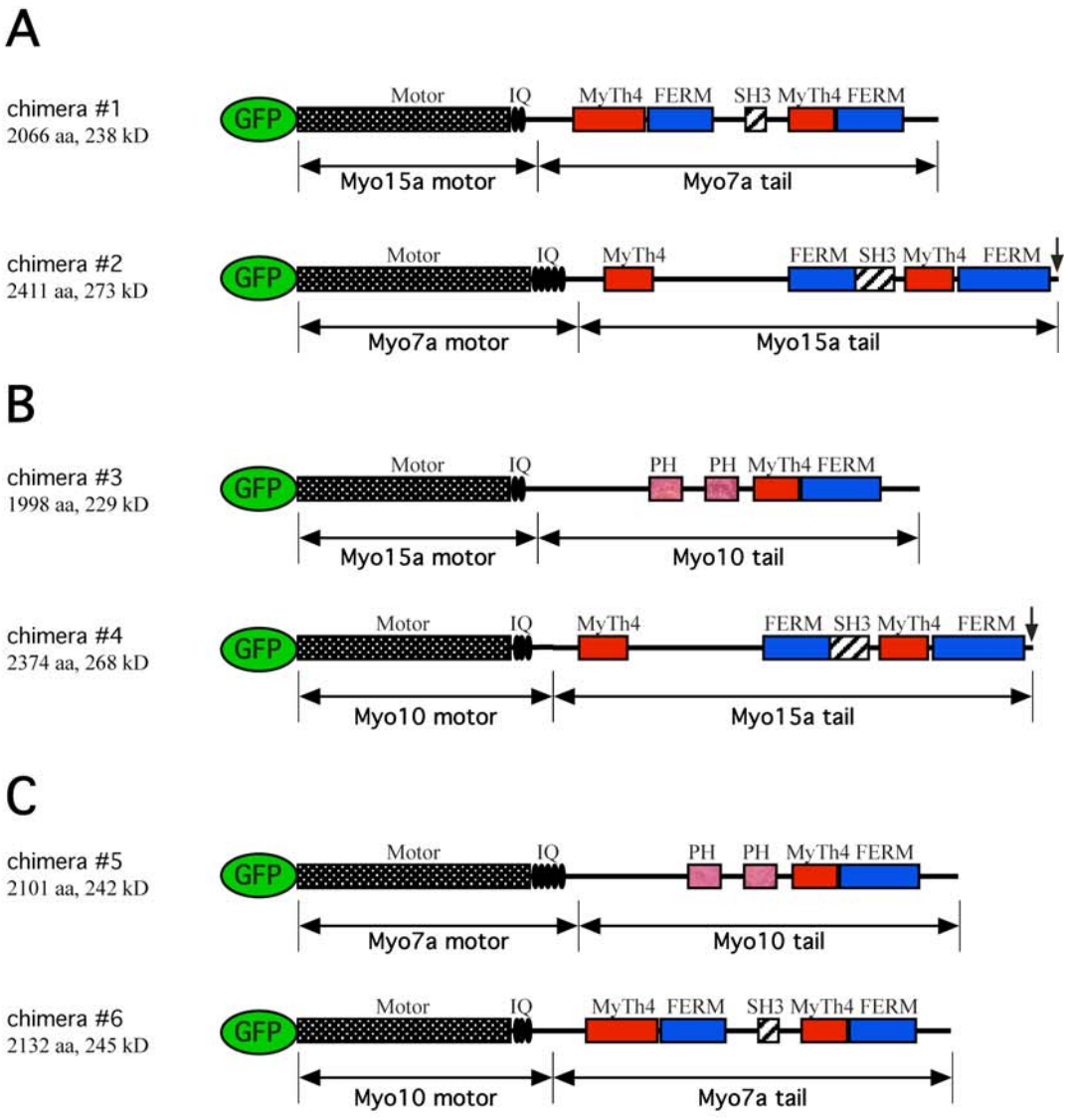

Figure 4-12. Representation of six chimeric myosins that interchange the motor and tail domains of myosins VIIa, X and XVa. **(A)** Myosin chimeras 1 and 2 swap the motor and tail domains of myosins VIIa and XVa **(B)** Myosin chimeras 3 and 4 swap the motor and tail domains of myosins X and XVa **(C)** Myosin chimeras 5 and 6 swap the motor and tail domains of myosins VIIa and X

GFP-mini-myosin XVa: a novel, in vivo protein-protein interaction assay

In chapter 3, the co-transfection of GFP-myosin XVa and dsRed-whirlin into COS-7 cells resulted in the accumulation of both proteins at filopodia tips (figure 3-8A; Belyantseva et al. 2005). The disruption of the protein-protein interaction between whirlin and myosin XVa resulted in myosin XVa accumulation at filopodia tips while dsRed-whirlin remained in the cell body (figure 3-8C and D; Belyantseva et al. 2005). The clarity of interpreting the co-localization of green and red fluorescent signals at filopodia tips in transfected COS-7 cells, far away from the cell body, would make a good assay system for detecting *in vivo* protein-protein interactions.

How would one determine whether or not an interaction occurred between protein A and B? I envision a three-step experiment. In the first step, three expression constructs would be generated; GFP-minimal myosin XVa-protein A, DsRed-protein A and DsRed-protein B. From our experiments described in chapter 4, we determined that a minimal GFP-myosin XVa comprised of the motor, IQ motifs, $MyTh4_2$ and $FERM_2$ domains (i.e. lacking the $MyTh4_1$, $FERM_1$ and SH3 domains) robustly accumulated at filopodia tips at levels nearly indistinguishable from full-length GFP-myosin XVa (figure 4-7B).

In general, as the size of a cloning plasmid decreases, it becomes easier to ligate inserts into it. The use of this minimal GFP-myosin XVa expression construct would therefore offer several advantages. The shorter cDNA insert of this minimal GFP-myosin XVa (3.8 kb instead of 7.0 kb for full-length myosin XVa cDNA) would permit the insertion of the cDNA sequence encoding protein A into the GFP-minimal

myosin XVa plasmid. The size of our GFP-minimal myosin XVa plasmid (8.5 kb) is easily amenable to the cloning of an additional insert. The size of the encoded minimal myosin XVa protein (146 kilodaltons) allows for the myosin XVa-protein A fusion protein to be expressed by the transfected cell. In our experience, proteins with molecular weights of 300 kilodaltons or greater are poorly translated in transfected cells.

The cDNA encoding protein A would be inserted in-frame into a multiple cloning site located upstream of the minimal myosin XVa cDNA insert or into a different plasmid with the multiple cloning site located after the minimal myosin XVa cDNA insert. The encoded protein would be comprised of GFP-myosin XVa fused to protein A. For the second expression construct, the cDNA encoding protein A would be cloned in-frame into the dsRed expression plasmid (Clontech). Finally the cDNA encoding protein B would be cloned into a dsRed expression plasmid.

In the second step of the experiment, COS-7 cells would be transfected using four different combinations of expression plasmids as listed in the table 4-3. After 24 hours of transfection, the cells would be fixed and the subcellular localization examined by confocal microscopy.

Table 4-4. Plasmids used in transfection of COS-7 cells for interaction assay

Transfection	Expression Plasmids	Comment
1	GFP-minimal myosin XVa-protein A DsRed-protein B	Test the interaction of proteins A and B

2	GFP-minimal myosin XVa-protein A	Control
3	DsRed-protein A	Control
4	DsRed-protein B	Control

If protein A interacted with protein B, then GFP-myosin XVa-protein A would be expected to transport the complex to filopodia tips of transfected COS-7 cells (figure 4-13). The co-localization of green and red fluorescent signals at filopodia tips, indicated by the yellow color in the merge panel, would indicate an interaction between protein A and B. If only a green fluorescent signal was observed at filopodia tips while red fluorescent signal was distributed throughout the cytoplasm, then this would indicate that no protein interaction had occurred. The three control transfections (Table 4-3) would indicate whether the assay was useful for studying the interaction of proteins A and B. If GFP-myosin XVa-protein A failed to traffic to filopodia tips (transfection 2), then the assay would not be suitable for studying protein A. If dsRed-protein A (transfection 3) or dsRed-protein B (transfection 4) accumulated at filopodia tips in the absence of myosin XVa transport, then the assay would not be suitable for studying the interactions of proteins A and B.

It remains to be determined if the filopodia targeting of our minimal GFP-myosin XVa would be disrupted if protein A were inserted after the $FERM_2$ domain or if protein A was inserted in front of the myosin XVa motor. The presence of a 1,187 amino acid N-terminal extension preceding the motor in class I myosin XVa isoforms suggest that insertion of some proteins would be well tolerated at this position. To ascertain the ideal position for the insertion of protein A, we will choose three to five

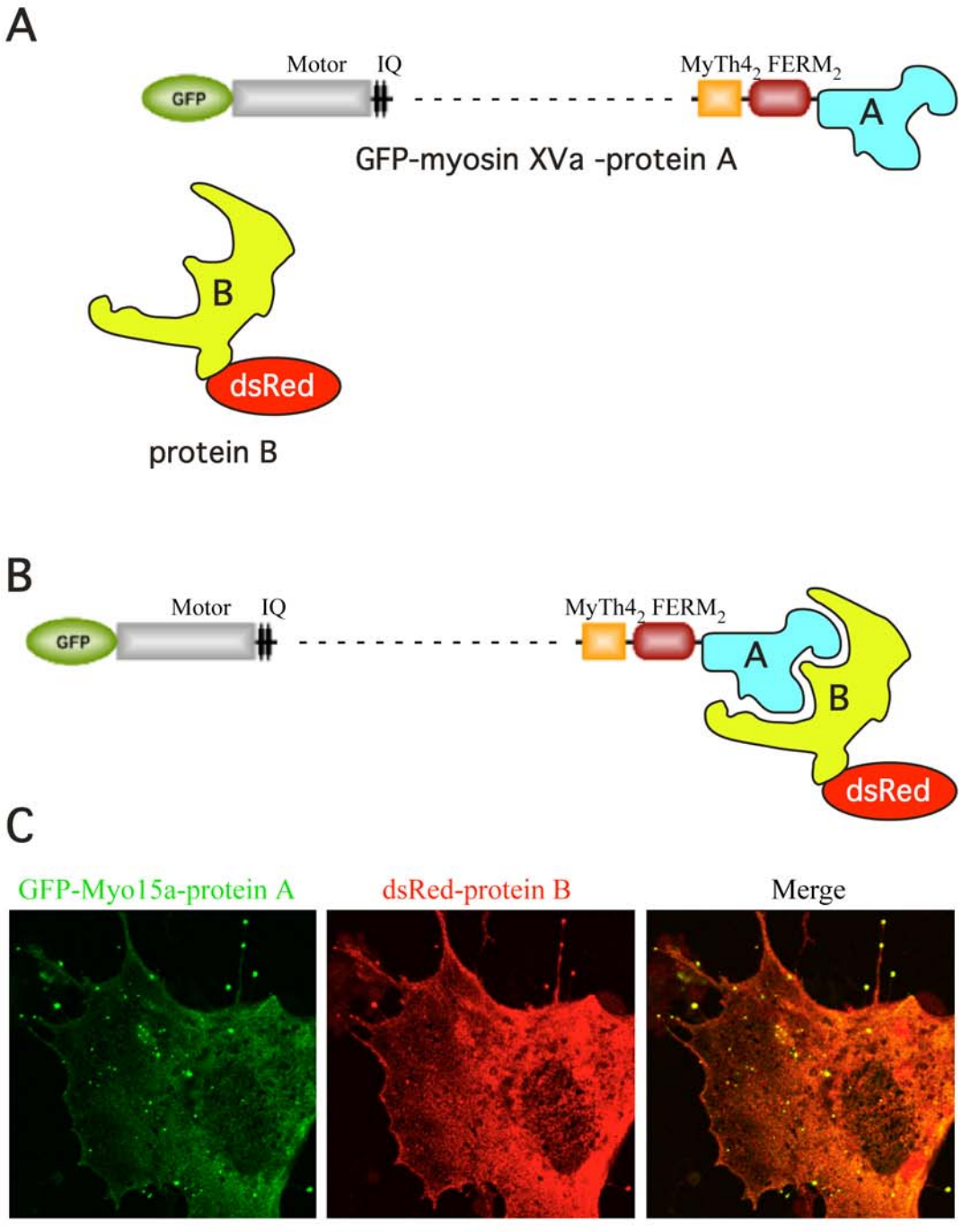

Figure 4-13. Hypothetical result of a "mini-GFP-Myosin XVa" assay showing the interaction of protein A and protein B and transport of protein A-B complex to filopodia tips in transfected COS-7 cells. **(A)** Schematic representation of GFP-myosin XVa-protein A and dsRed-protein B. **(B)** The interaction of of GFP-myosin XVa-protein A and dsRed-protein B. **(C)** GFP-myosin XVa-protein A (left panel) binds dsRed-protein B (middle panel) and transports it to filopodia tips (right panel). Yellow signal at filopodia tips indicates co-localization of GFP-myosin XVa-protein A and dsRed-protein B.

pairs of well-known cytoplasmic and nuclear protein partners and determine if a position effect is evident upon the filopodia targeting of our minimal GFP-myosin XVa. Clearly we should attempt to avoid choosing proteins known to be located endogenously at filopodia tips, since this will likely result in false positive localization at filopodia tips. Likewise cloned proteins should lack organelle-targeting tags such as nuclear localization signals or endoplasmic reticulum retention sequences. Since the proposed assay is cytoplasmic, transmembrane proteins or at least the membrane spanning segments should be avoided. Nonetheless, our choices of protein partner pairs should reflect a diversity of putative interactions from different sub-cellular contexts, not just optimal cytoplasmic protein interaction pairs.

Since the interaction between the two proteins will occur within the context of a living cell, correct folding of the protein partners will be essential for an interaction to occur, prior to transport out of the cell body and to filopodia tips. If the protein-protein interaction is transient and low-affinity, it is unlikely to persist while the protein complex is transported several micrometers along the length of the filopodia. In this respect, it will represent an advantage over *in vitro* pull down assays and immunoprecipitated over-expressed proteins from transfected cells that do not distinguish between true protein interaction and protein aggregation.

Chapter 5: The Role of Myosin XVa in Stereocilia Elongation and Staircase Formation

Abstract

Stereocilia are actin-filled protrusions on the apical surface of inner ear hair cells that convert mechanical stimuli of sound and head movement into electrical signals that are processed by the brain. In mouse hair cells that are homozygous for shaker 2 (*Myo15a*^{sh2}) mutation, stereocilia are abnormally short due to a failure of their actin filamentous core to elongate. The stereocilia bundle of homozygous *Myo15a*^{sh2} hair cells lack the characteristic staircase architecture found in wild type hair cell stereocilia bundles. The inability of mutant myosin XVa to deliver whirlin to stereocilia tips underlies the stereocilia dysmorphology in hair cells from homozygous *Myo15a*^{sh2} mice. Re-initiation of stereocilia elongation and staircase formation was observed in homozygous *Myo15a*^{sh2} hair cells transfected with wild type GFP-myosin XVa, which recruits and delivers endogenous whirlin to stereocilia tips. The subcellular localization and ability to promote stereocilia elongation and staircase formation of several GFP-myosin XVa constructs lacking one or more domains in the tail were evaluated in transfected wild type and homozygous mouse *Myo15a*^{sh2} hair cells. A functional myosin XVa motor was required for stereocilia tip localization as two myosin XVa mutants containing missense mutations in the motor domain failed to accumulate at stereocilia tips. Myosin XVa containing a deletion of the SH3 domain localized at stereocilia tips and elongated stereocilia in homozygous *Myo15a*^{sh2} hair cells. Two myosin XVa proteins containing deletions of multiple domains, the motor, IQ motifs plus MyTh4$_1$/FERM$_1$/SH3 domain and motor, IQ

motifs plus $MyTh4_2/FERM_2$ domains, localized at stereocilia tips but did not promote stereocilia elongation of homozygous *Myo15a*^{sh2} hair cells. Myosin XVa containing deletions of $MyTh4_1$ and $MyTh4_2$ domains failed to localize at stereocilia tips and accumulated in the cell body. Variable results of subcellular localization were obtained for myosin XVa containing deletions of $FERM_1$ and $FERM_2$ domains, more transfected hair cells will be required to draw a definitive conclusion. Therefore, these preliminary results suggest that a myosin XVa motor, IQ motifs plus either $MyTh4_1/FERM_1$ or $MyTh4_2/FERM_2$ domains are sufficient for targeting of this unconventional myosin to stereocilia tips of hair cells.

Introduction

Stereocilia are rod-like, actin protrusions on the apical surface of the sensory hair cells of the inner ear. Displacement of the stereocilia bundle opens mechanosensitive ion channels located either at the distal tips of stereocilia or at the attachment site of the tip link to the next taller adjacent stereocilium (Denk et al. 1995; Holt et al. 2000). In each inner ear hair cell, stereocilia are organized in rows of increasing height, forming the characteristic staircase-like architecture. The cytoskeletal core of each stereocilium is comprised of a rigid paracrystalline array of several hundred parallel, uniformly polarized cross-linked actin filaments (Tilney et al. 1983). The barbed ends of the actin filaments are located at the stereocilia tips while the pointed ends are located at the tapered base of the stereocilia (Tilney et al. 1983; Tilney et al. 1992). The actin cytoskeleton of stereocilia undergoes continuous renewal by the addition of actin monomers at the stereocilia tips, retrograde flow, and disassembly of actin monomers at the base (Schneider et al. 2002; Radzinska et al. 2004).

The development of stereocilia occurs in mouse hair cells in several stages, with these morphological changes observed in vestibular hair cells at an earlier time point than in cochlear hair cells (figure 5-1A). Initially, a single centrally positioned kinocilium surrounded by numerous equal-length microvilli is present on the apical surface of hair cells (Tilney et al. 1992; Forge et al. 1997; Frolenkov et al. 2004). The migration of the kinocilium to one edge of the apical surface establishes the orientation of the staircase bundle and differential elongation of stereocilia rows occurs (figure 5-1B). The stereocilia row closest to the kinocilium elongates first, followed by successively

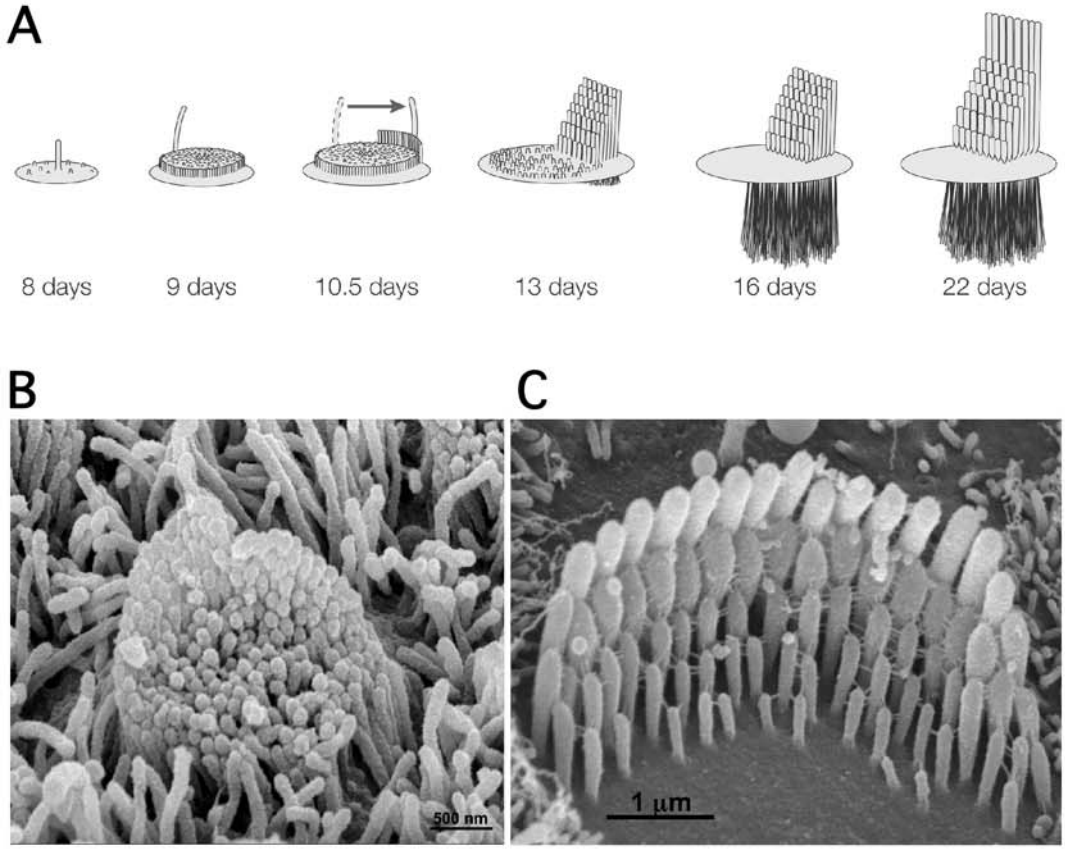

Figure 5-1. Stages of stereocilia development in inner ear hair cells.
(A) Stereocilia bundle development in chicken hair cells. Initially, a central positioned kinocilium is surrounded by numerous short, equal-length microvilli on the apical surface of hair cells. The migration of the kinocilium to one end of the apical surface sets the orientation of the staircase bundle. The stereocilia row closest to the kinocilium elongates first, followed by successively elongation of each row further away. Concurrent with differential elongation of stereocilia, dense packing of actin filaments increases the thickness of stereocilium while cross-linking of actin filaments confers rigidity. Excess microvilli on the apical surface are reabsorbed while differential elongation of stereocilia occurs until pre-determined lengths are achieved. **(B)** Scanning electron microscopy (SEM) image of an immature stereocilia bundle of a mouse post natal day 0 (P0) cochlear inner hair cell. The developmental stage corresponds to approximately day 13 in panel A. **(C)** SEM image of the stereocilia bundle of mouse P9 cochlear inner hair cell during the final stage of differential stereocilia elongation corresponding to days 16 through 22 depicted in panel A. Panel A was reproduced from Frolenkov (2004) and adapted from Tilney (1992). Panels B and C were reproduced from Frolenkov (2004).

elongation of each row further away. Concurrent with differential elongation of stereocilia, dense packing of actin filaments increases the thickness of stereocilium while cross-linking of filaments presumably confers rigidity. Excess microvilli on the apical surface of hair cells are reabsorbed while differential elongation of stereocilia occurs until pre-determined lengths are achieved (figure 5-1C; Tilney et al. 1992; Forge et al. 1997; Frolenkov et al. 2004). The evolutionary conservation of hair cell stereocilia staircase architecture suggests an essential role in mechanotransduction (Fay and Popper 2000; Manley 2000).

In homozygous *Myo15a*^{sh2} hair cells, a cysteine to tyrosine missense mutation in the myosin XVa motor domain disables the motility function, resulting in an absence of myosin XVa at stereocilia tips (figure 3-6A; Belyantseva et al. 2003a). The stereocilia of homozygous *Myo15a*^{sh2} hair cells fail to elongate and achieve a staircase architecture (figure 3-4). The stereocilia bundle development of homozygous *Myo15a*^{sh2} hair cells is arrested at time point analogous to between days 10.5 and 13 in chicken stereocilia development depicted in figure 5-1A. Restoration of the stereocilia bundle architecture was observed in homozygous *Myo15a*^{sh2} hair cells transfected with wild type GFP-myosin XVa (figure 3-11A, B and C).

We observed two events that are critical to re-initiation of stereocilia elongation and staircase formation in transfected *Myo15a*^{sh2} hair cells. The first event was that GFP-myosin XVa must localize at stereocilia tips. The accumulation of myosin XVa at distal tips of stereocilia appears to be an intrinsic property of the motor and/or tail

domains of myosin XVa. However, merely trafficking to the tips of stereocilia was insufficient as evidenced by the failure of myosin XVa lacking the PDZ ligand to re-initiate stereocilia elongation and staircase formation (Belyantseva et al. 2005).

The second event critical for restoration of the stereocilia bundle architecture in transfected *Myo15a*^{sh2} hair cells was the ability of GFP-myosin XVa to bind and deliver endogenous whirlin to stereocilia tips. GFP-myosin XVa[-PDZ_L], which lacks the carboxy four amino acids comprising the carboxy terminal PDZ ligand, localized at stereocilia tips but was unable to restore the stereocilia bundle due to a failure to bind and transport whirlin (figure 3-11D; Belyantseva et al. 2005).

In this study, we sought to answer two different but related questions about myosin XVa. First, what domains of myosin XVa are necessary for trafficking and localization at stereocilia tips in wild type and homozygous mouse *Myo15a*^{sh2} hair cells? Second, what domains of myosin XVa are necessary for re-initiation of stereocilia elongation and staircase formation in homozygous mouse *Myo15a*^{sh2} hair cells?

Methods

For the data in this dissertation, I initiated and completed all of the molecular biology and genotyping of animals. Inna Belyantseva, M.D., Ph.D. transfected my expression constructs into inner ear sensory epithelium cultures and captured the high-resolution confocal images of transfected hair cells. Together, Dr. Belyantseva and I evaluated all of the data.

Genotyping.

The procedure for genotyping wild type, heterozygous shaker 2 and homozygous shaker 2 animals is described in the Methods Section of Chapter 3.

Generation of GFP-Myo15a motor mutants and deletion constructs.

The generation of GFP-myosin XVa deletion constructs used in this study are described in the Methods Section of Chapter 4. Two full-length myosin XVa cDNA expression constructs containing mutations in the motor domain that were predicted to produce a non-motile motor were synthesized. The first motor mutant, GFP-myosin XVa(C592Y), contained a cysteine to tyrosine mutation of an invariant amino acid, which was identical to the shaker 2 mouse mutant (*Myo15a*^{sh2}). The second expression construct encoding a disabled motor, GFP-myosin XVa(R167A/G388A), contained two missense mutations of invariant amino acids that were shown to abolish motility and to lock myosin in a weak actin-binding state (Onishi et al. 1997; Shimada et al. 1997; Li et al. 1998; Onishi et al. 1998; Kambara et al. 1999). The R167A, G388A and C592Y missense mutations were introduced into the coding

sequence of mouse myosin XVa isoform 2a (NCBI Accession # AY331133) using the QuikChange II Site-Directed Mutagenesis Kit (Stratagene).

Myosins VIIa, VIIb and X expression constructs.
The construction mouse GFP-myosins VIIa, VIIb and X cDNA expression constructs are described in the Methods Section of Chapter 3.

Culture and transfection of inner ear sensory epithelium.
The culture, Helios gene-gun transfection, processing and examination of mouse and rat organ of Corti, saccule, utricle and ampulae were described in the Methods Section of Chapter 3.

Immunocytochemistry.
Cultured inner ear sensory epithelia explants were fixed overnight with 4% paraformaldehyde at 4°C. Immunostaining using anti-whirlin antibodies HL5136, HL5137, HL5140, HL5141 was performed as described (Belyantseva et al., 2003a). The specificity of anti-whirlin antibodies is described in chapter 3 (figure 3-13B).

Results

My goal was to determine which domains of myosin XVa are sufficient for trafficking to stereocilia tips and stimulating stereocilia elongation and staircase formation. Therefore, the subcellular localization of several green fluorescent protein (GFP) tagged mouse myosin XVa expression constructs containing deletions of the cDNA encoding individual or multiple domains were evaluated in transfected wild type and homozygous *Myo15a*^{sh2} hair cells (figure 5-2). The domain(s) missing from GFP-myosin XVa deletion protein products were designated in brackets. For example, if the SH3, second MyTh4 and second FERM domains were deleted, the protein was designated GFP-myosin XVa[-SH3,-MyTh4$_2$,-FERM$_2$]. Two myosin XVa motor mutants containing engineered missense mutations in the motor domain predicted to abolish motility were used in this study. The missense mutation(s) in the myosin XVa motor domain are listed in parenthesis. For example, GFP-myosin XVa(R167A/G388A) contains two missense mutations in the motor domain.

A functional myosin XVa motor is required but not sufficient for stereocilia tip localization.

In order to examine whether a functional myosin XVa was necessary for trafficking to stereocilia tips, the subcellular localization of two myosin XVa motor mutants was evaluated. GFP-myosin XVa(C592Y), which contains the missense mutation equivalent to the shaker 2 mouse mutant (*Myo15a*^{sh2}) accumulated in the cell body of transfected wild type hair cells and was absent from the stereocilia (figure 5-3A). The cell body localization of GFP-myosin XVa(C592Y) in transfected hair cells was the

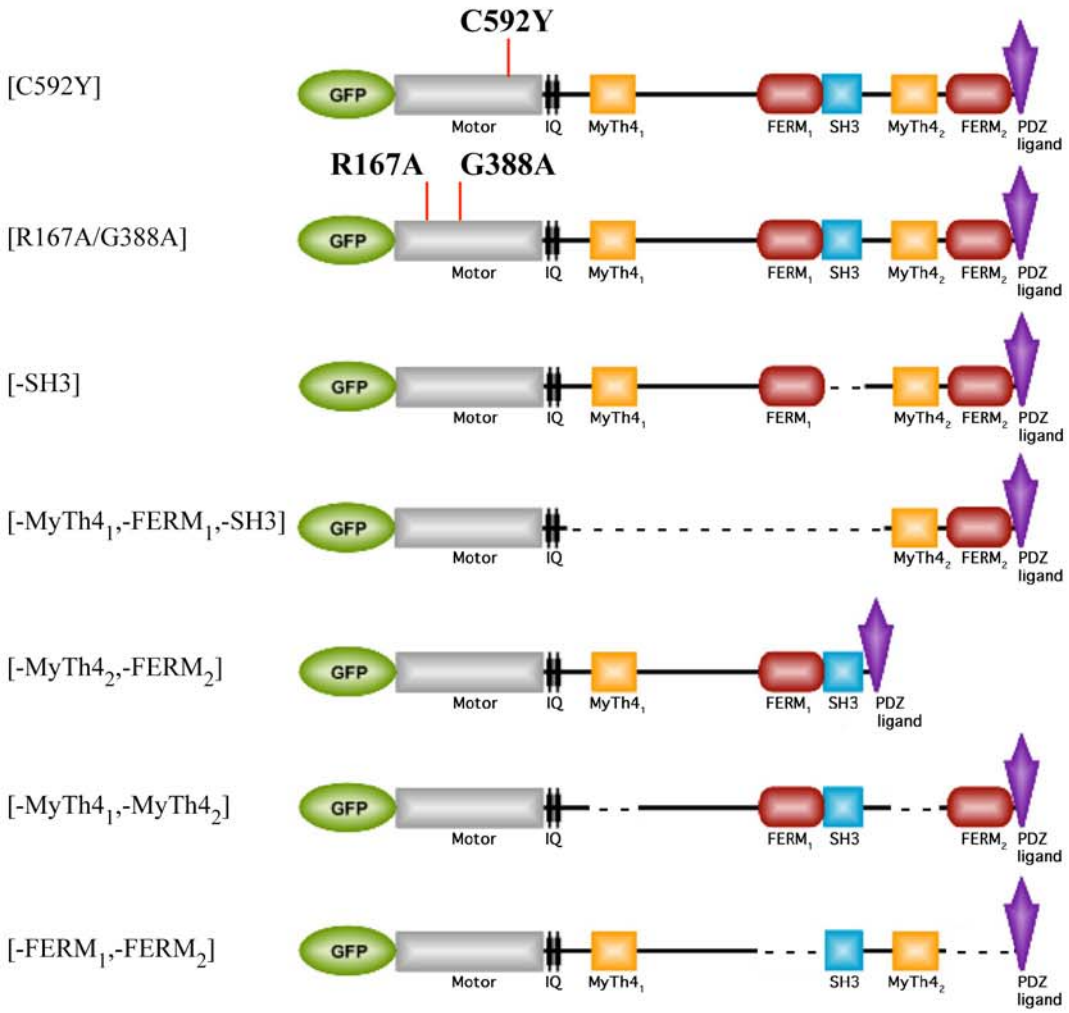

Figure 5-2. GFP tagged myosin XVa motor mutants and deletion proteins used in chapter 5 for studying the domains of myosin XVa necessary for trafficking to stereocilia tips and re-initiation of stereocilia elongation and staircase formation in homozygous *Myo15a*^{sh2} hair cells. GFP-myosin XVa[C592Y] and GFP-myosin XVa[R167A/G388A] are motor mutants containing engineered missense mutations in the cDNA encoding the myosin XVa motor domain. Five GFP-myosin XVa deletion proteins, GFP-myosin XVa[-SH3], GFP-myosin XVa [-MyTh4$_1$,-FERM$_1$,-SH3], GFP-myosin XVa[-MyTh4$_2$,-FERM$_2$], GFP-myosin XVa[-MyTh4$_1$,-MyTh4$_2$] and GFP-myosin XVa[-FERM$_1$,-FERM$_2$] are encoded by GFP-myosin XVa cDNA expression constructs containing deletions of the cDNA encoding individual or multiple domains. The domain(s) missing from these five GFP-myosin XVa deletion proteins are designated in brackets in the left column. For example, GFP-myosin XVa[-MyTh4$_1$,-FERM$_1$,-SH3] protein has the MyTh4$_1$, FERM$_1$ and SH3 domains deleted. Therefore, GFP-myosin XVa[-MyTh4$_1$,-FERM$_1$,-SH3] protein is comprised of the motor, IQ motifs, MyTh4$_1$, FERM$_1$ and PDZ ligand. Dotted lines represent deleted regions of myosin XVa.

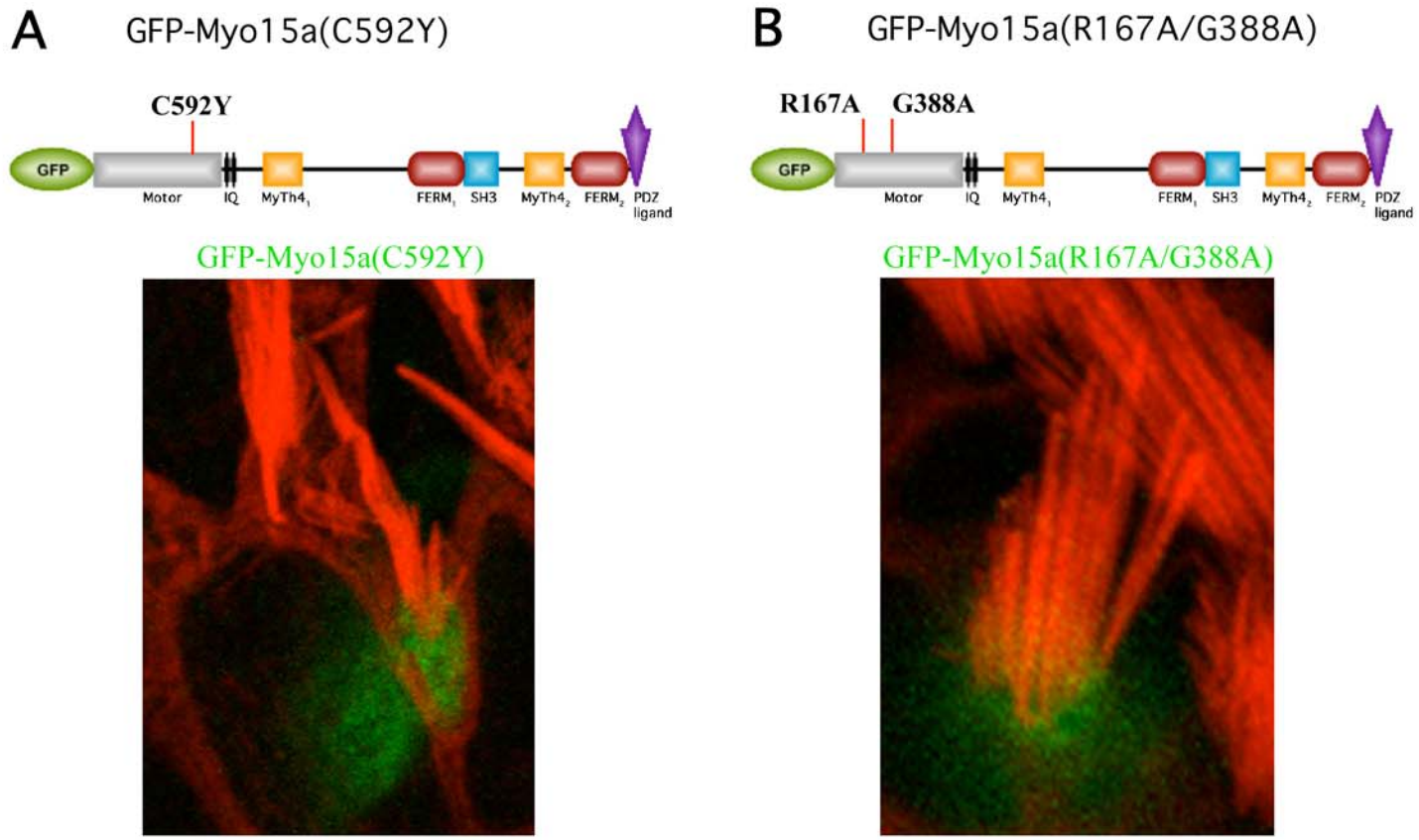

Figure 5-3. A functional motor is required for trafficking of myosin XVa to stereocilia tips. **(A)** GFP-myosin XVa(C592Y), which contains a engineered missense mutation in the motor domain identical to the *Myo15a*^{sh2} mouse, is absent from stereocilia and accumulates in the cell body of a transfected wild type ampulla hair cell. **(B)** GFP-myosin XVa[(R167A/G388A), which contains two missense mutations in the motor domain that are predicted to abolish motility, is absent from stereocilia and accumulates in the cell body of a transfected wild type saccule hair cell. Actin cytoskeleton is stained with rhodamine-phalloidin (red).

same as the localization of endogenous myosin XVa in homozygous *Myo15a*^{sh2} hair cells (figure 3-6A). GFP-myosin XVa(R167A/G388A), which contains two mutations of invariant amino acids in the motor that were demonstrated to abolish motility in other myosins (Onishi et al. 1997; Shimada et al. 1997; Li et al. 1998; Onishi et al. 1998; Kambara et al. 1999), also accumulated in the cell body and was absent from the stereocilia (figure 5-3B). The cell body localization of GFP-myosin XVa(C592Y) and GFP-myosin XVa(R167A/G388A) in transfected hair cells indicates that a functional myosin XVa motor is necessary for correct targeting. Myosin XVa is not passively transported by another mechanism or motor protein to stereocilia tips.

The SH3 domain is not required for stereocilia tip targeting or re-initiation of stereocilia elongation and staircase formation.

The transfection of wild type mouse and homozygous *Myo15a*^{sh2} hair cells with GFP-myosin XVa[-SH3], which lacks the SH3 domain, resulted in accumulation of GFP-myosin XVa[-SH3] at stereocilia tips (figure 5-4). In contrast to wild type GFP-myosin XVa that accumulated exclusively at stereocilia tips (figure 3-8A), some GFP-myosin XVa[-SH3] was observed in the cuticular plate of transfected hair cells. This suggested that the SH3 domain is not necessary for trafficking to stereocilia tips, however it appears to contribute to the efficiency of stereocilia tip targeting. The deletion of the SH3 domain might affect the proper folding of myosin XVa, thereby contributing to less efficient trafficking. Alternatively, disruption of a protein interaction mediated by the SH3 domain could affect the targeting efficiency of GFP-myosin XVa[-SH3].

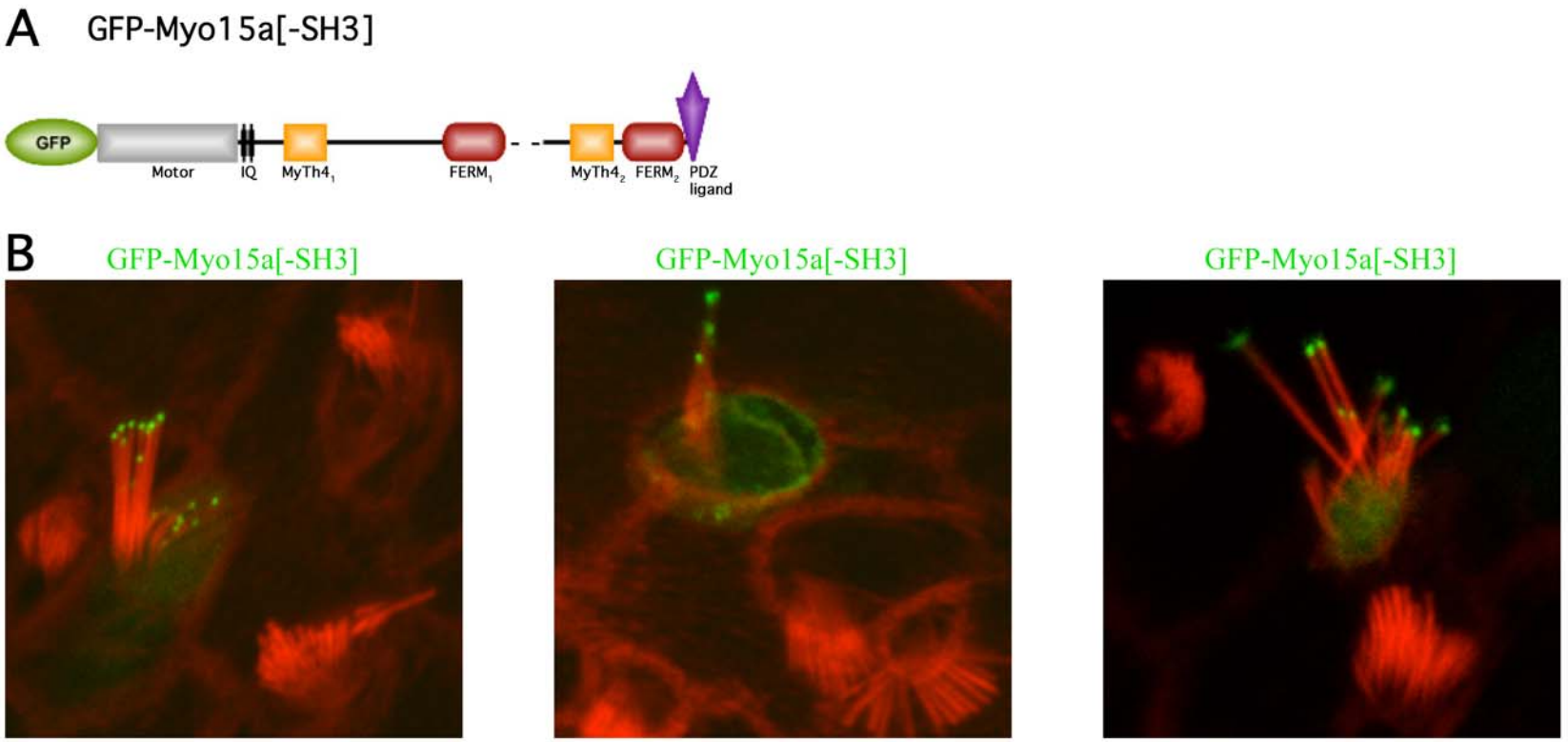

Figure 5-4. The SH3 domain is not required for trafficking of myosin XVa to stereocilia tips nor is it required for the re-initiation of stereocilia elongation and staircase formation in transfected homozygous *Myo15a*^{sh2} hair cells. **(A)** Schematic representation of GFP-myosin XVa[-SH3] protein product. The C-terminal PDZ ligand permits binding of whirlin. **(B)** GFP-myosin XVa[-SH3] accumulates at stereocilia tips and promotes re-initiation of stereocilia elongation and staircase formation in transfected homozygous *Myo15a*^{sh2} utricle (left and center panel) and saccule (right panel) hair cells. Actin cytoskeleton is stained with rhodamine-phalloidin (red).

When GFP-myosin XVa[-SH3] was transfected into homozygous *Myo15a*^{sh2} hair cells, re-initiation of stereocilia elongation and staircase formation was observed (figure 5-4B). This result implied that the SH3 domain is not necessary for re-initiation of stereocilia elongation and staircase formation. While the role of the SH3 domain in stereocilia tip targeting or stereocilia elongation is not evident, it is possible that the SH3 domain of myosin XVa mediates a protein interaction that functionally occurs downstream of stereocilia elongation.

Belyantseva (2005) demonstrated that the re-initiation of stereocilia elongation and staircase formation in transfected *Myo15a*^{sh2} hair cells was dependent upon the binding and delivery of endogenous whirlin to stereocilia tips by GFP-myosin XVa (figure 3-12A and B; Belyantseva et al. 2005). To determine whether GFP-myosin XVa[-SH3] was capable of binding and transporting whirlin in *Myo15a*^{sh2} hair cells, the subcellular localization of myosin XVa and whirlin in transfected COS-7 cells was determined. Co-transfection of COS-7 cells with GFP-myosin XVa[-SH3] and red fluorescently tagged (dsRed)-whirlin resulted in co-localization of both proteins at filopodia tips (figure 5-5). The transfection of dsRed-whirlin without myosin XVa resulted in no whirlin accumulation at filopodia tips (data not shown). This result suggested that GFP-myosin XVa[-SH3] bound and delivered dsRed-whirlin to filopodia tips of COS-7 cells. Indirectly, the COS-7 cell localization data implies that GFP-myosin XVa[-SH3] binds and transports whirlin to stereocilia tips in transfected *Myo15a*^{sh2} hair cells.

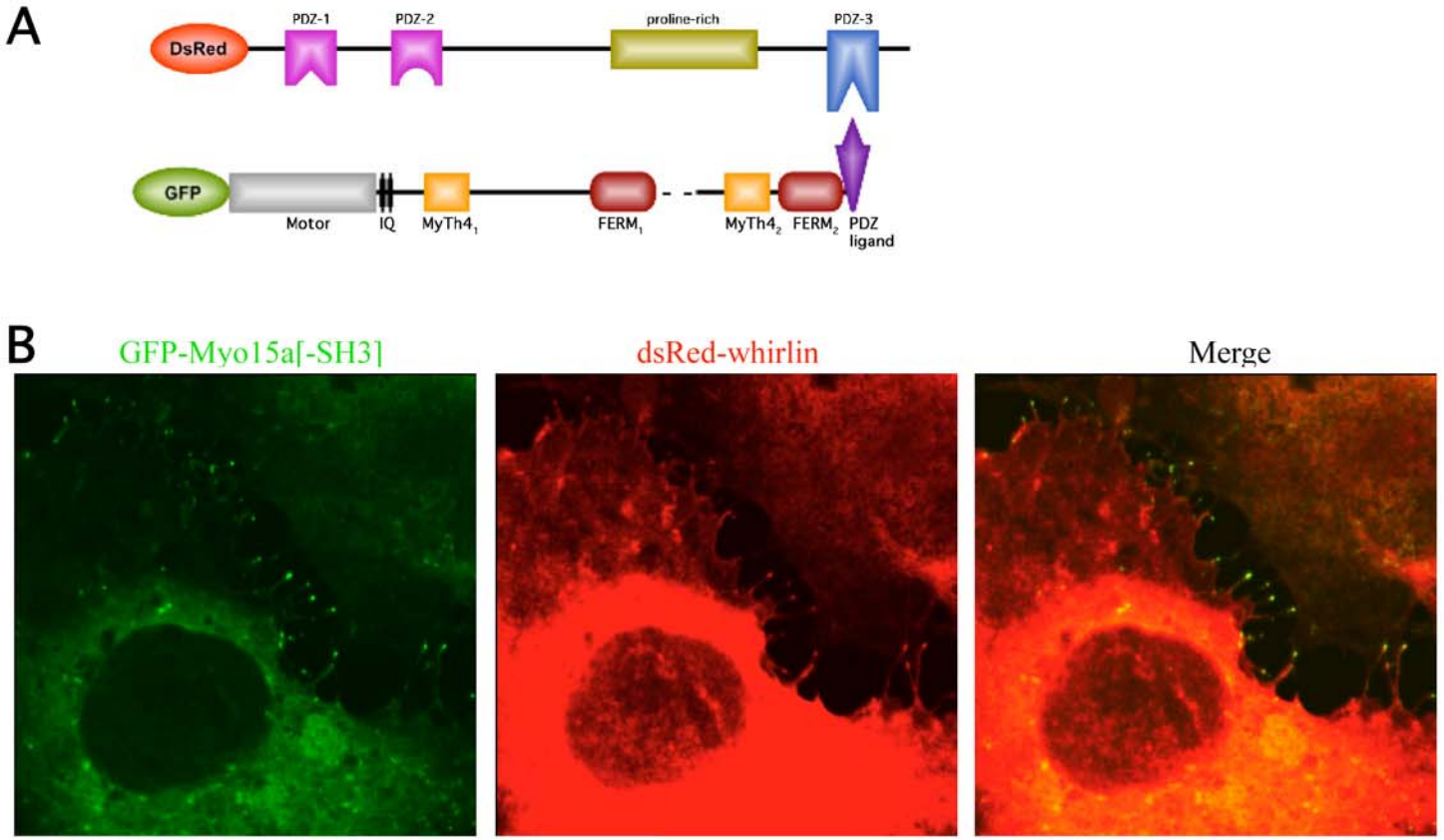

Figure 5-5. Myosin XVa lacking the SH3 domain binds and transports whirlin to filopodia tips of transfected COS-7 cells. **(A)** Representation of the GFP-myosin XVa[-SH3] and dsRed-whirlin protein products. The carboxy terminal PDZ ligand of myosin XVa interacts with the third PDZ domain of whirlin. **(B)** GFP-myosin XVa[-SH3] (left panel) and dsRed-whirlin (middle panel) co-localized at filopodia tips (right panel) of transfected COS-7 cells.

MyTh4$_2$/FERM$_2$ is sufficient for stereocilia tip targeting but not sufficient for re-initiation of stereocilia elongation and staircase formation.

Next, I examined the role of the MyTh4$_2$/FERM$_2$ domains in trafficking to stereocilia tips, stereocilia elongation and staircase formation. The transfection of homozygous *Myo15a*^{sh2} hair cells with GFP-myosin XVa[-MyTh4$_1$,-FERM$_1$,-SH3], which lacked the MyTh4$_1$, FERM$_1$ and SH3 domains, resulted in accumulation at stereocilia tips (figure 5-6). However, no elongation or restoration of the stereocilia bundle was observed in transfected mouse *Myo15a*^{sh2} vestibular hair cells.

One possible reason for the failure of GFP-myosin XVa[-MyTh4$_1$,-FERM$_1$,-SH3] to promote re-initiation of stereocilia elongation and staircase formation was an inability to deliver whirlin to stereocilia tips. Staining with anti-whirlin antibody of homozygous *Myo15a*^{sh2} hair transfected with GFP-myosin XVa[-MyTh4$_1$,-FERM$_1$,-SH3] will reveal whether endogenous whirlin is delivered to stereocilia tips, however this experiment has not been performed at this time. To partially address this question, GFP-myosin XVa[-MyTh4$_1$,-FERM$_1$,-SH3] and dsRed-whirlin were co-transfected into COS-7 cells. Both GFP-myosin XVa[-MyTh4$_1$,-FERM$_1$,-SH3] and dsRed-whirlin accumulated at filopodia tips of transfected COS-7 cells (figure 5-7). The ability of GFP-myosin XVa[-MyTh4$_1$,-FERM$_1$,-SH3] to bind and transport whirlin in COS-7 cells suggests that the failure to promote re-initiation of stereocilia elongation and staircase formation in *Myo15a*^{sh2} hair cells is due to the deletion of the MyTh4$_1$ and FERM$_1$ domains and not a failure to deliver whirlin to stereocilia tips.

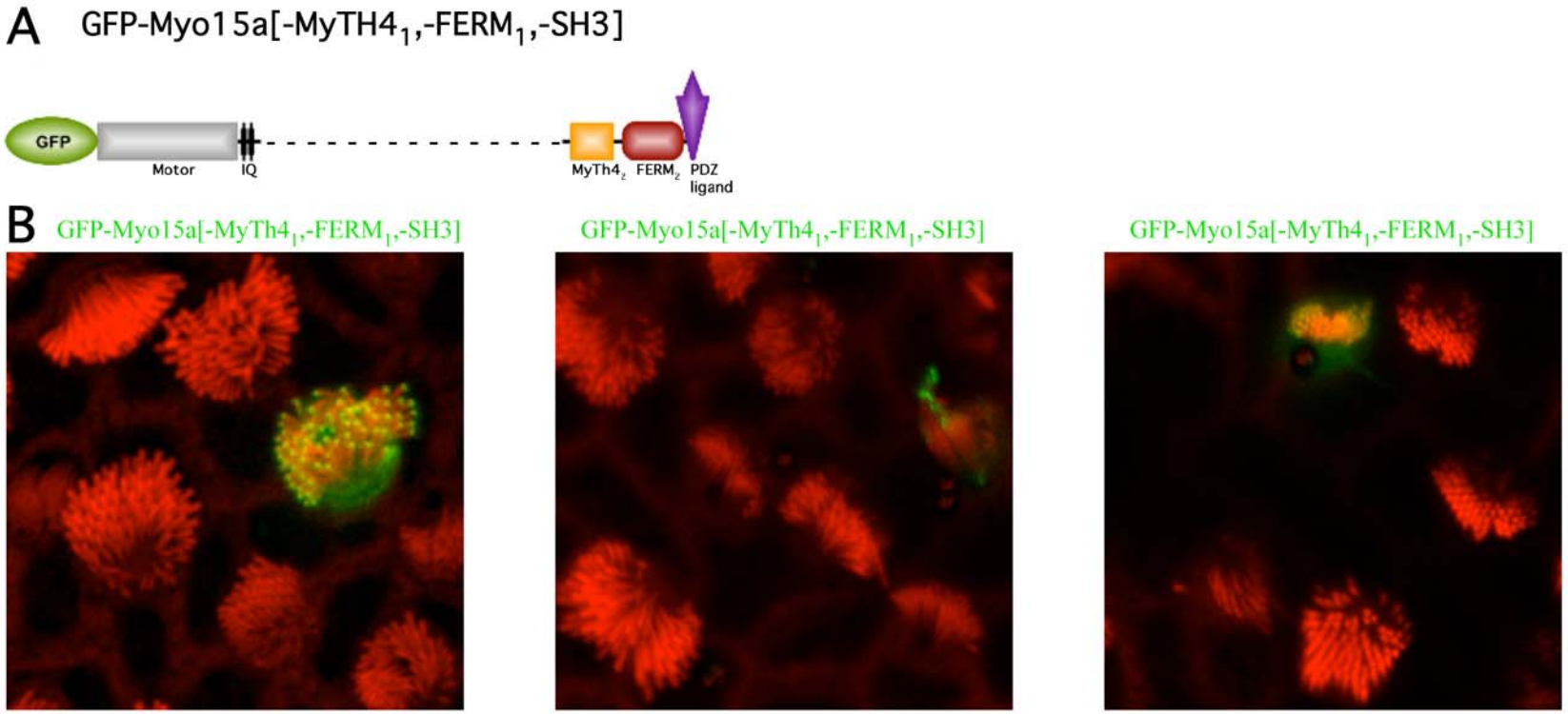

Figure 5-6. The MyTh4$_2$/FERM$_2$ tandem is sufficient for trafficking of myosin XVa to stereocilia but it is not sufficient for the re-initiation of stereocilia elongation and staircase formation in transfected homozygous *Myo15a*^{sh2} hair cells. **(A)** Schematic representation of GFP-myosin XVa[-MyTh4$_1$.-FERM$_1$,-SH3] protein product. The C-terminal PDZ ligand permits binding of whirlin. **(B)** GFP-myosin XVa[-MyTh4$_1$.-FERM$_1$,-SH3] accumulates at stereocilia tips of transfected homozygous *Myo15a*^{sh2}utricle (left panel) and ampulla (center and right panels) hair cells. Re-initiation of stereocilia elongation and staircase formation is not observed in transfected homozygous *Myo15a*^{sh2} utricle or ampulla hair cells. Actin cytoskeleton is stained with rhodamine-phalloidin (red).

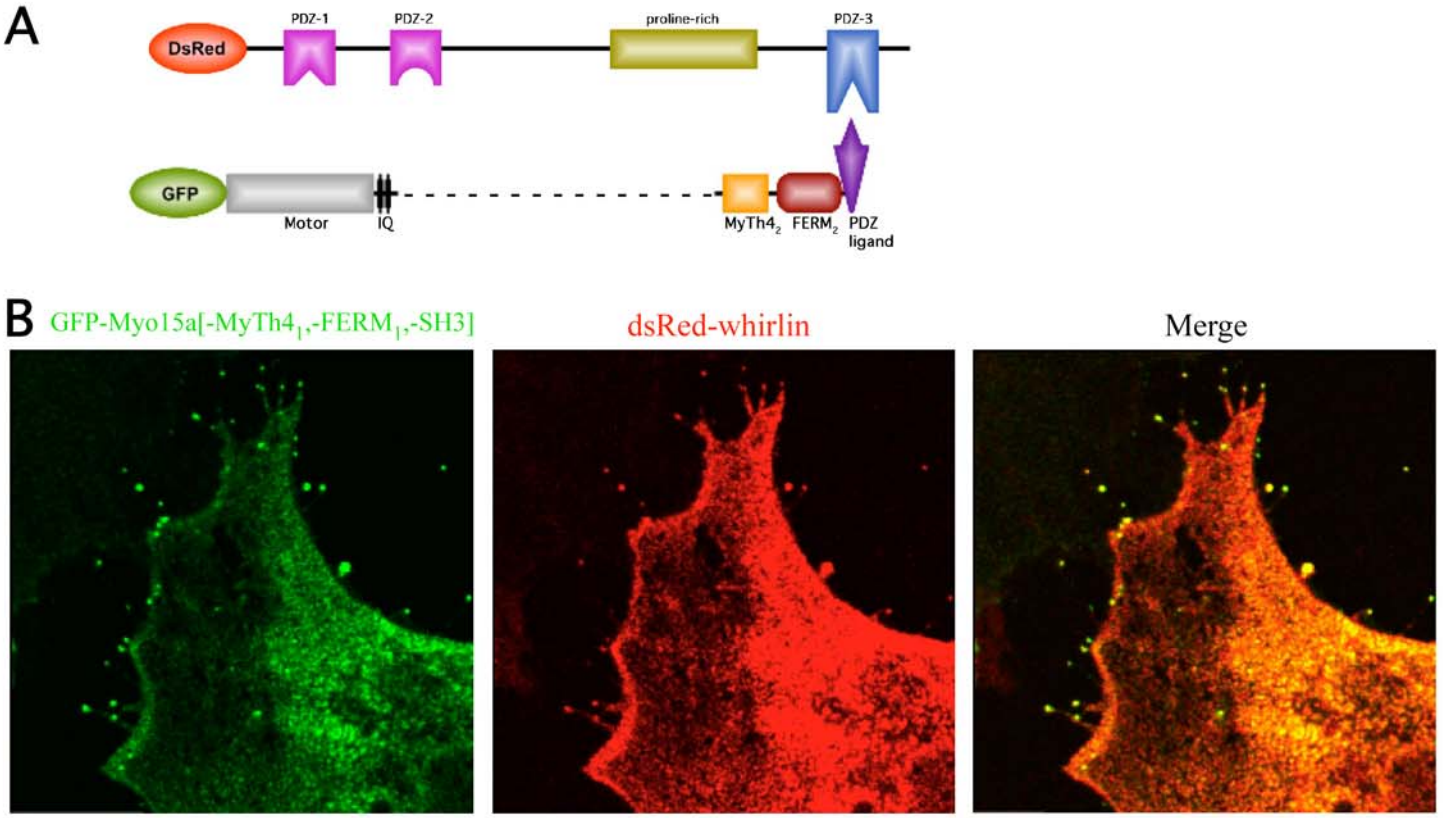

Figure 5-7. Myosin XVa lacking the MyTh4$_1$, FERM$_1$ and SH3 domains binds and transports whirlin to filopodia tips of transfected COS-7 cells. **(A)** Schematic representation of GFP-myosin XVa[-MyTh4$_1$,-FERM$_1$,-SH3] and dsRed-whirlin protein products. The carboxy terminal PDZ ligand of myosin XVa interacts with the third PDZ domain of whirlin. **(B)** GFP-myosin XVa[-MyTh4$_1$, -FERM$_1$,-SH3] (left panel) and dsRed-whirlin (middle panel) co-localized at filopodia tips (right panel) of transfected COS-7 cells.

MyTh4$_1$/FERM$_1$ is sufficient for stereocilia tip targeting but not sufficient for re-initiation of stereocilia elongation and staircase formation.

Our next question was whether the MyTh4$_1$ and FERM$_1$ domains were sufficient for trafficking to stereocilia tips, stereocilia elongation and staircase formation. The transfection of wild type mouse hair cells with GFP-myosin XVa[-MyTh4$_2$,-FERM$_2$] resulted in accumulation at stereocilia tips (figure 5-8A and B). This implied that the MyTh4$_1$ and FERM$_1$ domains were sufficient for trafficking to stereocilia tips.

The transfection of homozygous *Myo15a*^{sh2} hair cells with GFP-myosin XVa[-MyTh4$_2$,-FERM$_2$] did not cause the re-initiation of stereocilia elongation and staircase formation (figure 5-8C and D). *Myo15a*^{sh2} hair cells transfected with GFP-myosin XVa[-MyTh4$_2$,-FERM$_2$] and stained with anti-whirlin antibody showed that GFP-myosin XVa[-MyTh4$_2$,-FERM$_2$] bound and transported endogenous whirlin to the stereocilia tips, however no elongation or restoration of the stereocilia bundle was observed (figure 5-8D). The ability of GFP-myosin XVa[-MyTh4$_2$,-FERM$_2$] to bind and transport whirlin was also observed in COS-7 cells. The co-transfection of GFP-myosin XVa[-MyTh4$_2$,-FERM$_2$] and dsRed-whirlin resulted in the accumulation of both proteins at filopodia tips of COS-7 cells (figure 5-9). Despite the ability to deliver whirlin to stereocilia tips, the MyTh4$_1$ and FERM$_1$ domains were insufficient to promote re-initiation of stereocilia elongation and staircase formation in *Myo15a*^{sh2} hair cells. Collectively taken, the failure of both GFP-myosin XVa[-MyTh4$_1$,-FERM$_1$,-SH3] and GFP-myosin XVa[-MyTh4$_2$,-FERM$_2$] to restore the stereocilia

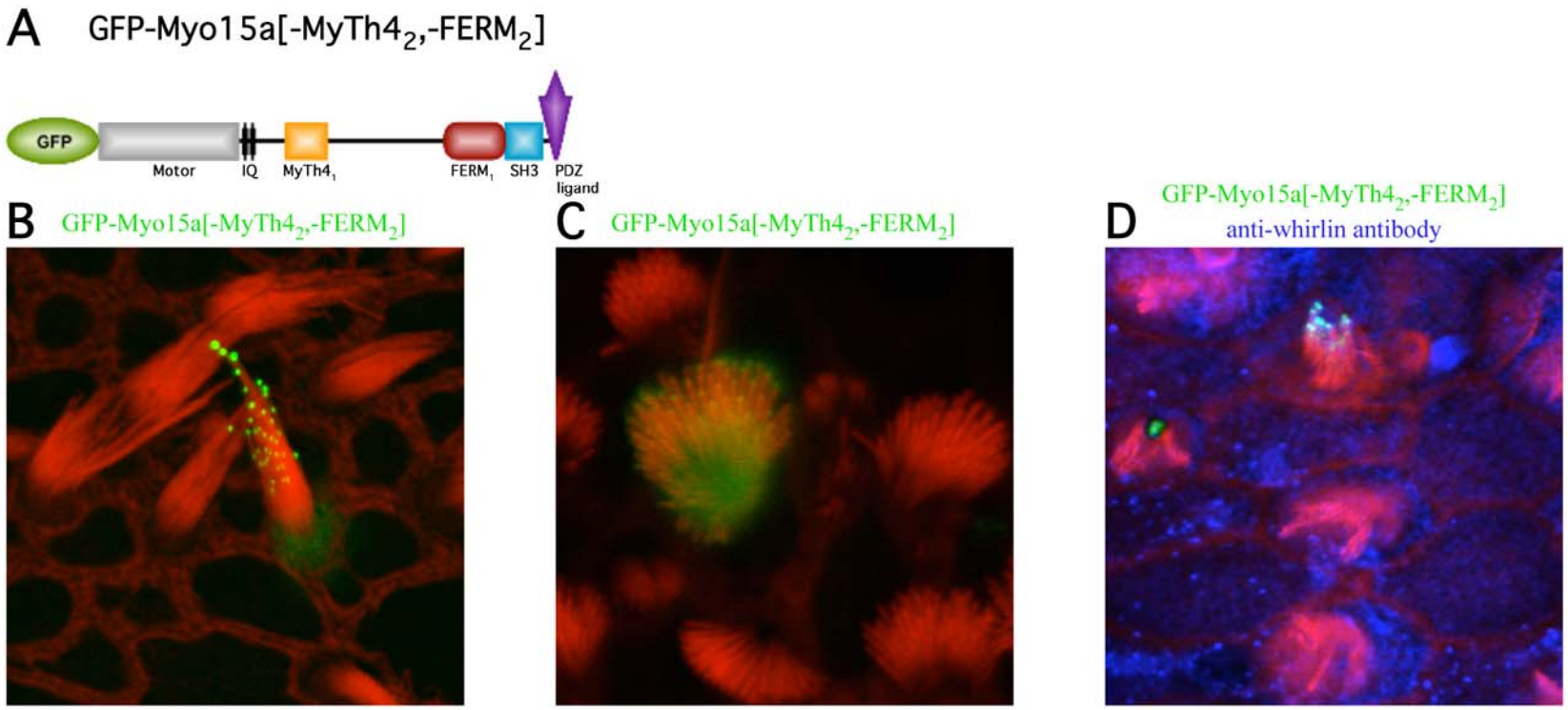

Figure 5-8. The MyTh4$_1$/FERM$_1$ tandem is sufficient for trafficking of myosin XVa to stereocilia tips but it is not sufficient for the re-initiation of stereocilia elongation and staircase formation in transfected homozygous *Myo15a*^{sh2} hair cells. **(A)** Schematic representation of GFP-myosin XVa[-MyTh4$_2$,-FERM$_2$] protein product. The C-terminal PDZ ligand permits binding of whirlin. **(B)** GFP-myosin XVa[-MyTh4$_2$,-FERM$_2$] accumulates at stereocilia tips of a transfected wild type utricle hair cell. **(C)** Re-initiation of stereocilia elongation and staircase formation is not observed in a transfected homozygous *Myo15a*^{sh2} utricle hair cell. **(D)** Endogenous whirlin is bound by GFP-myosin XVa[-MyTh4$_2$,-FERM$_2$] and transported to stereocilia tips of a transfected homozygous *Myo15a*^{sh2} organ of Corti hair cell. Despite the presence of whirlin at stereocilia tips, no restoration of the stereocilia bundle occurred. Actin cytoskeleton is stained with rhodamine-phalloidin (red).

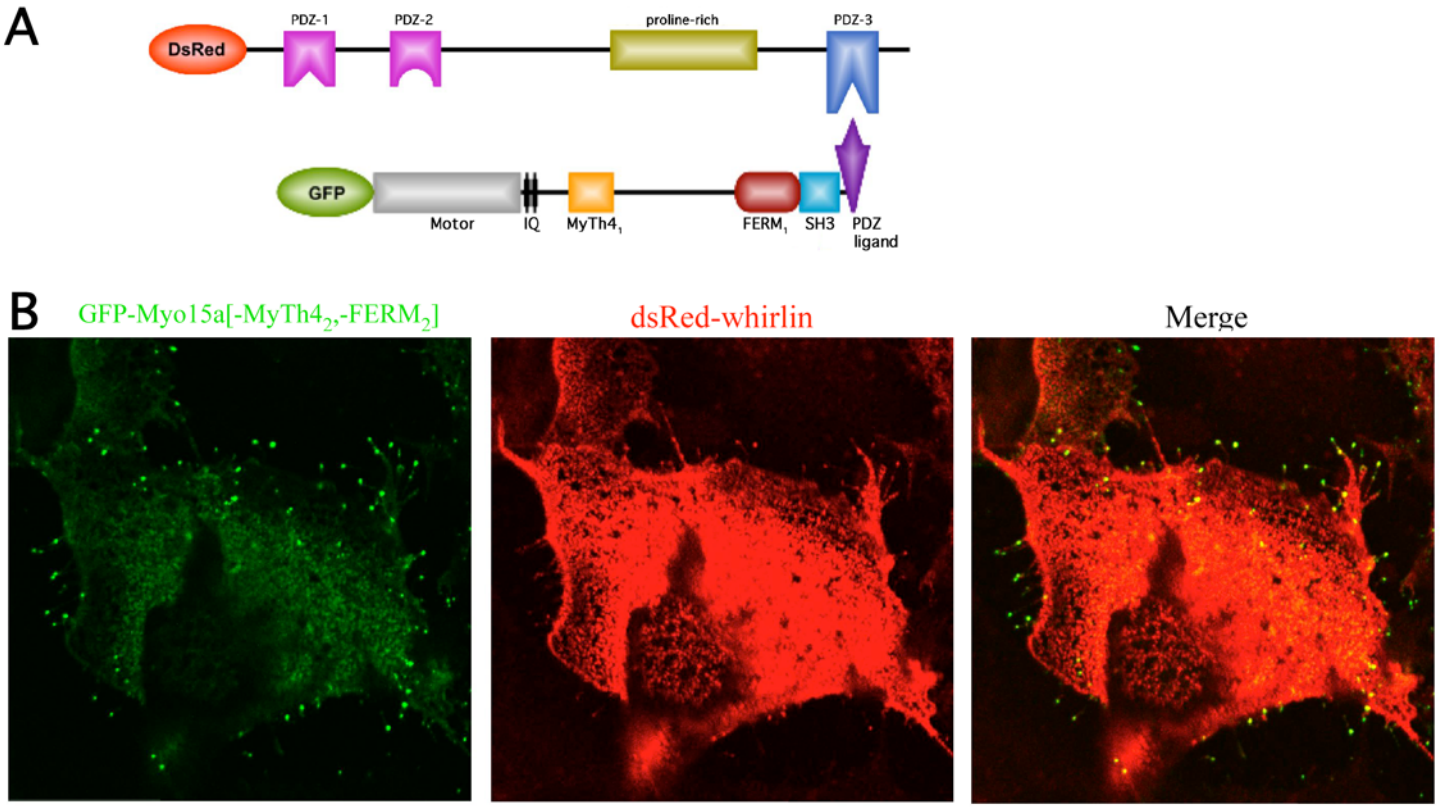

Figure 5-9. Myosin XVa lacking the MyTh4$_2$ and FERM$_2$ domains binds and transports whirlin to filopodia tips of transfected COS-7 cells. **(A)** Schematic representation of GFP-myosin XVa[-MyTh4$_2$,-FERM$_2$] and dsRed-whirlin protein products. The carboxy terminal PDZ ligand of myosin XVa interacts with the third PDZ domain of whirlin. **(B)** GFP-myosin XVa[-MyTh4$_2$,-FERM$_2$] (left panel) and dsRed-whirlin (middle panel) co-localized at filopodia tips (right panel) of transfected COS-7 cells.

bundle architecture, suggests that the MyTh4$_1$, FERM$_1$, MyTh4$_2$ and FERM$_2$ domains work in combination to mediate elongation and staircase formation of stereocilia.

Deletion of both MyTh4 domains abolished stereocilia tip localization

The ability of the myosin XVa motor plus the MyTh4$_1$/FERM$_1$ domains and myosin XVa motor plus the MyTh4$_2$/FERM$_2$ domains to traffic to stereocilia tips, suggests that either a MyTh4 domain or MyTh4/FERM domains are sufficient for stereocilia tip localization. To test the hypothesis that a single MyTh4/FERM tandem is necessary, I deleted both MyTh4 domains of myosin XVa (figure 5-10A). Transfection of GFP-myosin XVa[-MyTh4$_1$,-MyTh4$_2$] into wild type and homozygous *Myo15a*^{sh2} hair cells resulted in accumulation of the protein in the cell body and no detectable amounts in the stereocilia or at the tips of stereocilia (figure 5-10B). The absence of GFP-Myo15a[-MyTh4$_1$,-MyTh4$_2$] protein at stereocilia tips suggested that the normal trafficking of this protein into the stereocilia was altered by the loss of both MyTh4 domains. Moreover, GFP-myosin XVa[-MyTh4$_1$,-MyTh4$_2$] failed to promote re-initiation of stereocilia elongation and staircase formation in *Myo15a*^{sh2} hair cells (figure 5-10D).

One possibility to explain the cell body localization of GFP-myosin XVa[-MyTh4$_1$,-MyTh4$_2$] is that the protein is misfolded. However, two lines of evidence suggest that cell body localization of GFP-myosin XVa[-MyTh4$_1$,-MyTh4$_2$] protein is not due to accumulation of misfolded protein. First, GFP-myosin XVa[-MyTh4$_1$,-MyTh4$_2$]

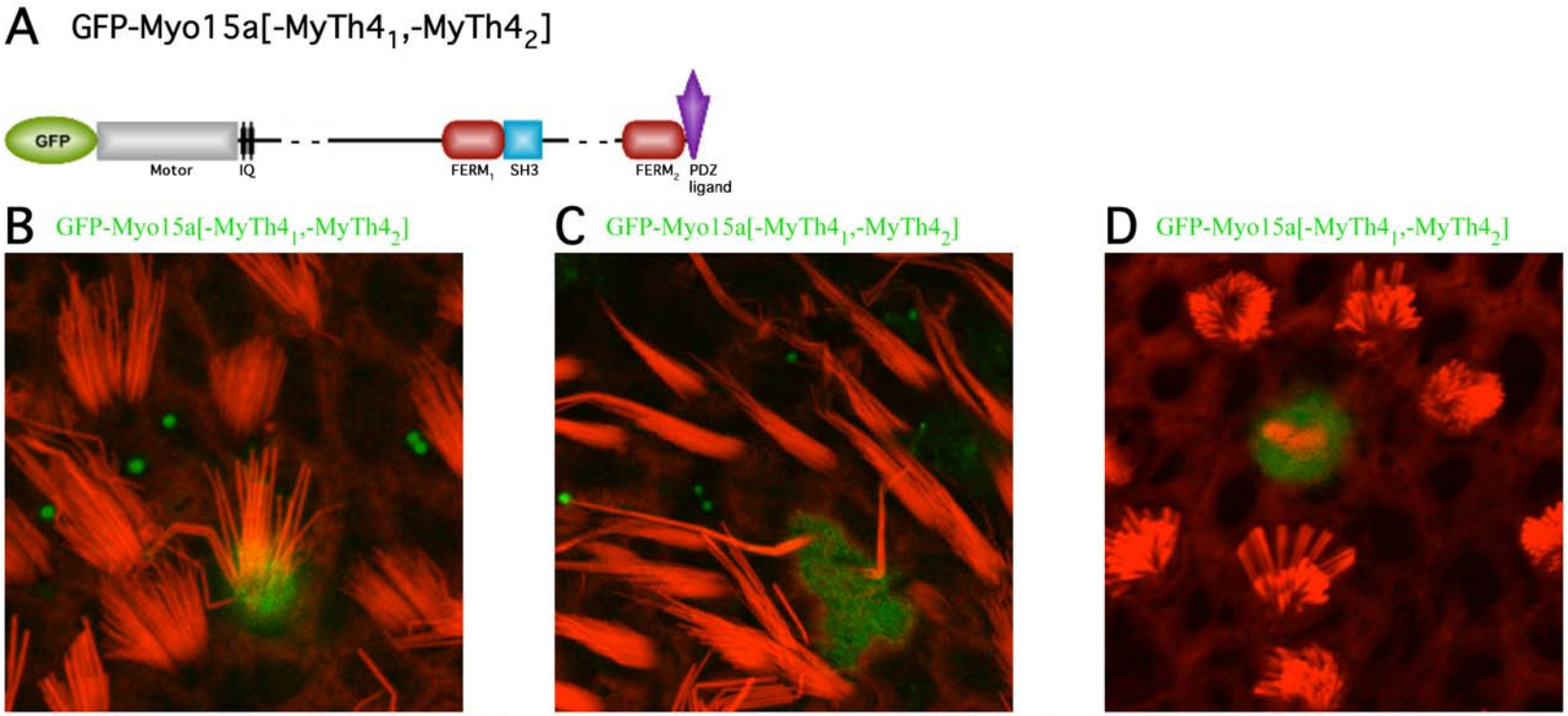

Figure 5-10. The deletion of MyTh4$_1$and MyTh4$_2$ domains abolished myosin XVa localization at stereocilia tips and was insufficient for the re-initiation of stereocilia elongation and staircase formation in transfected homozygous *Myo15a^{sh2}* hair cells. **(A)** Schematic representation of GFP-myosin XVa[-MyTh4$_1$,-MyTh4$_2$] protein product. The C-terminal PDZ ligand permits binding of whirlin. **(B)** GFP-myosin XVa[-MyTh4$_1$,-MyTh4$_2$] is absent from stereocilia and accumulates in the cell body of transfected wild type ampulla hair cell. **(C)** In transfected wild type ampulla hair cell with degenerating stereocilia bundles, GFP-myosin XVa [-MyTh4$_1$,-MyTh4$_2$] accumulates at tips of fused stereocilia. **(D)** Re-initiation of stereocilia elongation and staircase formation is not observed in transfected homozygous *Myo15a^{sh2}* saccule hair cell. Actin cytoskeleton is stained with rhodamine-phalloidin (red).

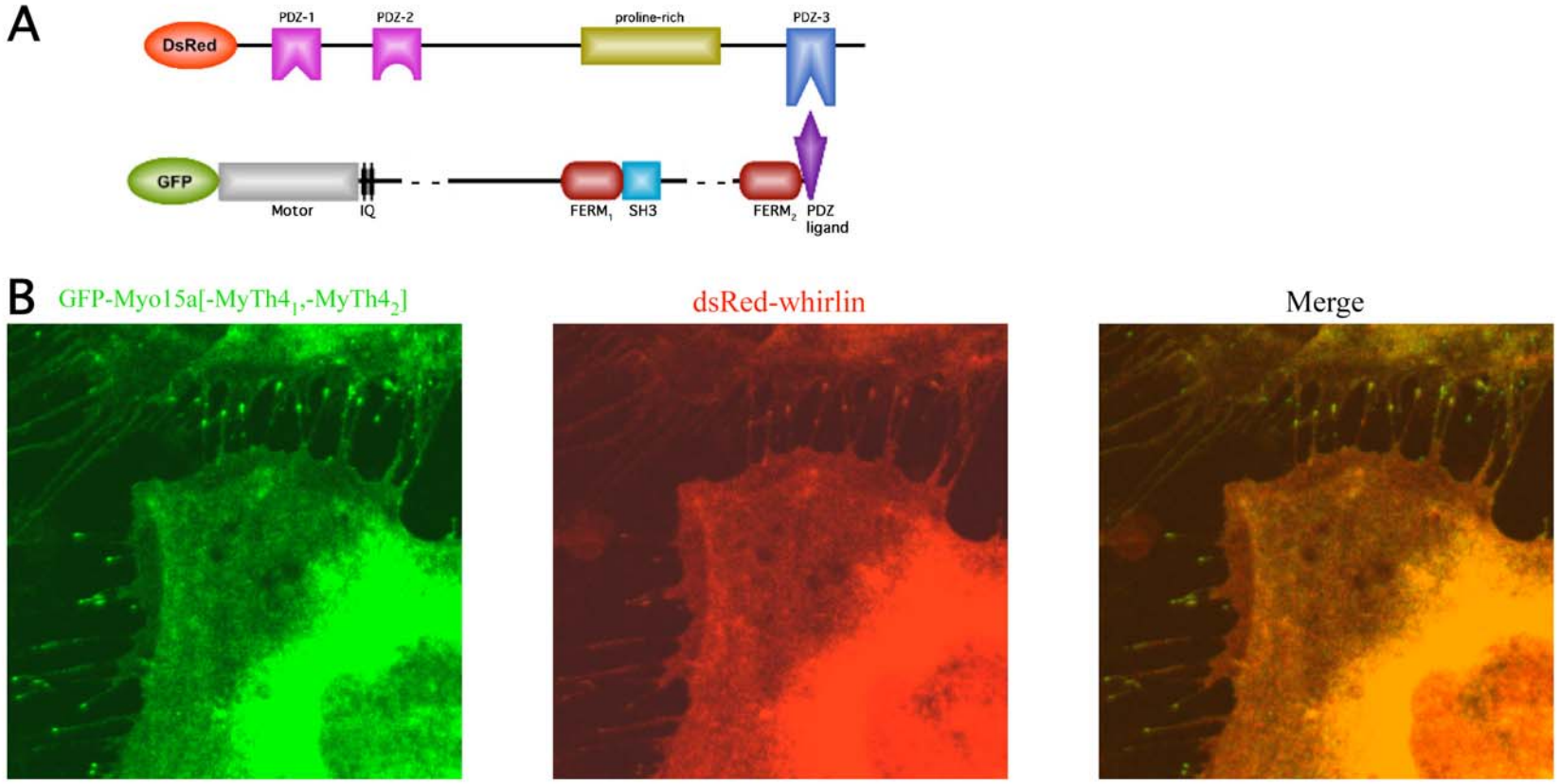

Figure 5-11. Myosin XVa lacking the MyTh4$_1$ and MyTh4$_2$ binds and transports whirlin to filopodia tips of transfected COS-7 cells. **(A)** Schematic representation of GFP-myosin XVa[-MyTh4$_1$,-MyTh4$_2$] protein product. The carboxy terminal PDZ ligand of myosin XVa interacts with the third PDZ domain of whirlin. **(B)** GFP-myosin XVa[-MyTh4$_1$,-MyTh4$_2$] (left panel) and dsRed-whirlin (middle panel) co-localized at filopodia tips (right panel) of transfected COS-7 cells.

accumulated at the tips of degenerating stereocilia bundles in transfected but damaged wild type hair cells (Figure 5-10C). In degenerating stereocilia bundles, individual stereocilium often fuse together to form large “antennae-like” structures. The gold ballistic particles used to transfect hair cells can fatal injure the cell, leading to necrotic signs such as stereocilia bundle degeneration. Second, co-transfection of GFP-myosin XVa[-MyTh4$_1$,-MyTh4$_2$] and dsRed-whirlin into COS-7 cells results in accumulation of GFP-myosin XVa[-MyTh4$_1$,-MyTh4$_2$] and dsRed-whirlin at filopodia tips (figure 5-11). The localization of GFP-myosin XVa[-MyTh4$_1$,-MyTh4$_2$] at filopodia tips suggests that it is a functional, motile myosin protein. If the GFP-myosin XVa[-MyTh4$_1$,-MyTh4$_2$] were misfolded, it would not be expected to accumulate at the tips of filopodia but rather it would be observed within the cell body. The possibility that misfolded GFP-myosin XVa[-MyTh4$_1$,-MyTh4$_2$] could be carried to filopodia tips by another endogenous myosin in COS-7 cells is not a likely explanation. Immunostaining with anti-myosin XVa antisera revealed that endogenous myosin XVa is not present in COS-7 cells (figure 4-2, Belyantseva et al. 2003a). This eliminates the possibility of GFP-myosin XVa[-MyTh4$_1$,-MyTh4$_2$] dimerizing with an endogenous myosin XVa molecule. Also, two non-motile GFP-myosin XVa proteins (GFP-myosin XVa(C592Y) and GFP-myosin XVaR167A/G388A]) accumulate in the cell body of transfected COS-7 cells (figure 3-9C, data not shown and Belyantseva et al. 2005). The failure to observe either non-motile GFP-myosin XVa protein at filopodia tips, indicates that other endogenous myosins are incapable of transporting these myosin XVa proteins with disabling motor mutations.

In summary, the absence of GFP-myosin XVa[-MyTh4$_1$,-MyTh4$_2$] in the stereocilia or at the tips of stereocilia, suggests a critical role for MyTh4 domains in correct trafficking to stereocilia tips in mouse hair cells. The mislocalization of GFP-myosin XVa[-MyTh4$_1$,-MyTh4$_2$] in the cell body does not appear to result from misfolding of the protein. Rather these observations suggest that either a MyTh4 domain or a single group of MyTh4/FERM domains is sufficient for stereocilia tip localization in mouse hair cells.

The incomplete results of the deletion of both FERM domains of myosin XVa

To examine the possibility that the myosin XVa motor plus a single group of MyTh4/FERM domains is sufficient for stereocilia tip localization, I examined the subcellular localization of myosin XVa lacking both FERM domains (figure 5-12A). If MyTh4/FERM domains are necessary for trafficking to stereocilia tips, then deletion of both FERM domains of myosin XVa should result in cell body localization. Despite several attempts, transfection of GFP-myosin XVa[-FERM$_1$,-FERM$_2$] was generally unsuccessful. Only three transfected hair cells were obtained. In two transfected hair cells, GFP-myosin XVa[-FERM$_1$,-FERM$_2$] accumulated at stereocilia tips (figure 5-12B and C) while cell body localization was observed in a third transfected hair cell (figure 5-12D). The small number of transfected hair cells and the conflicting subcellular localization results does not allow us to conclude whether FERM domains are essential for trafficking to stereocilia tips. Thus, we are unable to conclude if myosin XVa motor plus a MyTh4 domain or MyTh4/FERM

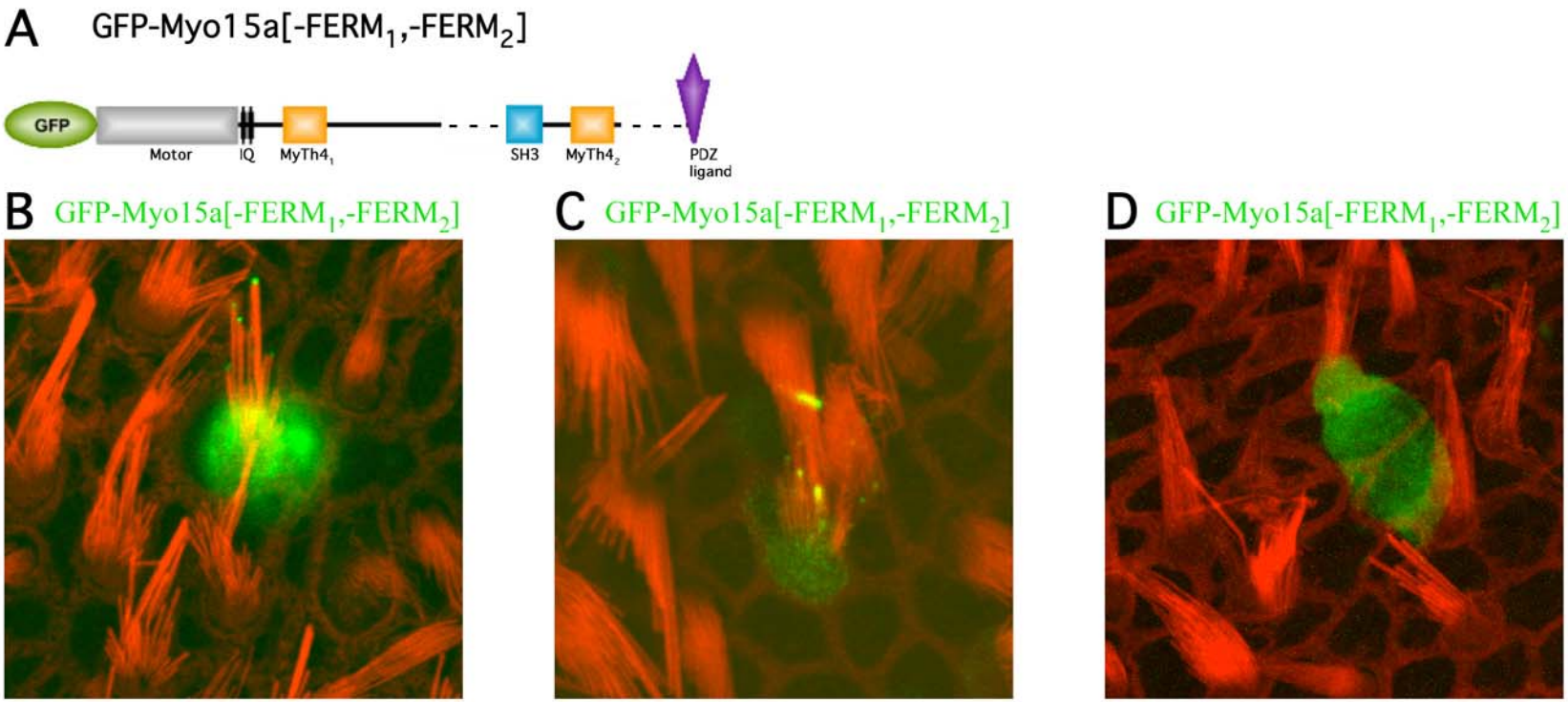

Figure 5-12. Variable results on the subcellular localization results for myosin XVa[-$FERM_1$,-$FERM_2$], which lacks the $FERM_1$ and $FERM_2$ domains. **(A)** Schematic representation of GFP-myosin XVa[-$FERM_1$,-$FERM_2$] protein product. The C-terminal PDZ ligand permits binding of whirlin. **(B)** GFP-myosin XVa[-$FERM_1$,-$FERM_2$] accumulates at stereocilia tips of a transfected rat wild type saccule hair cell. **(C)** In transfected heterozygous *Myo15a*^{sh2} utricle hair cell, GFP-myosin XVa[-$FERM_1$,-$FERM_2$] accumulates at stereocilia tips. **(D)** Computer three dimension reconstruction of serial optic sections taken through the optic plane reveals that GFP-myosin XVa[-$FERM_1$,-$FERM_2$] is localized in the cell body but absent from stereocilia of a transfected rat wild type ampulla hair cell. Actin cytoskeleton is stained with rhodamine-phalloidin (red).

domains is sufficient for stereocilia tip localization. No homozygous *Myo15a*^{sh2} hair cells were transfected with GFP-myosin XVa[-$FERM_1$,-$FERM_2$], so it is not known if FERM domains are essential for stereocilia elongation and staircase formation.

MyTh4 or MyTh4/FERM domains are not generic stereocilia targeting motifs

Our hair cell subcellular localization results of GFP-myosin XVa[-$MyTh4_1$,-$MyTh4_2$] and GFP-myosin XVa[-$FERM_1$,-$FERM_2$] suggests that either myosin XVa's MyTh4 domains or MyTh4/FERM domains are essential for trafficking to stereocilia tips. This raises the question of whether other myosins containing MyTh4 or MyTh4/FERM domains would target to stereocilia in hair cells. In the mammalian proteome, myosins VIIa, VIIb and X contain MyTh4 or MyTh4/FERM domains in their respective tails (figure 5-13A). Hair cell transfection of GFP tagged myosins VIIa, VIIb and X resulted in different subcellular localization. GFP-myosin VIIa accumulates along the length of stereocilia (figure 3-8E). Transfection of GFP-myosins VIIb and X resulted in accumulation in the cell body of hair cells (figure 5-13B and C). Flattened Z-stack of serial optical sections taken through the optical plane of transfected hair cells reveals that GFP-myosins VIIb and X are localized throughout the cell body and are absent from stereocilia. It is not known whether myosin VIIb or X are endogenously present within hair cells. The different subcellular localization of GFP-myosins VIIa, VIIb and X in transfected hair cells suggests that a non-myosin XVa MyTh4 domain or MyTh4/FERM domains are not sufficient for trafficking to stereocilia tips.

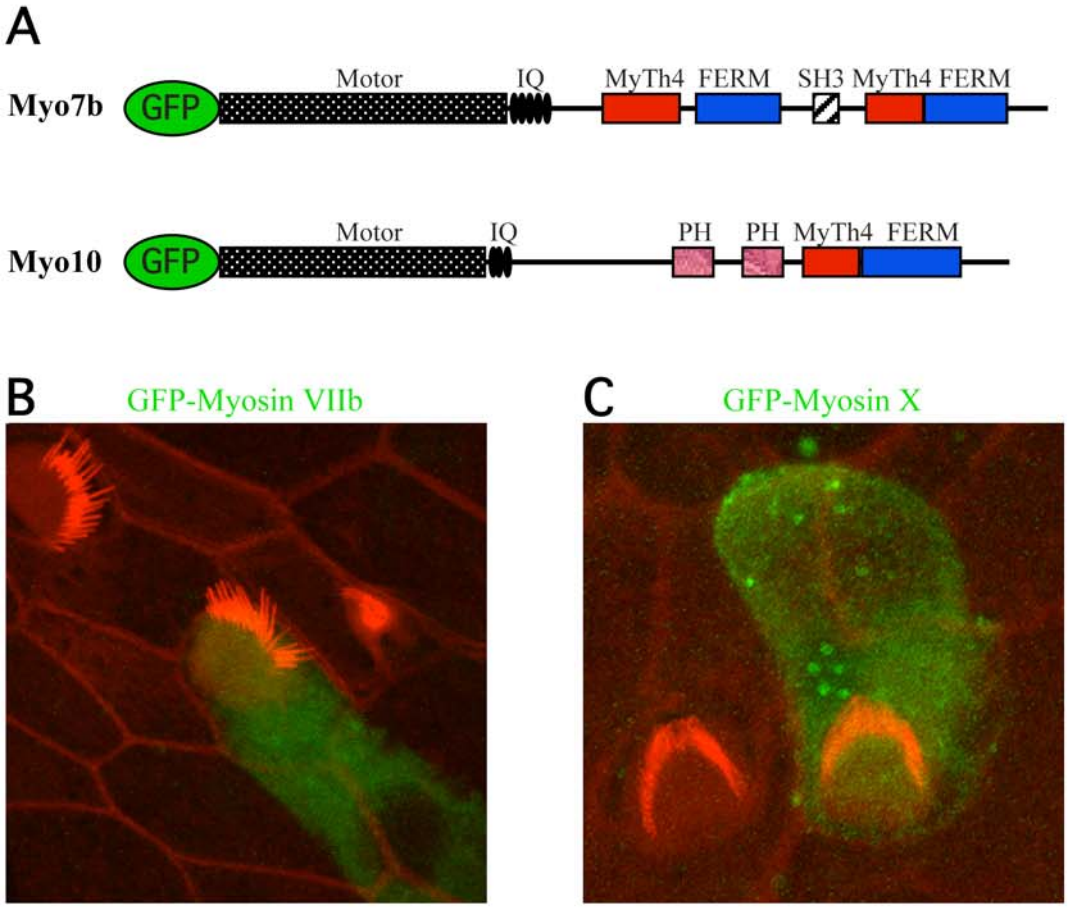

Figure 5-13. Mouse myosins VIIb and X are absent from stereocilia of transfected hair cells. **(A)** Schematic representations of the protein structures of mouse GFP-myosins VIIb and X. **(B)** Flattened Z-stack of serial optical sections taken through the optical plane (Z-stack) of a transfected wild type organ of Corti hair cell reveals that GFP-myosin VIIb is localized throughout the cell body and absent from stereocilia. **(C)** Z-stack of transfected wild type organ of Corti hair cell reveals that GFP-myosin X is localized throughout the cell body and absent from stereocilia. Actin cytoskeleton is stained with rhodamine-phalloidin (red).

Discussion

A preliminary assessment of which myosin XVa domains are necessary for stereocilia tip targeting

The results of our inner ear hair cell subcellular localization experiments using various GFP-myosin XVa motor mutants and deletion proteins are preliminary and do not allow a definitive assessment of what domains are sufficient for targeting to stereocilia tips (figure 5-14). The failure to observe accumulation of several GFP-myosin XVa deletion constructs at stereocilia tips could be due to either a failure to target to stereocilia tips, inability to associate with tethering proteins that retain myosin XVa at stereocilia tips, or increased turnover of myosin XVa mutant protein. A functional myosin XVa motor is necessary for stereocilia tip localization as evidenced by the cell body localization of two myosin XVa motor mutants, GFP-myosin XVa(C592Y) and GFP-myosin XVa(R167A/G388A) (figure 5-3). In transfected hair cells, GFP-myosin XVa[-SH3], GFP-myosin XVa[-$MyTh4_1$,-$FERM_1$,-SH3] and GFP-myosin XVa[-$MyTh4_2$,-$FERM_2$] accumulated at stereocilia tips (figures 5-4, 5-6 and 5-8). These results suggest that a myosin XVa motor plus either the $MyTh4_1/FERM_1$ or $MyTh4_2/FERM_2$ domains is sufficient for stereocilia targeting. If the myosin XVa motor plus the $MyTh4_1/FERM_1$ or $MyTh4_2/FERM_2$ domains functions as a basic unit for stereocilia tip targeting, then deletion of both MyTh4 or both FERM domains should abolish myosin XVa trafficking to stereocilia tips.

The deletion of both MyTh4 domains, GFP-myosin XVa[-$MyTh4_1$,-$MyTh4_2$], abolished accumulation at stereocilia tips (figure 5-10B). It is not clear whether the

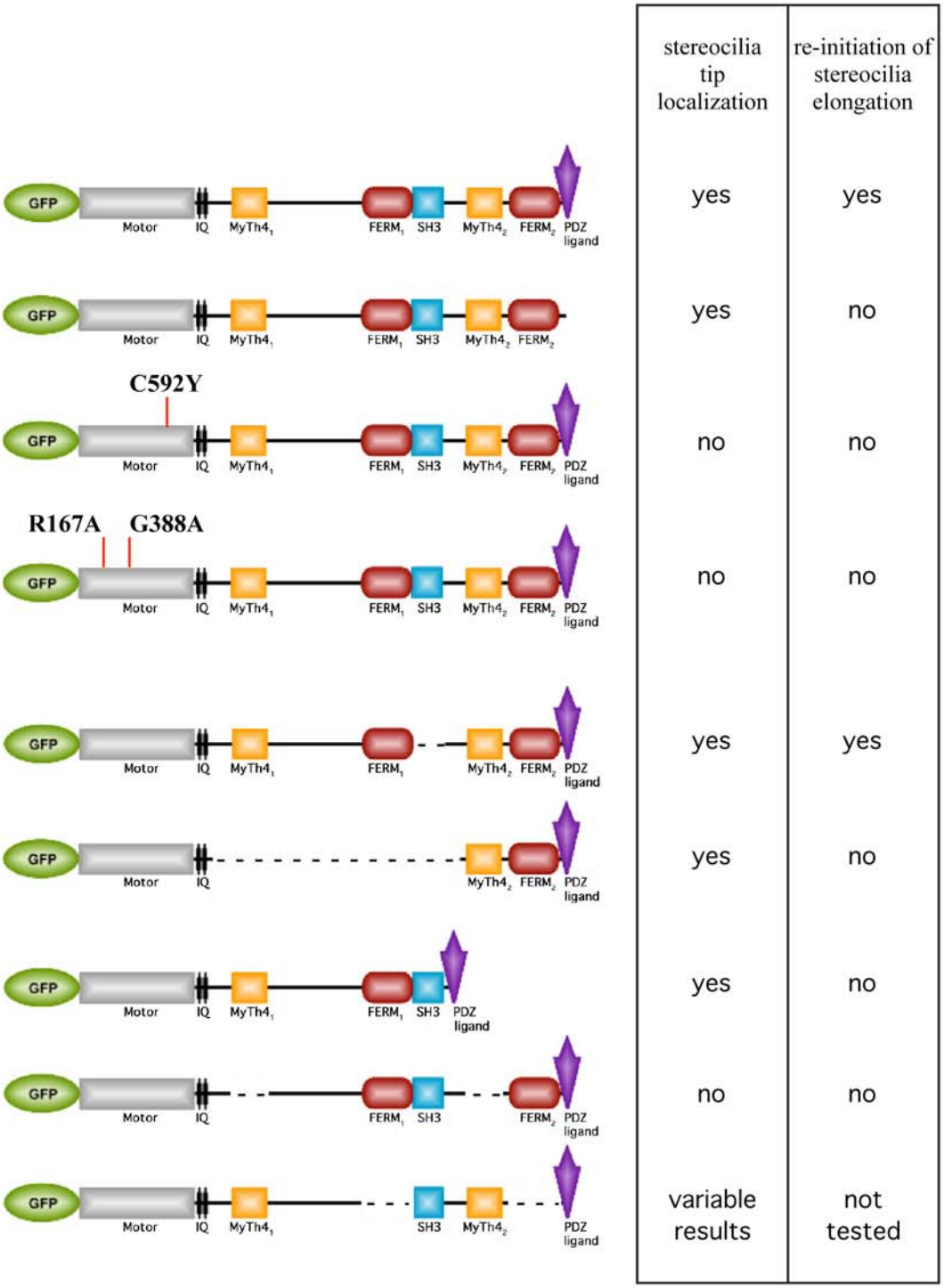

Figure 5-14. A summary of the results for the trafficking to stereocilia tips and re-initiation of stereocilia elongation and staircase formation in homozygous *Myo15a^{sh2}* hair cells of several GFP-myosin XVa deletion proteins. The results of the first two GFP-myosin XVa proteins are described in chapter 3 (figure 3-11). The results of the remaining seven GFP-myosin XVa motor mutants and deletion proteins are described in Chapter 5.Dotted lines represent deleted regions of myosin XVa.

failure to observe GFP-myosin XVa[-MyTh4$_1$,-MyTh4$_2$ at stereocilia tips was due to a deficiency in targeting to stereocilia tips, an inability to interact with a protein or lipid component of stereocilia tips responsible for retaining myosin XVa at stereocilia tips, or increased susceptibility to degradation of GFP-myosin XVa[-MyTh4$_1$,-MyTh4$_2$]. At this time, I am unable to rule out any of three aforementioned possibilities.

The conflicting subcellular localization results of GFP-myosin XVa[-FERM$_1$,-FERM$_2$], which lacks both FERM domains, does not allow us to conclude whether FERM domains are essential for targeting to stereocilia tips. Additional experiments with hair cells transfected with GFP-myosin XVa[-FERM$_1$,-FERM$_2$] will allow us to make a definitive assessment of targeting behavior.

The incomplete results from the GFP-myosin XVa[-FERM$_1$,-FERM$_2$] transfected hair cells combined with the stereocilia tip localization of GFP-myosin XVa[-SH3], GFP-myosin XVa[-MyTh4$_1$,-FERM$_1$,-SH3] and GFP-myosin XVa[-MyTh4$_2$,-FERM$_2$] implies at least two models of myosin XVa targeting. The first model suggests that the myosin XVa motor plus either the MyTh4$_1$ or MyTh4$_2$ domain is sufficient for stereocilia tip targeting in the case that neither FERM domain is required for targeting. The cell body localization of GFP-myosin XVa[-MyTh4$_1$,-MyTh4$_2$] suggests that MyTh4 domains are essential for targeting to stereocilia tips. The second model posits that the myosin XVa motor plus either the MyTh4$_1$/FERM$_1$ or MyTh4$_2$/FERM$_2$ domains is sufficient for targeting to stereocilia tips. If additional

transfected hair cells confirm that GFP-myosin XVa[-$FERM_1$,-$FERM_2$] accumulates in the cell body, then it will suggest that a single MyTh4/FERM domain is necessary for stereocilia tip targeting.

Not all MyTh4 containing myosins are trafficked to stereocilia

Analogous to the results observed in COS-7 cells, GFP-myosins VIIa, VIIb and X demonstrated different subcellular localization in transfected hair cells (figures 3-8E, 5-13B and 5-13C). Myosin VIIa is distributed along the length of the stereocilia while myosins VIIb and X accumulate in the cell body of transfected hair cells. The failure of myosin VIIb to accumulate within stereocilia was unexpected given its high protein sequence similarity to myosin VIIa (69%) and the localization of endogenous myosin VIIb at distal ends of kidney microvilli (Chen et al. 2001). Equally puzzling was the absence of myosin X from stereocilia, given the robust accumulation of myosin X at filopodia tips (Berg et al. 2002). These results suggest MyTh4 and FERM domains are not a generic stereocilia targeting motifs but rather the MyTh4 and FERM domains of myosin VIIa, VIIb, X and XVa are probably adapted for other functions.

SH3 domain of myosin XVa is not necessary for re-initiation of stereocilia elongation and staircase formation.

Re-initiation of stereocilia elongation and staircase formation was observed in homozygous *Myo15a*^{sh2} hair cells transfected with GFP-myosin XVa[-SH3] (figure 5-4). Previously, we demonstrated that delivery of endogenous whirlin to stereocilia tips by GFP-myosin XVa was essential to promote re-initiation of stereocilia

elongation and staircase formation in transfected homozygous *Myo15a*^{sh2} hair cells (figures 3-11 and 3-12). In transfected COS-7 cells, GFP-myosin XVa[-SH3] bound and delivered dsRed-whirlin to filopodia tips (figure 5-5). These two observations imply that stereocilia elongation in homozygous *Myo15a*^{sh2} hair cells is due to the delivery of endogenous whirlin to stereocilia tips by GFP-myosin XVa[-SH3].

Delprat and colleagues reported that the proline-rich domain of whirlin interacted with the SH3 domain of myosin XVa based upon results from *in vitro* binding assays using small fragments of myosin XVa and whirlin (Delprat et al. 2005). Our results demonstrated that the deletion of myosin XVa's SH3 domain did not disrupt the *in vivo* interaction necessary to target whirlin to filopodia tips, as evidenced by the ability of GFP-myosin XVa[-SH3] to deliver dsRed-whirlin to filopodia tips of COS-7 cells (figure 5-5).

Myosin XVa MyTh4$_1$, FERM$_1$, MyTh4$_2$ and FERM$_2$ domains are all required for re-initiation of stereocilia elongation and staircase formation.

In our preliminary results, the failure of either GFP-myosin XVa[-MyTh4$_1$,-FERM$_1$,-SH3] or GFP-myosin XVa[-MyTh4$_2$,-FERM$_2$] to re-initiate stereocilia elongation and staircase formation in homozygous *Myo15a*^{sh2} hair cells suggests a more complex role for myosin XVa than merely delivering whirlin to stereocilia tips. Despite the delivery of endogenous whirlin to stereocilia tips by GFP-myosin XVa[-MyTh4$_2$,-FERM$_2$], no restoration of the stereocilia bundle occurred (figure 5-8). This implies that the absence of the MyTh4$_2$ and FERM$_2$ domains, which likely mediate a critical

protein or lipid interaction, were responsible for the inability to promote stereocilia elongation.

The failure of GFP-myosin XVa[-MyTh4$_1$,-FERM$_1$,-SH3] to restore the stereocilia bundle indicated that the deleted MyTh4$_1$ and FERM$_1$ domains were essential for re-initiation of stereocilia elongation and staircase formation in homozygous *Myo15a*^{sh2} hair cells (figure 5-6). In COS-7 cells, GFP-myosin XVa[-MyTh4$_1$,-FERM$_1$,-SH3] binds and transports whirlin to filopodia tips (figure 5-7), suggesting that whirlin could be delivered to stereocilia tips by GFP-myosin XVa[-MyTh4$_1$,-FERM$_1$,-SH3]. Thus, these results suggest that, 1) the delivery of whirlin to stereocilia tips by myosin XVa is necessary but not sufficient to re-initiate stereocilia elongation and staircase formation, and 2) some combination of MyTh4$_1$, FERM$_1$, MyTh4$_2$ and FERM$_2$ domains is necessary for promoting stereocilia bundle elongation. Additional experiments with homozygous *Myo15a*^{sh2} hair cells transfected with GFP-myosin XVa[-MyTh4$_1$,-FERM$_1$,-SH3] or GFP-myosin XVa[-MyTh4$_2$,-FERM$_2$] will allow us to make a definitive assessment of the myosin XVa tail domains necessary for stereocilia elongation.

Myosin XVa targeting in COS-7 versus inner ear hair cells

My subcellular localization results in transfected COS-7 and inner ear hair cells indicate that the domains of myosin XVa sufficient for filopodia tip localization are different from the myosin XVa domains sufficient for stereocilia tip localization (figure 5-15). The larger subset of combinations of myosin XVa motor plus tail

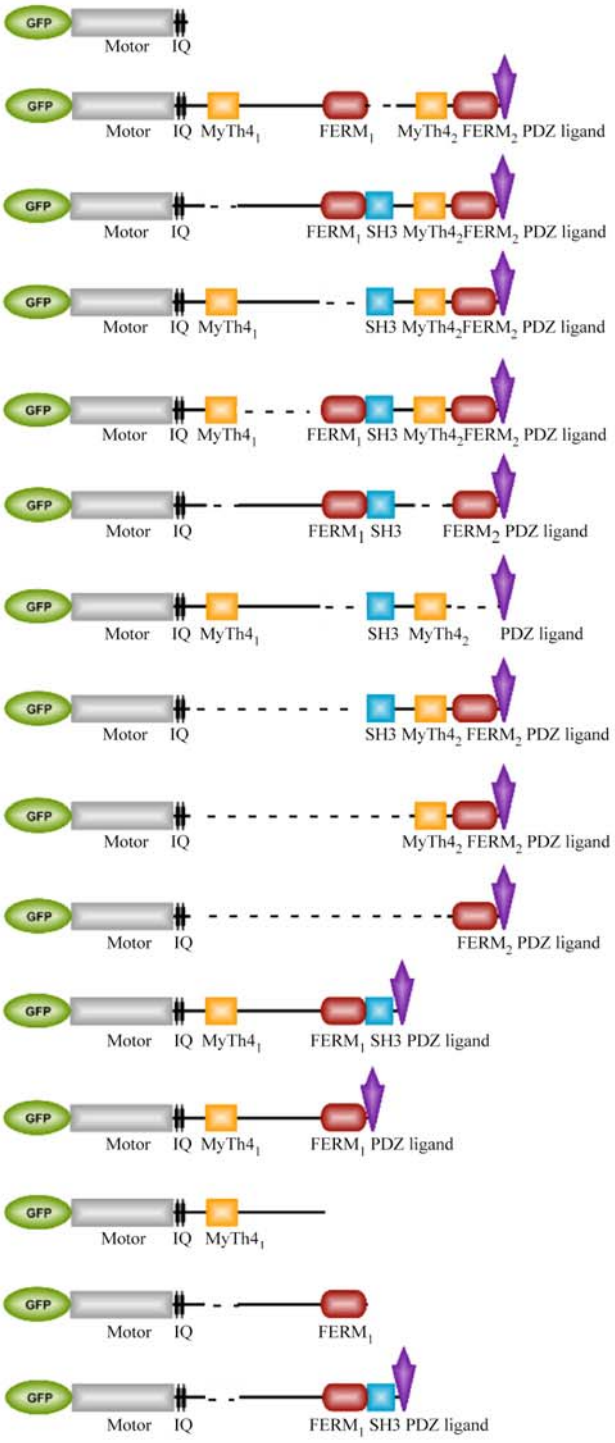

filopodia tip localization	stereocilia tip localization
no	-
yes	yes
yes	-
yes	-
yes	-
yes	no
yes/no	yes/no
yes	yes
yes	yes
yes	-
yes	yes
yes	-
no	-
no	-
yes	-

Figure 5-15. Summary of COS-7 and inner hair cell subcellular localization of GFP-Myosin XVa deletion expression cDNA constructs used in chapters 4 and 5. Dotted lines represent deleted regions of myosin XVa. A dash (-) in the filopodia tip and stereocilia tip localization results indicates the experiment has not been conducted.

domains that are permissible for filopodia tip targeting in COS-7 cells indicate a generic targeting and/or retention mechanism in epithelial cells. In contrast, only the myosin XVa motor plus MyTh4/FERM domains are sufficient for targeting to stereocilia tips in hair cells.

In both COS-7 and hair cells, a functional myosin XVa motor is required for filopodia and stereocilia tip localization. In hair cells, the myosin XVa motor plus the $MyTh4_1/FERM_1$ domains or myosin XVa motor plus the $MyTh4_2/FERM_2$ domains were sufficient for targeting to stereocilia tips. Deletion of both MyTh4 domains of myosin XVa abolished targeting to stereocilia tips while the deletion of both FERM domains yielded inconclusive results due to the small number of transfected hair cells. At this time, my preliminary results suggest that the motor plus a single grouping of MyTh4/FERM domains is sufficient for targeting to stereocilia tips. However, more experiments using other myosin XVa deletion constructs will be necessary to definitively conclude that the region is necessary for stereocilia tip targeting.

In COS-7 cells, several combinations of the myosin XVa motor plus tail domains are sufficient for filopodia tip localization (figure 5-15). Similar to the results observed in hair cells, either the myosin XVa motor plus the $MyTh4_1/FERM_1$ domains or myosin XVa motor plus the $MyTh4_2/FERM_2$ domains were sufficient for targeting to filopodia tips in COS-7 cells. In contrast to hair cell stereocilia tip targeting, the MyTh4 domains of myosin XVa are not necessary for filopodia tip targeting in COS-

7 cells. The myosin XVa motor plus the $FERM_2$ domain was sufficient to target filopodia tips but the myosin XVa motor plus the $FERM_1$ domain was unable to accumulate at filopodia tips. The myosin XVa motor plus either the $FERM_1$/SH3 domains or the myosin XVa motor plus either the $FERM_1$/SH3/$FERM_2$ domains were sufficient to target filopodia tips, however neither of these myosin XVa constructs were tested in hair cells.

At least three non-exclusive mechanisms can account for the differences in the subcellular localization of myosin XVa in COS-7 and inner ear hair cells. First, myosin XVa localization at filopodia and stereocilia tips is due to differential myosin motor activity along tropomyosin-coated actin filaments (Tsakraklides et al. 1999). Several tropomyosins were demonstrated to differentially influence the mechanochemistry of myosin I, II and V motor domains (Fanning et al. 1994; Wolenski et al. 1995). Tropomyosin is a component of most actin filaments and over 40 isoforms have been identified in non-muscle cells (Gunning et al. 2005). The subcellular localization of tropomyosin isoforms within COS-7 and hair cells is unknown, although tropomyosin was observed in stereocilia rootlets and cuticular plate by anti-tropomyosin antiserum recognizing a large number of tropomyosin isoforms (Slepecky et al. 1985; Anniko et al. 1995).

Second, there could be a putative gate-keeping complex located at the base of hair cell stereocilia which might allow entry of particular myosins into the actin cytoskeletal core of stereocilia. The cytoskeletal core of stereocilia, comprised of

approximately 3,000 actin filaments at the stereocilia tips, is narrowly tapered at the base with approximately 20 to 30 actin filaments inserting into the cuticular plate (Tilney et al. 1980). This dramatically tapered region of the stereocilia base could harbor a gate-keeping complex to regulate access of myosins to the actin cytoskeletal core of stereocilium. Conversely, a generalized epithelial cell such as a COS-7 might lack an analogous gate-keeping complex regulating entry to filopodia. How might a gate-keeping complex achieve selection? Myosins that have low affinity interactions with protein components of the gate-keeping complex would be allowed passage. Given the sequence conservation of myosin motors combined with the divergent sequence of the myosin tails, it is likely that selection might occur through myosin tail interactions with the putative gate-keeping complex.

A third possibility is that most myosin XVa deletion proteins target to filopodia tips and to stereocilia tips, but only some myosin XVa proteins are retained at tips. Accumulation is mediated by the interaction of regions of the myosin XVa tail with protein or lipid components of filopodia and stereocilia tips. By extension, this implies that most plus end directed myosins could traffick along the stereocilia but only myosins Ic, IIIa, VIIa and XVa are retained at their particular locations by specific protein or lipid interactions (Hasson et al. 1997; Belyantseva et al. 2003a; Rzadzinska et al. 2004; Belyantseva et al. 2005; Schneider et al. 2006). Other myosins that do not interact with protein or lipid components of stereocilia, fail to accumulate and are transported to stereocilia base by treadmilling of the actin cytoskeleton or by other means. In the case of myosin X, filopodia tip accumulation is

mediated by the interaction of the cytoplasmic tails of beta integrins with the FERM domain of myosin X (Zhang et al. 2004). Disruption of this interaction resulted in no myosin X accumulation at filopodia tips. This example suggests that myosin X is retained at filopodia tips by its interaction with beta integrins.

Future Plans

Engineered missense mutations in myosin XVa MyTh4$_1$, FERM$_1$ and MyTh4$_2$ domains

It is possible that the failure of GFP-myosin XVa[-MyTh4$_1$,-MyTh4$_2$] to accumulate at stereocilia tips was due to disrupted function of the tail caused by the juxtaposition of the FERM$_1$, SH3 and FERM$_2$ domains. To rule out this possibility, I suggest engineering missense mutations into the MyTh4$_1$ and MyTh4$_2$ domains of myosin XVa. In humans, several missense mutations located in the MyTh4$_1$, FERM$_1$ and MyTh4$_2$ domains of myosin XVa were reported to cause deafness (figure 5-16; Liburd et al. 2001; Nal et al. 2007). Of particularly note are the N890Y, I892F and T978I missense mutations in the MyTh4$_1$ domain, the Q1492H and D1496H mutations in the FERM$_1$ domain and the L1936F mutation in the MyTh4$_2$ domain. I propose to individual engineer these point mutations into the wild type myosin XVa cDNA expression construct. These various GFP-myosin XVa cDNA expression constructs containing individual missense mutations will be transfected into wild type hair cells and the subcellular localization will be determined. If any of the GFP-myosin XVa cDNA expression constructs containing individual missense mutations have a perturbed pattern of accumulation at stereocilia tips relative to wild type GFP-myosin XVa, then it can be assumed that the domain containing the missense

mutation is critical for correct localization. On the other hand, if no obvious change in stereocilia tip accumulation is observed, then it will suggest that the missense mutation affects a protein interaction critical for normal auditory function.

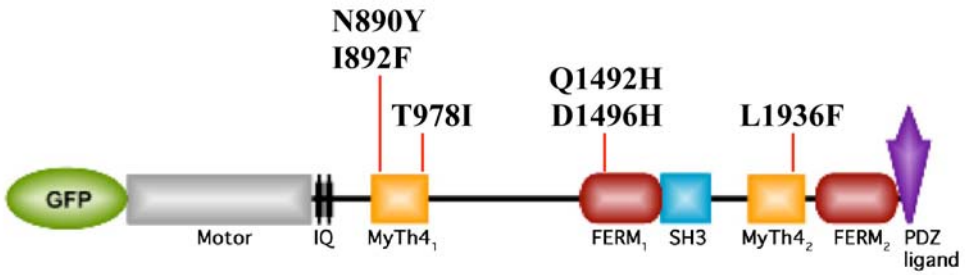

Figure 5-16. Locations of several human myosin XVA missense mutations within the tail of mouse myosin XVa protein isoform 2a associated with nonsyndromic deafness in humans. Liburd et al. 2001 and Nal et al. 2007 identified three missense mutations in the MyTh4$_1$ domain, two missense mutations in the FERM$_1$ domain, and one missense mutation in the MyTh4$_2$ domain.

Chimeric MyTh4/FERM myosin trafficking in hair cells

The distinct subcellular localization of myosin VIIa along the length of stereocilia, myosin X in the cell body and myosin XVa at stereocilia tips will provide an opportunity to examine the respective contributions of the motors and tails to the subcellular localization in hair cells. In the Future Plans Section of chapter 4, I described six chimeric myosin expression constructs that represent all possible mixed combinations of motor and tails of myosins VIIa, X and XVa (figure 4-12). First, the GFP-chimeric myosins will be evaluated in transfected COS-7 cells. Accumulation of a GFP-chimeric myosin along the length of the filopodia or filopodia tips will

indicate that the GFP-chimeric myosin expression constructs encode a motile myosin. Next, GFP-chimeric myosins will be transfected into wild type hair cells and their subcellular localization will be assessed by confocal microscopy.

The subcellular localization will allow us to answer some of the following questions. Will the fusion of the myosin X motor and myosin XVa tail result in accumulation at stereocilia tips or along the length of stereocilia? If so, this will imply that the tail is capable of determining localization. Will the myosin X motor fused to the myosin XVa tail be capable of initiating stereocilia elongation and staircase formation in transfected homozygous *Myo15a*^{sh2} hair cells? Will the fusion of the myosin XVa motor and myosin X tail result in cell body localization or accumulation in stereocilia? Will the fusion of the myosin VIIa motor with the tail of myosin XVa tail result in stereocilia tip localization? If so, will the myosin VIIa motor fused to the myosin XVa tail be capable of initiating stereocilia elongation and staircase formation in transfected homozygous *Myo15a*^{sh2} hair cells? Will the motor be the sole determinant of hair cell subcellular localization regardless of the fusion tail? The GFP-chimeric myosin localization in hair cells will provide the first step in interpreting the complex phenomena of myosin localization in hair cells.

Which MyTh4 and/or FERM domains are required for re-initiation of stereocilia elongation and staircase formation?

In this chapter, we attempted to demonstrate that both myosin XVa motor plus the MyTh4$_1$/FERM$_1$ domains and myosin XVa motor plus the MyTh4$_2$/FERM$_2$ domains targeted stereocilia tips but were unable to promote the re-initiation of stereocilia

elongation and staircase formation in homozygous *Myo15a*^{sh2} hair cells. This preliminary data suggests that some combination of MyTh4$_1$, FERM$_1$, MyTh4$_2$ and FERM$_2$ domains is necessary. To determine which of these domains are essential for of stereocilia elongation and staircase formation, four GFP-myosin XVa deletion constructs lacking one of the four domains (GFP-myosin XVa[-MyTh4$_1$], GFP-myosin XVa[-FERM$_1$], GFP-myosin XVa[-MyTh4$_2$], GFP-myosin XVa[-FERM$_2$]), will be evaluated in transfected homozygous *Myo15a*^{sh2} hair cells (figure 5-17). For

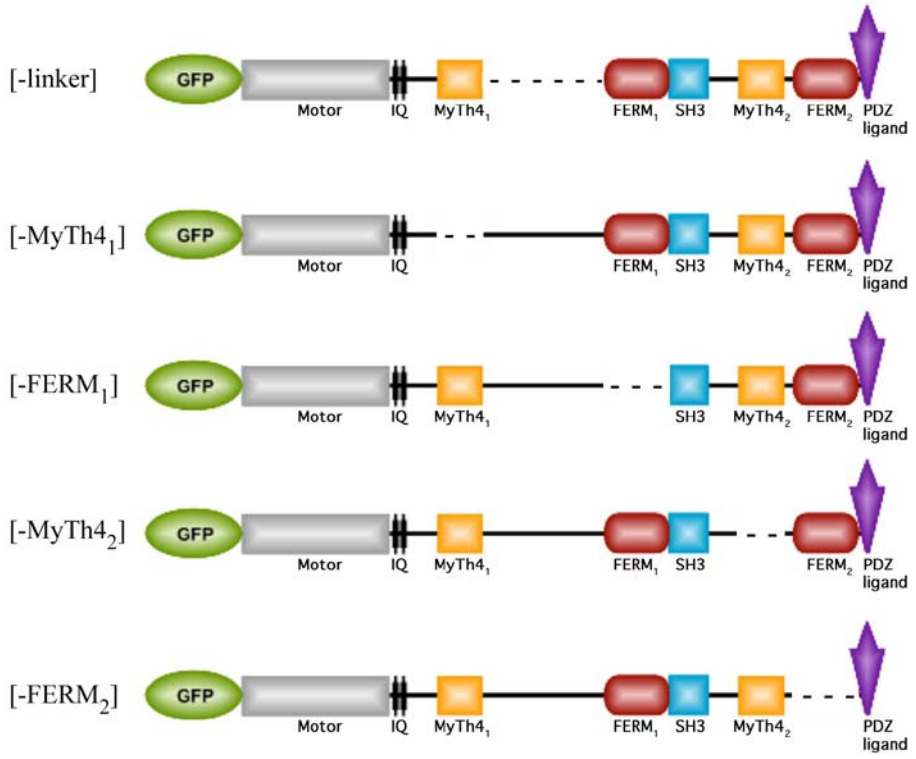

Figure 5-17. Future experiments to determine trafficking behavior of GFP-myosin XVa deletion proteins to stereocilia tips or ability to elongate stereocilia and form a staircase structure in homozygous *Myo15a*^{sh2} hair cells. Dotted lines represent deleted regions of myosin XVa.

example, if transfection of GFP-myosin XVa[-$FERM_1$], which lacks the first FERM domain, causes stereocilia elongation and staircase formation in *Myo15a*^{sh2} hair cells, this would imply this domain is not necessary for the process. Conversely, failure of GFP-myosin XVa[-$FERM_1$] to promote re-initiation of stereocilia elongation and staircase formation in transfected *Myo15a*^{sh2} hair cells would imply the domain is essential for the process. It is anticipated that each of the four GFP-myosin XVa deletion constructs will localize at stereocilia tips due to the presence of one MyTh4 or MyTh4/FERM domains. If all four GFP-myosin XVa deletion constructs, each lacking one of the four domains, fail to restore the stereocilia bundle, then one can conclude that all four domains are required.

References

Adato A, Lefevre G, Delprat B, Michel V, Michalski N, Chardenoux S, Weil D, El-Amraoui A, Petit C. Usherin, the defective protein in Usher syndrome type IIA, is likely to be a component of interstereocilia ankle links in the inner ear sensory cells. *Hum Mol Genet.* **14**: 3921-32 (2005).

Ahmed ZM, Goodyear R, Riazuddin S, Lagziel A, Legan PK, Behra M, Burgess SM, Lilley KS, Wilcox ER, Riazuddin S, Griffith AJ, Frolenkov GI, Belyantseva IA, Richardson GP, Friedman TB. The tip-link antigen, a protein associated with the transduction complex of sensory hair cells, is protocadherin-15. *J Neurosci.* **26**: 7022-34 (2006).

Alberts AS. Identification of a carboxyl-terminal diaphanous-related formin homology protein autoregulatory domain. *J Biol Chem.* **276**:2824-30 (2001).

Anderson DW, Probst FJ, Belyantseva IA, Fridell RA, Beyer L, Martin DM, Wu D, Kachar B, Friedman TB, Raphael Y, Camper SA. The motor and tail regions of myosin XV are critical for normal structure and function of auditory and vestibular hair cells. *Hum Mol Genet.* **9**: 1729-38 (2000).

Anniko M, Arnold W, Stigbrand T, Takumida M. Cytoskeletal basis for contractility of outer hair cells in the normal adult human organ of Corti: comparisons with vestibular hair cells. *ORL J Otorhinolaryngol Relat Spec*. **57**:61-7 (1995).

Asaba N, Hanada T, Takeuchi A, Chishti AH. Direct interaction with a kinesin-related motor mediates transport of mammalian discs large tumor suppressor homologue in epithelial cells. *J. Biol. Chem.* **278**: 8395-8400 (2003).

Ashmore J, Gale J. The cochlea. *Curr Biol.* **10** :R325-7 (2000).

Ashmore JF, Mammano F. Can you still see the cochlea for the molecules? *Curr Opin Neurobiol.* **11**: 449-54 (2001).

Aspenstrom P, Fransson A, Saras J. Rho GTPases have diverse effects on the organization of the actin filament system. *Biochem J.* **377**: 327-37 (2004).

Assad JA, Shepherd GM, Corey DP. Tip-link integrity and mechanical transduction in vertebrate hair cells. *Neuron.* **7**: 985-94 (1991).

Assad JA, Corey DP. An active motor model for adaptation by vertebrate hair cells. *J Neurosci.* **12** :3291-309 (1992).

Avraham KB, Hasson T, Steel KP, Kingsley DM, Russell LB, Mooseker MS, Copeland NG, Jenkins NA. The mouse Snell's waltzer deafness gene encodes an unconventional myosin required for structural integrity of inner ear hair cells. *Nat Genet.* **11**: 369-75 (1995).

Baker JP, Titus MA. Myosins: matching functions with motors. *Curr Opin Cell Biol.* **10**: 80-86 (1998).

Balla T. Inositol-lipid binding motifs: signal integrators through protein-lipid and protein-protein interactions. *J Cell Sci.* **118**: 2093-104 (2005).

Belyantseva IA, Boger ET, Friedman TB. Myosin XVa localizes to the tips of inner ear sensory cell stereocilia and is essential for staircase formation of the hair bundle. *Proc Natl Acad Sci U S A.* **100**: 13958-63 (2003a).

Belyantseva IA, Labay V, Boger ET, Griffith AJ, Friedman TB. Stereocilia: the long and the short of it. *Trends Mol Med.* **9**:458-61 (2003b).

Belyantseva IA, Boger ET, Naz S, Frolenkov GI, Sellers JR, Ahmed ZM, Griffith AJ, Friedman TB. Myosin-XVa is required for tip localization of whirlin and differential elongation of hair-cell stereocilia. *Nat Cell Biol.* **7**:148-56 (2005).

Berg JS, Powell BC, and Cheney RE. A millennial myosin census. *Mol Biol Cell.* **12**: 780-794 (2001).

Berg JS, Cheney RE. Myosin-X is an unconventional myosin that undergoes intrafilopodial motility. *Nat Cell Biol.* **4**:246-50 (2002).

Bezprozvanny I, Maximov A. Classification of PDZ domains. *FEBS Lett.* **509**:457-62 (2001).

Bohil AB, Robertson BW, Cheney RE. Myosin-X is a molecular motor that functions in filopodia formation. *Proc Natl Acad Sci U S A.* **103**:12411-6 (2006).

Chang AC, Sohlberg B, Trinkle-Mulcahy L, Claverie-Martin F, Cohen P, Cohen SN. Alternative splicing regulates the production of ARD-1 endoribonuclease and NIPP-1, an inhibitor of protein phosphatase-1, as isoforms encoded by the same gene. *Gene*. **240**:45-55 (1999).

Chen ZY, Hasson T, Zhang DS, Schwender BJ, Derfler BH, Mooseker MS, Corey DP. Myosin-VIIb, a novel unconventional myosin, is a constituent of microvilli in transporting epithelia. *Genomics.* **72**: 285-96 (2001).

Cheney RE, Mooseker MS. Unconventional myosins. *Curr Opin Cell Biol.* **4** :27-35 (1992).

Chevesich J, Kreuz AJ, Montell C. Requirement for the PDZ domain protein, INAD, for localization of the TRP store-operated channel to a signaling complex. *Neuron.* **18**:95-105 (1997).

Crawford AC, Evans MG, Fettiplace R. Activation and adaptation of transducer currents in turtle hair cells. *J Physiol.* **419** :405-34 (1989).

Crawford AC, Evans MG, Fettiplace R. The actions of calcium on the mechano-electrical transducer current of turtle hair cells. *J Physiol.* **434** :369-98 (1991).

Delprat B, Michel V, Goodyear R, Yamasaki Y, Michalski N, El-Amraoui A, Perfettini I, Legrain P, Richardson G, Hardelin JP, Petit C. Myosin XVa and whirlin, two deafness gene products required for hair bundle growth, are located at the stereocilia tips and interact directly. *Hum Mol Genet.* **14**:401-10 (2005).

Denk W, Holt JR, Shepherd GM, Corey DP. Calcium imaging of single stereocilia in hair cells: localization of transduction channels at both ends of tip links. *Neuron.* **15**:1311-21 (1995).

Dobrovolskaia-Zavasdkaia N. L'irradiation des testicules et l'heredite chez la souris. *Arch. Biol*. **38**: 457-501 (1928).

Donaudy F, Ferrara A, Esposito L, Hertzano R, Ben-David O, Bell RE, Melchionda S, Zelante L, Avraham KB, Gasparini P. Multiple mutations of MYO1A, a cochlear-expressed gene, in sensorineural hearing loss. *Am J Hum Genet.* **72**:1571-7 (2003).

Doyle DA, Lee A, Lewis J, Kim E, Sheng M, MacKinnon R. Crystal structures of a complexed and peptide-free membrane protein-binding domain: molecular basis of peptide recognition by PDZ. *Cell.* **85**:1067-76 (1996).

Dumont RA, Zhao YD, Holt JR, Bahler M, Gillespie PG. Myosin-I isozymes in neonatal rodent auditory and vestibular epithelia. *J Assoc Res Otolaryngol.* **3**:375-89 (2002).

Eatock RA, Corey DP, Hudspeth AJ. Adaptation of mechanoelectrical transduction in hair cells of the bullfrog's sacculus. *J Neurosci.* **7**: 2821-36 (1987).

Eatock RA. Adaptation in hair cells. *Annu Rev Neurosci.* **23**: 285-314 (2000).

Edds KT. Dynamic aspects of filopodial formation by reorganization of microfilaments. *J Cell Biol.* **73**:479-91 (1977).

Espreafico EM, Cheney RE, Matteoli M, Nascimento AA, De Camilli PV, Larson RE, Mooseker MS. Primary structure and cellular localization of chicken brain myosin-V (p190), an unconventional myosin with calmodulin light chains. *J Cell Biol.* **119**:1541-57 (1992).

Evangelista M, Zigmond S, Boone C. Formins: signaling effectors for assembly and polarization of actin filaments. *J Cell Sci.* **116**: 2603-2611 (2003).

Fanning AS, Wolenski JS, Mooseker MS, Izant JG. Differential regulation of skeletal muscle myosin-II and brush border myosin-I enzymology and mechanochemistry by bacterially produced tropomyosin isoforms. *Cell Motil Cytoskeleton.* **29**:29-45 (1994).

Fay RR, Popper AN. Evolution of hearing in vertebrates: the inner ears and processing. *Hear Res.* **149** :1-10 (2000).

Fleming J, Rogers MJ, Brown SD, Steel KP. Linkage analysis of the whirler deafness gene on mouse chromosome 4. *Genomics.* **21**: 42-8 (1994).

Forge A, Souter M, Denman-Johnson K. Structural development of sensory cells in the ear. *Semin Cell Dev Biol.* **8**: 225-237 (1997).

Friedman TB, Liang Y, Weber JL, Hinnant JT, Barber TD, Winata S, Arhya IN, Asher JH Jr. A gene for congenital, recessive deafness DFNB3 maps to the pericentromeric region of chromosome 17. *Nat Genet.* **9**: 86-91 (1995).

Frolenkov GI, Belyantseva IA, Friedman TB, Griffith AJ. Genetic insights into the morphogenesis of inner ear hair cells. *Nat Rev Genet.* **5**: 489-98 (2004).

Garcia-Anoveros J, Corey DP. The molecules of mechanosensation. *Annu Rev Neurosci.* **20**: 567-94 (1997).

Gerhardt H, Golding M, Fruttiger M, Ruhrberg C, Lundkvist A, Abramsson A, Jeltsch M, Mitchell C, Alitalo K, Shima D, Betsholtz C. VEGF guides angiogenic sprouting utilizing endothelial tip cell filopodia. *J Cell Biol.* **161**: 1163-77 (2003).

Gibson F, Walsh J, Mburu P, Varela A, Brown KA, Antonio M, Beisel KW, Steel KP, Brown SD. A type VII myosin encoded by the mouse deafness gene shaker-1. *Nature.* **374**: 62-4 (1995).

Gillespie PG and Walker RG Molecular basis of mechanosensory transduction. *Nature.* **413**: 194-202 (2001).

Graveley BR. Alternative splicing: increasing diversity in the proteomic world. *Trends Genet.* **17**: 100-107 (2001).

Gunning PW, Schevzov G, Kee AJ, Hardeman EC. Tropomyosin isoforms: divining rods for actin cytoskeleton function. *Trends Cell Biol.* **15**:333-41 (2005).

Gustincich S, Sandelin A, Plessy C, Katayama S, Simone R, Lazarevic D, Hayashizaki Y, Carninci P. The complexity of the mammalian transcriptome. *J*

Physiol. **575**:321-32 (2006).

Hamada K, Shimizu T, Matsui T, Tsukita S, Hakoshima T. Structural basis of the membrane-targeting and unmasking mechanisms of the radixin FERM domain. *EMBO J.* **19**: 4449-62 (2000).

Han W, Kim KH, Jo MJ, Lee JH, Yang J, Doctor RB, Moe OW, Lee J, Kim E, Lee MG. Shank2 associates with and regulates Na+/H+ exchanger 3. *J Biol Chem.* **281**: 1461-9 (2006).

Harris BZ and Lim WA. Mechanism and role of PDZ domains in signaling complex assembly. *J. Cell Sci.* **114**: 3219-3231 (2001)

Harris ES, Li F, Higgs HN. The mouse formin, FRLalpha, slows actin filament barbed end elongation, competes with capping protein, accelerates polymerization from monomers, and severs filaments. *J Biol Chem.* **279**: 20076-87 (2004).

Harteneck C, Kuchta SN, Huber A, Paulsen R, Schultz G. The PDZ scaffold protein INAD abolishes apparent store-dependent regulation of the light-activated cation channel TRP. *FASEB J.* **16**: 1668-70 (2002).

Hasson T, Gillespie PG, Garcia JA, MacDonald RB, Zhao Y, Yee AG, Mooseker MS, Corey DP. Unconventional myosins in inner-ear sensory epithelia. *J Cell Biol.* **137**:1287-307 (1997).

Higgs HN. Formin proteins: a domain-based approach. *Trends Biochem Sci.* **30**:342-53 (2005a).

Higgs HN, Peterson KJ. Phylogenetic analysis of the formin homology 2 domain. *Mol Biol Cell.* **16**:1-13 (2005b).

Hodge T, Cope MJ. A myosin family tree. *J Cell Sci.* **113**:3353-4 (2000).

Holme RH, Kiernan BW, Brown SD, Steel KP. Elongation of hair cell stereocilia is defective in the mouse mutant whirler. *J Comp Neurol.* **450**:94-102 (2002).

Holt JR, Corey DP. Two mechanisms for transducer adaptation in vertebrate hair cells. *Proc Natl Acad Sci U S A.* **97**:11730-5 (2000).

Howard J, Hudspeth AJ. Mechanical relaxation of the hair bundle mediates adaptation in mechanoelectrical transduction by the bullfrog's saccular hair cell. *Proc Natl Acad Sci U S A.* **84** : 3064-8 (1987).

Howard J, Hudspeth AJ. Compliance of the hair bundle associated with gating of mechanoelectrical transduction channels in the bullfrog's saccular hair cell. *Neuron.* **1**: 189-99 (1988).

Hudspeth AJ, Corey DP. Sensitivity, polarity, and conductance change in the response of vertebrate hair cells to controlled mechanical stimuli. *Proc Natl Acad Sci U S A.* **74** : 2407-11 (1977).

Hung AY, Sheng M. PDZ domains: structural modules for protein complex assembly. *J Biol Chem.* **277**:5699-702 (2002).

Jelen F, Oleksy A, Smietana K, Otlewski J. PDZ domains - common players in the cell signaling. *Acta Biochim Pol.* **50**:985-1017 (2003).

Kachar B, Parakkal M, Kurc M, Zhao Y, Gillespie PG. High-resolution structure of hair-cell tip links. *Proc Natl Acad Sci U S A.* **97**: 13336-41 (2000).

Kambara T, Rhodes TE, Ikebe R, Yamada M, White HD, Ikebe M. Functional significance of the conserved residues in the flexible hinge region of the myosin motor domain. *J Biol Chem.* **274**:16400-6 (1999).

Karthikeyan S, Leung T, Ladias JA. Structural basis of the Na+/H+ exchanger regulatory factor PDZ1 interaction with the carboxyl-terminal region of the cystic fibrosis transmembrane conductance regulator. *J Biol Chem.* **276**:19683-6 (2001).

Kay BK, Williamson MP, Sudol M. The importance of being proline: the interaction of proline-rich motifs in signaling proteins with their cognate domains. *FASEB J.* **14**:231-41 (2000).

Kendrick-Jones J, Hodge TP, Lister IMB, Roberts RC and Buss F. *The Myosin Home Page*, www.mrc-lmb.cam.ac.uk/myosin/myosin.html. (2001)

Kikkawa Y, Mburu P, Morse S, Kominami R, Townsend S, Brown SD. Mutant analysis reveals whirlin as a dynamic organizer in the growing hair cell stereocilium. *Hum Mol Genet.* **14**:391-400 (2005).

Kim E. and Sheng M. PDZ domain proteins of synapses. *Nature Reviews: Neuroscience* **5**:771-81. (2004).

Klaavuniemi T, Kelloniemi A, Ylanne J. The ZASP-like motif in actinin-associated LIM protein is required for interaction with the alpha-actinin rod and for targeting to the muscle Z-line. *J Biol Chem.* **279**:26402-10 (2004).

Kozlov MM, Bershadsky AD. Processive capping by formin suggests a force-driven mechanism of actin polymerization. *J Cell Biol.* **167**:1011-7 (2004).

Lalwani AK, Goldstein JA, Kelley MJ, Luxford W, Castelein CM, Mhatre AN. Human nonsyndromic hereditary deafness DFNA17 is due to a mutation in nonmuscle myosin MYH9. *Am J Hum Genet.* **67**: 1121-8 (2000).

Les Erickson F, Corsa AC, Dose AC, Burnside B. Localization of a class III myosin to filopodia tips in transfected HeLa cells requires an actin-binding site in its tail domain. Mol Biol Cell. **14**:4173-80 (2003).

Li XD, Rhodes TE, Ikebe R, Kambara T, White HD, Ikebe M. Effects of mutations in the gamma-phosphate binding site of myosin on its motor function. *J Biol Chem.* **273**:27404-11 (1998).

Liang Y, Wang A, Probst FJ, Arhya IN, Barber TD, Chen KS, Deshmukh D, Dolan DF, Hinnant JT, Carter LE, Jain PK, Lalwani AK, Li XC, Lupski JR, Moeljopawiro S, Morell R, Negrini C, Wilcox ER, Winata S, Camper SA, Friedman TB. Genetic mapping refines DFNB3 to 17p11.2, suggests multiple alleles of DFNB3, and supports homology to the mouse model shaker-2. *Am J Hum Genet.* **62** :904-15 (1998).

Liang Y, Wang A, Belyantseva IA, Anderson DW, Probst FJ, Barber TD, Miller W, Touchman JW, Jin L, Sullivan SL, Sellers JR, Camper SA, Lloyd RV, Kachar B, Friedman TB, Fridell RA. Characterization of the human and mouse unconventional myosin XV genes responsible for hereditary deafness DFNB3 and shaker 2. *Genomics*. **61**: 243-58 (1999).

Liburd N, Ghosh M, Riazuddin S, Naz S, Khan S, Ahmed Z, Riazuddin S, Liang Y, Menon PS, Smith T, Smith AC, Chen KS, Lupski JR, Wilcox ER, Potocki L, Friedman TB. Novel mutations of MYO15A associated with profound deafness in consanguineous families and moderately severe hearing loss in a patient with Smith-Magenis syndrome.
Hum Genet. **109**:535-41 (2001).

Lin HW, Schneider ME, Kachar B. When size matters: the dynamic regulation of stereocilia lengths. *Curr Opin Cell Biol.* **17**:55-61 (2005).

Lloyd RV, Vidal S, Jin L, Zhang S, Kovacs K, Horvath E, Scheithauer BW, Boger ET, Fridell RA, Friedman TB. Myosin XVA expression in the pituitary and in other neuroendocrine tissues and tumors. *Am J Pathol.* **159**:1375-82 (2001).

Lo PK, Wang FF. 5'-Heterogeneity of mouse Dda3 transcripts is attributed to differential initiation of transcription and alternative splicing. *Arch Biochem Biophys.* **425**:221-232 (2004).

Manley GA. Cochlear mechanisms from a phylogenetic viewpoint. *Proc Natl Acad Sci U S A.* **97**:11736-43 (2000).

Marfatia SM, Morais-Cabral JH, Kim AC, Byron O, Chishti AH. The PDZ domain of human erythrocyte p55 mediates its binding to the cytoplasmic carboxyl terminus of glycophorin C. Analysis of the binding interface by in vitro mutagenesis. *J Biol Chem.* **272**:24191-7 (1997).

Markin VS, Hudspeth AJ. Gating-spring models of mechanoelectrical transduction by hair cells of the internal ear. *Annu. Rev. Biophys. Biomol. Struct.* **24**: 59-83 (1995).

Martin P, Mehta AD, Hudspeth AJ. Negative hair-bundle stiffness betrays a mechanism for mechanical amplification by the hair cell. *Proc Natl Acad Sci U S A.* **97** : 12026-31 (2000).

Mburu P, Mustapha M, Varela A, Weil D, El-Amraoui A, Holme RH, Rump A, Hardisty RE, Blanchard S, Coimbra RS, Perfettini I, Parkinson N, Mallon AM, Glenister P, Rogers MJ, Paige AJ, Moir L, Clay J, Rosenthal A, Liu XZ, Blanco G, Steel KP, Petit C, Brown SD. Defects in whirlin, a PDZ domain molecule involved in stereocilia elongation, cause deafness in the whirler mouse and families with DFNB31. *Nat Genet.* **34**:421-8 (2003).

Mburu P, Kikkawa Y, Townsend S, Romero R, Yonekawa H, Brown SD. Whirlin complexes with p55 at the stereocilia tip during hair cell development. *Proc Natl Acad Sci U S A.* **103**:10973-8 (2006).

Mermall V, Post PL, Mooseker MS. Unconventional myosins in cell movement, membrane traffic, and signal transduction. *Science* **279**:527-533 (1998).

Mok H, Shin H, Kim S, Lee JR, Yoon J, Kim E. Association of the kinesin superfamily motor protein KIF1Balpha with postsynaptic density-95 (PSD-95), synapse-associated protein-97, and synaptic scaffolding molecule PSD-95/discs large/zona occludens-1 proteins. *J. Neurosci*. **22**:5253-5258 (2002).

Mooseker MS, Cheney RE. Unconventional myosins. *Annu Rev Cell Dev Biol.* **11**:633-75 (1995).

Mustapha M, Chouery E, Chardenoux S, Naboulsi M, Paronnaud J, Lemainque A, Megarbane A, Loiselet J, Weil D, Lathrop M, Petit C. DFNB31, a recessive form of sensorineural hearing loss, maps to chromosome 9q32-34. *Eur J Hum Genet.* **10**:210-2 (2002).

Nagase T, Kikuno R, Ishikawa K, Hirosawa M, Ohara O. Prediction of the coding sequences of unidentified human genes. XVII. The complete sequences of 100 new cDNA clones from brain which code for large proteins in vitro. *DNA Res.* **7**:143-50 (2000).

Naisbitt S, Valtschanoff J, Allison DW, Sala C, Kim E, Craig AM, Weinberg RJ, Sheng M. Interaction of the postsynaptic density-95/guanylate kinase domain-associated protein complex with a light chain of myosin-V and dynein. *J. Neurosci*. **20**:4524-4534 (2000).

Nal N, Ahmed ZM, Erkal E, Alper O, Lüleci G, Dinç O, Riazuddin S, Kabra M, Ghosh M, Riazuddin S, Morell RJ, Friedman TB. Spectrum of mutations of *MYO15A* associated with hearing loss yield insight into the function of myosin XVA. *Manuscript in Preparation* (2007).

Niggli V. Structural properties of lipid-binding sites in cytoskeletal proteins. *Trends Biochem Sci.* 2001 **26**:604-11.

O'Connor TP, Duerr JS, Bentley D. Pioneer growth cone steering decisions mediated by single filopodial contacts in situ. *J Neurosci.* **10**:3935-46 (1990).

Oliver TN, Berg JS, Cheney RE. Tails of unconventional myosins. *Cell Mol Life Sci.* **56**: 243-257 (1999).

Onishi H, Morales MF, Kojima S, Katoh K, Fujiwara K. Functional transitions in myosin: role of highly conserved Gly and Glu residues in the active site. *Biochemistry.* **36**:3767-72 (1997).

Onishi H, Kojima S, Katoh K, Fujiwara K, Martinez HM, Morales MF. Functional transitions in myosin: formation of a critical salt-bridge and transmission of effect to the sensitive tryptophan. *Proc Natl Acad Sci U S A.* **95**:6653-8 (1998).

Passey S, Pellegrin S, Mellor H. What is in a filopodium? Starfish versus hedgehogs. *Biochem Soc Trans.* **32**:1115-7 (2004).

Pearson MA, Reczek D, Bretscher A, Karplus PA. Structure of the ERM protein moesin reveals the FERM domain fold masked by an extended actin binding tail domain. *Cell.* **101**:259-70 (2000).

Pellegrin S, Mellor H. The Rho family GTPase Rif induces filopodia through mDia2. *Curr Biol.* **15**:129-33 (2005).

Peters, LM, Belyantseva IA, Lagziel A, Battey JF, Friedman TB, Morell RJ. Signatures from tissue-specific MPSS libraries identify transcripts preferentially expressed in the mouse inner ear. *Genomics.* Oct 16; [Epub ahead of print] (2006).

Pickles JO, Comis SD, Osborne MP. Cross-links between stereocilia in the guinea pig organ of Corti, and their possible relation to sensory transduction. *Hear Res.* **15**: 103-12 (1984).

Probst FJ, Fridell RA, Raphael Y, Saunders TL, Wang A, Liang Y, Morell RJ, Touchman JW, Lyons RH, Noben-Trauth K, Friedman TB, Camper SA. Correction of deafness in shaker-2 mice by an unconventional myosin in a BAC transgene. *Science.* **280**:1444-7 (1998).

Pruyne DW, Schott DH, Bretscher A. Tropomyosin-containing actin cables direct the Myo2p-dependent polarized delivery of secretory vesicles in budding yeast. *J Cell Biol.* **143**:1931-45 (1998).

Ramirez-Weber FA, Kornberg TB. Signaling reaches to new dimensions in Drosophila imaginal discs. *Cell.* **103**:189-92 (2000).

Reilein AR, Rogers SL, Tuma MC, Gelfand VI. Regulation of molecular motor proteins. *Int Rev Cytol.* **204**: 179-238 (2001).

Rossman KL, Der CJ, Sondek J. GEF means go: turning on RHO GTPases with guanine nucleotide-exchange factors. *Nat Rev Mol Cell Biol.* **6**:167-80 (2005).

Rzadzinska AK, Schneider ME, Davies C, Riordan GP, Kachar B. An actin molecular treadmill and myosins maintain stereocilia functional architecture and self-renewal. *J Cell Biol.* **164**:887-97 (2004).

Sako Y, Uyemura T. Total internal reflection fluorescence microscopy for single-molecule imaging in living cells. *Cell Struct Funct.* **27**:357-65 (2002).

Schafer DA, Jennings PB, Cooper JA. Dynamics of capping protein and actin assembly in vitro: uncapping barbed ends by polyphosphoinositides. *J Cell Biol.* **135**:169-79 (1996).

Schirenbeck A, Bretschneider T, Arasada R, Schleicher M, Faix J. The Diaphanous-related formin dDia2 is required for the formation and maintenance of filopodia. *Nat Cell Biol.* **7**:619-25 (2005).

Schliwa M, Woehlke G. Molecular motors. *Nature.* **422**: 759-65 (2003).

Schneckenburger H. Total internal reflection fluorescence microscopy: technical innovations and novel applications. *Curr Opin Biotechnol.* **16**:13-8 (2005).

Schneider ME, Belyantseva IA, Azevedo RB, Kachar B. Rapid renewal of auditory hair bundles. *Nature.* **418**:837-8 (2002).

Schneider ME, Dose AC, Salles FT, Chang W, Erickson FL, Burnside B, Kachar B. A new compartment at stereocilia tips defined by spatial and temporal patterns of myosin IIIa expression. *J Neurosci*. **26**:10243-52 (2006).

Sellers JR. Myosins: a diverse superfamily. *Biochim Biophys Acta* **1496**: 3-22 (2000).

Setou M, Seog DH, Tanaka Y, Kanai Y, Takei Y, Kawagishi M, Hirokawa N. Glutamate-receptor-interacting protein GRIP1 directly steers kinesin to dendrites. *Nature* **417**:83-87 (2002).

Seri M, Cusano R, Gangarossa S, Caridi G, Bordo D, Lo Nigro C, Ghiggeri GM, Ravazzolo R, Savino M, Del Vecchio M, d'Apolito M, Iolascon A, Zelante LL, Savoia A, Balduini CL, Noris P, Magrini U, Belletti S, Heath KE, Babcock M, Glucksman MJ, Aliprandis E, Bizzaro N, Desnick RJ, Martignetti JA. Mutations in MYH9 result in the May-Hegglin anomaly, and Fechtner and Sebastian syndromes. The May-Heggllin/Fechtner Syndrome Consortium. *Nat Genet.* **26:** 103-5 (2000).

Sheng M and Sala C. PDZ domains and the organization of supramolecular complexes. *Annu. Rev. Neurosci.* **24**:1-29 (2001).

Shepherd GM, Barres BA, Corey DP. "Bundle blot" purification and initial protein characterization of hair cell stereocilia. *Proc Natl Acad Sci U S A.* **86**: 4973-7 (1989).

Shimada T, Sasaki N, Ohkura R, Sutoh K. Alanine scanning mutagenesis of the switch I region in the ATPase site of Dictyostelium discoideum myosin II. *Biochemistry* **36**:14037-43 (1997).

Shiraki T, Kondo S, Katayama S, Waki K, Kasukawa T, Kawaji H, Kodzius R, Watahiki A, Nakamura M, Arakawa T, Fukuda S, Sasaki D, Podhajska A, Harbers M, Kawai J, Carninci P, Hayashizaki Y. Cap analysis gene expression for high-throughput analysis of transcriptional starting point and identification of promoter usage. *Proc Natl Acad Sci USA*. **100**:15776-81 (2003).

Shotwell SL, Jacobs R, Hudspeth AJ. Directional sensitivity of individual vertebrate hair cells to controlled deflection of their hair bundles. *Ann N Y Acad Sci.* **374**: 1-10 (1981).

Slepecky N, Chamberlain SC. Immunoelectron microscopic and immunofluorescent localization of cytoskeletal and muscle-like contractile proteins in inner ear sensory hair cells. *Hear Res*. **20**:245-60 (1985).

Snell GD, Law LW. A linkage between shaker-2 and wavy-2 in the house mouse. *J. Hered*. **30**: 447 (1939).

Sorokina EM, Chernoff J. Rho-GTPases: new members, new pathways. *J Cell Biochem.* **94**:225-31 (2005).

Sousa AD, Cheney RE. Myosin-X: a molecular motor at the cell's fingertips. *Trends Cell Biol.* **15**:533-9 (2005).

Sousa AD, Berg JS, Robertson BW, Meeker RB, Cheney RE. Myo10 in brain: developmental regulation, identification of a headless isoform and dynamics in neurons. *J Cell Sci.* **119**:184-94 (2006).

Stepanyan R, Belyantseva IA, Griffith AJ, Friedman TB, Frolenkov GI. Auditory mechanotransduction in the absence of functional myosin-XVa. *J Physiol.* 2006 Sep 14; [Epub ahead of print]

Taoka M, Ichimura T, Wakamiya-Tsuruta A, Kubota Y, Araki T, Obinata T, Isobe T. V-1, a protein expressed transiently during murine cerebellar development, regulates actin polymerization via interaction with capping protein. *J Biol Chem.* **278**:5864-70 (2003).

Tilney LG, Derosier DJ, Mulroy MJ. The organization of actin filaments in the stereocilia of cochlear hair cells. *J Cell Biol.* **86**:244-59 (1980).

Tilney LG, Bonder EM, DeRosier DJ. Actin filaments elongate from their membrane-associated ends. *J Cell Biol.* **90**:485-94 (1981).

Tilney LG, Egelman EH, DeRosier DJ, Saunder JC. Actin filaments, stereocilia, and hair cells of the bird cochlea. II. Packing of actin filaments in the stereocilia and in the cuticular plate and what happens to the organization when the stereocilia are bent. *J Cell Biol.* **96**:822-34 (1983).

Tilney LG, Tilney MS, DeRosier DJ. Actin filaments, stereocilia, and hair cells: how cells count and measure. *Annu Rev Cell Biol.* **8**:257-74 (1992).

Tsakraklides V, Krogh K, Wang L, Bizario JC, Larson RE, Espreafico EM, Wolenski JS. Subcellular localization of GFP-myosin-V in live mouse melanocytes. *J Cell Sci.* **112** :2853-65 (1999).

Vale RD. The molecular motor toolbox for intracellular transport. *Cell.* **112**:467-80 (2003).

van Wijk E, van der Zwaag B, Peters T, Zimmermann U, Te Brinke H, Kersten FF, Marker T, Aller E, Hoefsloot LH, Cremers CW, Cremers FP, Wolfrum U, Knipper M, Roepman R, Kremer H. The DFNB31 gene product whirlin connects to the Usher protein network in the cochlea and retina by direct association with USH2A and VLGR1. *Hum Mol Genet.* **15**:751-65 (2006).

Walker RG, Hudspeth AJ, Gillespie PG. Calmodulin and calmodulin-binding proteins in hair bundles. *Proc Natl Acad Sci U S A.* **90**: 2807-11 (1993).

Walker RG, Hudspeth AJ. Calmodulin controls adaptation of mechanoelectrical transduction by hair cells of the bullfrog's sacculus. *Proc Natl Acad Sci U S A.* **93**: 2203-7 (1996).

Wallar BJ, Alberts AS. The formins: active scaffolds that remodel the cytoskeleton. *Trends Cell Biol.* **13**:435-46 (2003).

Walsh T, Walsh V, Vreugde S, Hertzano R, Shahin H, Haika S, Lee MK, Kanaan M, King MC, Avraham KB. From flies' eyes to our ears: mutations in a human class III

myosin cause progressive nonsyndromic hearing loss DFNB30. *Proc Natl Acad Sci U S A.* **99**:7518-23 (2002).

Wang A, Liang Y, Fridell RA, Probst FJ, Wilcox ER, Touchman JW, Morton CC, Morell RJ, Noben-Trauth K, Camper SA, Friedman TB. Association of unconventional myosin MYO15 mutations with human nonsyndromic deafness DFNB3. *Science.* **280**:1447-51 (1998).

Wang FS, Wolenski JS, Cheney RE, Mooseker MS, Jay DG. Function of myosin-V in filopodial extension of neuronal growth cones. *Science.* **273**:660-3 (1996).

Weber KL, Sokac AM, Berg JS, Cheney RE, Bement WM. A microtubule-binding myosin required for nuclear anchoring and spindle assembly. *Nature.* **431**:325-9 (2004).

Wolenski JS. Regulation of calmodulin-binding myosins. *Trends Cell Biol.* **5**:310-6 (1995).

Wood W, Jacinto A, Grose R, Woolner S, Gale J, Wilson C, Martin P. Wound healing recapitulates morphogenesis in Drosophila embryos. *Nat Cell Biol.* **4**:907-12 (2002).

Wu H, Nash JE, Zamorano P, Garner CC. Interaction of SAP97 with minus-end-directed actin motor myosin VI. Implications for AMPA receptor trafficking. *J. Biol. Chem.* **277**:30928-30934 (2002).

Yang C, Pring M, Wear MA, Huang M, Cooper JA, Svitkina TM, Zigmond SH. Mammalian CARMIL inhibits actin filament capping by capping protein. *Dev Cell.* **9**:209-21 (2005).

Yap CC, Liang F, Yamazaki Y, Muto Y, Kishida H, Hayashida T, Hashikawa T, Yano R. CIP98, a novel PDZ domain protein, is expressed in the central nervous system and interacts with calmodulin-dependent serine kinase. *J Neurochem.* **85**:123-34 (2003).

Zhang M, Wang W. Organization of signaling complexes by PDZ-domain scaffold proteins. *Acc. Chem. Res.* **36**:530-538 (2003).

Zhang H, Berg JS, Li Z, Wang Y, Lang P, Sousa AD, Bhaskar A, Cheney RE, Stromblad S. Myosin-X provides a motor-based link between integrins and the cytoskeleton. *Nat Cell Biol.* **6**:523-31 (2004).

Zhao Y, Yamoah EN, Gillespie PG. Regeneration of broken tip links and restoration of mechanical transduction in hair cells. *Proc Natl Acad Sci U S A.* **93**:15469-74 (1996).

Zigmond SH, Evangelista M, Boone C, Yang C, Dar AC, Sicheri F, Forkey J, Pring M. Formin leaky cap allows elongation in the presence of tight capping proteins. *Curr Biol.* **13**:1820-3 (2003).

Zigmond SH. Formin-induced nucleation of actin filaments. *Curr Opin Cell Biol.* **16**:99-105 (2004).